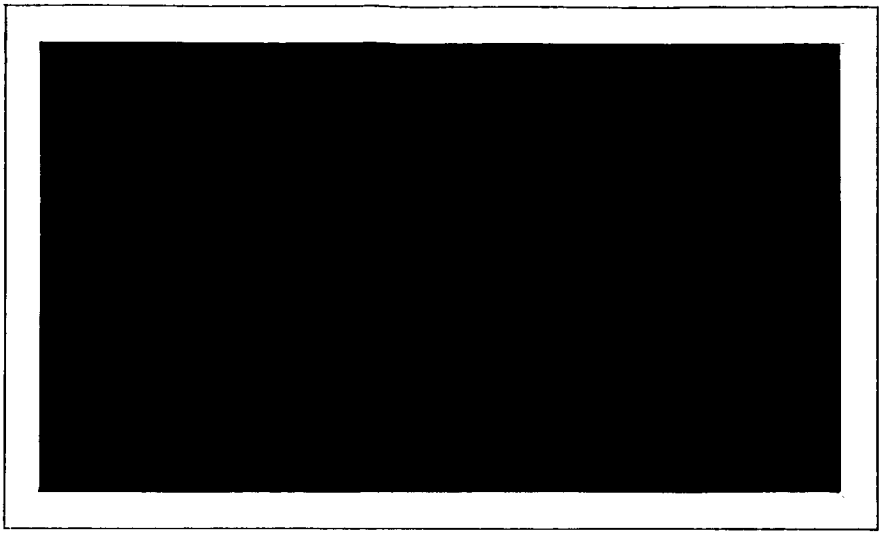

UNIVERSITY OF PENNSYLVANIA

ELECTROCHEMISTRY LABORATORY

PHILADELPHIA, PENNSYLVANIA 19104

THREE-QUARTER PROGRESS REPORT

1 OCT. 1964 TO 30 JUNE 1965

STUDIES IN FUNDAMENTAL CHEMISTRY OF FUEL CELL REACTIONS

NsG-325

Submitted to:

NATIONAL AERONAUTICS AND SPACE ADMINISTRATION

Washington 25, D.C.

Submitted by:

Professor John O'M. Bockris

The Electrochemistry Laboratory

The University of Pennsylvania

Philadelphia, Pa. 19104

TABLE OF CONTENTS

I. POTENTIALS OF ZERO CHARGE

1. Introduction

In the reported period a review of the theory and methods of determination of points of zero charge was prepared (see Appendix I).

On the experimental side, the differential capacitance method for the determination of potential of zero charge was used. The principle of the method has been described in a previous report.[1]

2. Experimental

The existing apparatus was modified so that a better accuracy of measurement was possible. The separate oscillator and wave analyzer arrangement was replaced by a Hewlett-Packard 302-A wave analyzer which has a better resolution (frequency wise) and accuracy. The oscilloscope presently being used (Tektronix type 564 storage oscilloscope) is also capable of detecting smaller signals. Preliminary measurements were made on a dropping mercury electrode to test the accuracy as well as to get familiar with the technique. The data obtained were in good agreement with previous results and the accuracy of measurement was better than 0.5% in the potential range of minimum capacitance plateau. The program was then continued to measure the capacitance-potential behavior of solid electrodes. The first metal studied was platinum.

Preparation and Purification of Platinum Electrode:

To have least possible frequency dispersion a spherical geometry

is preferred, i.e. a spherical platinum bead surrounded by a spherical platinized platinum gauze basket. Platinum bead was formed as follows. Platinum wire 0.2 mm diameter, cleaned in hot conc. HNO_3, was sealed by a Housekeeper seal at the end of a long 'true-bore' tubing so that a thin glass capillary was surrounding at least 3/4" of platinum wire. The wire was melted down to a spherical ball touching the tip of the glass capillary by a hydrogen-oxygen flame. Thus no part of the wire was exposed to the solution. The bead was again cleaned in HNO_3 along with the glass, washed with distilled water and double distilled water. Then it was introduced in a 'Vycor' furnace made to fit on top of the cell. The bead was heated to 350°C in an argon atmosphere (99.9975 % A purified further by passing over Cu filing heated to 400°C and subsequently over molecular sieves cooled down to - 78°C) for about 1/2 hr. Then hydrogen (purified by passing through heated Ag-Pd alloy tube) was introduced for a few minutes to remove any surface oxides. As hydrogen diffuses into platinum (changing the surface and also bulk properties of platinum) it seemed necessary to remove any hydrogen gone into the bulk. So the platinum was heated at a higher temperature $\sim$ 450°C in argon atmosphere up to 3 hours.

Preparation of the Solution:

It is necessary to have highly purified solutions, in order to reduce the drift of capacitance and potential with time and obtain meaningful results. The perchloric acid used was 'Baker Analyzed reagent'. The double distilled water was distilled into a pre-electrolysis cell under a nitrogen (N_2 purified by passing over hot Cu filings and

activated charcoal cooled to - 78°C) atmosphere. The requisite amount of perchloric acid was added and the solution was pre-electrolyzed for 72 hours with the help of very large platinized platinum electrodes at a current density of $1\mu A/cm^2$. The area of the electrode was more than 1200 cm^2. The volume of solution pre-electrolyzed was $\sim$ 500 ml.

Cleaning of glass cells was done as follows: The cells were steeped overnight with 1:3 nitric acid; sulfuric acid, subsequently washed with distilled and double distilled water. The glass ware was steamed and finally with distilled double-distilled-water under purified N_2 atmosphere.

3. Results and Discussion

Figure 1 shows the capacitance vs. potential plot. The capacitance minimum is seen to be at +620 mv (r.h.e.) which is 460 mv (N.H.E.) (pH $\sim$ 2.7) in very good agreement with the result obtained by the first method. Another quite interesting feature of this figure is that with small amount of hydrogen on the surface the p.z.c. shifts in the negative direction if the surface is covered with hydrogen, as was the case in the work of Krasikov and Kheifets. The results obtained on electrodes which contained hydrogen are in fair agreement with the results of Krasikov and Kheifets. Thus the data obtained on metals like platinum with hydrogen on the surface is bound to be different from that measured on the same metal, from which hydrogen has been carefully eliminated. In almost all of the cases, the data seen in the literature is for platinum with hydrogen on it.

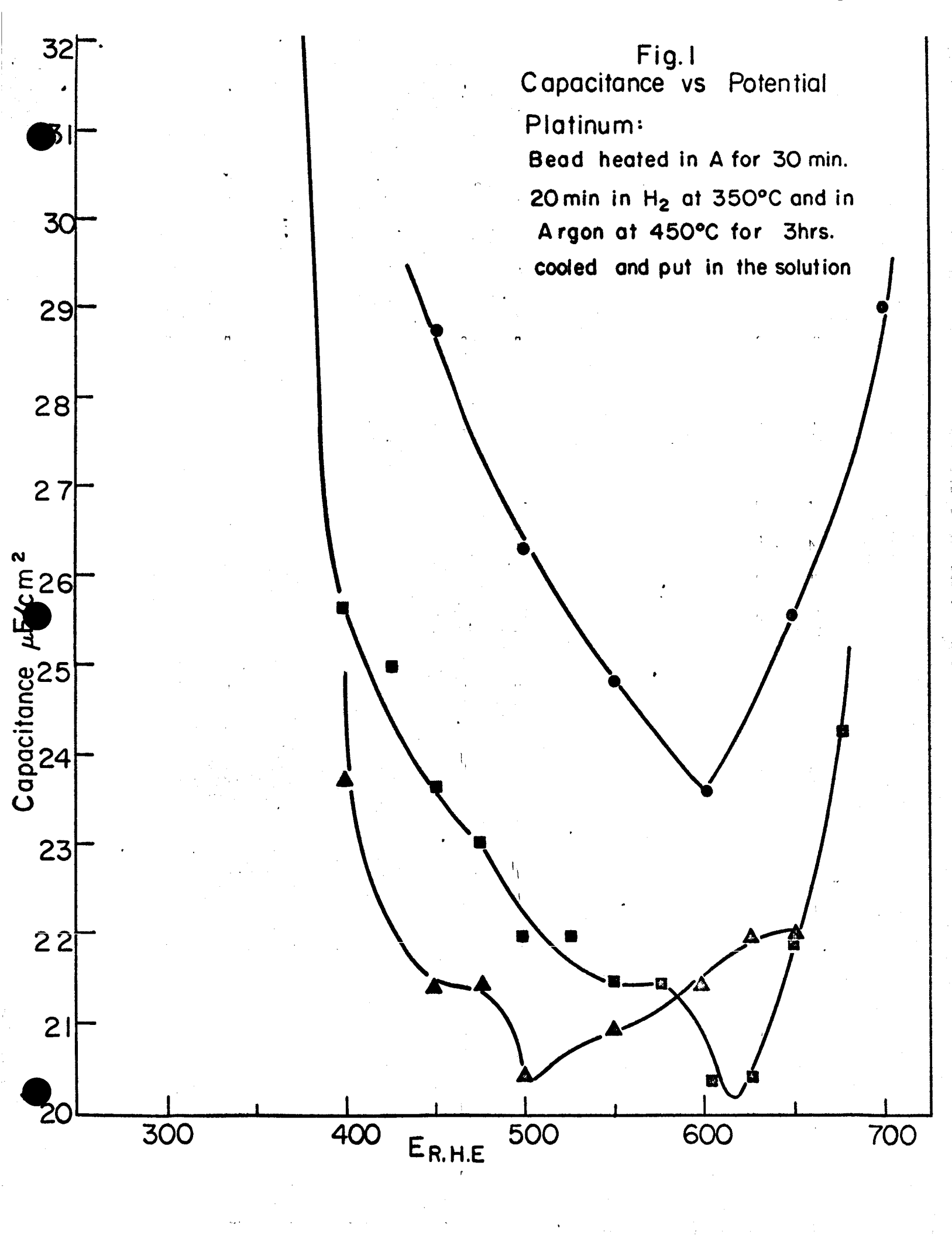
Fig. I
Capacitance vs Potential
Platinum:
Bead heated in A for 30 min.
20 min in H_2 at 350°C and in
Argon at 450°C for 3hrs.
cooled and put in the solution
Capacitance $\mu F/cm^2$
32
31
30
29
28
27
26
25
24
23
22
21
20
300
400
500
600
700
$E_{R.H.E}$

4. Future Work

The program will be continued to obtain the values of the potential of zero charge on several other solid metals, specifically, gold, silver and nickel. Further experiments will be done with platinum to determine the pH dependence of the potential of zero charge of this metal and its relation to the hydrogen content of the metal.

Preparations for setting up a third method for the determination on the p.z.c. on metals will be made.

The role of the surface potential χ_m and the electronic work function in determining the value of the potential of zero charge will be looked into in more detail.

II. THEORETICAL STUDIES

The numerical calculations in the "theoretical analysis of the potential sweep method" have been finished and are reported in Appendix II.

The present report contains also the paper "Proton Transfer across double layers: mechanism evaluation from isotopic effects," Appendix III, which was presented at the Faraday Society Meeting in April, 1965. This paper demonstrates the usefulness of an isotope effect study in elucidating the mechanism of electrolytic hydrogen evolution on a number of metals and also ascertain the degree of proton tunneling in the case of the hydrogen evolution reaction on mercury.

III. ELECTROCATALYSIS

A brief outline of electrocatalysis, presented at the Fuel Cells Meeting of S.E.R.A.I. in Brussels, on June 22, 1965, is enclosed (Appendix IV).

An attempt is reported to correlate the catalytic activities and physical properties of noble metal electrocatalysts, using ethylene oxidation at 80°C, in 1 N sulfuric acid as a test reaction. Relative catalytic activities are measured by a comparison of current values at an arbitrarily chosen potential.

A correlation was found between catalytic activity and both Latent Heat of Sublimation of the metal (L_s), which according to Pauling's formula reflects the adsorbate-adsorbent bond strength, and also the number of unpaired "d" electrons in the metal. Both of these parameters gave a "volcano" type relationship, when plotted against reaction rate.* (Figs. 1 and 2).

Oxygen coverage on the noble metals has been shown[2] to be proportional to the number of unpaired "d" electrons, and similar behavior might be expected for ethylene. Thus on gold, ethylene is known to be very slightly adsorbed,[1] while on platinum, the saturation coverage is that amount that might be predicted on the basis of 0.55 "d" electrons per Pt atom.[3] The apparent weak adsorption of ehtylene on rhodium, appears to result from competitive adsorption with oxygen,

---

*The almost identical behavior of Au and Pd (see Table I A) suggests that under the conditions of the experiment, hydrogen or hydrogen containing species are absorbed in the Pd, thus filling the "d" band vacancies.

TABLE I A

Metal	Tafel Slope (mv)	i_{600}	$\frac{d\log i}{dP_{eth}}$	$\frac{d\log i}{dpH_{\eta}}$	Reaction Products
Platinum	140	5×10^{-6}	-0.2	0	CO_2
Palladium	190	2×10^{-7}	+0.5	0*	50% CO_2 balance aldehydic
Rhodium	180	1×10^{-7}	+0.5	0	CO_2
Iridium	160	3×10^{-7}	+0.5	0	CO_2
Gold	200	2×10^{-7}	+0.5	0*	As Pd
Osmium	---	$< 1 \times 10^{-8}$	+ ?	--	--
Ruthenium	165	1×10^{-7}	+ ?	--	--
Silver	---	5×10^{-8}	+ ?	--	--
Mercury	---	$< 1 \times 10^{-8}$	+ ?	--	--

i_{600} denotes current at 0.6 volts vs R.H.E.

0* denotes that pH effect was zero in the range pH = 0 to 4.0. The reaction did not appear to proceed in alkaline solutions

--- denotes parameter not measured due to experimental difficulties

+ ? denotes positive pressure effect of unknown magnitude

TABLE I B

Alloy	Tafel Slope	i_{600}	$d.i/d.P_{eth}$
Pd-Au			
20-80 At%	2RT/F	6×10^{-7}	+ve $\sqrt{p}$
46-54 At%		3×10^{-7}	
78-22 At%		4×10^{-7}	
Rh-Pd			
25-75 At%	2RT/F	7.0×10^{-7}	+ve
50-50 At%		1.5×10^{-6}	
75-25 At%		3.0×10^{-6}	
Cu-Rh			
10-90 At%	2RT/F	4.0×10^{-6}	+ve $\sqrt{p}$
Cu-Au			
25-75 At%	---	1×10^{-7}	---
Pt-Ru			
80-20 At%	2RT/F	8×10^{-7}	+ve
50-50 At%		5×10^{-7}	
Pt-Ni			
85-15 At%	2RT/F	4.0×10^{-7}	---

which is known to adsorb more strongly on this metal than on Pt[4]. The presence of less than 10% oxygen coverage is known to inhibit adsorption of organic species.[5]

In the case of Platinum, previously described by [7], the following mechanism was suggested,

$$C_2H_4 \quad C_2H_{4_{ads}} \tag{1}$$

$$H_2O \quad OH^{\bullet} + H^{+} + e \tag{2}$$

$$C_2H_{4_{ads}} + OH^{\bullet} \quad C_2H_4O + H^{+} + e. \tag{3}$$

where step (2) was rate determining. This mechanism is obviously not applicable to other metals, where a positive fractional order of reaction with respect to ethylene indicates that an adsorbed organic species is involved in the rate determining step. In order to interpret the observed empirical rate equation:

$$i = k\, e^{FV/RT}\, p^{1/n}\, c_{H^+}^{-0.5} \tag{1}$$

two mechanisms are proposed.

I. Radical Attack

In this mechanism, the sequence suggested above still applies, except that step (3) is now rate determining. Such a mechanism would give rise to an equation such as the above if coverage with $OH^{\bullet}$ or $O^{\bullet\bullet}$ were to change linearly with potential, as is often the case. The change of rate control from step (3) in the case of Au to step (2)

for Pt and back to (3) for Rh, and the various factors controlling it, are considered in Table II.

TABLE II

Parametric Change	Forward Rate of (2)	Forward Rate of (3)
Increase in θ_{OH}	decreases	increases
Increase in θ_{eth}	decreases	increases
Metal-OH bond strength	increases	rises to max, then decreases
Metal-ethylene bond strength	----	rises to max, then decreases.

Thus an optimum value exists, lying between the extremes of weak adsorption (not true chemisorption) and strong adsorption (immobile species, metal-adsorbate bond hard to break). The rate of step (3) will be highest on catalysts with high coverages of both adsorbed species, and intermediate values of bond strengths. It seems that Pt fulfills these conditions, having however a relatively slow rate for step (2) owing to the high coverage of ethylene.

This accounts for step (2) being rate determining. On gold, very low coverages and low bond strengths of adsorbed radicals result in step (3) proceeding slowly. The same is true on Rhodium, again because of very low ethylene coverage but also because of the much higher Metal-Oxygen bond strength. In both cases, step (3) becomes

rate determining. The weakness of the Metal-Organic chemi-bond in the case of gold, is the probable reason for desorption of intermediates such as aldehydes, as opposed to the complete oxidation to CO_2 observed on other metals.

II Electron Transfer from Organic Species

In this second possible mechanism, which has already been proposed for many oxygen containing organic species,[6] the sequence is:

$$C_2H_4 \quad C_2H_{4_{ads}} \tag{1}$$

$$C_2H_{4_{ads}} \quad C_2H_3^{\bullet} + H^+ + e \tag{2}$$

$$C_2H_3^{\bullet} + H_2O \quad C_2H_4O + H^+ + e \tag{3}$$

Such a mechanism is possible wherever zero or positive pressure effects with respect to concentration of organic species are observed.

An attempt to distinguish between mechanisms I and II is presently under way, involving H/D isotope effects.

References

1. B. Rubin, E. Gileadi and J. O'M. Bockris, to be published.
2. M. L. Rao, A. Damjanovic and J. O'M. Bockris, J. Phys. Chem. 67, 2508 (1963).
3. E. Gileadi, B. Rubin and J. O'M. Bockris, J. Phys. Chem., in press.
4. H. Dahms and J. O'M. Bockris, J. Electrochem Soc. 111, 728 (1964).
5. M. Breiter and S. Gilman, J. Electrochem Soc. 109, 1099 (1962).

6. V. S. Bagotskii and Yu. B. Vasilyev, Electrochimica Acta 9, 869 (1964).

7. H. Wroblowa, B. J. Piersma and J. O'M. Bockris, J. Electroanal Chem. 6, 401 (1963).

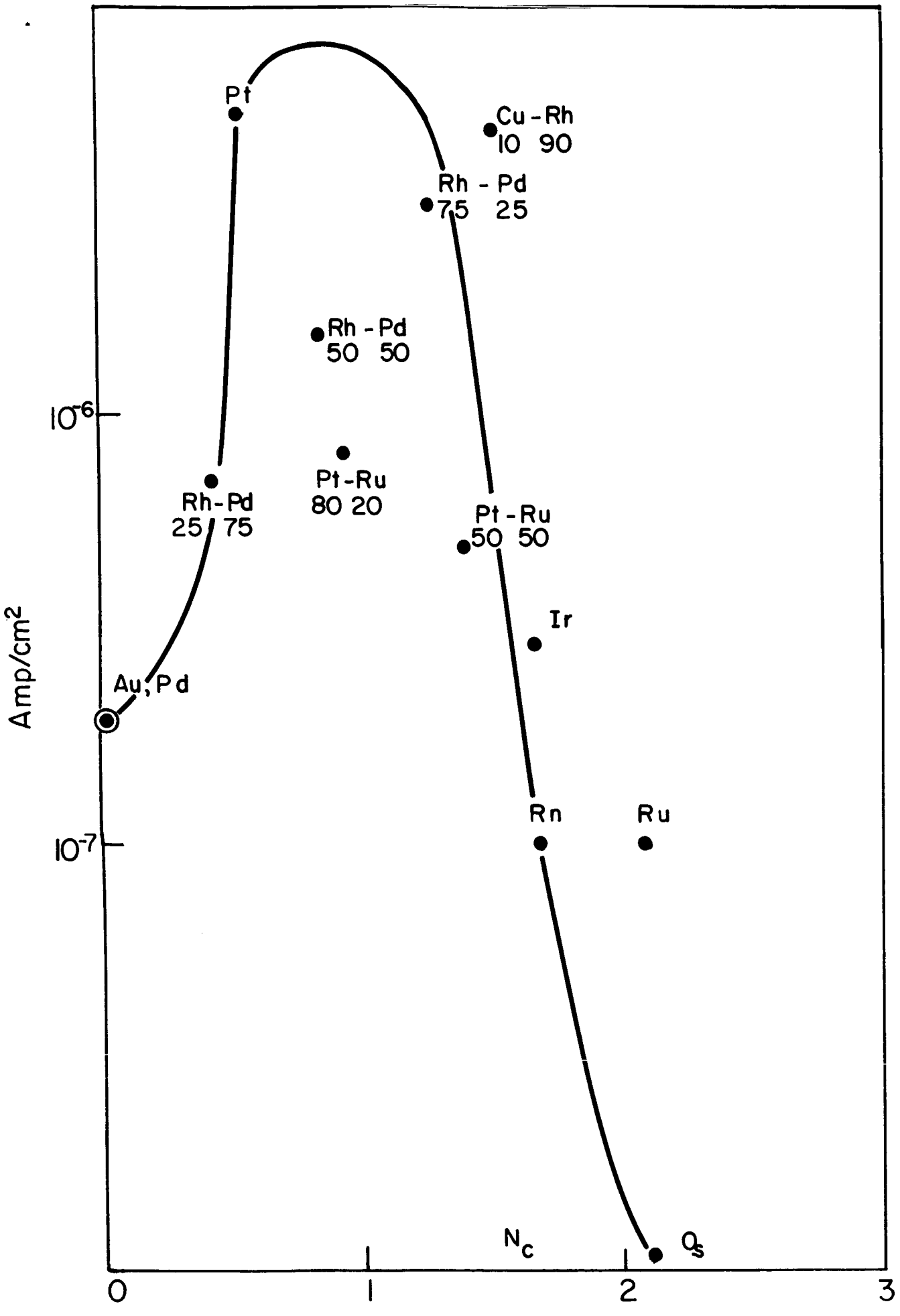
Pt
Cu - Rh
10 90
Rh - Pd
75 25
Rh - Pd
50 50
Pt-Ru
80 20
Rh-Pd
25 75
Pt - Ru
50 50
Ir
Au; Pd
Rn
Ru
10^{-6}
10^{-7}
Amp/cm^2
N_c
O_s
0
1
2
3

FIG. 1

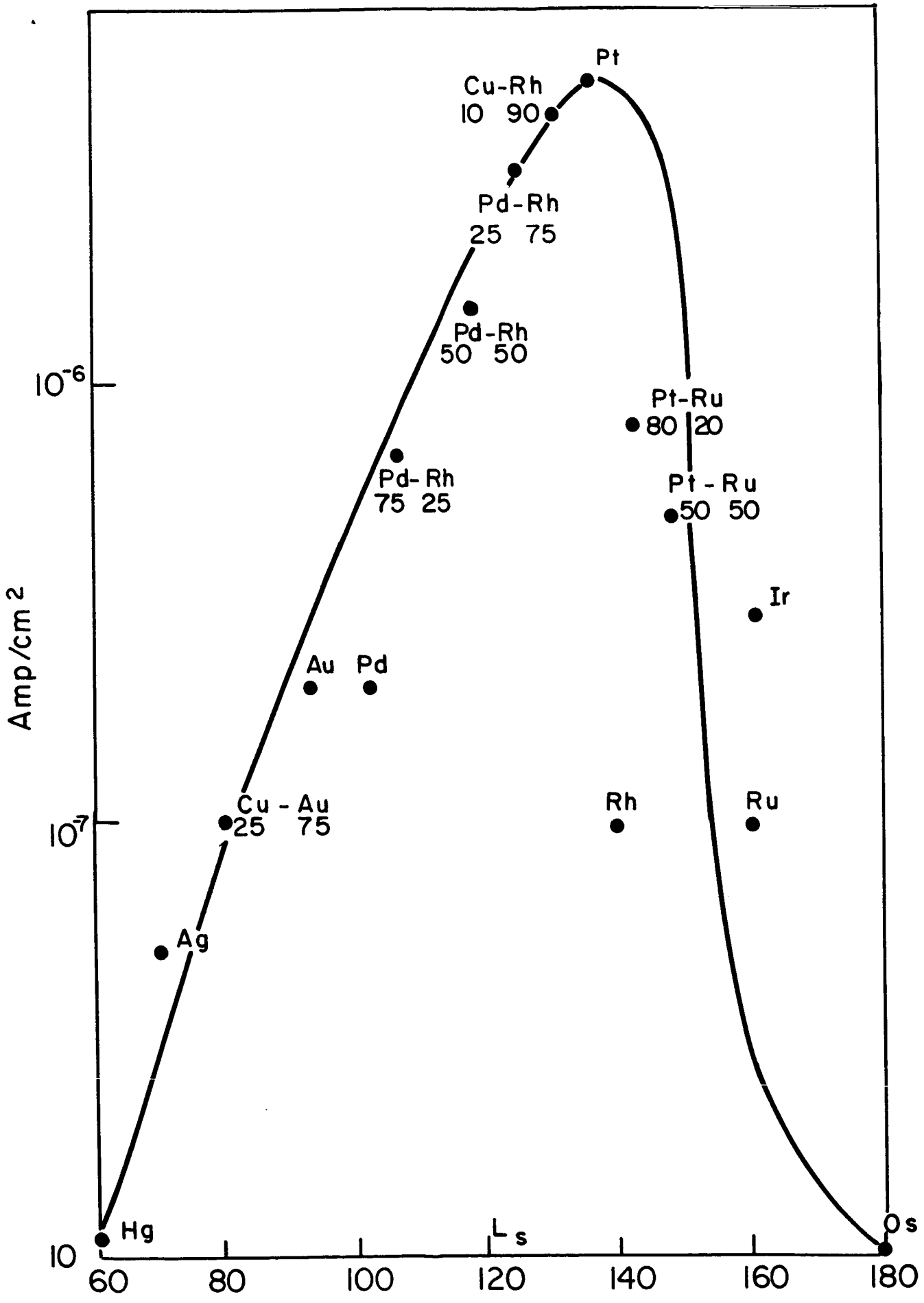
Pt
Cu-Rh
10 90
Pd-Rh
25 75
Pd-Rh
50 50
Pt-Ru
80 20
Pd-Rh
75 25
Pt-Ru
50 50
Ir
Au
Pd
Cu - Au
25 75
Rh
Ru
Ag
Hg
Os
Ls
Amp/cm 2
10^{-6}
10^{-7}
10
60
80
100
120
140
160
180

FIG 2

IV. CATALYTIC ACTIVITY FOR SIMPLE ELECTRODE REACTIONS

1. Introduction

In previous Reports,[1,2] data were given on the catalytic activity for hydrogen evolution reaction on a number of noble metals and on their alloys in acid solution. In this Report, work on the catalytic activity in alkaline media on various noble and some non-noble metals and their alloys is described and data presented.

2. Electrode Material

Catalytic activity for hydrogen electrode reaction of Pt, Rh, Ir, Pd, Ni, Au, and Cu electrodes in alkaline solution have been examined. Also, activities on alloys of Au-Pt, Au-Pd, Au-Cu in alkaline, and of Pt-Pd in acid solution have been studied.

3. Experimental Procedure

The cell and the set up for the experiments were essentially the same as described in previous Reports.[1,2] 'Fisher' reagent grade 50% NaOH solution was purified by recrystallization in N_2 atmosphere. The solution in a crystallization vessel was cooled by an acetone-dry ice mixture bath. At the appearance of the first crystals, cooling was slowed down to decrease the rate of crystallization and to obtain purer crystals. The residual liquid was extracted by a suction pump. After crystals remelted, process of recrystallization was repeated twice more. The crystals obtained after the third crystallization were allowed to melt

and the liquid was transferred through ball and socket arrangement into a closed graduated tube. The liquid was then standardized by titrating a measured amount of NaOH against standard HCl acid solution. The amount needed to make a 0.1 N NaOH solution was transferred into the counter-electrode compartment without exposing the solution to the atmosphere. Required volume of the conductivity water was redistilled into this compartment. This solution was then introduced into the test and reference electrode compartments of the cell, after which it was further purified by pre-electrolysis on a large Pt electrode for about 15 - 18 hours. Both cathodic and anodic Tafel lines were determined and thereby the slope and the exchange current densities obtained.

4. Pretreatment of Electrodes

To obtain reproducible and meaningful results, it was required to standardize the pre-treatment of electrodes. With metals this is not a difficult problem, and the final treatment might include short anodic and then cathodic pulse. On a Pt electrode, for instance, this treatment is supposed to remove organic impurities which might be adsorbed on the electrode, and also to create, at least partially, a fresh surface in the cycle of oxide formation-oxide reduction. With alloy, this treatment might lead to a radical change on the surface. Thus, if a Au-Cu electrode is anodized, some oxides might form which during the cathodic pulse will reduce. During the reduction, gold may deposit on the electrode preferentially and change the character of the latter. At the potentials of 200 - 300 mV anodic with respect to the rest

potential, a Cu-Au electrode with only a few (< 5) at. % of Au in N_2 saturated $CuSO_4$ solution soon becomes covered by "redeposited" gold.[3] In order to avoid anodic formation of oxides on the electrodes and possible change of the electrode during the electrochemical reduction of these oxides, no anodic pulse above 1.05 V was applied in the pretreatment of the electrodes. If an electrode is potentiostated at 1 V (N.H.E.) for a few milliseconds it is expected that no oxides form on noble metals. On such electrodes subsequently reduced, reproducible results have been obtained. In figure 1, line a, a Tafel line was shown for an Au-Pt (20 at.%) alloy which has been treated as described. Subsequently, the same electrode has been anodized at higher potential of 1.7 V for less than 0.1 sec and then cathodically reduced. With this treatment the electrode changed its active and slope of Tafel line. These changes are indicative of the change in the mechanism of the reaction.

The procedure which was used in previous experiments, and which consisted of heating of the electrodes at 1/3 of their respective melting points, first in H_2 for about 5 min., and then in N_2 for another 10 - 15 min., was discontinued. The reason for it was that it was shown[4] that in some alloys (Au-Pt, for instance) the change in the surface concentration may occur if electrodes were heated for an extended period (order of 1) at 600°C. In order to avoid any uncertainty in the results, thermal treatment was discontinued and electrochemical treatment described above was used throughout except in case of non-noble metals (e.g., Cu, Ni) and their alloys. In the latter cases, after chemical

treatment cathodic pulses were applied to the electrodes.

5. Description of the Results

In Table 1, the values of the exchange current densities (i_o's) and of Tafel slopes (b's) for both cathodic and anodic reactions in 0.1 N NaOH solutions are given. As was observed before in acid solution,[2] a definite relationship between the alloy composition and the activity of the electrode exists, both in Au-Pt and Au-Pd series of alloys (Fig. 2).

Only one Cu-Au alloy was tested: no significant change either in Tafel slope or in the activity was observed from that of pure Cu or pure Au. Tafel slopes were $\sim$120 mv, and the i_o of 3×10^{-6} amp/cm^2.

In the Pt-Pd alloy system, Pt and Pd have approximately the same activity (i_o's) but different mechanisms of reaction as indicated by different Tafel slopes in acid solution. The way in which the Tafel slopes would change with alloy composition might throw light on the factors affecting the mechanism and the catalytic activities for this reaction. It was observed that the Tafel slopes, and thus possibly the mechanism of the reaction on these alloys, are close to those of the corresponding end members. More alloys are required to see if there would be a sharp change in the mechanism in a narrow range of alloy composition. Further accumulation of experimental facts are still needed before final analysis and conclusion could be made regarding the factors affecting the activity for hydrogen evolution reaction on these noble metals and on their alloys.

TABLE 1

EXCHANGE CURRENT DENSITIES AND TAFEL SLOPES IN ALKALINE SOLUTION

Electrodes		i_o (amp/cm^2)	b (mv)
Au	Cathodic	4×10^{-6}	112
	Anodic	2×10^{-6}	130
Pt	Cathodic	6×10^{-4}	122
	Anodic	4×10^{-4}	108
Pd	Cathodic	3×10^{-4}	115
	Anodic	2.5×10^{-4}	105
Cu	Cathodic	5×10^{-6}	115
Au-Pd(25%at)	Cathodic	3.5×10^{-6}	125
	Anodic	3.5×10^{-6}	128
Au-Pd(50%at)	Cathodic	10^{-5}	130
	Anodic	10^{-5}	128
Au-Pd(75%at)	Cathodic	2×10^{-5}	115
	Anodic	2×10^{-5}	125
Au-Pd(90%at)	Cathodic	4.5×10^{-5}	140
	Anodic	4.5×10^{-5}	130
Au-Pt(10%at)	Cathodic	4×10^{-6}	120
	Anodic	7×10^{-6}	
Au-Pt(20%at)	Cathodic	5×10^{-6}	125
	Anodic	5×10^{-6}	130
Au-Pt(95%at)	Cathodic	4×10^{-6}	112
	Anodic	4×10^{-6}	116
Ni(1N H_2SO_4)	Cathodic	5×10^{-6}	120

References

1. NASA Semi-annual Progress Report, Dated 1st Oct., 1963 to 31st March, 1964.

2. NASA Semi-annual Progress Report, dated 1st March to 30th Sept., 1964.

3. Gerischer, H., Anodic Behavior of Noble Metal Alloys and Resistance Limits of the Corrosion of Such Alloys, Korrosion, 16, 21-7 (1963).

4. Bockris, J. O'M., Damjanovic, A., Kundu, K., Private Communication.

Legend to Figures

Fig. 1 - Effect of electrode treatment on the electrode behavior in H_2 reduction. Alloy Au - 20 at% Pt. a: electrode potentiostated at 1.05 V for about 0.1 sec and then cathodically reduced. b: electrode potentiostated at 1.7 V for about 0.1 sec and then chemically reduced.

Fig. 2 - Change of the activity for H_2 reduction into alloy in Au-Pt and Au-Pd alloys. Alkaline (0.1 N) solution.

Fig. 3 - Plot of Tafel slopes for H_2 reduction on Pt, Pd and a Pt-Pd alloys. Sharp change in expected at mid range of atomic

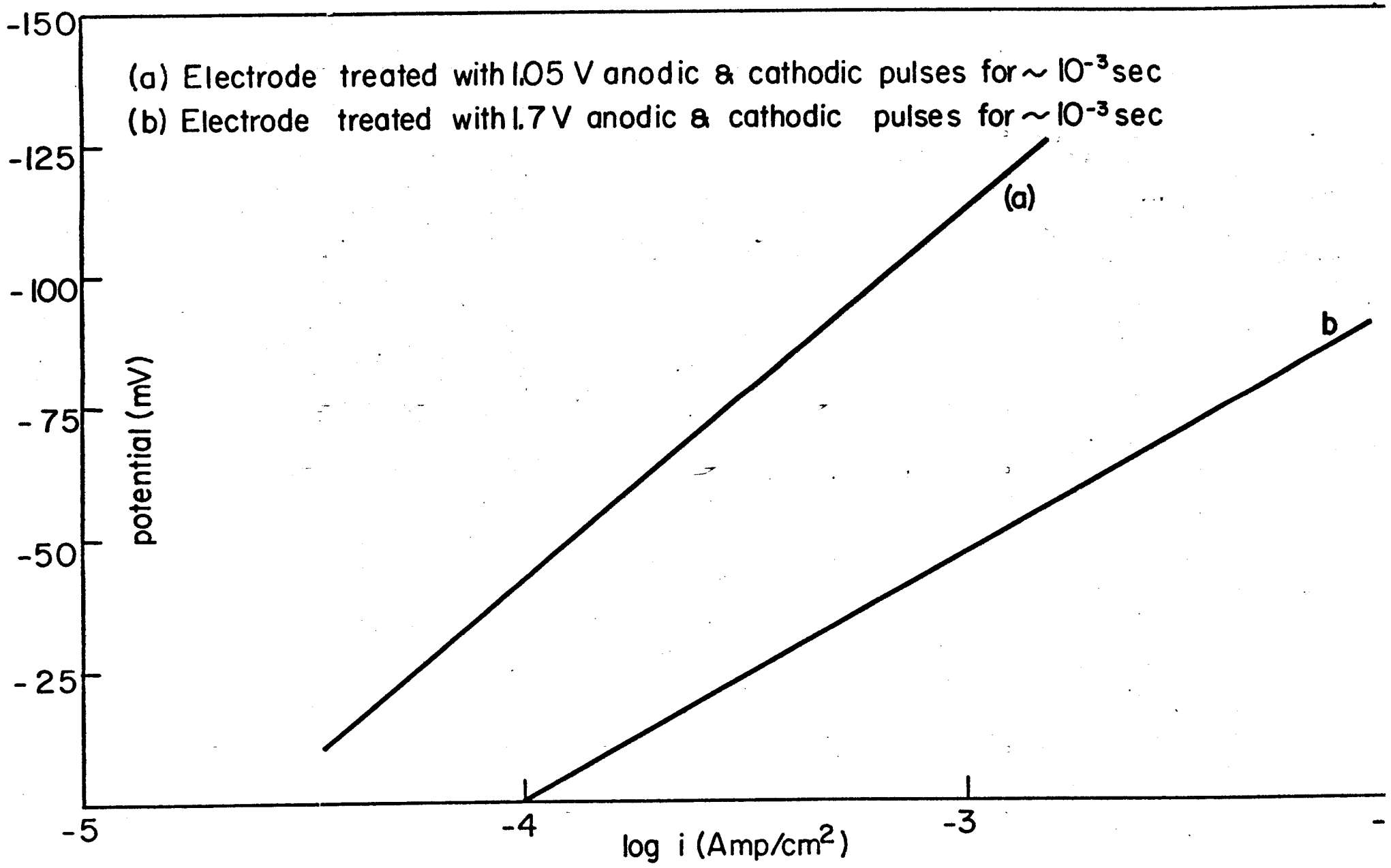
(a) Electrode treated with 1.05 V anodic & cathodic pulses for ~ 10^{-3} sec
(b) Electrode treated with 1.7 V anodic & cathodic pulses for ~ 10^{-3} sec
-150
-125
-100
-75
-50
-25
potential (mV)
(a)
b
-5
-4
-3
log i (Amp/cm^2)

FIG. 1

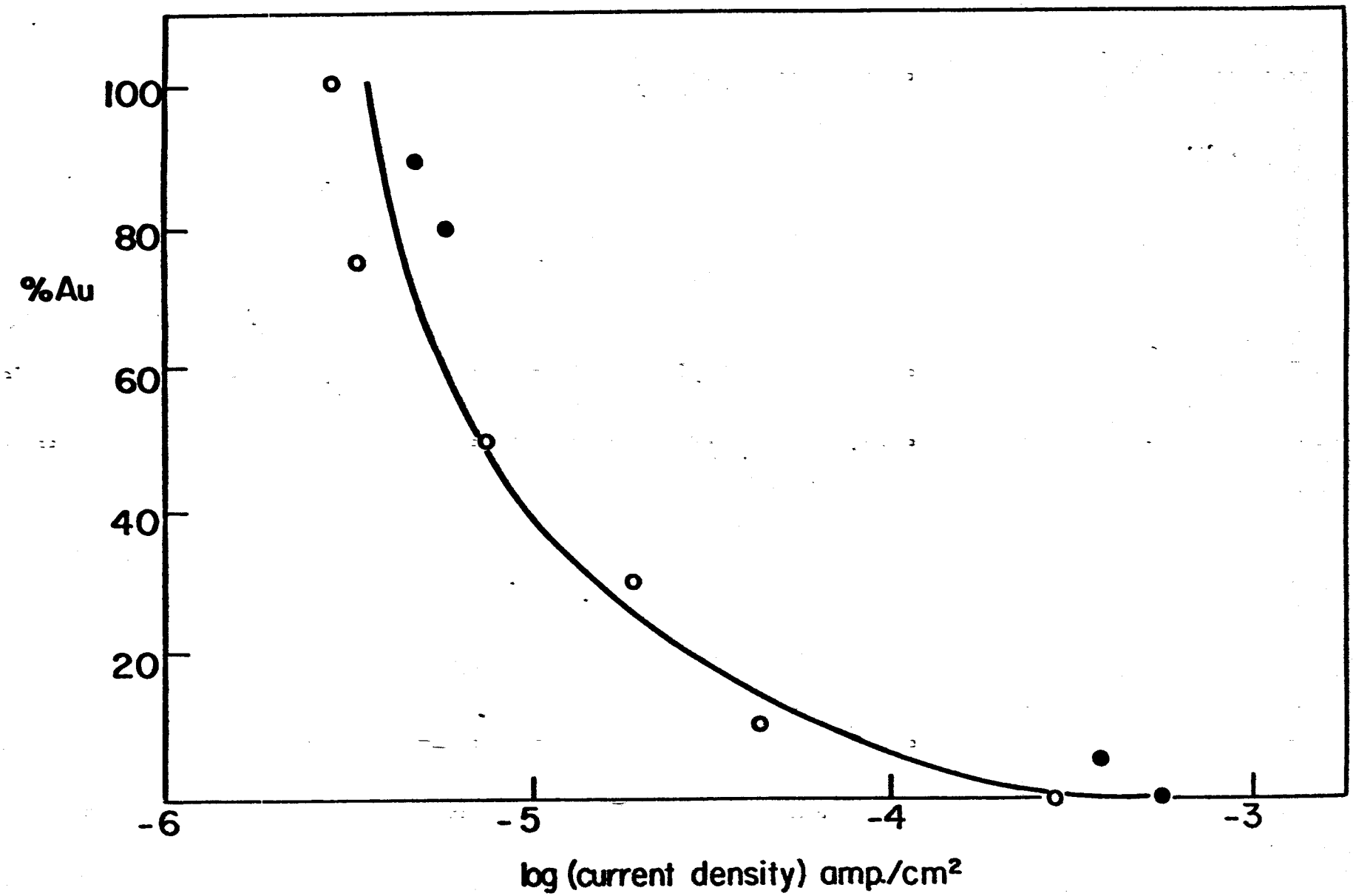

FIG.2

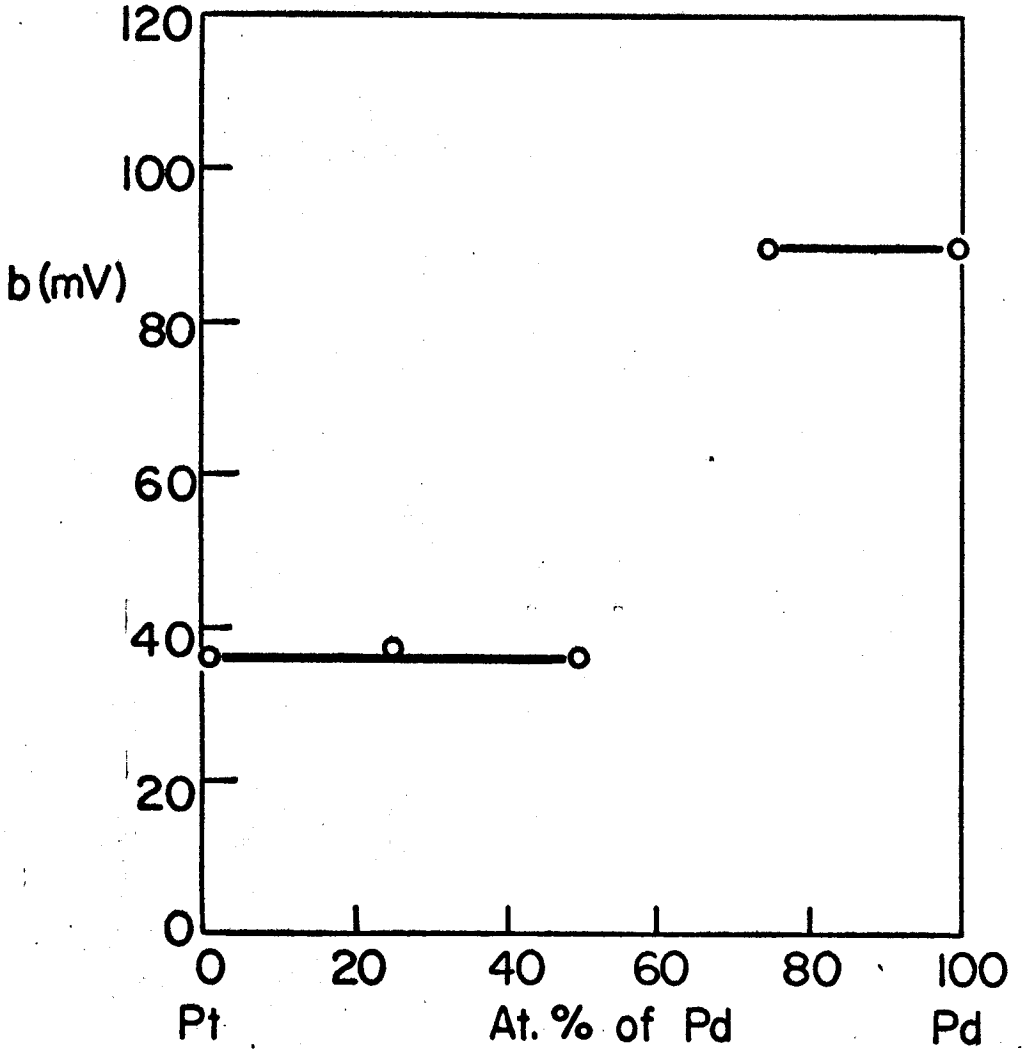

FIG. 3

V. MODEL POROUS ELECTRODE

TRANSIENT MEASUREMENTS

I. Introduction

The transient (i vs t) measurements made thus far can be divided into two categories. (1) The shorter time (.1 msec to ~1 - 10 sec) with fast switching of potentials and the (2) longer time transients made on the recorder with manual setting of the potentiometer, thus producing a time uncertainty in t = 0 of 1 - 2 seconds, besides making the conditions inside the pore completely undefined (see appendix for details of analysis of transients on "slot" electrodes) since a complicated input function is produced rather than a well defined step.

II. Description of Technique

The empty cell is adjusted to desired width, and H_2 gas flushed through cell to remove last traces of air. H_2 gas is also bubbled from cell through electrolyte in external reservoir to purge majority (at least) of dissolved air. The H_2 is standard Airco H_2 with no special attempts at purification except for passing through distilled H_2O to saturate the H_2 w/H_2O vapor to eliminate evaporation of the electrolyte and incidentally to scrub out any gross soluble contaminant. The electrolyte was made from water from the conductivity still, and H_2SO_4 (A.R. - from bottle) to make 1 N solution. The electrolyte is carefully filled into the cell from the bottom to minimize trapped bubbles of H_2

(which require several days to remove by reaction and diffusion, if produced) and the final level adjusted with a piston microburette. During the filling procedure, the reference electrode (a Pd bead) is charged at a low current till visible H_2 evolution occurs.

III. Transient technique (1)

The cell is then allowed to equilibrate on open circuit, the potential measured with an electrometer, and the potentiostat adjusted to the same potential and attached to the cell. Final adjustments of the potentiostat ($\pm$ 2 - 3 mv) are then made so that the net current into the cell is zero. The desired potential step is set on the "adding" potential dial, and the oscilloscope, channel 2, is connected to measure current differentially to the appropriate scale (determined by prior experiment), and the time scale set at 0.1 msec/cm. The potential is turned on, the transient recorded on the scope, and the potential switched back to zero as soon as possible (i.e. $\sim$ 0.1 - .2 sec). The current (now in a cathodic direction) is allowed to decay back to zero (or very close to it, which takes several minutes), the time scale is increased by a decade, and the current range is set so that the value at the 10th cm (1msec for first sweep) will just be on scale after the first cm at the new time. The transient is repeated, and stored on the oscilloscope screen. This process is repeated until the scope sweep is in its slowest position of 1 sec/cm.

(Experimentally, it is found that if the transients are only allowed to proceed for the time required to produce the transient, the

results are precise, well within 1%, the limit of measurement accuracy, and reproducible within 10%. If times much longer than 10 sec are allowed, the system becomes disturbed and results can vary by several hundred per cent. During the measurement, no auxiliary measuring equipment such as recorders can be connected to the system, because of the "loading" effect on the measured system. This applies to steady state measurements after the 10 sec sweep also, because they affect the next series of transients at the next potential.)

The 5 transients produced are thus stored on the scope and photographed (if satisfactory) at the end, noting carefully which transient is which. The adding potential is changed to the next value and the process repeated.

IV. Slow Transients (2)

The slower transients run more recently and recorded only on a recorder, were set up in the following fashion. The cell is adjusted and filled according to the same procedure as in III above, and a potential of 50 mv is set on the adding potential, recorder at 1"/minute and sensitivity at 5.0 ma full scale (i.e. 50 mv full scale across 10 Ω measuring resistor) and the potential switched on. As the current drops to lower values, the sensitivity is advanced to 1 ma or .5 ma full scale as required. The chart is allowed to run for at least 10 minutes or until an apparent steady state is reached, and the potential advanced manually to the next potential. (With the apparatus in its present form, sequential automatic switching is impossible, although a setup could be

produced relatively easily.) For this reason all i-t curves above 50 mv are relatively meaningless (or at least very difficult to interpret) and bear little or no relationship to the shorter time transients (1). "Steady state" measurement, taken after ten minutes also depend drastically on prior history, as described later.

V. Results

A. Fast transients (1)

Detailed sets of data were obtained for a 1.05 mm slit at top, middle and bottom meniscus regions, and are plotted as follows:

Fig. 1. 1.05 mm width full slit, potential steps of 100, 200, 300, 400 and 600 mv with times from .1 msec to 10 sec plotted as i vs log t.

Fig. 2. Same electrode steps of 100, 200, 300 mv, on expanded current scale.

Fig. 3. Same electrode spacings, 400, 600, 800 and 1000 mv.

Fig. 4. Repeat of Fig. 3, but after electrode is activated at 1.000 volt (for unknown period).

Fig. 5. 1.05 mm wide middle height.
Solid lines - 100, 200, 300, 400, 500, 600, 800 and 1000 mv steps also for comparison P-14-2 and P-14-1 (400 and 600 mv respectively) from Fig. 4 in dotted lines; and - in 200 and 400 mv steps at bottom meniscus with dashed lines.

Fig. 6. .15 mm slit-top meniscus only. 200-400-600-800 mv steps.

Fig. 7. .15 mm slit showing effects of pre-exhaustion 200 mv steps starting at 100, 200, 300 and 500 mv with one (P-9-2) from OCV for comparison.

Fig. 8. From Fig. 7, top and bottom curve plotted vs $t^{-1/2}$.

Also measured but not shown in figures (data is available but not plotted because of poor reliability of electrode) is data on wide slit, but this data will be discussed in generalities under discussion.

VI. Discussion - transients (1)

The transients in Fig. 1 show two definite segments linear in log t, with slopes and maximum initial currents proportional to the size of the input step. Both segments of the lowest four curves extrapolate to a common point at ~.15 sec and 1 - 2 sec. Fig. 2 is an expansion of the lowest three curves. Fig. 3 (at higher steps) also shows two segment behavior, but the curves extrapolate to different points, the initial segment also to .15 sec, but the second point to about .4 sec. (The 600 mv step does not fit well, and there may have been an experimental problem, or there may just be something peculiar about 600 mv, though I expect the former. Slight unobserved shifts in instrumental zero could cause such deviations easily.)

However, Fig. 4 is a set of runs taken after the electrode was activated (unintentionally at the time, just as a result of the earlier runs.) Note only one linear segment extrapolating to about .1 sec, but at a somewhat higher current than Figures 1, 2, 3. (Compare this result with triangular sweep data presented in appendix on mechanism changes for H_2 oxidation.)

Fig. 5 shows a marked deviation from Figures 1 - 4. A linear segment is observed, but terminates rather abruptly at 20 - 30 msec. Apparently, a 1 mmslot in this setup is just on the borderline between wide and narrow slot behavior. The flooded slot then shows the "modified transmission line" behavior over all times, while the half-slot starts out that way for short times, but is terminated by the meniscus after 20 - 30 msec after which time it behaves like a macro-slot. Data taken on 4 and 5 mm slots show similar, even more marked, inflections, but no linear segments are observable. Note that the portions in Fig. 5 which are linear do tend to extrapolate to a common point at 5 - 6 sec.

Data taken on a .15 mm slit, flooded, shown in Fig. 6, show even a more marked linearity with log t, and similar extrapolation to "common" points, but, of course, slightly lower initial currents, although higher than would be expected from the ratios of the slit thicknesses.

Figure 7 shows a very interesting result. Here, the 200 mv transient has been replotted together with 4 other 200 mv transients taken at different starting potentials. The purpose of this set of runs was to determine the effects of pre-reducing H and H_2 conc. in the slit, both on (and in) the surface and in the solution. While the current is decreased, the decrease is not as great as expected, although the linearity vs log t is destroyed. After prepolarization at 500 mv, the conc of dissolved H_2 in solution should drop to negligible amounts, and the H_{ads} should also be reduced to very small quantities. If only C_{DL} is then left, the area under Curve P-10-4 should be about 1% of that under P-9-2. The reason for this discrepancy is not too clear, but may be in part due

to the non-equipotential distribution in the slot. If we assume a slot resistance control (as compared to a meniscus control in the wider slot) we may expect an area under the curve P-10-4 as great as 30% of P-9-2!

It has been shown elsewhere, that on the basis of pure linear transmission line theory one expects a $i\text{-}t^{-1/2}$ decay rather than i-log t. I suspect that the finite "q" allowed on the C_ϕ causes some of the deviation from $t^{-1/2}$ behavior in this slit. Pre-exhaustion, if it removed the hydrogen totally from the slit should tend to produce $t^{-1/2}$ behavior. But as Fig. 8 shows (although P-10-4 tends slightly more to tend to this behavior), no good straight lines can really be drawn to these curves over any appreciable period, while the same curve shows 3 decades of linearity on log t.

VII. Results of Recorder Longterm Work

Little can be said about the results of the transients obtained on the recorder, except that the primary transient was obtained at the first step of 50 mv (Fig. 9) and at least 10 minutes was required to reach a quasi-steady state. Subsequent voltage changes (not steps) were quicker to reach a more stable value (Fig. 10).

An example of the problems involved are shown in Fig. 11,a which are pictorial examples of what sometimes occurred when approaching the same potential from above and below. One would expect the curves to look more like Fig. 11b, but definite maxima were usually observed. The "Quasi-steady state" (taken after 10 min) values are shown plotted in several graphs. The results below are extremely dependent on activation

(see Fig. 12 which shows the result of going up to 1 volt (1) and returning from the "activated" state via (2), where the currents in the lower voltage regions can be increased by an order of magnitude. If reasonable care is exercised not to exceed .6 - .7 volts, the results are more reproducible, but still vary by some 10% (compare to about .1 - .12% with slow polarographic sweep methods or 1% with faster transients (1)). Fig. 13 and 14 show some selected-runs which had about the best reproducibility.

Three heights were run at 3 widths (top, middle, bottom at 4 mm, 1mm and .3 mm). The curves using increasing voltages are plotted at constant width for the three heights in Fig. 15a, b, c in a relatively unactivated condition (although there was usually some activation because of the prior run) and Fig. 15d is a repeat of 15b, but after the electrodes were partially "activated".

Fig. 16a, b, c show the same data replotted with constant position, and variable height. Fig. 17 is another graph showing the effects of "partial activation" on the 1 mm meniscus only.

VIII. Discussion

The data obtained is practically impossible to interpret quantitatively, and only a few rough qualitative generalizations were made. No comparison of any slow transient data can be made with the rapid transient systems. In general, currents were highest at the bottom position for all widths studied, and if the electrodes were "unactivated" linear behavior was usually observed.

A. Behavior of porous electrodes

In an attempt to solve the problems of a porous electrode, the following points were assumed:

(1) that we knew something about the actual microstructure of a porous electrode,

(2) that we know something about the "shape" of the meniscus interface in this porous structure.

(3) On this basis, we assume that we could set up some sort of a model for the porous electrode structure. Though all of these points rest on somewhat shaky ground (but see Supplement I), point # (3) may be the weakest.

B. Statement of problem

Let us divide the problem into two parts.

(1) Macro-treatment

The first part in the bulk processes that occur considering the electrode as a porous mass with some kind of distribution of electrode, liquid, and fuel. This is the type of procedure adopted by Newman and Tobias,[1] Wagner,[2] Bonnemay[3] and some others. Here, the tacit assumption is that we can take some average distribution function of material in the bulk of the porous body and that we can treat the problem in terms of the average bulk resistance of the electrode and electrolyte, and that the concentration term for the fuel can be reduced to a one-dimensional problem (by replacing the

complex pore distribution with a simplified, one dimensional array of tubes aligned in the thickness direction) and by assuming that the gas liquid interface can be localized to some definite region of the plate, thus producing a determinable concentration gradient in the porous matrix. Though this may be roughly true for some special geometries, such as a "homoporous" electrode (which is in reality far from homoporous), or the totally "wet" or totally "dry" electrode, it can be far from true for most other electrodes, and the actual interface is a vastly different arrangement, and gas space may extend well into the liquid phase and vice versa.

(2) Micro-treatment

The second phase of the problem deals with the localization of the activity in an electrode on a micro-scale, and assuming a knowledge of capillary shape, calculating local current distributions on an idealized electrode pore. This is essentially the approach used by Will[4] and Urbach[5] and in some aspects by myself. Here, one assumes some shape of the meniscus, tries to simplify the boundary conditions, inserts diffusion, resistance, and possibly activation and attempts to solve the resultant differential equations. Unfortunately, the equations, in general, become highly non-linear, and intractable to analytic solution. In most cases, computer solution would be feasible, and useful. The experimental verification of these systems is relatively simple, but the applicability to actual fuel cells is questionable. It can be shown that even in a simple setup such as Will's and/or

mine the behavior is a strong function of the actual shape of the meniscus in an extremely small region, and so the translation of these simplified systems to a real porous electrode may be questionable.

(3) Combined approach

The sort of treatment given by Burstein in an attempt to unify the two points of view. Penetration of the gas is provided for, and the control of the reaction is assumed in small pores interconnections the larger gas and liquid pores. Cylindrical interconnections are again assumed, and some of the weak points of the other macro treatments are still inherent, because a tacit assumption of the micro behavior is implied. The most usual (i.e. the easiest) is to assume that the capillaries are long compared to the diameters, and that the radial concentration distribution is constant, and is only a function of the distance from the gas interface. The problem then reduces to one dimension and is more easily solvable. However, I feel that it can be shown that if these approximations apply (i.e., the capillary is very long) in a uniform capillary the meniscus region is effectively isolated by the high resistance of the capillary, and contributes little to the total current. The implications of Supplement I are that the only really effective pores are the short ones, and that the shape is far from cylindrical.

C. Current Project

At the time of origination of the project, the only information available on the behavior of the meniscus was that of the paper by Will. At the time, the wetted film hypothesis seemed an interesting approach, but question was raised about the effect of small pore sizes on the meniscus behavior. To investigate this effect the "slot electrode" system was constructed.

The first systematic study was of the transient response of the slot system to a potentiostatic step function. Unfortunately, measurements at a slot electrode are not quite as simple as originally proposed. The following points must be considered.

1. Mechanism of reaction of H_2

Contrary to popular belief, the anodic dissolution of H_2 on Pt is not a well studied and understood reaction. No potentiostatic studies of this reaction are in the literature that I have been able to find.

I have evidence (Supplement II) that the potentiostatic dissolution proceeds along at least two different paths although not simultaneously. I do not know what the two paths are, nor do I know what the criteria for the changeover is, but I suspect that it is due to either: (a) Coverage by $H_{2,ads}$, (b) coverage by H_{ads} or (c) surface concentration of H dissolved in the Pt.

2. Solubility of hydrogen in Pt

Even before the determination of the solubility of hydrogen in Pt by Gileadi and Fullenwider,* I had obtained fairly strong secondary proof of this solubility and showed that something leads (Supplement II) to a definite change in mechanism.

3. Non-equipotential nature of pore

In the study by potentiostat, of a slot electrode, it is not possible to say that the electrode has a constant potential on its surface. Indeed, as shown by DeLevie, and by Bonnemay, (and others) the simplest, linear plot electrode behaves as an RC transmission line, (so-called because the diff. eqns. involved were first worked out for the "Telegrapher's Equation"), which has characteristics very much like a "Warburg" impedance (Note: - while it is true that a "Warburg" impedance (-W-) cannot be represented for all frequencies by a simple R + C combination, it can be represented by an infinite array of infinitesimal ΔR's + ΔC's, and approximated to any degree of accuracy desired for any finite frequency spread by a "lumped constant" array of a finite number of components). One of the properties of these transmission lines is that for no finite time is the potential anywhere inside the line equal to that at the input, and, indeed, if the line is terminated by a resistive component, this holds even for infinite time. Fig. 18 shows how such an equivalent line could

---

*Private communication.

represent the slot electrode. dC is the equiv. capacitance per dL length, and dR the solution resistance. (C is about 1500μfd/cm and R ranges from 10 - 10KΩ/cm depending on slit width.) For this simple transmission line the voltages at points A, B, C, D, and E will look as shown in Fig. 19.

Note that even at A, the potential does not reach the $E_{applied}$ even with an ideal system for a finite time because of the solution resistance between Ref. electrode and Working electrode. The finer the slot, the longer time to reach a steady state (not $E_{applied}$).

4. Non-linearity problem

A potentiostatic study of even simple electrode systems (i.e. one and only one reaction with one and only one step) is not a simple study for anything larger than a few mv step because of the non-linearity of the reaction term. (Indeed, I have shown that even to ~50 mv where E^2 terms are incorporated, the curve looks like $E = k_1 \tanh k_2 t$ and if cube terms are added ($100 > E > 50$ mv) a curve in log tanh t results.)

For larger steps results are even worse.

5. Frequency response on equivalent circuit basis

For reactions in which two consecutive steps occur (which can be represented schematically as in Fig. 20 if one of the steps is pseudocapacitive for small perturbations) at least three time constants occur, namely a) $C_{DL} \times R_F$, b) $C_\phi R_F$ and c) $C_\phi R_s$, where R_F is the

equivalent reaction resistance of the fast step and R_s is the slow step, and C_ϕ is the pseudocapacitance. This can be represented diagramatically as below in Fig. 21 where the values C_{DL} = 16μfd, C_ϕ = 1600μfd, R_s = 1000Ω, R_F = 1Ω have been chosen arbitrarily. Also shown are two curves for C_ϕ = 160μfd and C_ϕ = 0. A further simplification of the equivalent circuit is shown drawn near the curve showing the predominant nature of the electrode system during each frequency band (or time interval). At very high frequencies the swamping effect of series cable, solution and/or film resistance, which are <u>inseparable</u> from the main circuit are shown. Note that for each order of magnitude change of C_ϕ or of added resistance for R_s the low frequency point drops one decade. Thus, response time is $>$ 10 sec for R_s = 1000Ω; $>$ 100 sec for R_s - $10^4\Omega$ etc.

6. <u>"Proper time" problem</u>

Coupling of the transmission line problem with the non-linear pseudocapacitance problem can create even longer response times, since there is a propagation delay (see Fig. 19) in the transmission line before a point in the slit even sees a change of potential to react to. Thus, different parts of the electrode reach the state of "interest to fuel cells" at very different times.

7. <u>Analysis of "transient" problems</u>

What are the probable reactions that occur? a) oxidation of adsorbed H on the surface, b) oxidation of adsorbed H_2 on the surface;

c) oxidation of dissolved H_2 in the electrolyte as it diffuses to the surface, and d) the oxidation of H_2 in the meniscus region. All but (d) should cease in the steady state, but this may take a very long time ($\delta \doteq \sqrt{\pi Dt}$ and forms a secondary pseudocapacitance).

In point of fact, forgetting any theoretical reasons, all four reactions above occur simultaneously, and at different times in different parts of the slot. Variation of the "shape" of the slot (i.e. length and width) not only changes the values of current at a specific time, but changes drastically the whole shape of the curve.

8. Some experimental observations

Attempts to obtain "steady state" require about 15 hours for stabilization of values. Measurements after "short times" (i.e. $>$10 sec) are drastically dependent on prior history. Results vary over almost an order of magnitude depending on whether the electrode was at high or low potentials and whether for a long or short time.

Probably the best method of measuring the meniscus currents is to allow the system to equilibrate, and make a series of small perturbations first in one direction and then in the other.

When these perturbations are made infinitismally small, of course, they degenerate into a slow scan of current vs. potential. When the currents are the same for a given potential whether ascending or descending then and only then can one be sure that the effects of prior history are rendered negligible.

D. Quasi Steady State

Fig. 12 shows some of the results obtained just on the meniscus illustrating the time variation effects on the current obtained. (It is impossible to arrange that only the meniscus is studied, since some portion of the electrode is always immersed, giving effects that add to the meniscus current. However, this system was measured with only 1 mm of free electrode below the intersection.) The electrode, initially at rest in the solution overnight is made anodic in small (50 - 100 mv) steps, and the current obtained after $\sim$10 minutes plotted (green x's). The current rises linearly until a potential of about 0.6 volts (at which point OH deposition begins) and then the surface passivates. Practically steady state currents are reached in about 1 minute at each point. As the potential is raised above 0.7 V the electrode apparently passivates, and the current drops off slightly with potential. On decrease of potential with the same size step, (green O's) much larger currents (electrode apparently becomes activated at higher potentials, see Supplement II) are produced which do not reach steady state even after 10 minutes which continuously and slowly decay. After the potential is reduced to zero and reversed (red X's) the current follows a similar curve but at slightly reduced currents (the current was dropping during the first run and presumably these lower currents are equivalent to these extrapolated time values. A slow "polarographic scan" immediately following (.0003 V/sec) from 0 - 400 V gives data plotted as black dots, practically superimposed on the red curve.

E. Calculations

A theoretical treatment of the "non-wetted" meniscus is given in Supplement III. These calculations call for an ohmic (i.e. linear I-V) behavior for this meniscus as observed in experiments on non-activated electrodes. Additional calculations should be done on a computer, including the effects of activation polarization, which is even more difficult to solve analytically.

Supplement I

The exact localization of the sites of raction in a porous electrode structure is an extremely complex problem. The structure of the simplest of porous electrodes for fuel cell use is at best only porrly understood from a microscopic point of view, and these simple structures are purposely made much more complex in actual fuel cell electrodes by any or all of the following construction practices: (1) graded porosity; (2) sandwich construction; (3) partial or total waterproofing; (4) catalyst deposition; (5) inert fillers or matrices. The pores themselves vary widely in shape and size, depending on whether they are made from (1) compressed powders; (2) sintered compacts; (3) "Raney-metal"-type surface treatments; or (4) chemically or electrochemically precipitated fillers or catalysts.

Once prepared, fuel cell electrodes can be operated in any of several fashiion; (1) electrode flooded; (2) electrode "dry"; (3) wet electrode, gas bubbled through pores; (4) wet electrode, gas statically balanced by bubble pressure.

Obviously, no single theoretical treatment can possibly cover all cases of fuel cell operation, and some reasonable estimate must be made of the types of behavior to be expected in each, and the relative importance of each mode.

I. Evaluation of Structures of Electrodes and Treatments

A. Powder Compacts

This type of structure probably applies to many carbon electrodes, at least in the raw state. They can be made by compacting a powder, consisting of particles of approximately spherical shape of fairly uniform diameter. The resulting pore structure can be envisioned by picturing the spaces between a random pile of round balls. The pores would then consist of a series of larger cavities, of fairly uniform size with cross sections shaped as in Fig. 22, connected together in all directions through narrower, but similarly shaped, passages, so as to look like a network of pointed beads on a 3-dimensional random lattice. Measurement of this type of structure with a Winslow (mercury intrusion) porosimeter would yield a characteristic pore spectrum as shown in Fig. 23. No mercury can enter the pores in region A until a critical pressure P_o is reached, corresponding to a mean-radius r_o according to the Washburn formula

$$P = \frac{2\gamma \cos \theta}{r}$$

where P is the pressure, γ the surface tension of Hg, θ is the contact angle, and r is the effective radius. At this point, the Hg gains access to the larger volume of voids between the particles and a large volume of pores (area B) of apparent radius r_o is measured. An appreciable pore volume is also measured (area C) at successively smaller pores as the Hg is squeezed into the smoothly tapering region between the granules. (In addition, with a brittle starting material, such as

carbon or ceramic, some of the particles would fracture, leaving thin flat crivices, whose volume would show up in section C.)

B. Sintered compacts

Porous electrodes made from "green" compacts are usually structurally too weak to be used successfully as electrodes, and some degree of sintering is usually employed. During the sintering process, sharp points, such as crystallite tips and edges, are generally rounded, dislocations annealed out, and the regions of contact between particles and fissures grow together, decreasing the area under the curve of Fig. primarily in the region "C" as shown in Fig. 24. The higher the temperature of sintering, the stronger the compact grows mechanically. However, even though the pore volume changes only a small per cent, the available free surface decreases markedly, since the area "C" has the largest surface to free volume ratio.

C. Thermal Activation

Some compacts (notably carbon) are made with resinous binders in the green state. When heated in a reducing atmosphere, these resins cake and volatalise leaving a fine pore structure behind and a cementing residue of graphite between the particles. This procedure will tend to give a structure similar to that shown in Fig. 24, with the addition of a region of pores in the very small radius area as shown in Fig. 25 region D. The volume in these pores, is only a small fraction of the total pore volume, but the surface to volume ratio is very high.

D. Catalyst Deposition

Many types of catalysts have been introduced into the pores of electrodes in many different manners. They can be summed up into three basic groupings.

(1) Impregnation of the pores with a dilute solution of a catalyst salt (e.g. $AgNO_3/H_2O$ $H_2PtCl_6/PtOH$, sugar/H_2O, etc.) removal of the solvent, and heating to decompose and/or sinter the catalyst in place. Since the catalyst is usually present in small amounts for economy's sake, appreciable decrease of pore volume does not take place, but a marked increase in the BET surface area usually results.

(2) Impregnation of the pores with a suspension of catalyst metal powder or insoluble catalyst compound of fine particle size, and sintering in situ into the electrodes. Unless the particle size is kept extremely small, this type of treatment generally deposits catalyst primarily on the outer surfaces because of a filtering action of the electrode pores. This process precludes the deposition of catalyst in the finest pores, but is compensated in part by the large surface area of the catalyst particles themselves.

(3) "Raney" type catalysts: If the metal from which the plate is fabricated contains an alloy, one component of which is readily soluble, and the other component is a catalytically active material as a separate phase, it is possible to dissolve out the one component, leaving a highly porous, active residue of catalyst. When an alloy like this is used as one component of a metal powder sinter, the macro-pore structure can be as shown in Fig. 24 but the "active" surface area can be drastically increased by etching after sintering.

E. Waterproofing

Two main types of waterproofing are used today for fuel cell electrodes.

(1) Paraffin

A dilute solution of paraffin in a suitable solvent, such as petroleum ether is soaked into the pores of an electrode, and the solvent is allowed to evaporate, leaving a fairly uniform, but powdery layer behind. This layer is usually melted into the electrode at 100 - 200°C. Since the paraffin wets the electrode, it will fill the small pores preferentially and round out the crevices between particles, producing an effect similar to severe sintering. If the electrode has been precatalyzed, the paraffin also serves to cover the catalyst with a thin film.

(2) Teflon

A dilute suspension of Teflon (or similar fluoroplastic) is soaked into the pores and the suspensoid is evaporated. The particles of Teflon, usually about 0.1 to 0.5 microns, do not penetrate the finest of the pores, but tend to remain in the larger cavities. Since the Teflon is hydrophobic, and has a contact angle greater than 90°, it repels the electrolyte, while the pore walls wet. The electrolyte then forms a film on the walls, allowing the fuel gas to penetrate. The very fine pores ($< 0.1\mu$) are filled with electrolyte in electrodes treated by this process.

II. Evaluation of Mode of Operation in Relation to Structure

Depending on the mode of operation, different areas of the porous electrode become of importance.

A. Electrode Flooded

This type of electrode is probably the poorest from the standpoint of practical fuel cells. Current is limited by the amount of relatively insoluble gas that can diffuse through the surface film to the electrode itself, and the voltage is limited at higher currents by the large IR drop through the pores of the electrode. This type of operation can sometimes be useful for a qualitative study of catalysts deposited on the surface of the electrode, since the pore structure itself is rendered relatively unimportant.

B. Electrode "Dry"

Truly waterproofed electrodes will have a contact angle greater than 90° and positive pressure on the electrolyte side is required to force liquid into the pores. The larger pores will fill first. In a real fuel cell, operated with vertical electrodes, the hydrostatic pressure at the bottom causes greater penetration and consequently greater electrode-electrolyte contact there. However, in a uniform pore size electrode, once the critical pressure for pore entry has been exceeded, only a small additional pressure is needed to force electrolyte all the way through and the electrode is then partially flooded.

Since the electrolyte is held largely in the larger pores, the smaller pores are left free for gas transport and the lower resistance large pores are used for current and reaction product transport. Since fuel transport in the gas phase is faster than diffusion of a slightly soluble gas in liquid, this type of electrode is very useful for mixed gas (i.e. air) consumption.

(2) Partially waterproofed electrodes, such as those treated with Teflon will behave in a similar fashion from the macroscopic (or penetration) point of view, but since the pore walls are not completely coated, they will wet, forming thin electrolyte films which cover most of the free surface. (Not all of this surface can be electrochemically active, as shown by Will[1]). The very fine pores, however, are probably completely filled with electrolyte.

C. Wet Electrodes

(1) Gas bubbled through electrode

This type of operation gives a behavior similar to that of B, except that the particles of Teflon are replaced by air bubbles. These bubbles will be of a relatively uniform size, controlled by the Washburn relation (p. 2) and the gas flow resistance. Within limits, once actual gas bubbling has occurred at the solution side, the maximum pressure is fixed and with it the minimum size of pore gas can enter. If the bubbling rate is excessive, misleading results can be obtained with a mixed gas, because a steady state concentration cannot be reached in the gas phase. This system is physically the easiest to control experimentally, but

presents difficulties in real batteries because of wasted fuel.

(2) Gas pressure balanced, no bubbles

This system is similar to (1) above, but the interface location is difficult to control, and results can be highly erratic.

III. Surface Utilization of Various Structures

While a number of authors[1-4] have formulated mathematical models for porous electrodes, it must be realized that no one of these is applicable to all types of electrode systems. A porous electrode at rest will become saturated with reactant, both in the solution, and any that may adsorb on or in the electrode wall.

Initially, when a load is placed on the cell, most of this is accessible immediately, and will yield relatively high currents, limited primarily by the IR drop in the system. Within relatively short times, this material is exhausted and the current becomes limited by the rate at which fresh fuel can diffuse to the active areas. (Of course, assuming lack of activation control.) The question of location and availability of these active areas is then of primary importance.

Will[1] has shown that in large pores, with the surface wetted by electrolyte, at most a region .1 to .3 mm long of the wet film adjacent to the bulk electrolyte can contribute to the available current because of the extremely high resistance of thin electrolyte films. This treatment will be most valid for well sintered electrodes, in which most micro fissures and intergranular spaces have been smoothed out, or have been filled with an inert material such as paraffin. We can also deduce that

in those systems where electrolyte is forced out of the pores with gas pressure only the outer few tenths of a millimeter are electrochemically active.

We can also observe that transient methods such as interrupters and step-functions must be interpreted with care, since the initial portions of transients are not representative of steady state conditions.

The availability of small pores and microfissures (5 microns diameter) for electrode reaction is strongly dependent on the rest of the structure. In order to be useable, the fissure must have ready access to the fuel and to a low resistance electrolyte path. A drop of electrolyte between two granules of an electrode may be saturated with gas, but if there is no immediate connection to a low resistance electrolyte pore, it is unavailable electrically. It can be shown that if the distance in a micropore from the gas interface to the electrolyte in a macropore is much greater than an order of magnitude longer than the width, its contribution is rendered negligible by the large IR drop. Therefore, long tortuous micropores, if filled with electrolyte, are valueless from the point of view of surface utilization. If these micropores and hydrophobic, however, and electrolyte is only slightly forced into them from a large pore, and the fuel gas has access to the other end, they can contribute significantly to the overall current yield.

References

1. F. G. Will, J. Elec. Soc., 110, 152 (1963).
2. J. S. Newman and C. W. Tobias, J. Elec. Soc., 109, 1183 (1962).
3. J. Euler and W. Nonnermacher, Elect. Acta, 2, 268 (1960).
4. A. Winsel, Zeitschrift fur Elektrochemie 66, 287 (1962).

Supplement II

A study of the transient development of triangular sweep data at various sweep rates shows an interesting short (1 - 10 second) time variation in the shape of the curve (which corresponds in this case to a "Breiter-type" curve) in the deposition of H_2 from anodic potentials, which would not have been observed had not a storage scope been used. Two precursor peaks to hydrogen deposition were observed, and on successive sweeps, one disappeared and was replaced by a third at more anodic potentials. At casual observation, this appeared to be a shift in the deposition potential of the first peak, (as I think Breiter or Will has mentioned) but closer examination showed clearly that one peak was being replaced by another! Without going into an elaborate discussion, I theorize (with some prior thought) that this is evidence of a change in the surface due to absorption of H into the surface, changing the character thereof and changing the reaction path. This change of reaction path would not show up in steady state where this step is a fast one in pseudoequilibrium, but is clearly resolved by more transient methods. The triangular sweep displays it quite clearly although it also shows up in potentiostatic step function data, but not as clearly as in the sweep. This mechanism change may be a principle cause of time variation in study of the H_2 dissolution in a meniscus.

Fig. 26 shows the typical curve (expanded for resolution and showing only a small portion of one branch of the loop) obtained. H_2 evolution is to the left in this curve, but to the right in the other two sweeps. (Fig. 27 and 28). The electrode stood at $\sim$500 mv anodic for

several minutes. This potential is sufficient to desorb and oxidize any H or H_2 on or in the surface, but not enough to oxidize the surface or deposit OH. From this potential the sweep drives to about + 20 mv, reverses to about + 500 and cycles back (i.e. all H or H_2 deposited should redissolve during the upper part of the curve, and impurities should not have too much chance to adsorb, and there should be no oxidation and reduction of Pt to change the surface). The upper curve is the first sweep, and successive sweeps are shown below it with the final value slightly brighter. Note that the middle peak disappears and is replaced by a more anodic one at the right. Fig. 27 shows the first four sweeps only, and the 4th curve shows fairly clearly the presence of two peaks simultaneously, demonstrating a switchover of mechanism (rather than a change of position of only one peak).

Fig. 28 is a series of curves where the sweep rate is varied in the critical region by a factor of ten. The lowest sweep is the slowest, about 100 mv/sec, and the upper one is 1 v/sec. Note that in the slow sweep, the stationary-state mechanism has time to develop, while at 3 - 400 mv/sec, both mechanisms are clearly distinguishable, and at 1v/sec only the other mechanism is resolved.

Fig. 29 shows the time effect with potentiostatic steps of about 500 mv. Here the electrode was held at + 500 for several minutes, brought to H_2 evolution for about 0.5 sec, and immediately made anodic again. The upper curve shows this first step. After this step, the electrode was held at H_2 potential for successively longer times, and the curves got lower. (In the first curve, the initial flat portion is

potentiostatic saturation, i.e. the amplifier could not supply sufficient current, over 300 ma in this case.) Note the inflection in the first curve, on the "bare" electrode. This peak probably corresponds to one of the peaks in the sweep curves, and the initial portion of the curve to the other. After H_2 treatment, the initial, faster portion disappears, and only the other one remains.

(One would expect the currents to <u>increase</u> with longer times of H_2 evolution, simply because of increased amounts of H_2 which could be evolved and subsequently reduced.)

Fig. 30 shows another series of curves similar to Fig. 4. Although the inflections is not as clear, a definite change in shape is observed between the first two and second two.

These potentiostatic inflections are not too obvious by themselves, but are pointed out clearly by comparison with sweep data, which in effect "differentiates" the step function data. A shift in the <u>position</u> of the peak in the sweep could have been due to a change in some activity of some species, but a <u>replacement</u> shows fairly clearly a change in mechanism for the hydrogen deposition. I hypothesize that this change is due to a change of the structure of the surface caused probably by a formation of a "Pt-H alloy" in the surface layers.

Supplement III

Observation of the actual meniscus on the electrode shows that in the region of the intersection the meniscus has a shape similar to Figure 31. If, instead of a contact angle of zero, as postulated in the 'thin film theory', we assume a linear slope of 45°, the following equations can be established:

$$i = - dI/dx,1 \tag{1}$$

where i is the local current density, and I_x is the total current generated from zero to x. In any thin slice 'dx' of solution

$$dE = - I_x dR = - I_x \rho\, dx/x \tag{2}$$

where ρ is resistivity and x is the distance from the meniscus edge to the slice dx. (Note: This equation is not strictly true, but is a sufficiently accurate approximation for this calculation.) Differentiating (2)

$$\frac{x^2 d^2E}{dx^2} = - x\rho \frac{dI}{dx} + I\rho \tag{3}$$

and substituting equations (1) and (2) we obtain

$$\frac{x^2 d^2E}{dx^2} + \frac{xdE}{dx} = x\rho i \tag{4}$$

but from Nernst's equation and Fick's first law

$$i = k \frac{\sqrt{2}}{x} (1 - e^{-z\phi E}) \tag{5}$$

$$k = zc_o FD \tag{5a}$$

$$\phi = F/RT \tag{5b}$$

where c_o is the equilibrium concentration of H_2 in the solution. The

term $\sqrt{2}/x$ is $1/\delta$ where δ is the diffusion path length from the point x to the gas-liquid interface.

Substituting (5) into (4) we obtain

$$\frac{x^2 d^2E}{dx^2} + \frac{xdE}{dx} = \sqrt{2}\, k\rho(1 - e^{-2\phi E}) \qquad (6)$$

Solving (6) by Euler's method; let $x = e^z$ and $dE/dz = x(dE/dx)$ we obtain:

$$\frac{d^2E}{dz^2} = \sqrt{2}\, k\rho(1 - e^{-2\phi E}) \qquad (7)$$

and integrating once:

$$dE/dz = \left[2\sqrt{2}k\rho\left(E + \frac{1}{2\phi}\, e^{-2\phi E} + C_1\right)\right]^{1/2} = xdE/dx = -I\rho \qquad (8)$$

At $x = 0$, where $\delta = 0$, the concentration of H_2 must be the equilibrium bulk value (assuming no kinetic dissolution of H_2 limitations, and no activation control). Therefore, $E_{x=0} = 0$ and $I_o = 0$. Therefore,

$$C_1 = -1/2\phi \qquad (9)$$

and

$$dE/dz = \left\{2\sqrt{2}\, k\rho\left[E + \frac{1}{2\phi}\,(e^{-2\phi E} - 1)\right]\right\}^{1/2} = -I\rho \qquad (10)$$

An analytic integration of this expression is not possible but we may substitute the exponential term by the approximate expression

$$1 - 2\phi E \doteq b(2\phi E)^2 \qquad (11)$$

where $b = .3925$, which is with 6% up to $2\phi E = 1$ or $E \cong 50$ mv. (Note: It is shown later that the region of $E > 50$ mv does not materially contribute to the total effect.) Equation (10) then becomes

$$dE/dz = (4\sqrt{2}\, k\rho\phi b)^{1/2}\, E \qquad (12)$$

Solving:

$$\ln E = (4\sqrt{2}\, k\rho\phi b)^{1/2}\, z + c \qquad (13)$$

Substituting for $z = \ln x$ and taking the antilog of both sides

$$E = cx^{(4\sqrt{2}k\rho\phi b)^{1/2}} \qquad (14)$$

at some $x = \ell$, let $E = E_\ell$. Then

$$c = E_\ell\, \ell^{-(4\sqrt{2}\, k\rho\phi b)^{1/2}}$$

and

$$E_x = E_\ell\, (x/\ell)^{(4\sqrt{2}\, k\rho\phi b)^{1/2}}$$

Using approximation (11) and equation (5) and (15)

$$i = \frac{\sqrt{2}k}{x}\left[2\phi E_\ell \left(\frac{x}{\ell}\right)^{S^{1/2}} - b(2\phi E_\ell)^2 \left(\frac{x}{\ell}\right)^{S} \right] \qquad (16)$$

where $S = (4\sqrt{2}\, k\rho\phi b)$ and using euqations (10), (11) and (15)

$$I_x = -\frac{S^{1/2}}{\rho} E_x = -\frac{S^{1/2}}{\rho} E_\ell \left(\frac{x}{\ell}\right)^{S^{1/2}}$$

at $x = \ell$, $I_x = -\frac{S^{1/2}}{\rho} E_\ell$.

Choosing a value of $E_\ell = 1/2\phi = .051$ volts, where approximation (11) is still valid,

$$I_\ell = .0139 \text{ ma/cm}$$

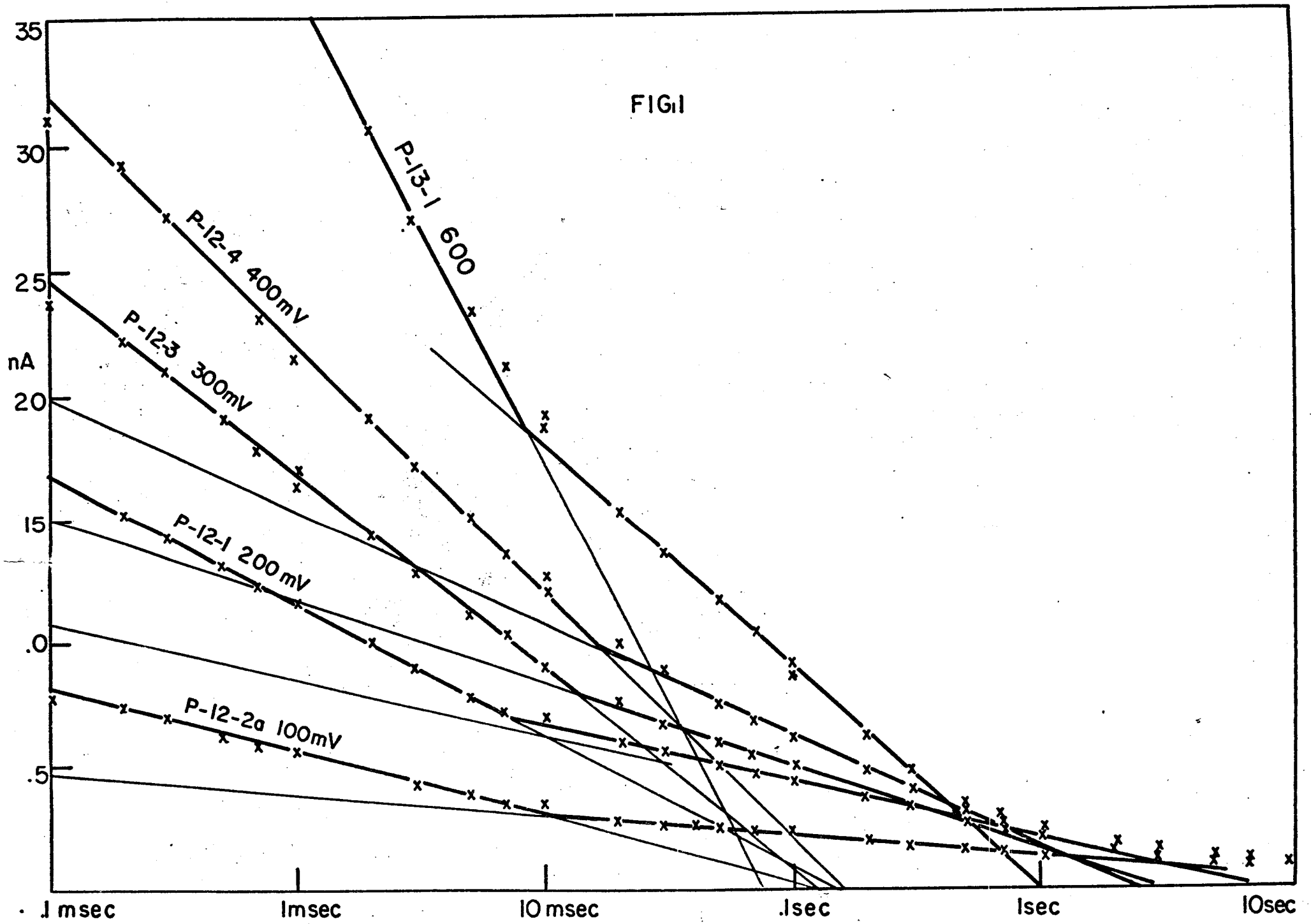
FIG1
35
30
25
nA
20
15
.0
.5
P-13-1 600
P-12-4 400mV
P-12-3 300mV
P-12-1 200mV
P-12-2a 100mV
.1msec
1msec
10msec
.1sec
1sec
10sec

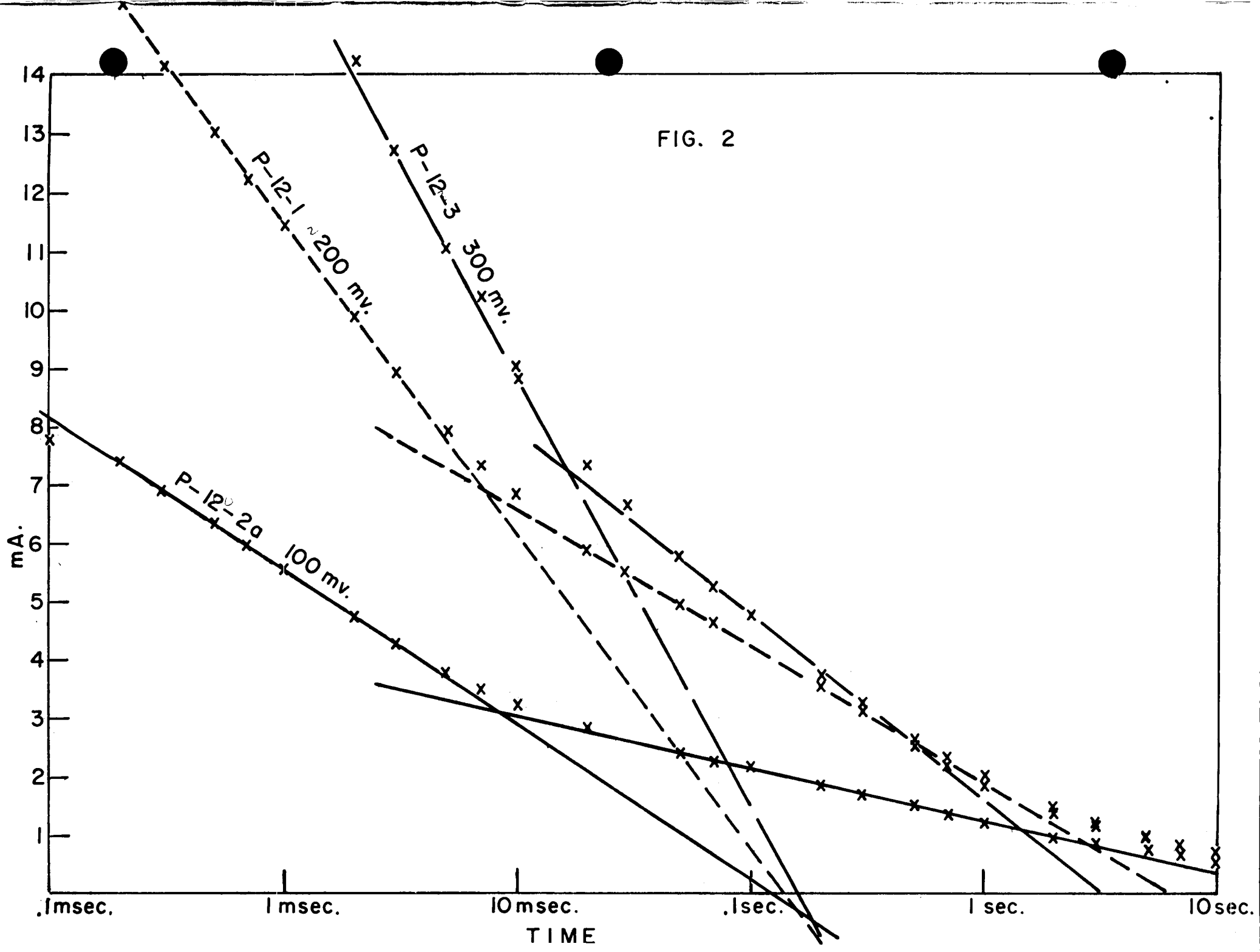
FIG. 2
P-12-1 200 mv.
P-12-3 300 mv.
P-12-2a 100 mv.
mA.
14
13
12
11
10
9
8
7
6
5
4
3
2
1
.1msec.
1 msec.
10 msec.
.1sec.
1 sec.
10 sec.
TIME

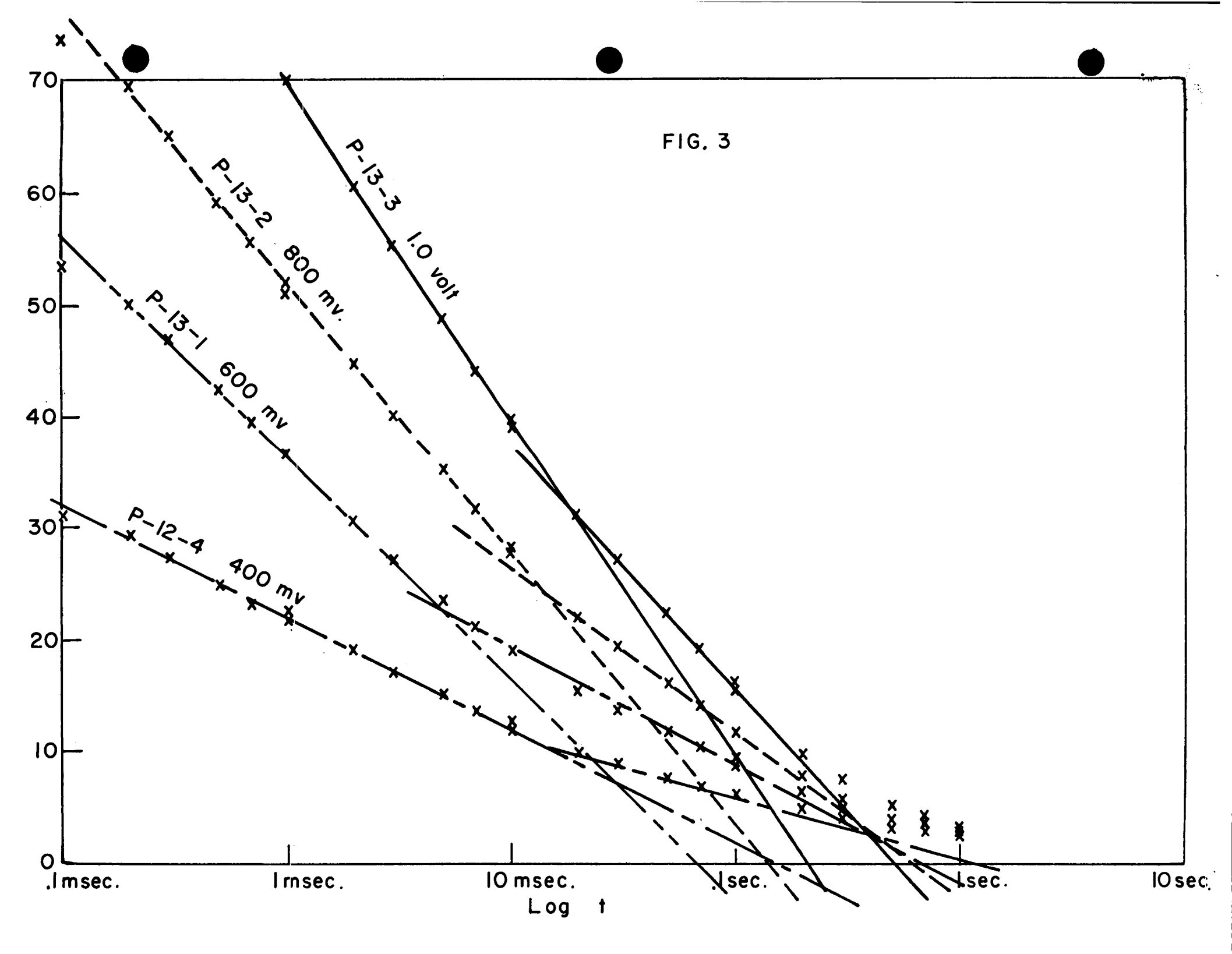
FIG. 3
P-13-3 1.0 volt
P-13-2 800 mv.
P-13-1 600 mv
P-12-4 400 mv
70
60
50
40
30
20
10
0
.1msec.
1msec.
10 msec.
1sec.
1sec.
10sec.
Log t

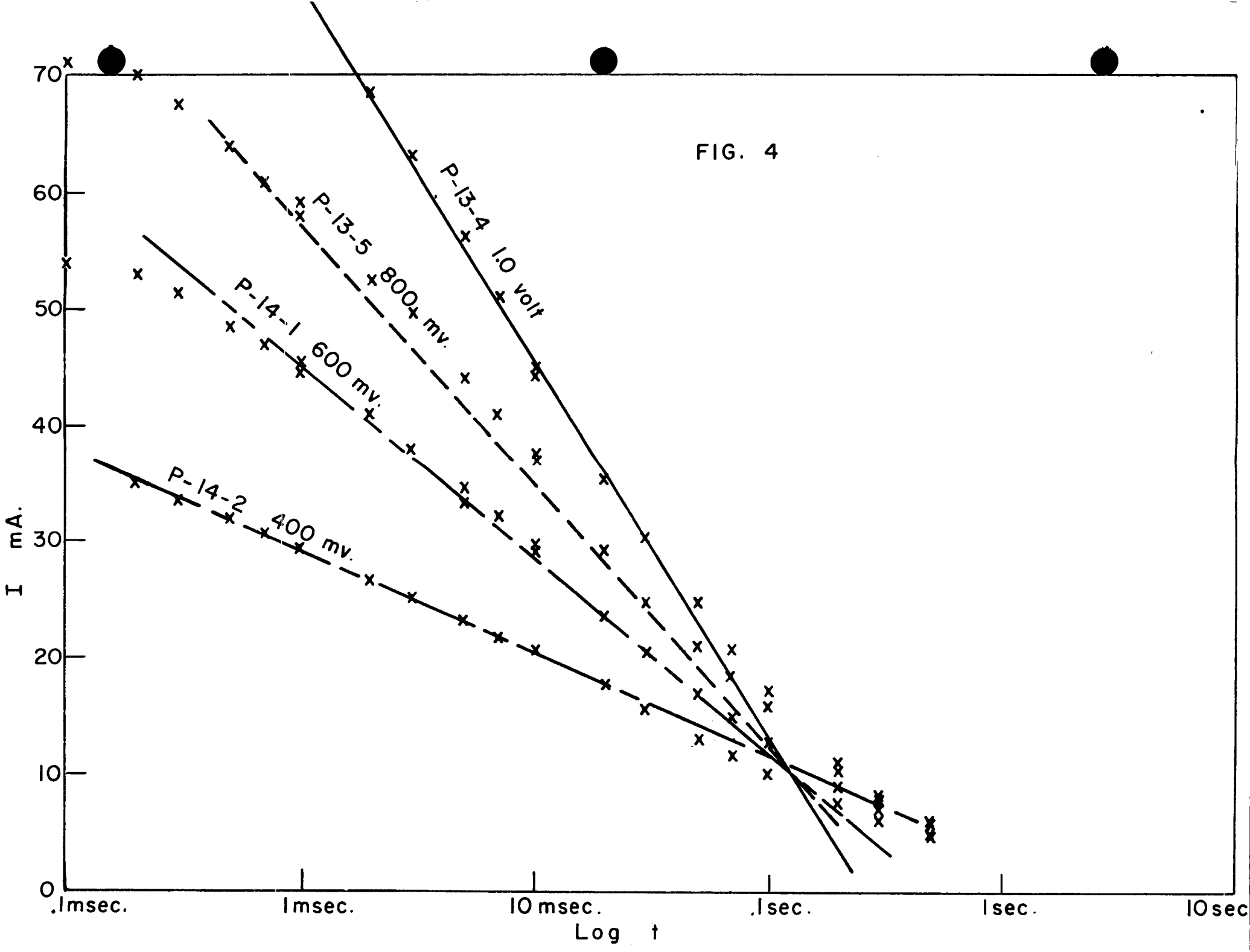
FIG. 4
P-13-4 1.0 volt
P-13-5 800 mv.
P-14-1 600 mv.
P-14-2 400 mv.
I mA.
70
60
50
40
30
20
10
0
.1msec.
1msec.
10 msec.
.1sec.
1sec.
10sec
Log t

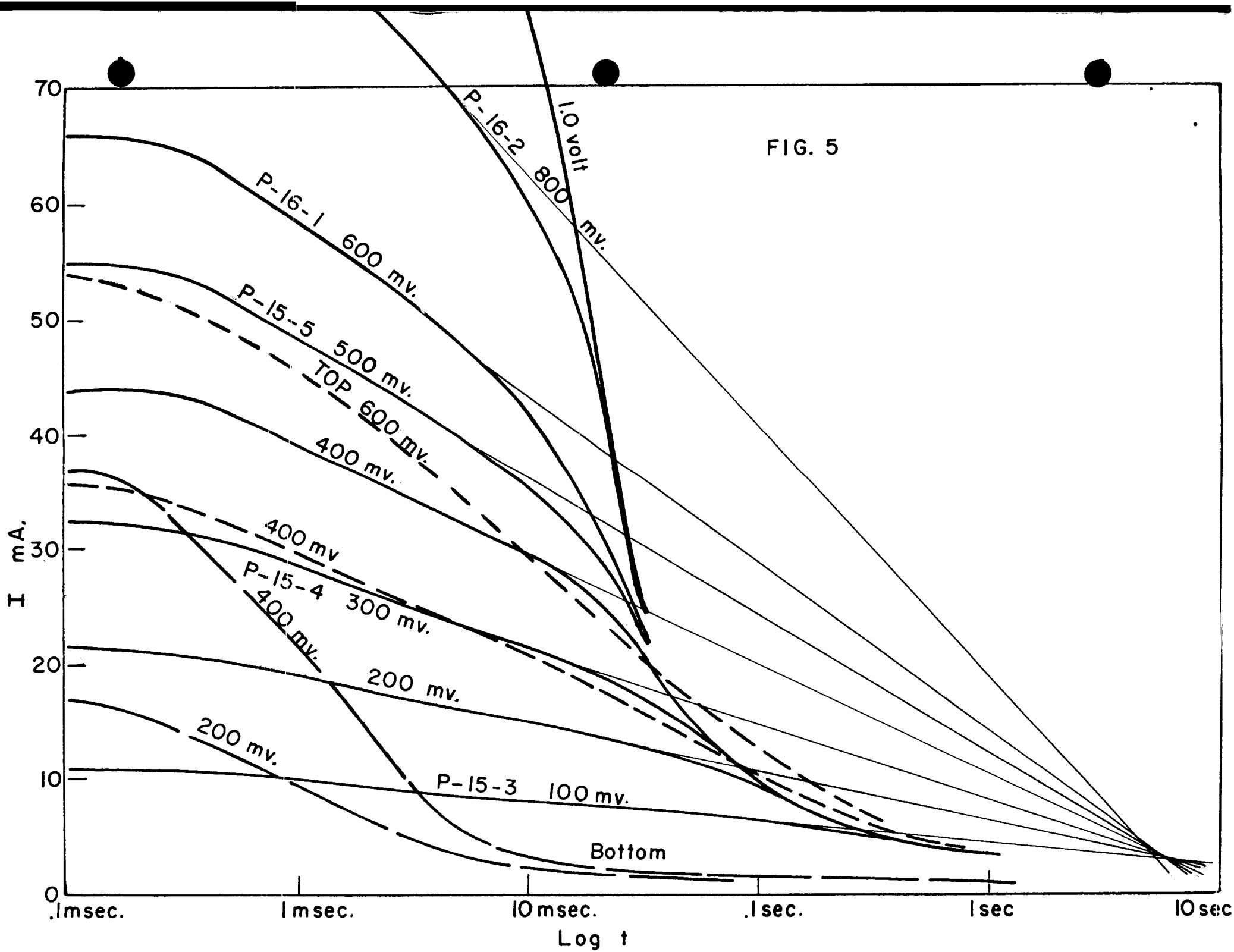
FIG. 5
P-16-2 800 mv.
1.0 volt
P-16-1 600 mv.
P-15-5 500 mv.
TOP 600 mv.
400 mv.
400 mv
P-15-4 300 mv.
400 mv.
200 mv.
200 mv.
P-15-3 100 mv.
Bottom
I mA.
70
60
50
40
30
20
10
0
.1msec.
1msec.
10msec.
.1sec.
1sec
10sec.
Log t

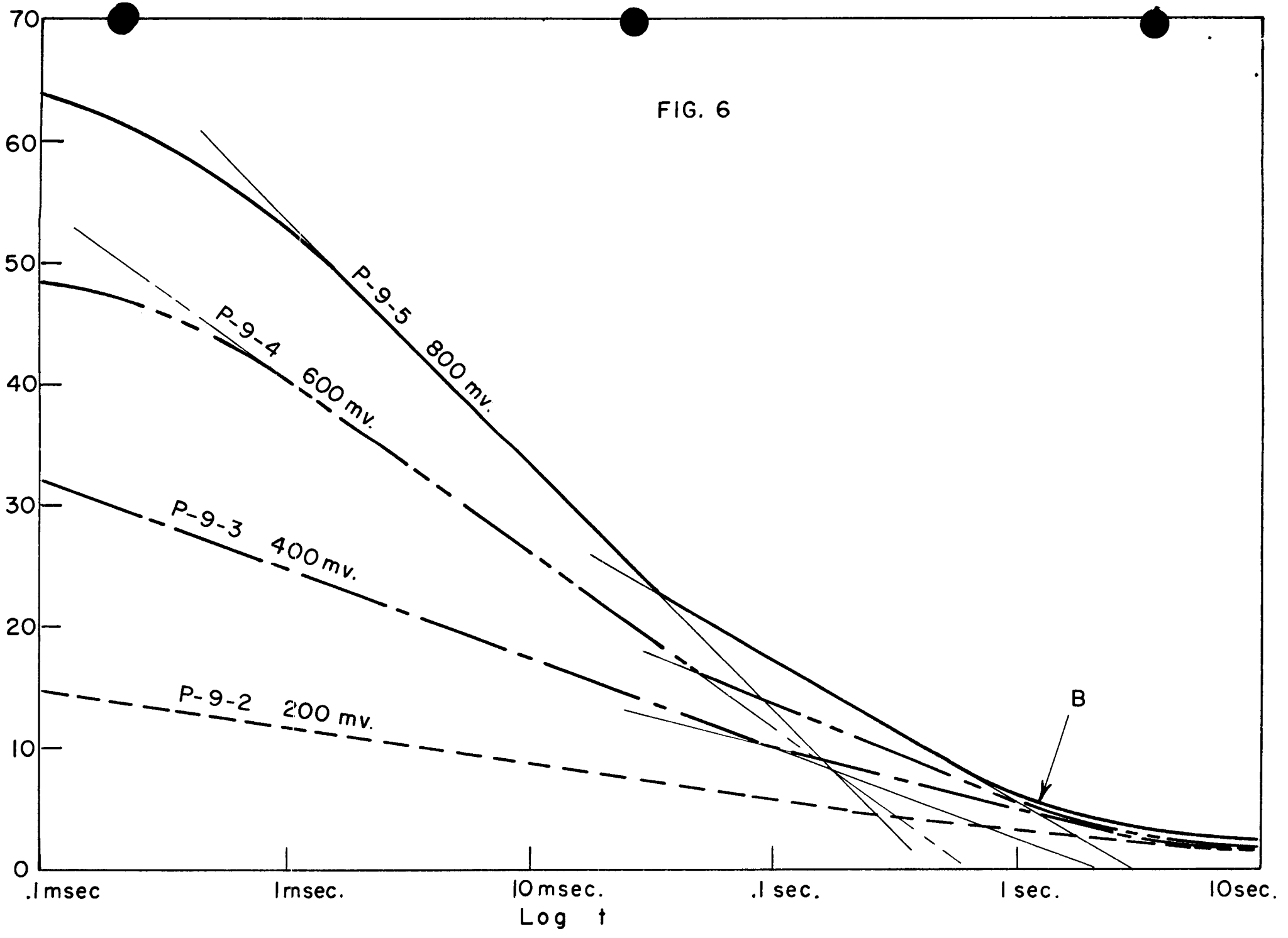
70
60
50
40
30
20
10
0
P-9-5 800 mv.
P-9-4 600 mv.
P-9-3 400 mv.
P-9-2 200 mv.
B
.1 msec
1 msec.
10 msec.
.1 sec.
1 sec.
10 sec.
Log t

FIG. 6

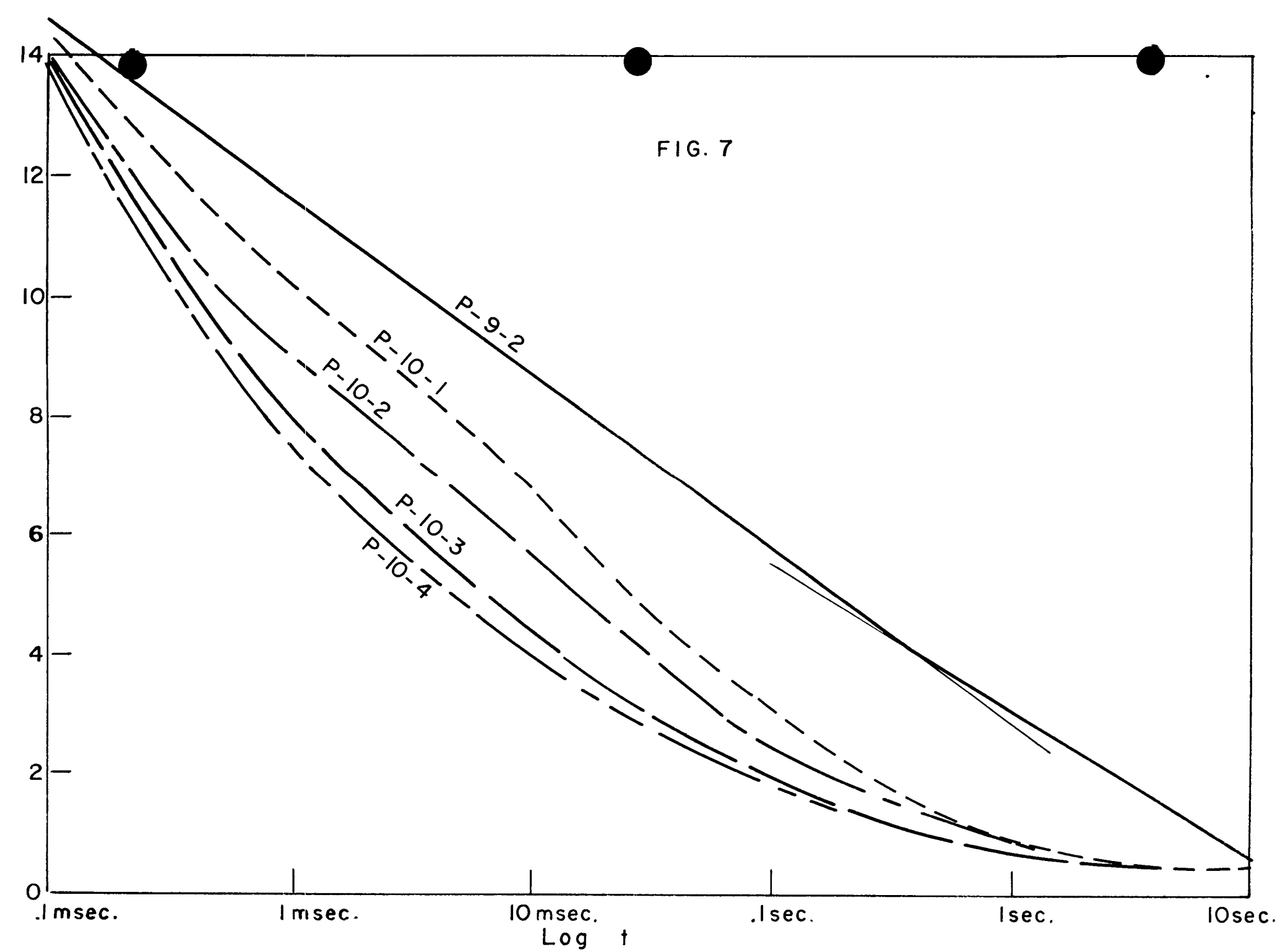
14
12
10
8
6
4
2
0
P-9-2
P-10-1
P-10-2
P-10-3
P-10-4
.1 msec.
1 msec.
10 msec.
.1 sec.
1 sec.
10 sec.
Log t

FIG. 7

FIG. 8

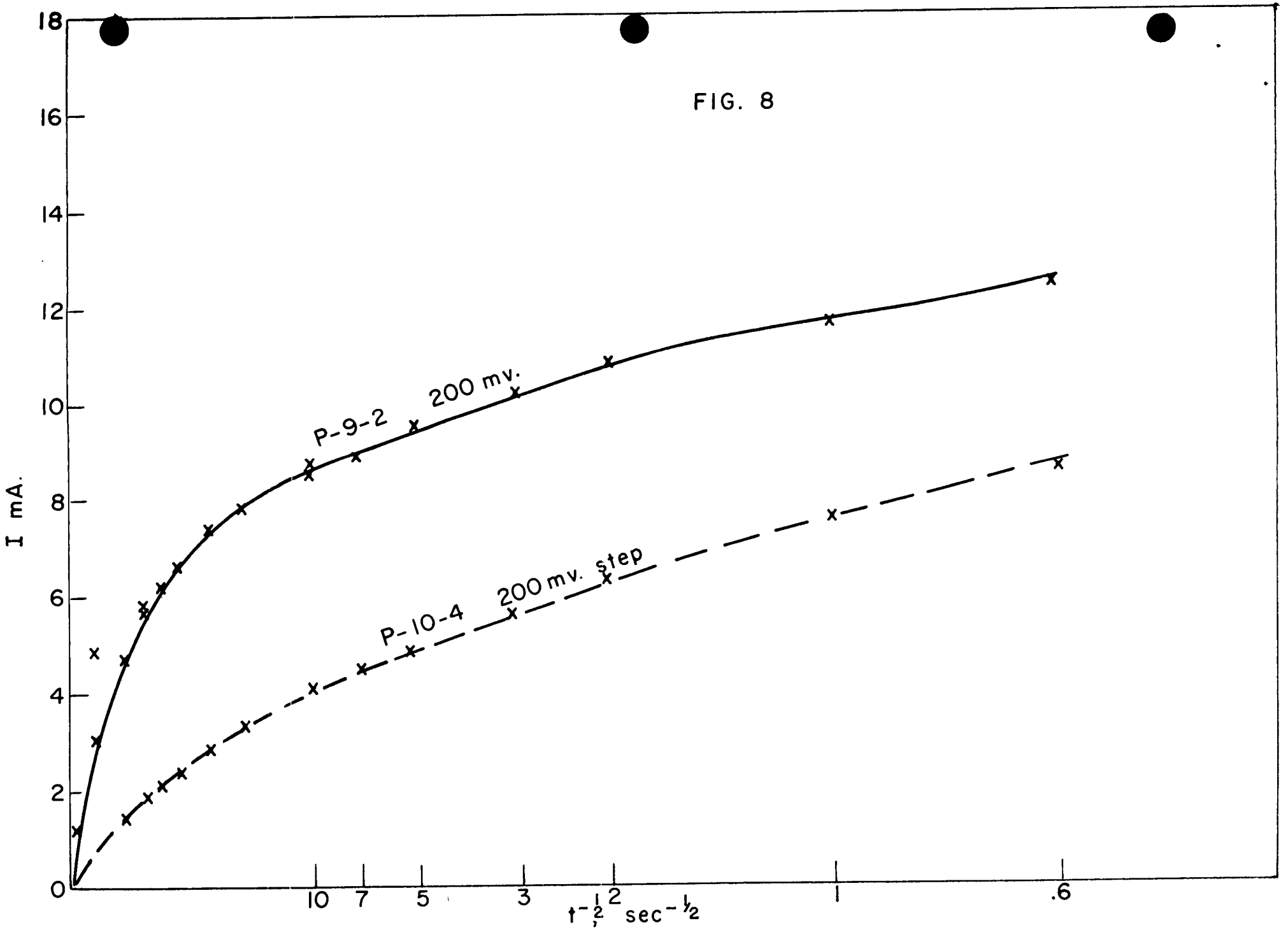
18
16
14
12
10
8
6
4
2
0
I mA.
P-9-2
200 mv.
P-10-4
200 mv. step
10
7
5
3
2
1
.6
$t^{-\frac{1}{2}}$ sec$^{-\frac{1}{2}}$

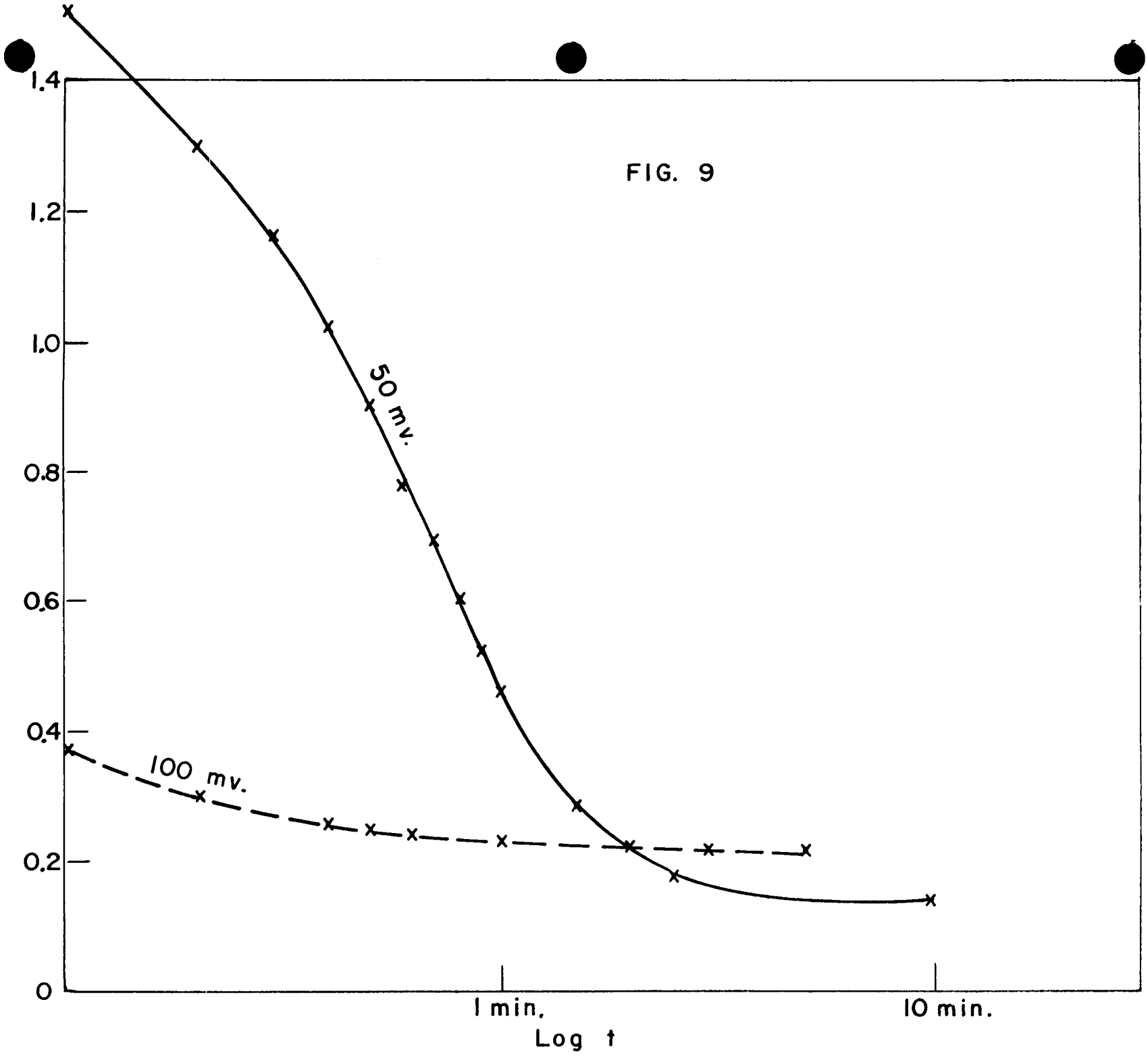

FIG. 9

FIG. 10

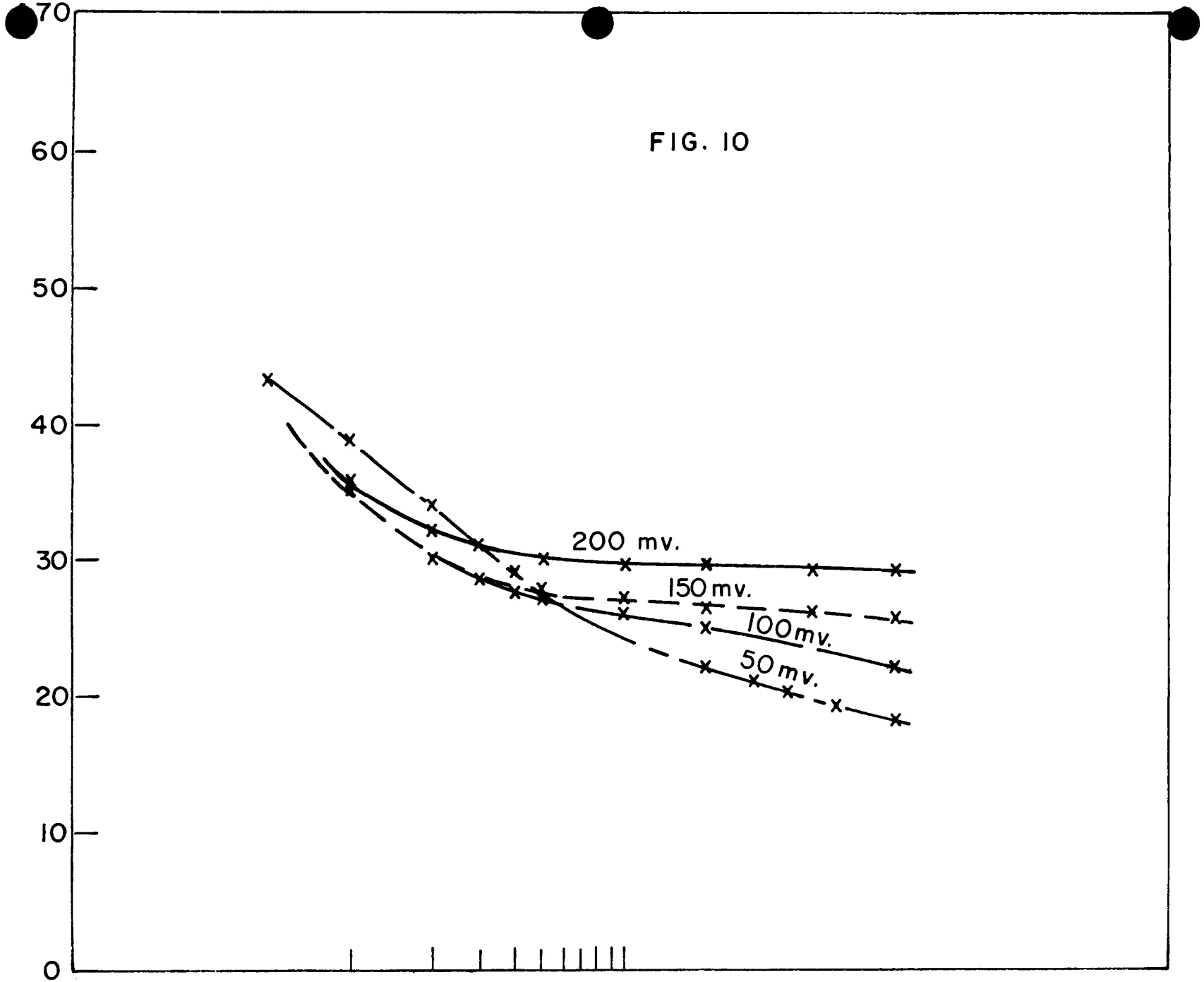

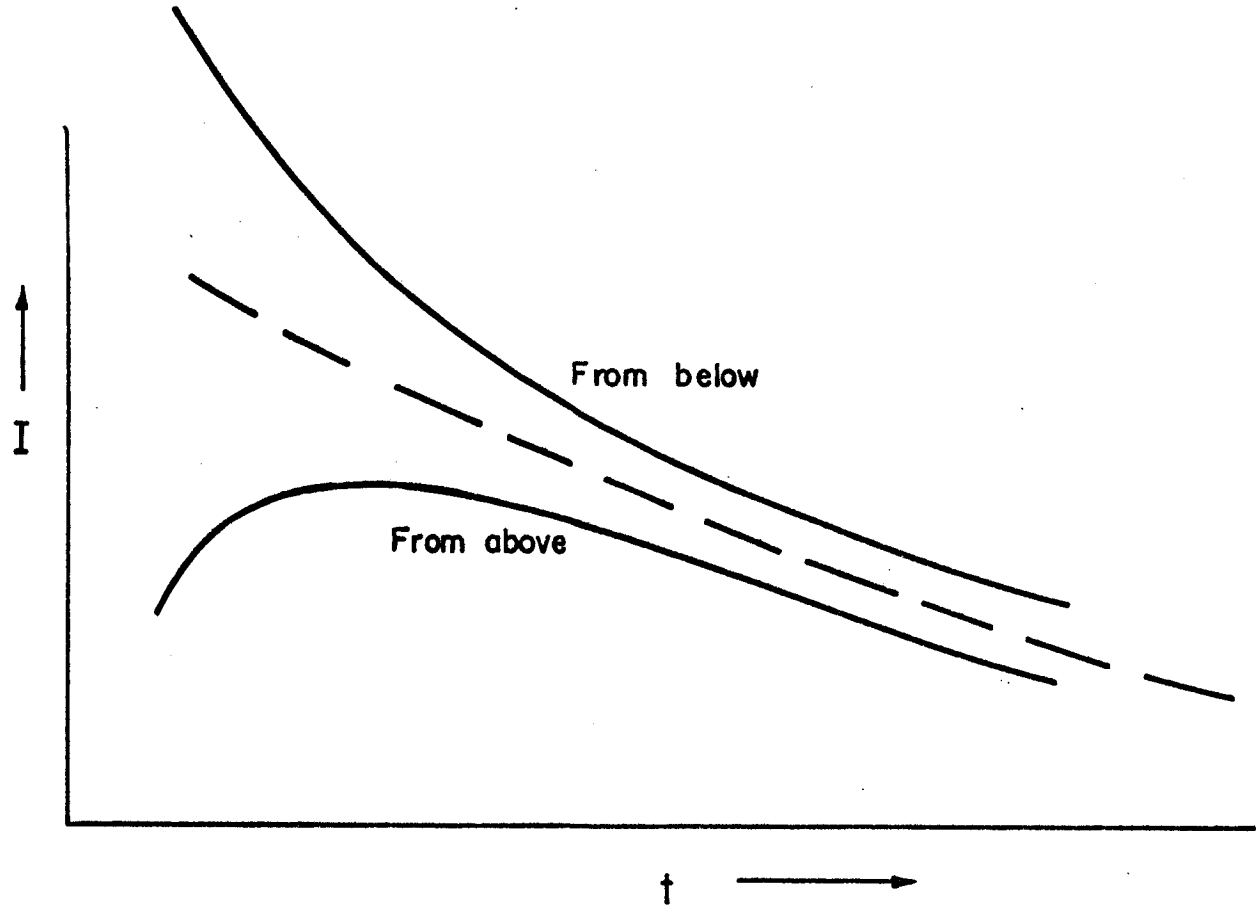

Fig IIa

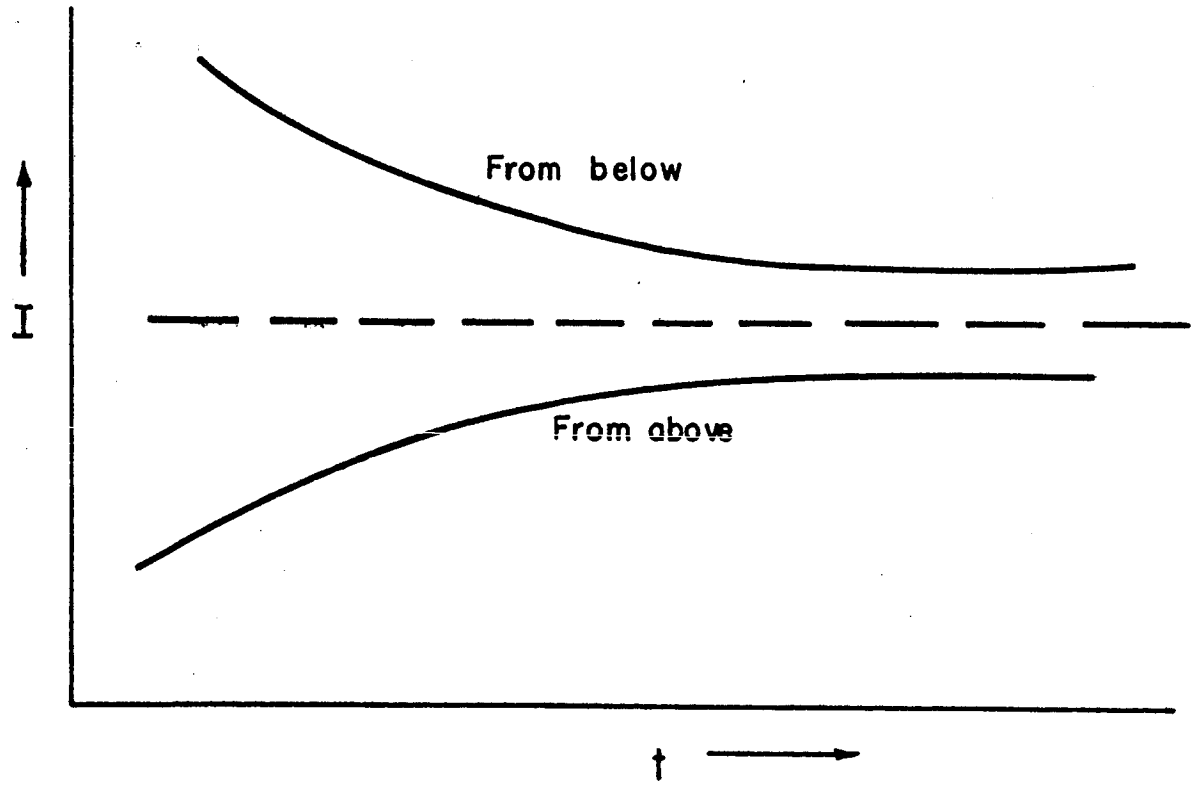

Fig. II b

FIG. 12

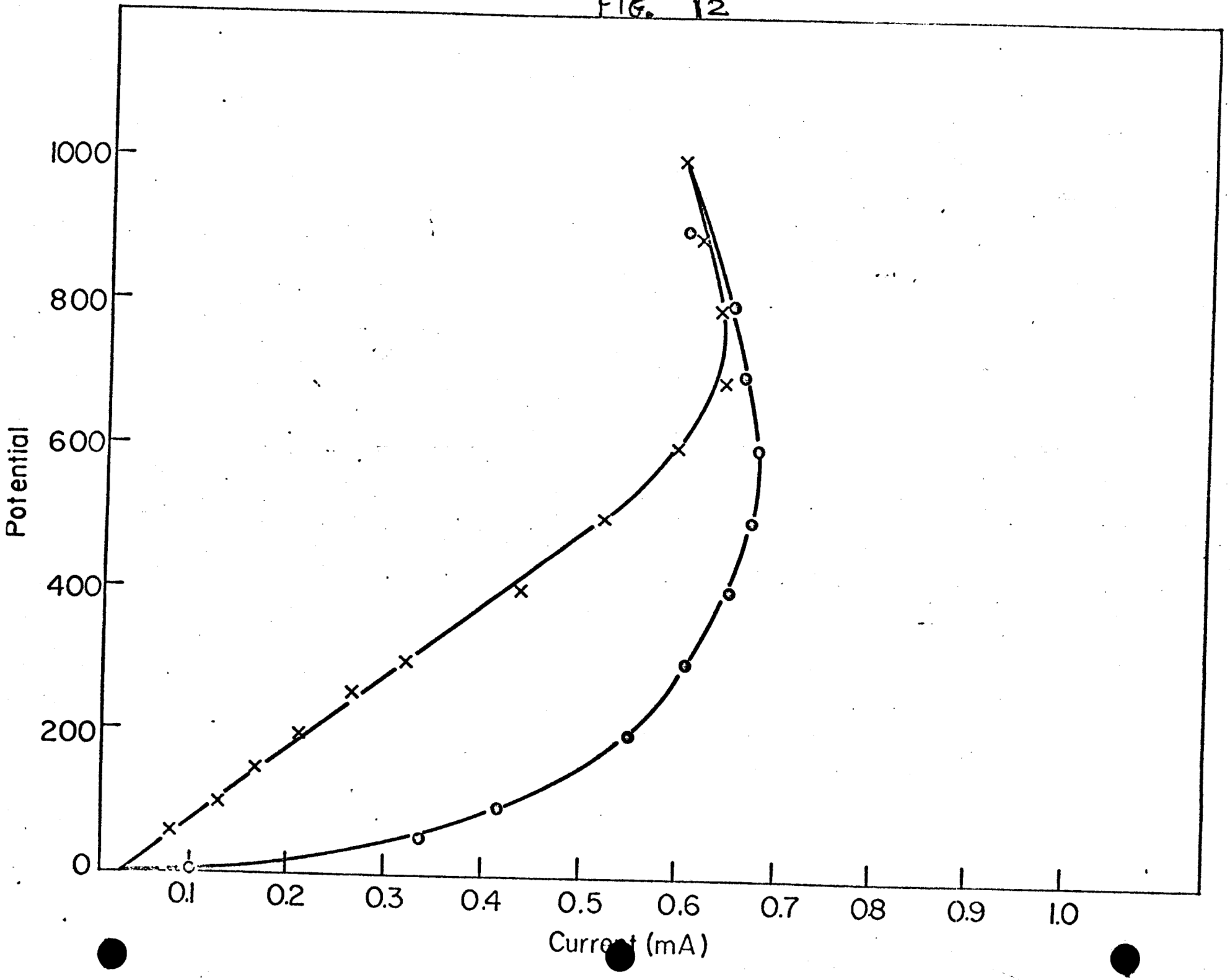
1000
800
600
400
200
0
Potential
0.1
0.2
0.3
0.4
0.5
0.6
0.7
0.8
0.9
1.0
Current (mA)

FIG. 13

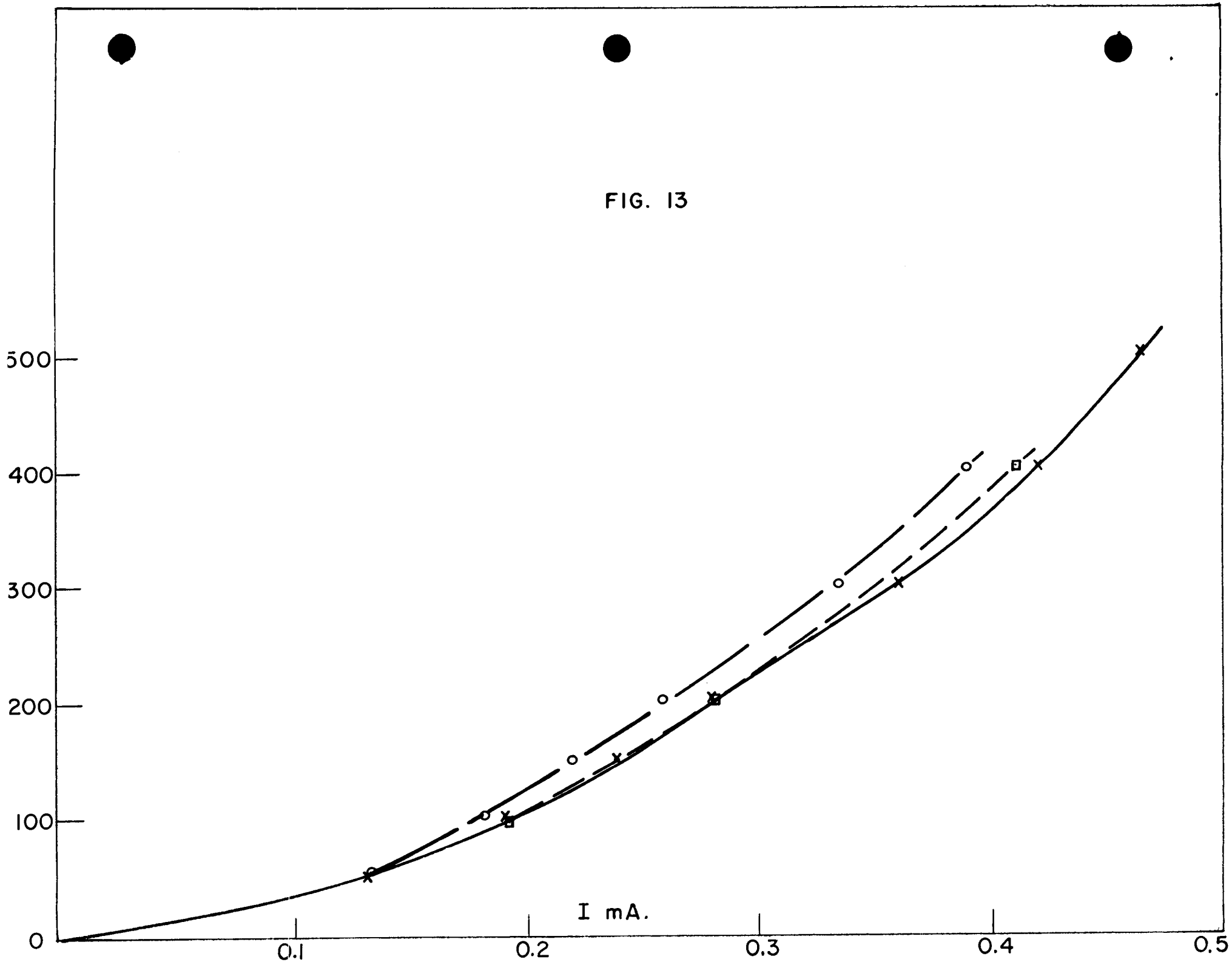

FIG. 14

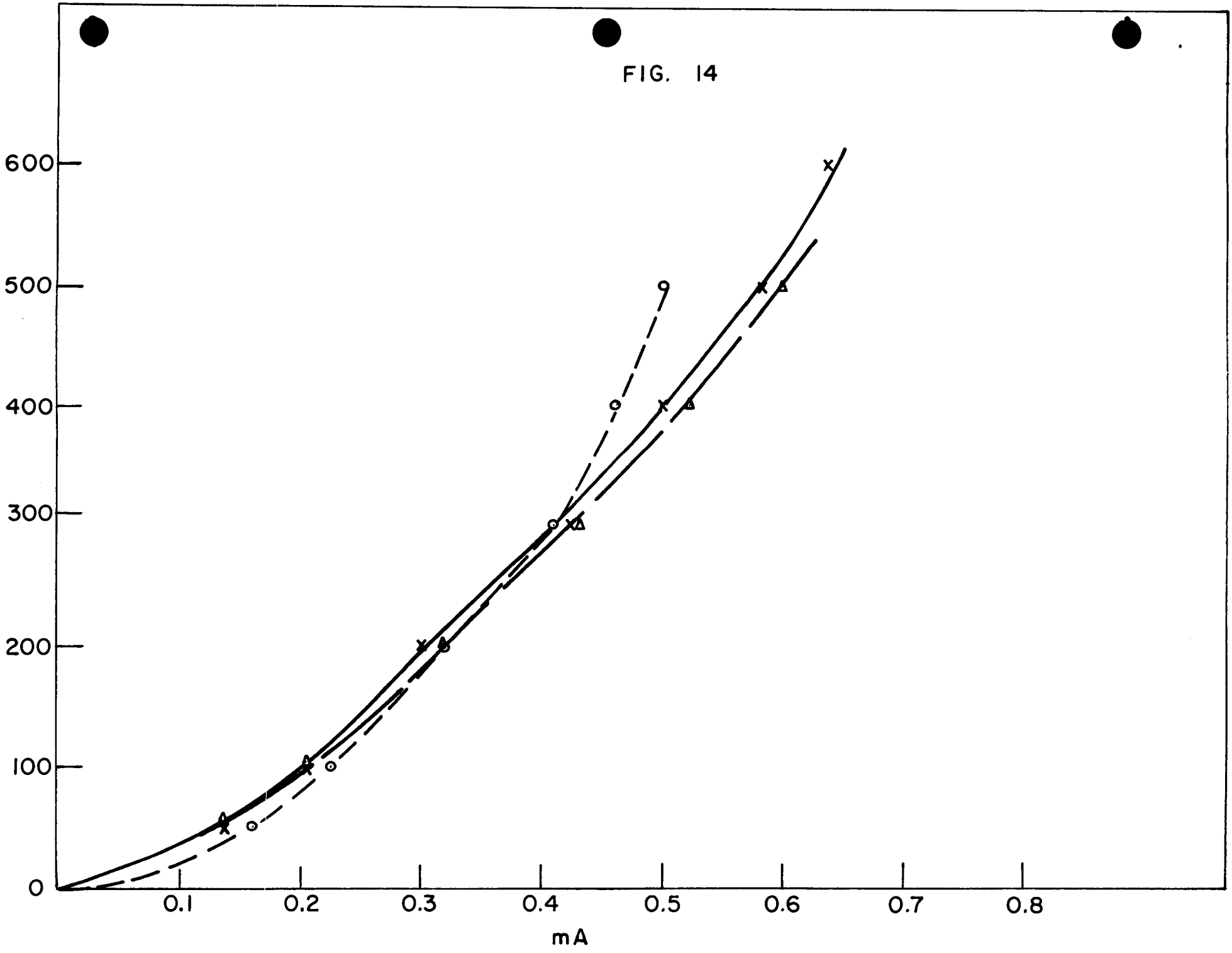

FIG. 15a

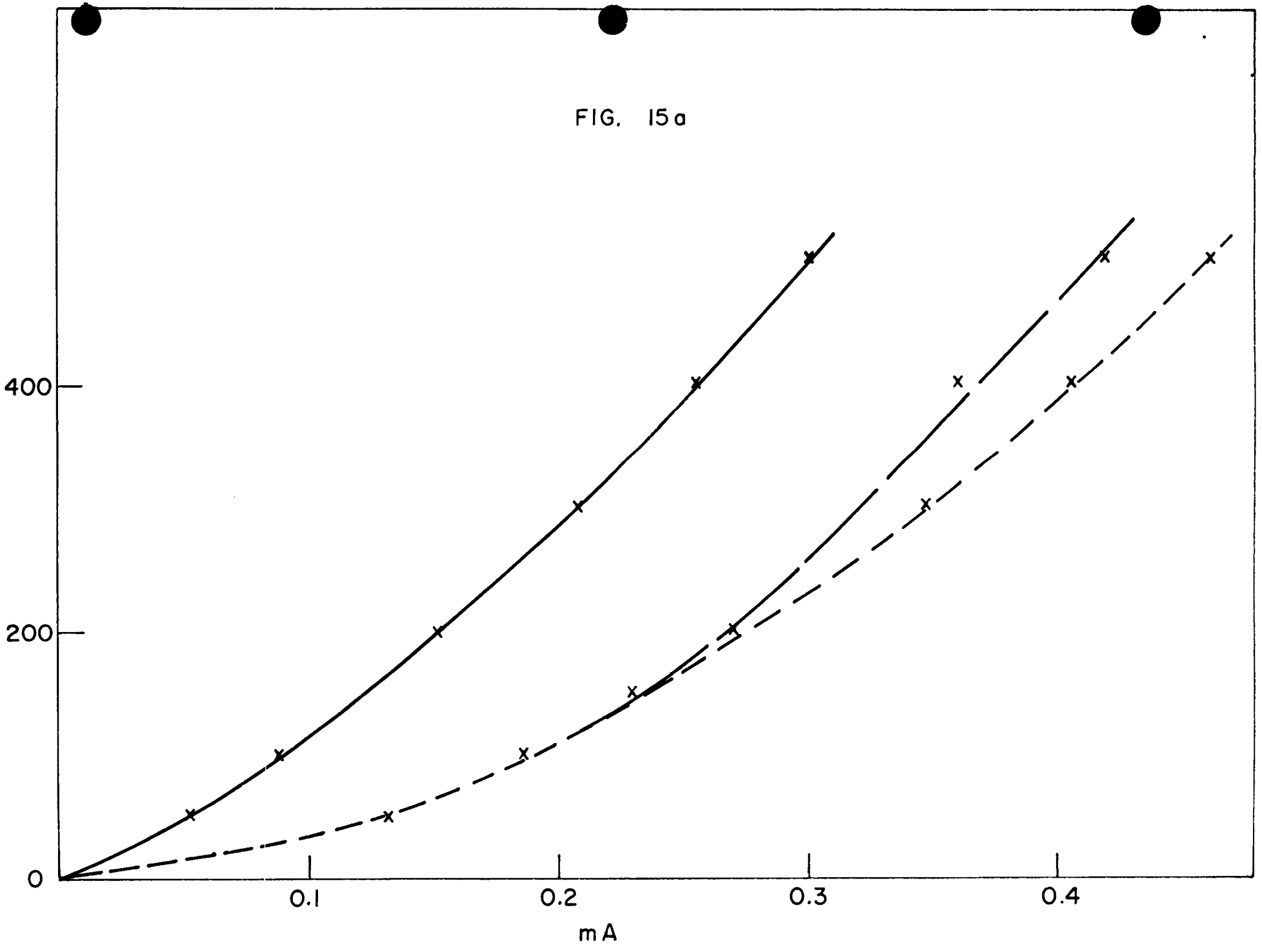

FIG. 15 b

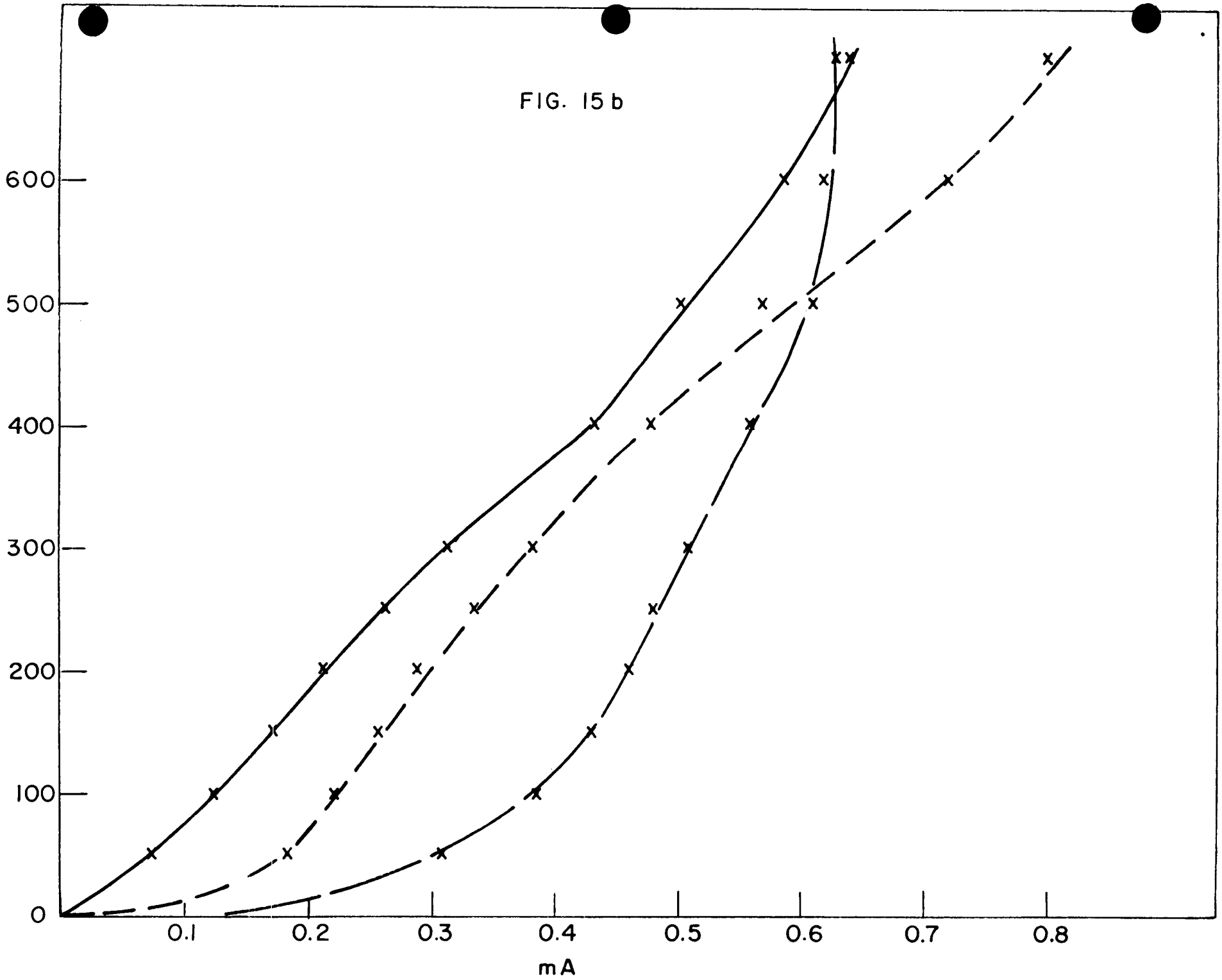

FIG. 15 c

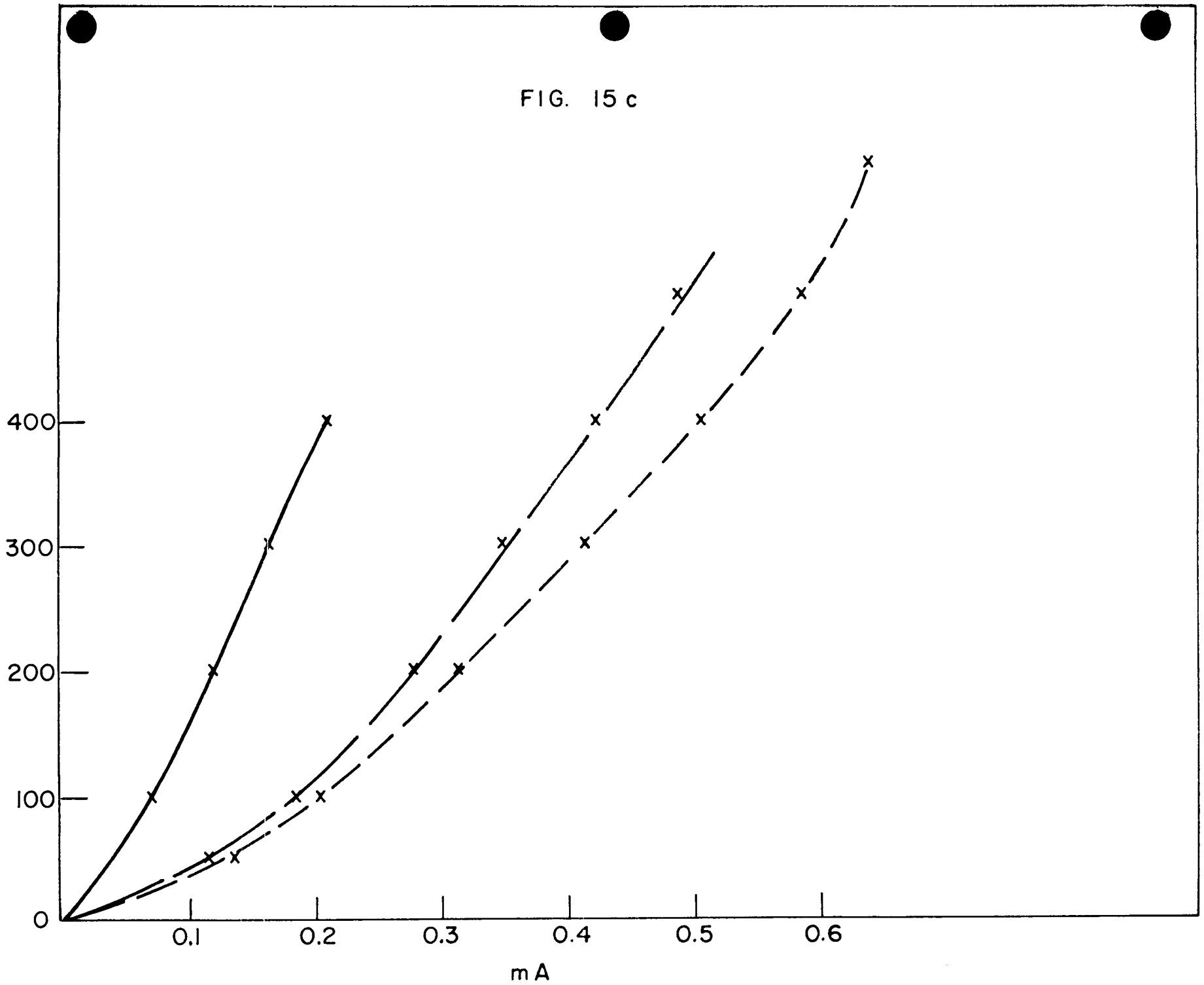

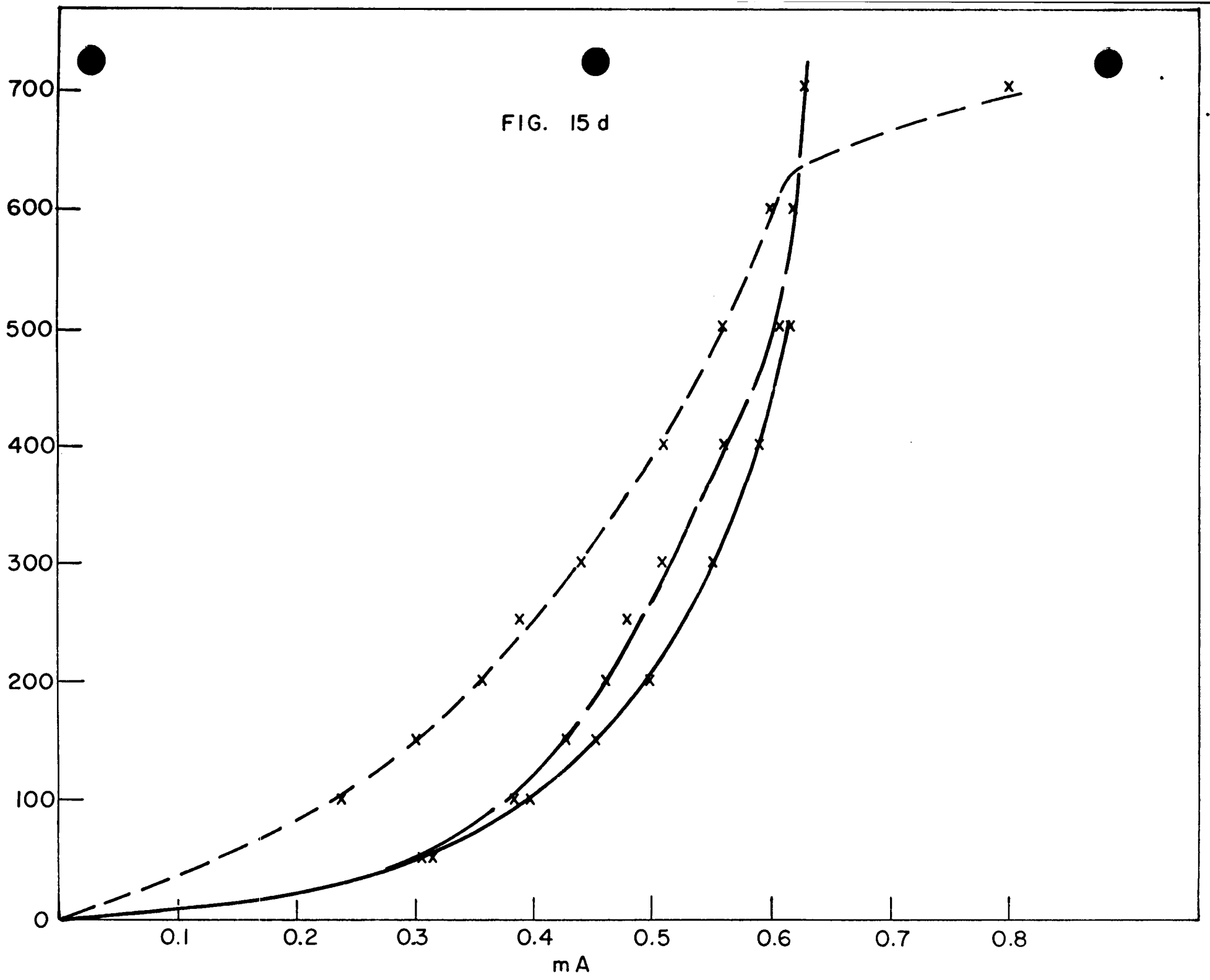

FIG. 15 d

FIG. 16 a

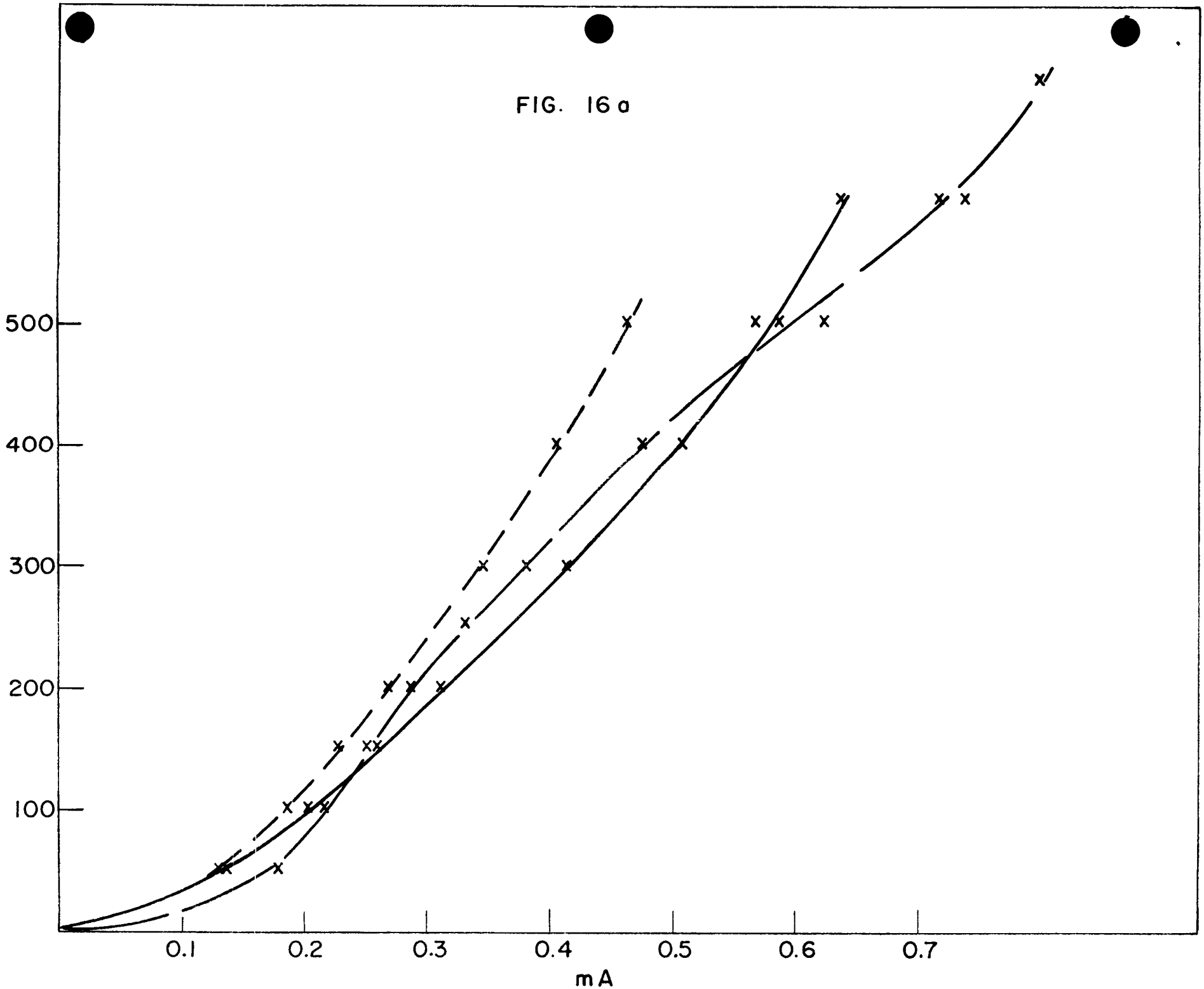

FIG. 16 b

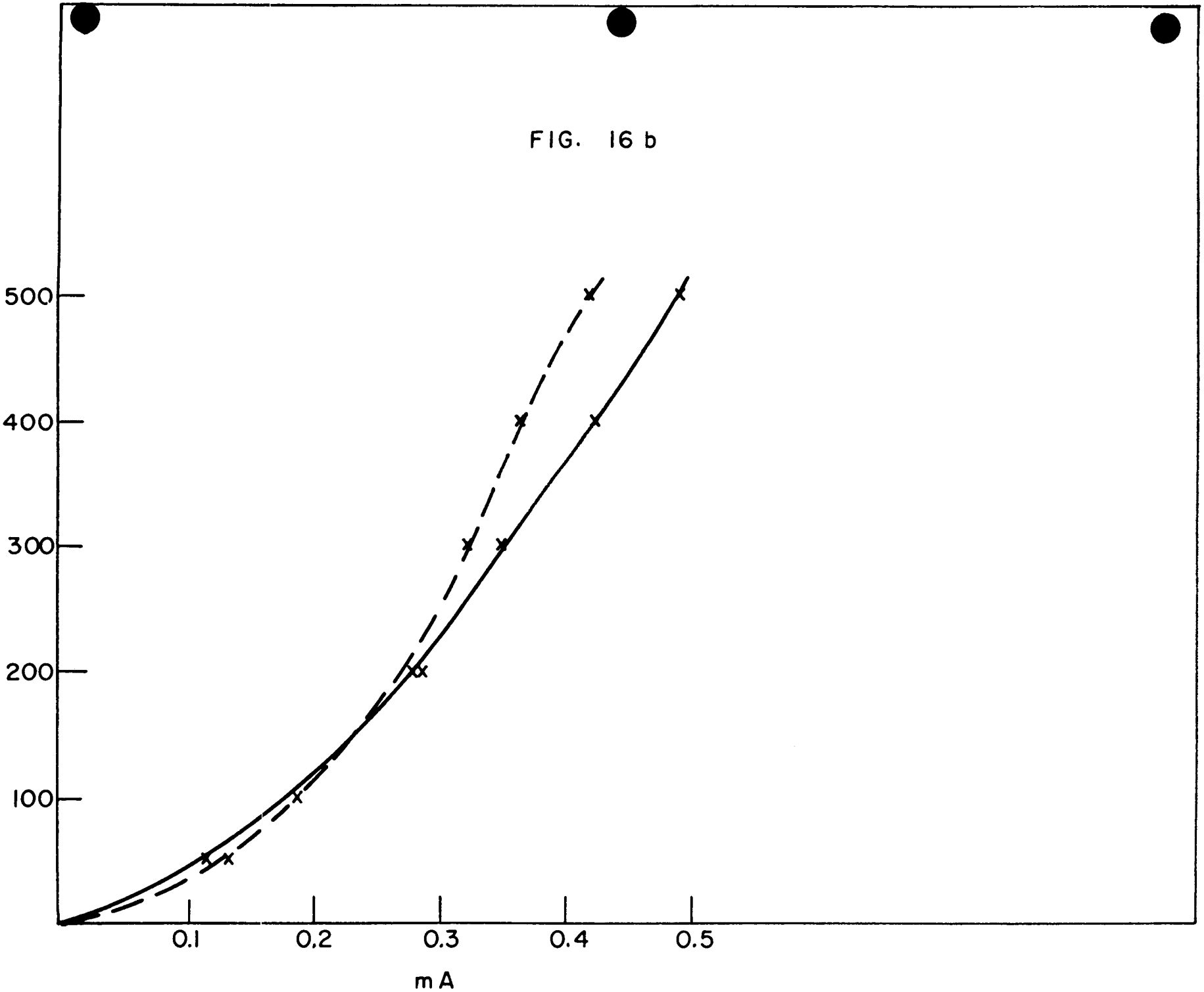

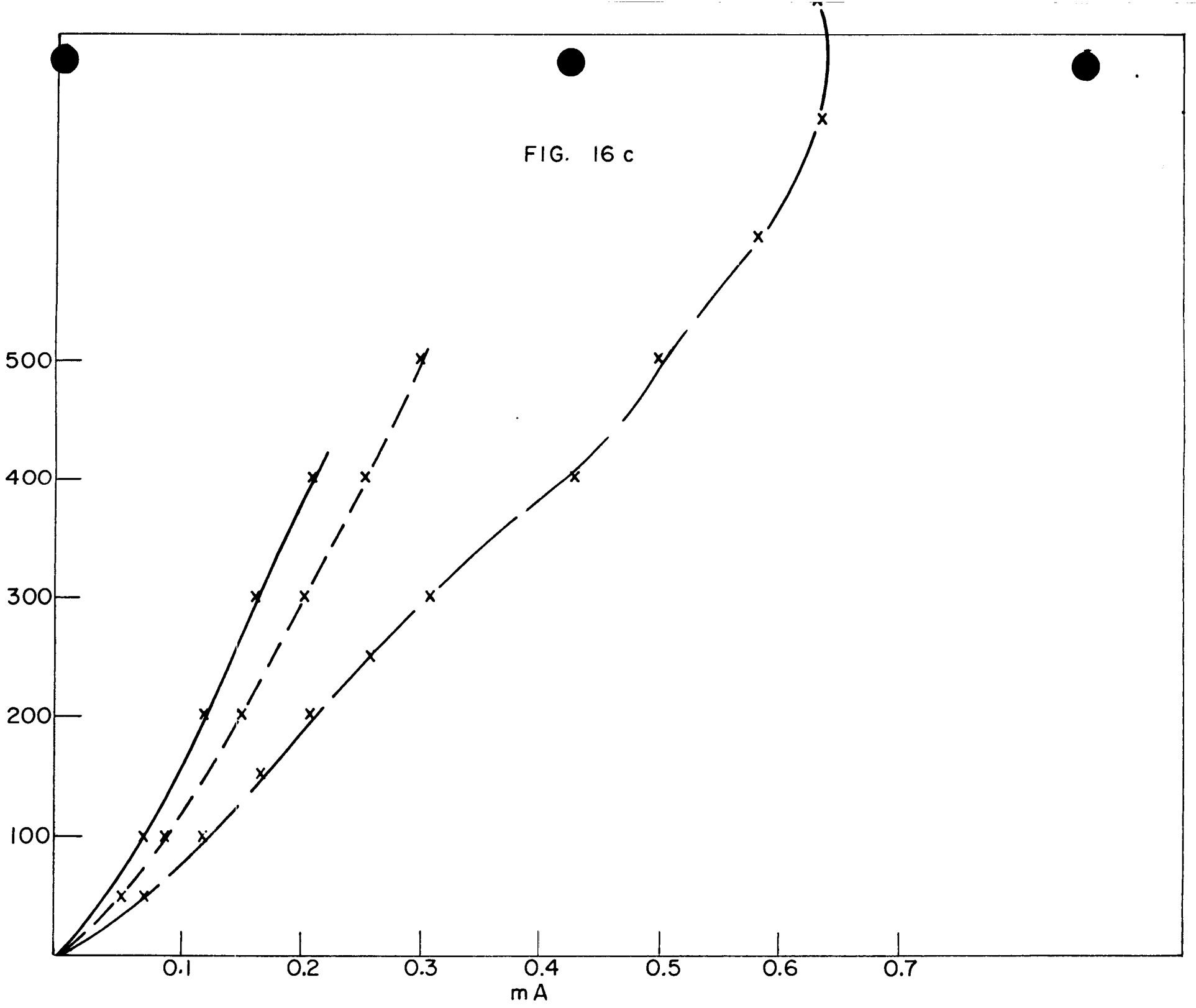

FIG. 16 c

FIG. 17

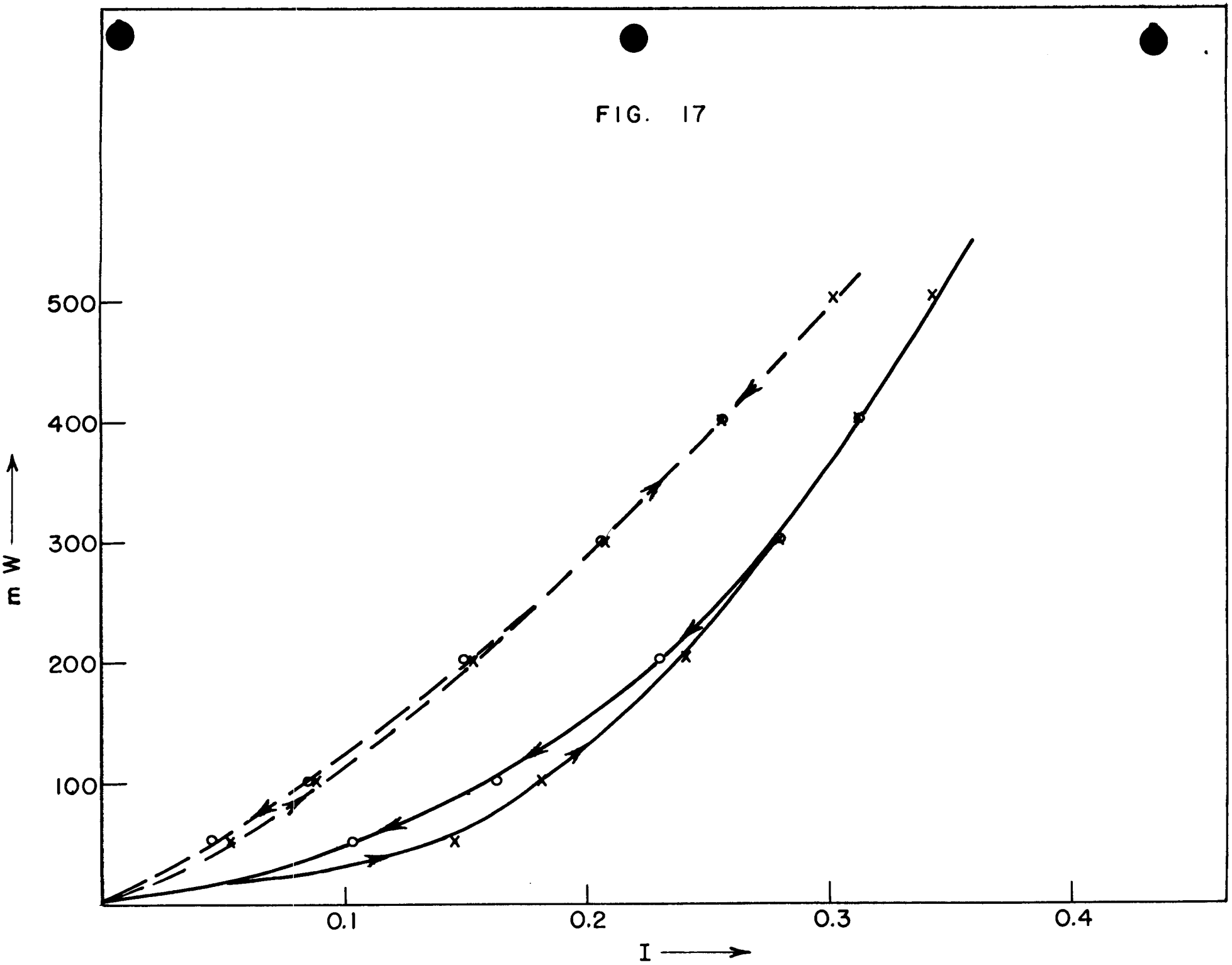

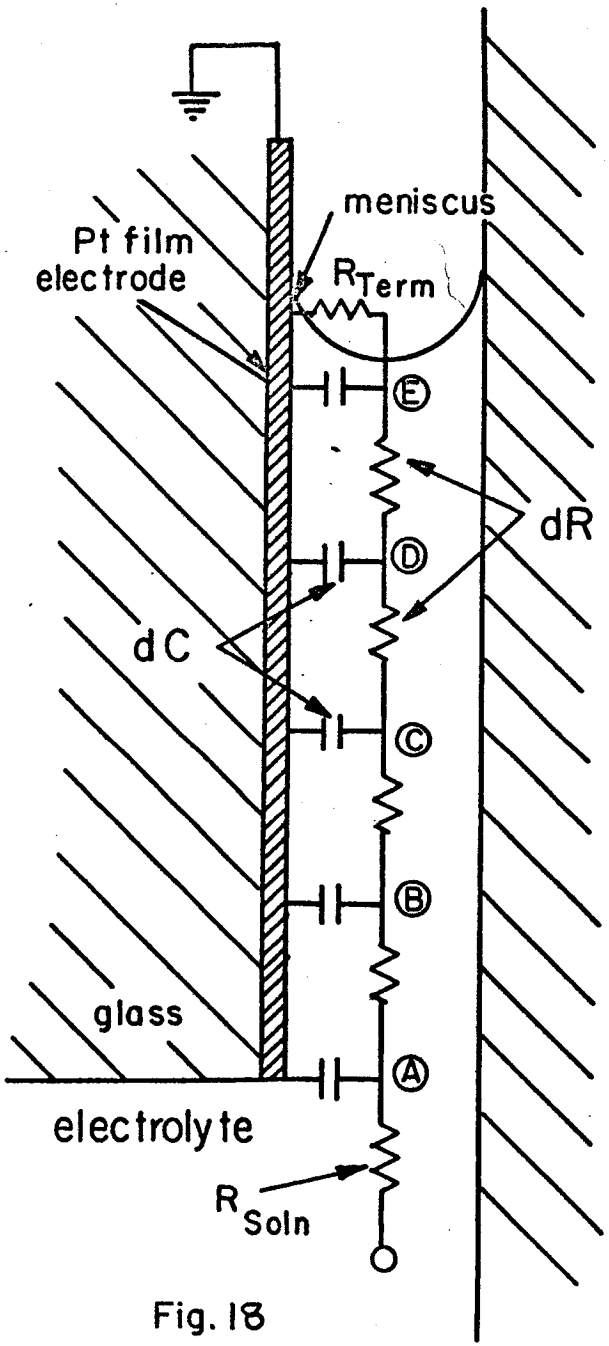
meniscus
Pt film electrode
R_{Term}
E
D
C
B
A
dR
dC
glass
electrolyte
R_{Soln}
$E_{Applied}$

Fig. 18

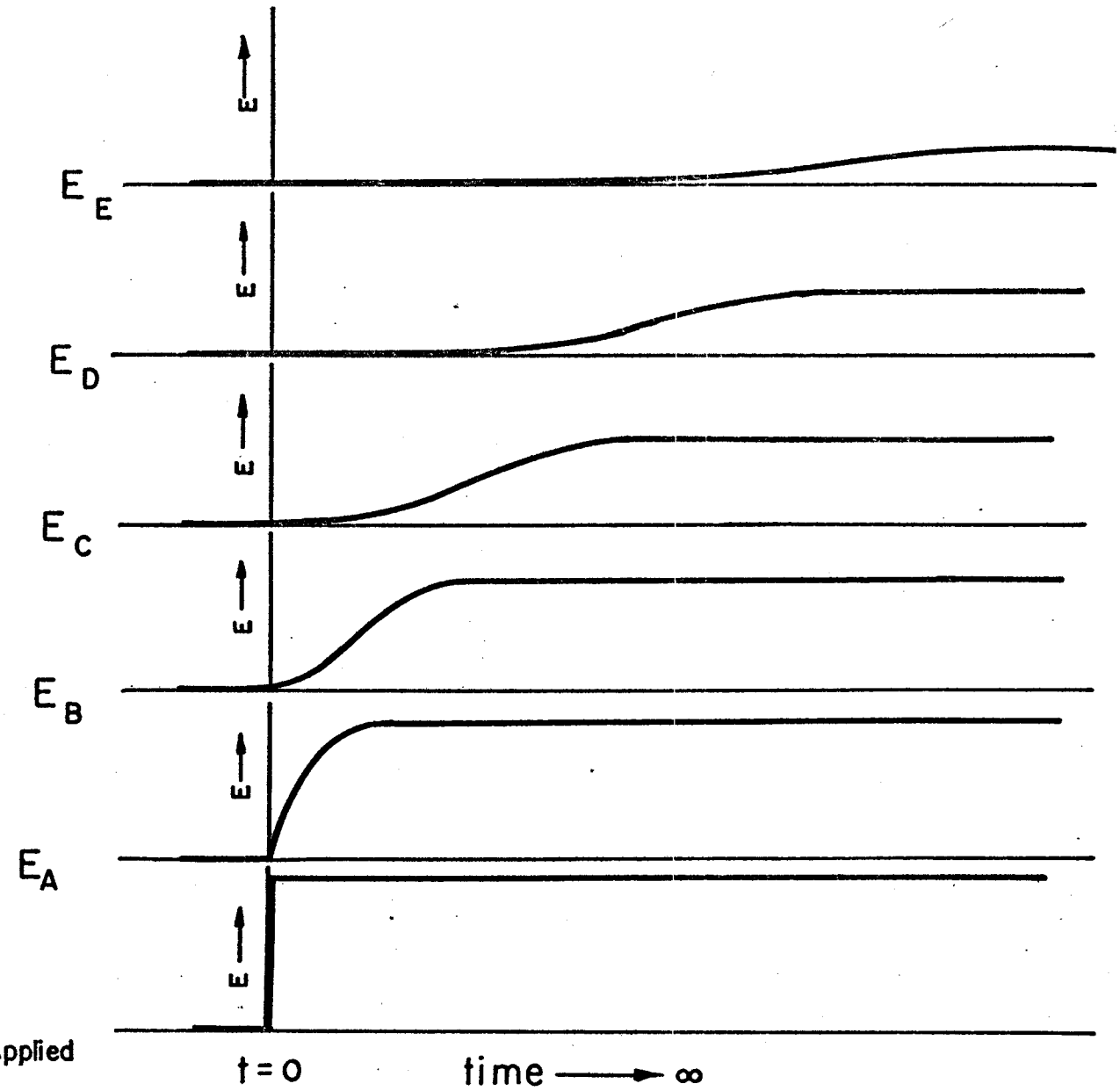
E_E
E_D
E_C
E_B
E_A
E
t = 0
time ⟶ ∞

Fig. 19

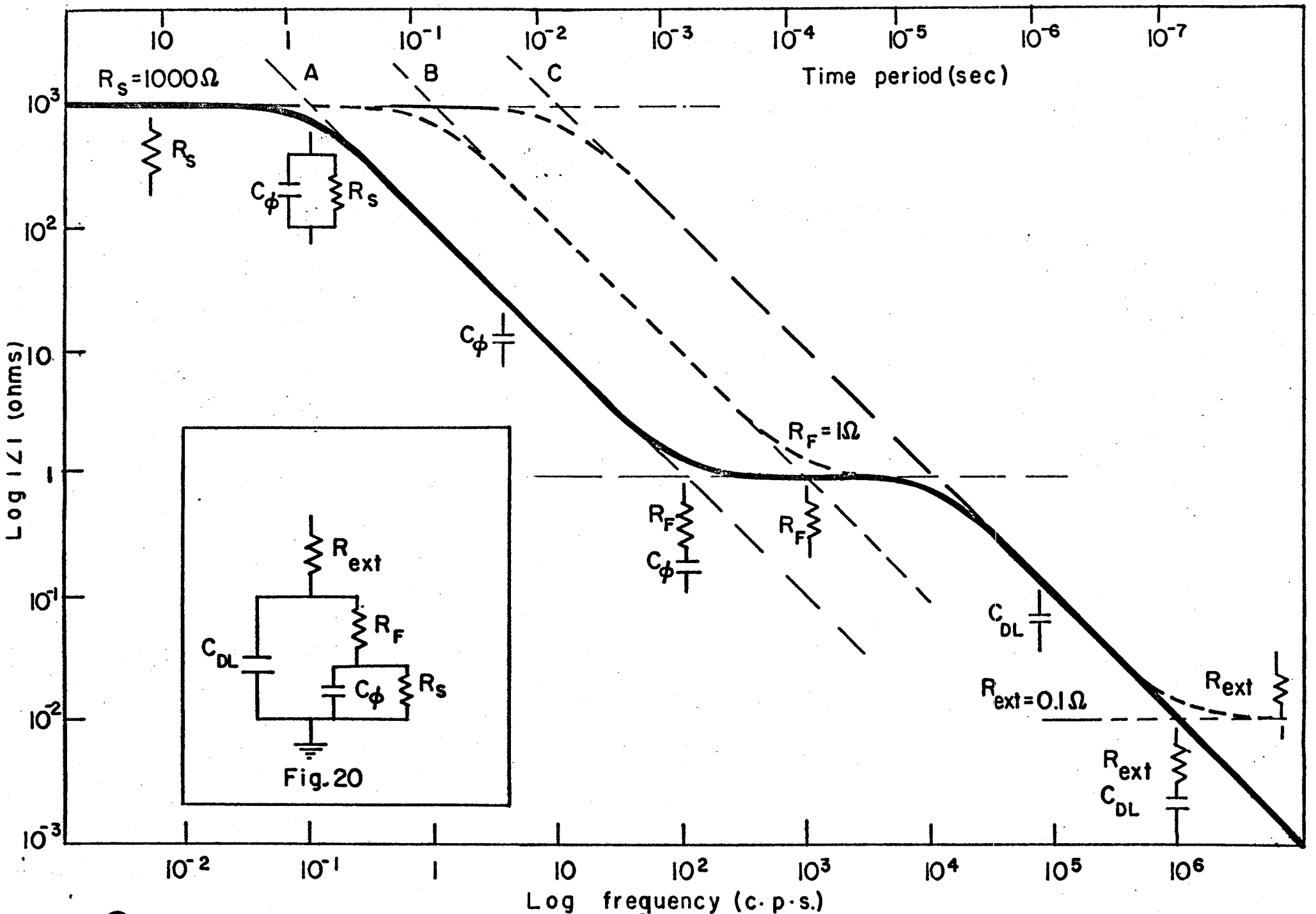
10
1
10^{-1}
10^{-2}
10^{-3}
10^{-4}
10^{-5}
10^{-6}
10^{-7}
Time period (sec)
$R_S = 1000\Omega$
A
B
C
10^3
10^2
10
1
10^{-1}
10^{-2}
10^{-3}
Log |Z| (ohms)
R_S
C_ϕ
R_S
C_ϕ
$R_F = 1\Omega$
R_F
C_ϕ
R_F
C_{DL}
R_{ext}
$R_{ext} = 0.1\Omega$
R_{ext}
C_{DL}
10^{-2}
10^{-1}
1
10
10^2
10^3
10^4
10^5
10^6
Log frequency (c·p·s.)

R_{ext}
R_F
C_{DL}
C_ϕ
R_S

Fig. 20

FIG. 2

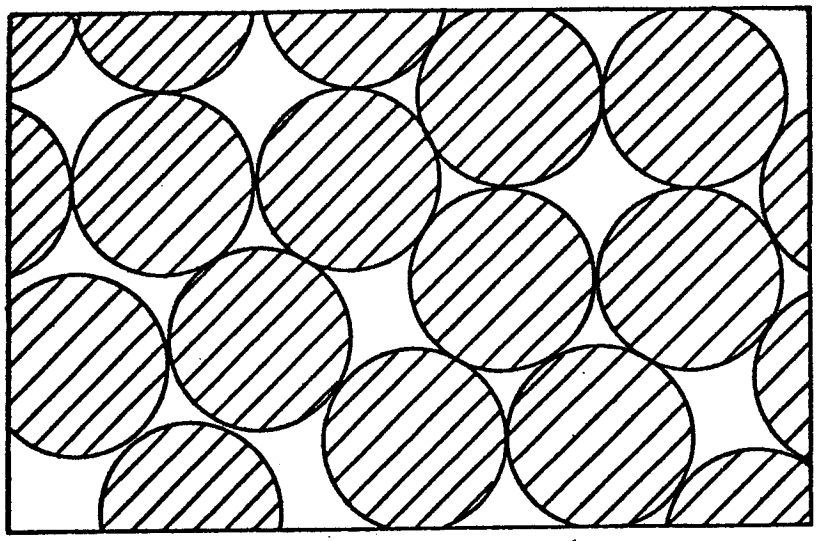

FIG. 22

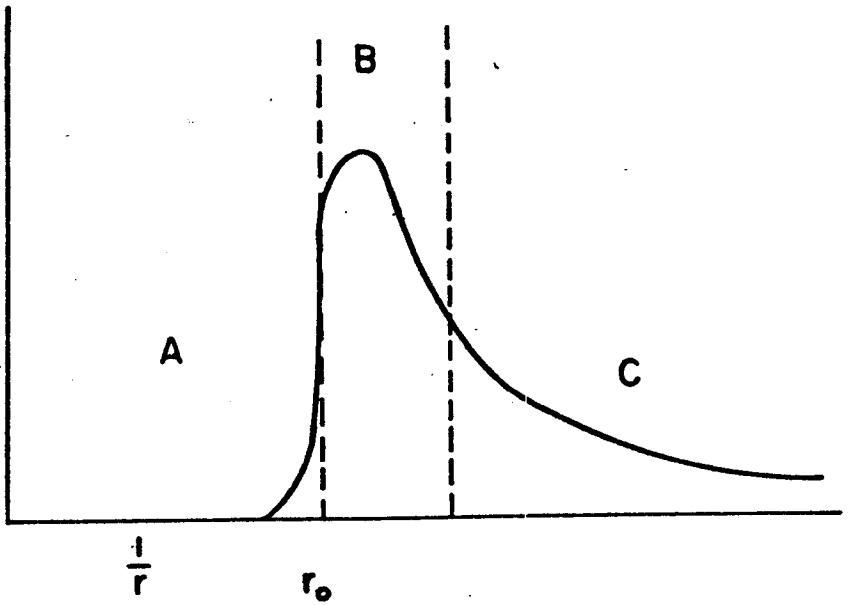

FIG. 23

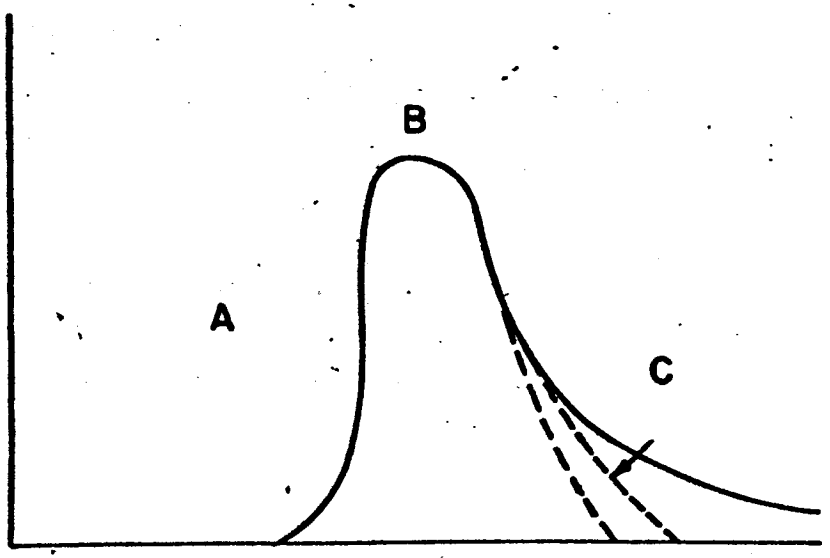

FIG. 24

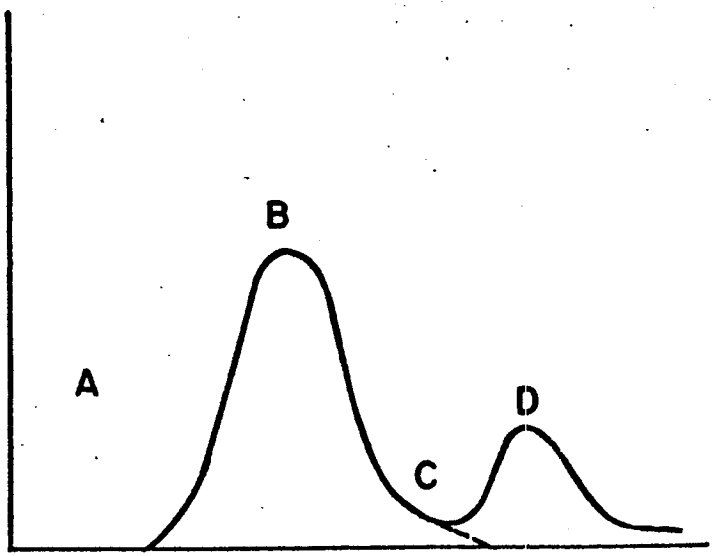

FIG. 25

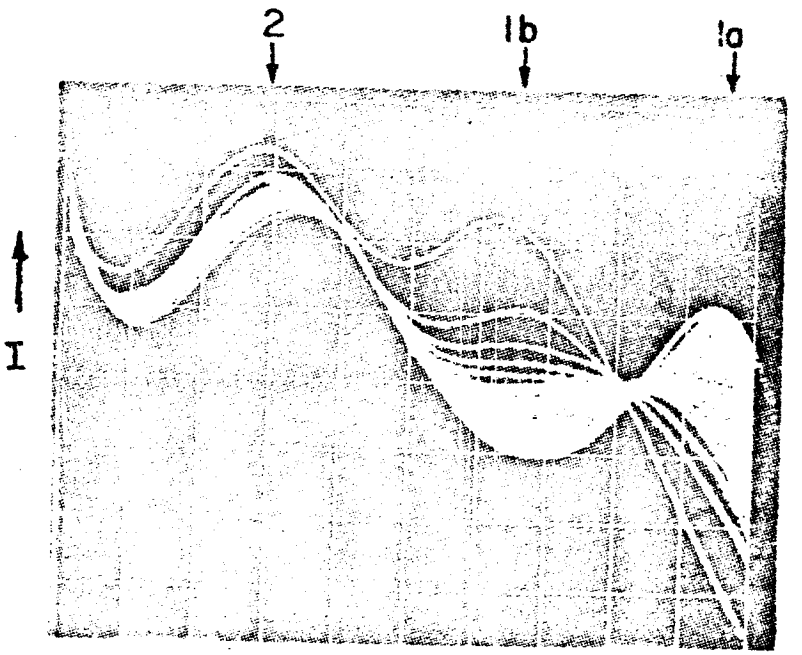

Fig.26

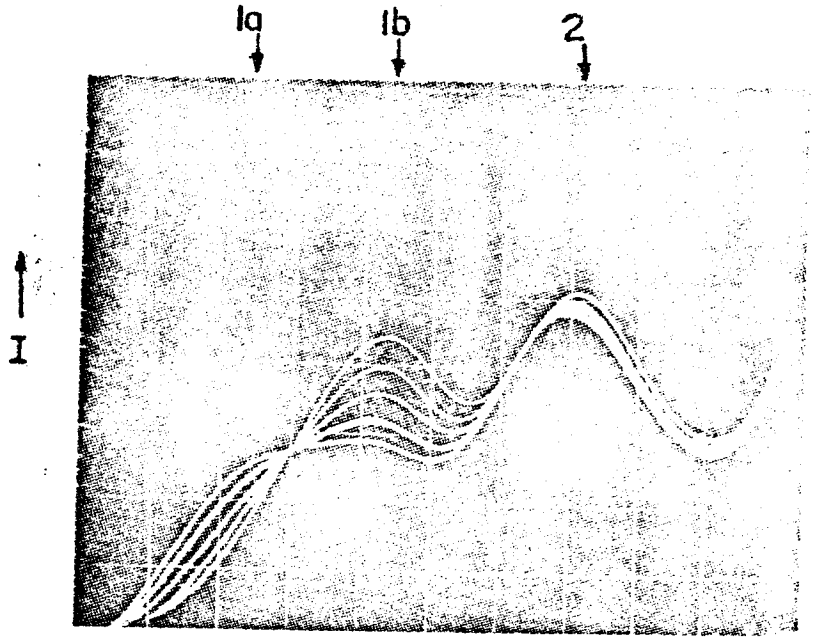

Fig.27

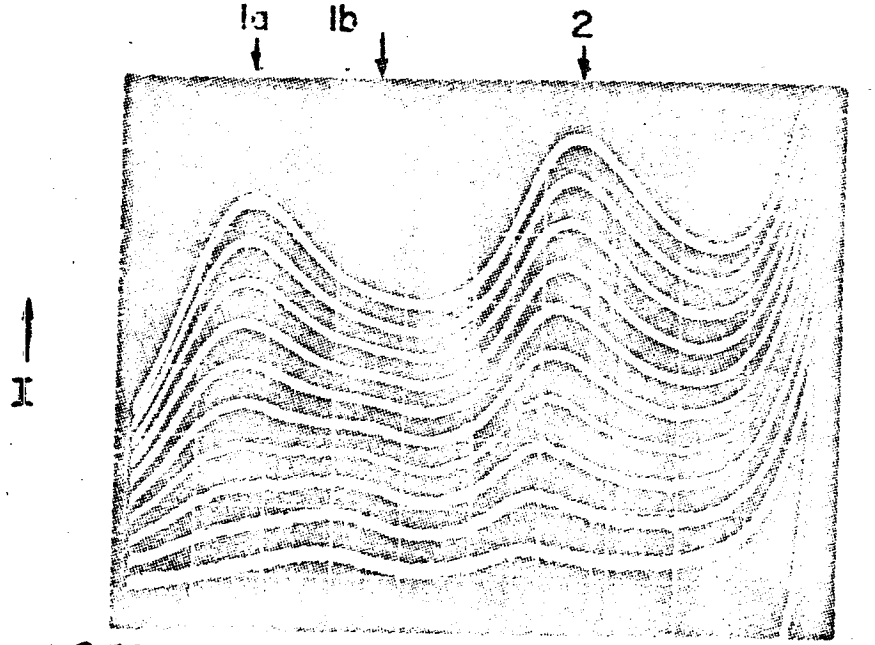

FIG.28

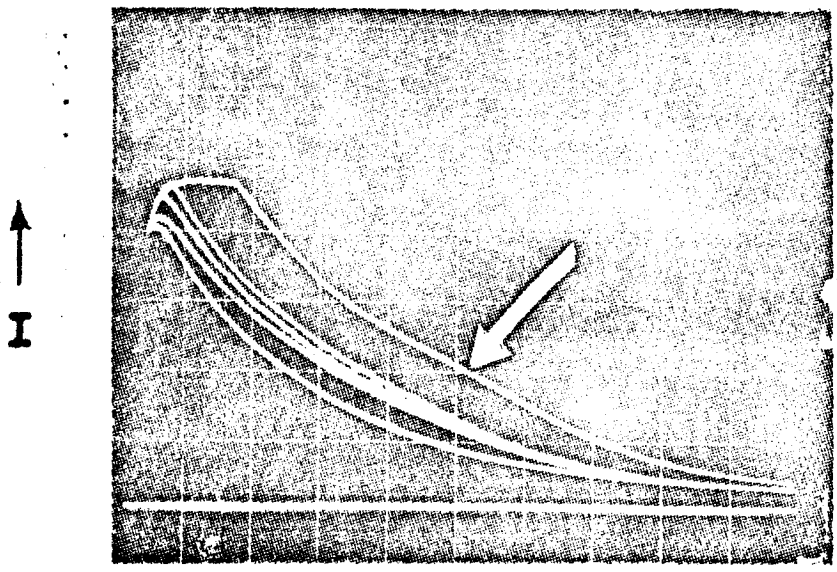

Fig.29

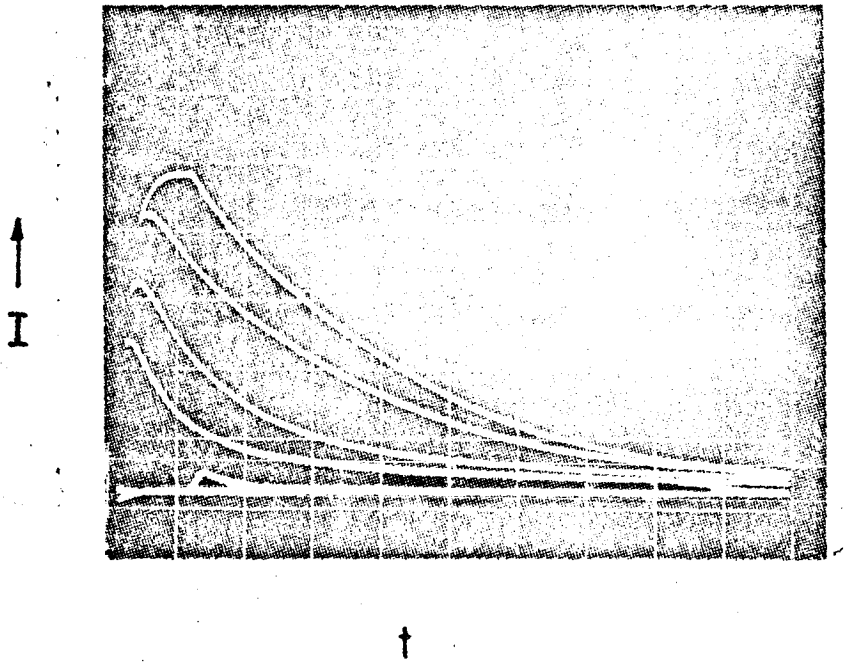

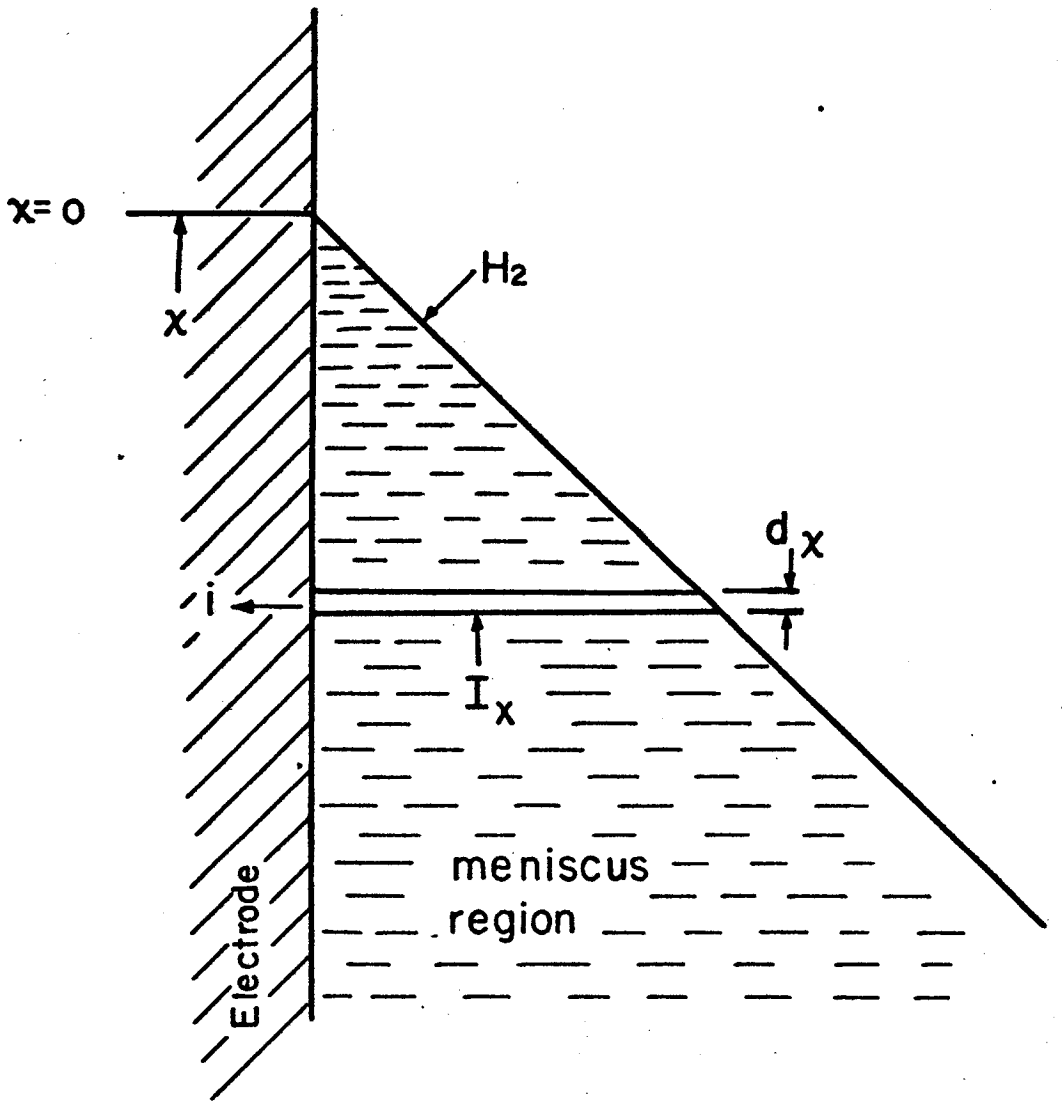

Fig. 31

VI. THE NATURE OF THE CATALYST SURFACE

An electropolished electrode is sometimes used in electrocatalysis studies. To the extent that the surface of such catalyst surface has not been determined, the interpretation of electrode kinetic studies on such surfaces is associated with a measure of uncertainty.

The central question is whether an electropolished electrode is oxide-covered or not. Considerable controversy hangs over this question. Some authors aver that an oxide film is essential to the mechanism of electropolishing. Others dispute this claim and demand a thick, liquid layer (Jacquet layer) of high viscosity.

It was decided, therefore, to carry out an in situ ellipsometric study of an electrode surface during electropolishing. Since most of the controversies have revolved around the mechanism of electropolishing of copper in phosphoric acid solution, this system was chosen for study.

As a first step, the copper electrode was potentiostated at two potentials: one in the etching region and one in the polishing region (Fig. 1). At each of these potentials, ellipsometric measurements are made on the polarization state of the reflected light. The values of the relative phase retardation Δ and relative amplitude diminution ($\tan\chi$) are shown in Table 1. Proceeding on the rule-of-thumb basis that 0.1° in Δ corresponds approximately to 1 Å, it can be seen that the results argue for a film thickness of several hundred angstroms.

When, however, an etching electrode and a polishing electrode are taken out of the polishing electrolyte, quickly flooded with alcohol, dried and ellipsometrically examined in air, there is only a small change

in Δ and χ (table 2). The conclusion was, therefore, drawn that any 'oxide' film which may be present in solution is under a thick liquid film. Attempts were consequently made to isolate the oxide film from the liquid layer and study it.

A simple technique was evolved. During the electropolishing, an organic liquid was placed above the polishing solution. The latter was then sucked out, thus allowing the organic liquid to displace the liquid film and cover the polishing anode without allowing it to come into contact with air. Then the ellipsometric measurements were made repeating the liquid displacement procedure on an etching electrode and a polishing electrode. The difference in the readings are shown in Table 3.

The instrument readings were then converted into thickness values using the Drude-Tronstad approximation (which assumes a non-absorbing film). The solid film appears to be a copper oxide film ($n = 2.63$) of 28 Å thickness.

In order to eliminate the doubt that the organic liquid had not successfully displaced the liquid layer, the experiments were repeated with other organic materials (Table 3). It turns out that, independent of the organic used to displace the liquid layer, the thickness of the oxide was the same. This result proves the validity of the technique used.

Once the thickness of the oxide is determined, it is easy to establish the thickness of the liquid layer. It was 88 Å.

An additional check on the oxide thickness was carried out by an electrochemical determination of the thickness. The galvanostatic method proved futile because after the reduction of about a monolayer of some species (probably oxygen adsorbed on the oxide) the potential jumped to the hydrogen evolution value. Hence, the method of potentiostatic build-up was used - the potential being switched from the etching region to the polishing region. From the quantity of electricity used (Fig. 2) it was found that the oxide thickness was $\sim$25 Å.

From these ellipsometric and electrochemical measurements, it can be concluded that the anode is covered with a thin oxide film during electropolishing. There are, however, characteristic changes in the ellipsometric data (Fig. 3) as the potential is changed. The inflection at the onset of polishing is of particular interest. In order to explore this inflection further, it is necessary to free the ellipsometric analysis from the assumption that the absorption coefficient of the oxide film is zero. This work is in progress.

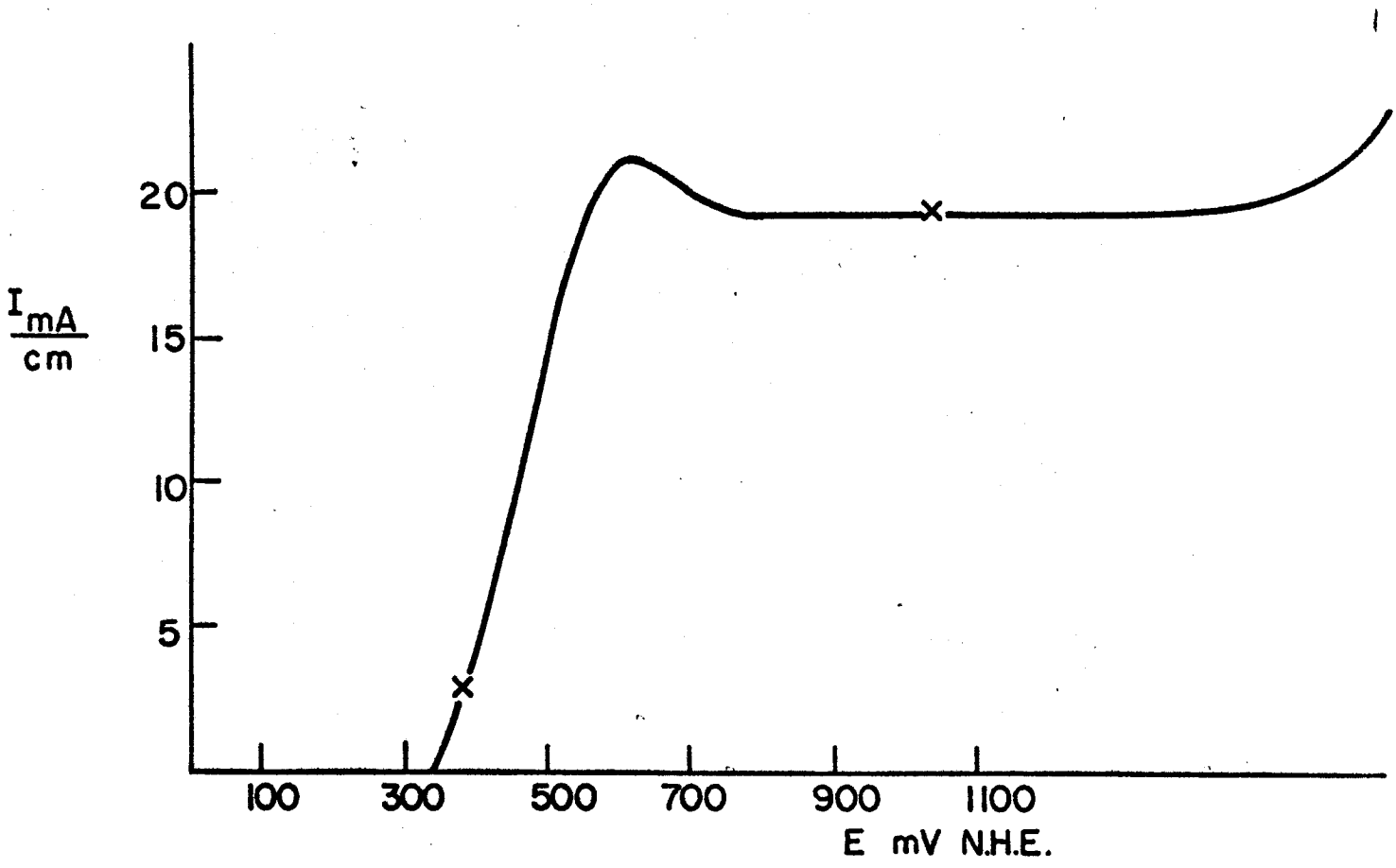

Fig. 1

mV	Δ	Ψ
420	-77,82	-36,43
1040	-102,86	-40,91

Table 1

Table 2

mV	Δ	Ψ
420	106,27	- 38,46
1040	104,46	- 37,15

Table 3

organic	Δ		d thickness
	420 mV	1040 mV	Å
glycerol	-72,84	-79,60	26
glycol	- 74,32	-80,50	28
ethyl-octinol	-71, 78	-19.04	28

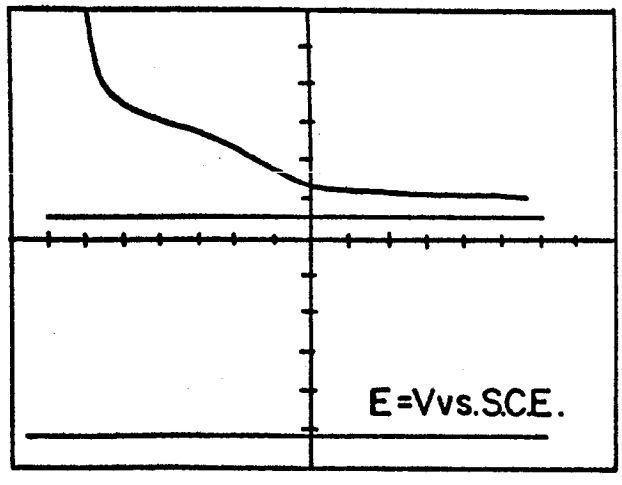

FIG.2 0.1 V/cm ; 0.2 sec / cm 20 mA

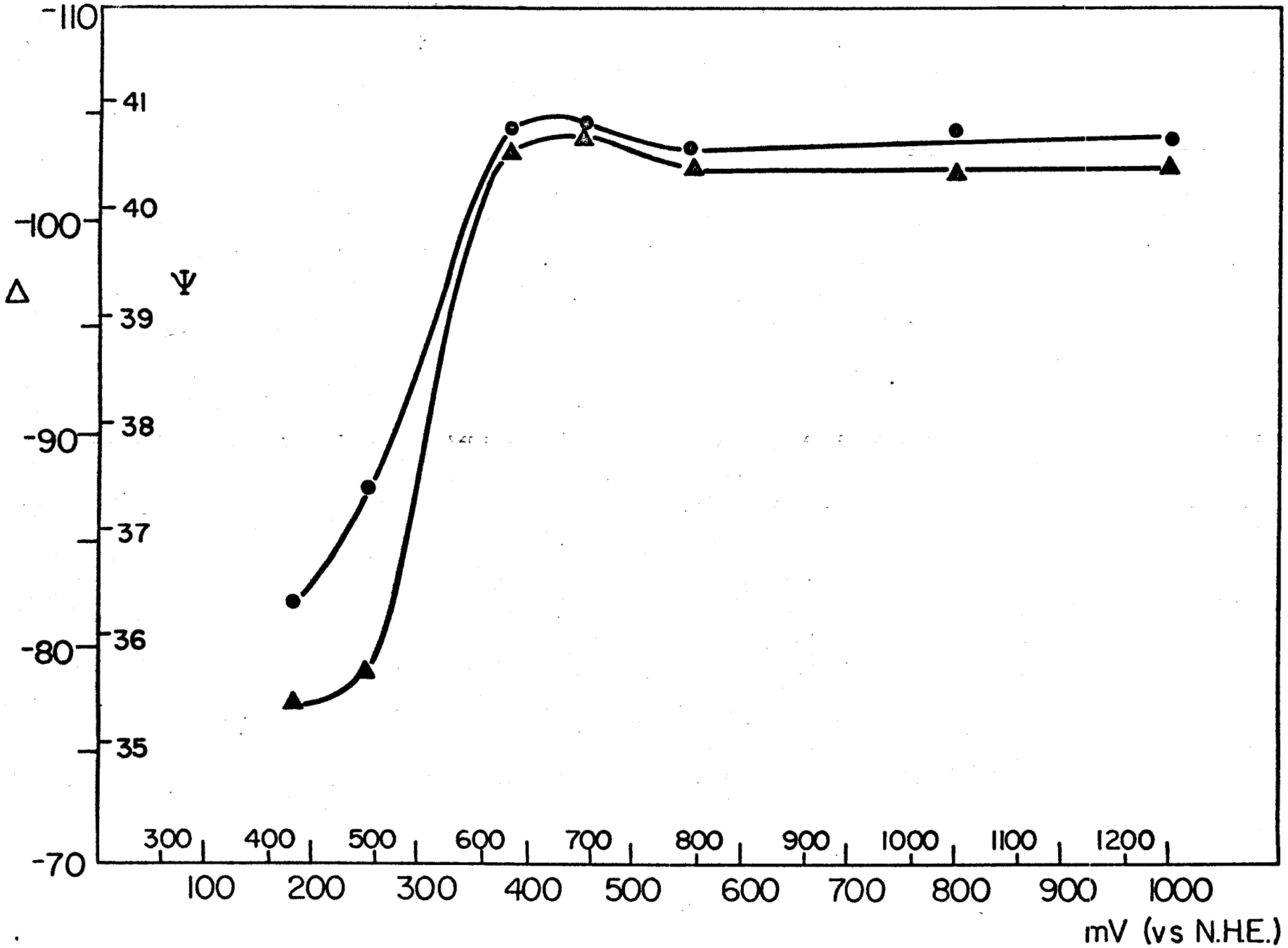
-110
-100
-90
-80
-70
Δ
41
40
39
38
37
36
35
Ψ
300
400
500
600
700
800
900
1000
1100
1200
100
200
300
400
500
600
700
800
900
1000
mV (vs N.H.E.)

FIG. 3a

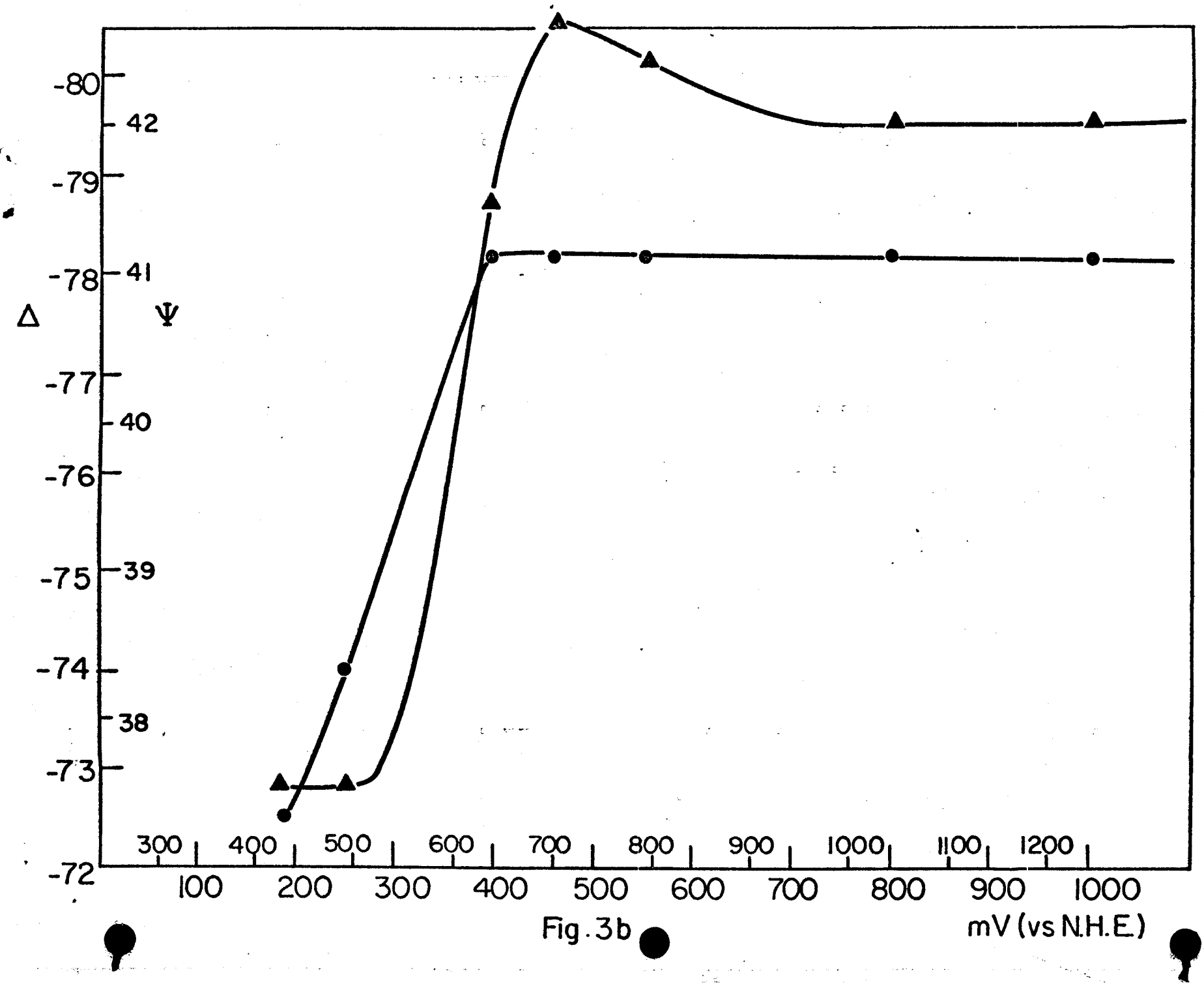
-80
42
-79
-78
41
Δ
Ψ
-77
40
-76
-75
39
-74
38
-73
-72
300
400
500
600
700
800
900
1000
1100
1200
100
200
300
400
500
600
700
800
900
1000
mV (vs N.H.E.)

Fig. 3b

POTENTIAL OF ZERO CHARGE

Shyam D. Argade and E. Gileadi

I. INTRODUCTION

1. What is Potential of Zero Charge?

When a metal is immersed in a solution of an electrolyte, a double layer is set up at the interface such that there can be an excess charge on the metal side of the interface and an ionic atmosphere with a net excess of one kind of ions in the solution side of the double layer to maintain electroneutrality over all of the system. The charge on the metal per unit area is given by

$$q^m = - F \sum_i \Gamma_i z_i \qquad (1)$$

where the summation is limited to the solution side of the double layer, F the Faraday, z_i the valence of the ionic species i including the sign of charge, and Γ_i is the surface excess of that component in the double layer in moles per unit area of the interface. The charge on the solution side of the double layer, q^s, is equal and opposite in sign to the charge on the metal, q^m. ($q^m = - q^s$). Consider this as an ideally polarized electrode, in which case the Gibbs' adsorption equation at constant temperature and pressure can be written as

$$(d\gamma)_{T,P} = \sum_i \Gamma_i d\mu_i - q^m dE \qquad (2)$$

and

$$(\partial\gamma/\partial E)_{T,P,\mu_i} = - q^m \qquad (3)$$

where μ_i is the chemical potential of the species i, E the electrode potential and γ the interfacial tension. In principle one can determine the interfacial tension as a function of the electrode potential with respect to some suitable reference electrode. Then the potential at which the derivative $(\partial \gamma / \partial E)_{T,P,\mu_i}$ is zero, the metallic side of the double layer will have no excess charge. This potential is defined as the potential of zero charge.

2. The Use of Rational Scale of Potentials

The potential of zero charge offers itself as a natural reference point. This point of view was originally put forward by Frumkin[1] and applied by Grahame[2] to devise a rational scale of potentials and stressed further by Antropov.[3] The rational scale of potentials is defined as follows

$$\bar{E} = E - E_{q=o} \qquad (4)$$

where $\bar{E}$ is the potential in the rational scale, E is the potential in which one is interested, and $E_{q=o}$ is the potential of zero charge of the electrode. What is rational about this scale of potentials is that the potential on this scale gives an approximate idea regarding the charge on the electrode. Also the rational potential, as can be seen from the equation (4), is independent of the scale of reference. It is absolutely necessary to have at least an approximate idea regarding the charge on the electrode in order to apprehend the processes taking place at the electrode-solution interface. The charge on the metal is fundamentally responsible for the distribution of ions and dipoles in the solution side of the double layer.

The importance of representing the double layer phenomena as a function of charge on the electrode is illustrated by an example as follows.[4] Consider the energy of adsorption of dipoles on the electrode surface. A dipole with a dipole moment μ in a field X has an energy μX when the dipole is in the direction of the field. In this particular case we will leave aside the other interactions just to make the point cited. If we know the charge on the electrode, $X = 4\pi q^m/\varepsilon$. But if we try to equate, $X = \Delta V/\delta$, difficulties arise because we do not know the precise value of δ, the double layer thickness and ΔV is the potential difference across the double layer (which includes the diffuse double layer p.d. and other contributions).

The advantage of representing double layer phenomena in terms of charge is demonstrated by Bockris, Devanathan and Müller[4] in the case of adsorption of various aliphatic compounds on Hg. It was found that (the coverage) versus q^m plots had a simple and symmetrical shape and the maximum of coverage occurred between -2 to -3 coul. cm^{-2} for various compounds. Whereas the θ - V plots were much more complex and there was no definite relation between θ_{max} and V. Fig. 1 shows θ--q^m and θ --V plots for the case of the adsorption of butanol.

Thus it may be realized that the knowledge of the charge on the electrode is very important. In the case of solid electrodes it is not possible to get very accurate values of potential of zero charge and also determination of q--V plots on solid electrodes presents difficulties and in such a case rational scale is quite useful.

At slightly negative charges or at slightly negative rational potential the water molecules at the electrode-solution interface are

oriented in such a way that the number of molecules of water in each orientation is the same. At this point several organic compounds will get adsorbed to the maximum extent because, on the basis of competitive model of adsorption, at this point the interaction between the organic and the metal may be larger than that with water. In case of some of the aromatic organic molecules this may happen at slightly positive rational potentials because of the specific interaction involved.

For charged particles, roughly the opposite sign of charge on the electrode is favorable for adsorption. Cations which do not get specifically adsorbed, are adsorbed when the rational potential is negative. For anions the picture is much more complicated as anions have a larger tendency for specific adsorption. Also whenever the interaction of the field in the double layer with some other species, charged or uncharged, becomes larger than that of the adsorbed ion, get desorbed. In the absence of specific adsorption, at $\bar{E} = 0$, there is no net excess of one kind of ions.

3. Electrode Kinetics and Potential of Zero Charge

Potential of zero charge serves as a reference point for comparison of rates of electrochemical reactions on different metals. Let us consider an electrochemical reaction whose rate is activation controlled. The exchange current density (i_o) of this reaction can be written as,

$$i_o = nF/\nu\,(kT/h) \prod a_j \exp(-\Delta G^{\neq})/RT \exp(-n\beta\,\Delta\phi_{rev}F)/RT \qquad (5)$$

and the rate of this electrochemical reaction (i)

$$i = i_o \exp(-n\beta\eta F)/\nu RT \qquad (6)$$

where k is the Boltzmann constant, h is the Planck constant, n is the number of the electrons required for the overall reaction, F is the Faraday, ν is the stoichiometric number, a_j's are the activities, $\Delta G^{\neq}$ is the chemical free energy, β is the symmetry factor, $\Delta\phi_{rev}$ is the metal-solution potential difference at the reversible potential and η is the overpotential. We would like to compare the rates of the electrochemical reactinn where the field dependent part of the free energy of activation ($n\beta\Delta\phi F$) is zero. At potential of zero charge the charge dependent part of the metal-solution p.d. ($\Delta\psi$) is zero and the only contribution to the metal-solution p.d. ($\Delta\phi$) is that of $\Delta\chi$. If we can assume, in the case of metals being compared for the catalytic activity, that $\Delta\chi$ is constant we have in effect a fair comparison of the chemical rate constants. Whereas if we compare the rates of the electrochemical reaction at the reversible potential, we are nowhere near the ideal situation of comparing the chemical rate constants. Because the charge dependent field in the case would be far different from metal to metal.

A very interesting point is the usage of rational scale of potentials in electrode reactions. We will mention two examples here, namely, hydrogen evolution reaction on different metals having the same β and the electrodeposition reaction of some metals. From equation (5), if we plot log i_o versus the reversible potential on the rational scale for hydrogen evolution reaction we would get a straight line with a slope of $n\beta F/RT$ and this is found to be the case (cf. Fig. 2). Several early

attempts[5-8] were made to list the metals in the order of their electrodeposition exchange current densities, On the basis of these data Antropov[3] put the metals in the decreasing order of their i_o's as: Hg, Ag, Pb, Tl, Cd, Bi, Sn, Cu, Zn, Co, Ni, Fe. This series is not rigorous and it can be explained on the basis of none of the considerations like the electronic structure of the metal ions, potential energy diagrams, nor the electromotive series. The sequence is fairly well elucidated by the consideration of the rational scale of potentials. As can be seen from Table 1, some of the positions of $\bar{E}_{rev}$ which forms a similar sequence

TABLE 1. REVERSIBLE POTENTIALS OF METALS IN THE RATIONAL SCALE AND THEIR EXCHANGE CURRENT DENSITIES

Metal	PZC	E_{rev}	$\bar{E}_{rev}$	i_o^* A cm^{-2}
Hg	-0.21	0.80	1.01	14 ± 1
Ag	+0.05	0.80	0.75	24 ± 5
Pb	-0.67	-0.13	0.54	--
Tl	-0.82	-0.34	0.48	--
Cd	-0.72	-0.40	0.32	1.4×10^{-2}
Cu	-0.04	+0.34	0.38	2.4×10^{-2}
Co	-0.51	-0.27	0.24	8×10^{-7}
Sn	-0.34	-0.14	0.20	2×10^{-5}
Zn	-0.60	-0.76	-0.16	2×10^{-5}
Fe	-0.38	-0.44	-0.06	1×10^{-8}
Ni	-0.34	-0.23	+0.11	2×10^{-9}

*i_o values are taken from the compilation of N. Tanaka and R. Tamamushi.[10]

as of i_o's, seem to be reversed but the general order is maintained.

Thus, the potential of zero charge is a very significant quantity in electrochemistry. It serves as a reference point for comparison and also in some cases it is useful for the purposes of interpretation, e.g., the case of electrodeposition of metals. It is also advantageous in some of the practical applications, viz. electroreduction, corrosion inhibition, etc.[3,9]

II. ASPECTS OF POTENTIAL OF ZERO CHARGE IN CONNECTION WITH THE METAL

1. The relation between Potential of Zero Charge, Contact Potential Difference and Work Function

It was pointed out by Frumkin[11] that the difference in the potential of zero charge of two metals is approximately equal to their contact potential difference.

$$\Delta\Psi_{\text{contact}} = E^1_{q=0} - E^2_{q=0} \qquad (7)$$

where $E_{q=0}$ potential of zero charge, 1 and 2 subscripts refer to the metal. $V_{1,2}$ is the contact potential difference between the two metals. Also Frumkin pointed out that the different orientation of the dipolar molecules of the solvent (water in aqueous media) at the electrode interface, causes the deviations to the above rule, Eqn. (7). It was Vasenin[12] who pointed out first the relation between potential of zero charge and work function. His was the first attempt to relate the potential of zero charge to a property of the metal semi-empirically. He took on the argument of Frumkin that contact p.d. is equal to the

difference of potentials of zero charge of metals. Vasenin said this correspondence serves as a basis for the approximate calculation of potential of zero charge from work function. From equation (7)

$$E_1^{q=0} - E_2^{q=0} \doteq V_{1,2}$$

$$E_2^{q=0} = E_1^{q=0} - V_{1,2} \tag{8}$$

Now

$$V_{1,2} = \phi_1 - \phi_2 \tag{9}$$

where ϕ's are work functions.

From (8) and (9)

$$E_2^{q=0} = E_1^{q=0} - (\phi_1 - \phi_2) \tag{10}$$

An assumption involved is that equality of difference in potential of zero charge and contact potential difference. A better approximation may be obtained by introducing a parameter b which corrects for the interaction of oriented dipole layer with the metal surface. Thus,

$$E_2^{q=0} = E_1^{q=0} - b(\phi_1 - \phi_2) \tag{11}$$

since we know the values of potential of zero charges and work function for one metal (mercury) Eqn. (11) can be rewritten as,

$$E^{q=0} = a + b\phi \tag{12}$$

The most probable values of constants of this line are given by Vasenin as, $a = -4.25$ and $b = 0.86$. b is dimensionless and a is in volts. The value of b according to Vasenin gives an indication of oriented water dipoles with the metal surface, which must depend upon the structure of the water molecule, in case of aqueous solution. The

fact that the experimental line lies below that of the slope b = 1, there is an interaction between the surface dipolar layer of oriented water dipoles and the surface layer of the metallic phase. The more negative the potentials of zero charge to these values on the line, it was proposed, that more was the interaction between surface dipoles adsorbed at the metal solution interface. Also the larger the work function the greater is the interaction between the two electric layers which are present in the different phases. The magnitude of the variation of the potential caused by this interaction is different for different metals and changes from 0.25 to 0.5 v for the alkali and alkaline earth metals and from 0.5 to 0.7 v for the remaining metals, increasing with increasing the electronic work function of the metal.

The relation Vasenin gets in figure (3) shows there is a lot of scatter due to the inaccuracy of measurement of both of these quantities, namely, work function and potential of zero charge.

Thus there seems to be an empirical relation between potentials of zero charge and work function. But it is difficult to check the validity of the Vasenin equation due to an extremely large scatter in the experimental data of work functions and potentials of zero charge of metals. Also, both of these quantities vary with the surface of the metal and particularly the potential of zero charge depends on ionic adsorption (cf. Section III).

2. Physicochemical Properties of the Metal

The potential of zero charge can be split up into two terms, according to Ukshe[13] and Levin[14] as follows

$$E_{q=0} = E_{q=0}^{bulk} + E_{q=0}^{surface} \qquad (13)$$

where $E_{q=0}$ is the potential of zero charge determined experimentally, $E_{q=0}^{bulk}$ is component due to the bulk of the metal and $E_{q=0}^{surface}$ is the surface component of the potential of zero charge.

According to equation (13) in the attempt of establishing any dependence of potential of zero charge upon the properties of metal. One should think of the bulk component of potential of zero charge and not experimentally determined potential of zero charge. The difference between $E_{q=0}$ and $E_{q=0}^{bulk}$ may be appreciable (see Section III).

Thus, one cannot expect to have an ideal agreement between a mathematical formula connecting a bulk property and the potential of zero charge of metal. Ukshe and Levin found that there exists some relation between the atomic weight of a metal and the potentials of zero charge as obtained experimentally or calculated from work function vs. potential of zero charge plot. This attests of some relation between two quantities. Accordingly they come up with a relation as follows

$$(Dn/A)^{1/3} = a \pm b \sin \omega (E_{q=0} + c) \qquad (14)$$

where $a \doteq 0.565$, $b \doteq 0.115$, $\omega \doteq 0.6$, $c \doteq 0.28$. D is the density of the metal, A is the atomic weight, n is the number of free electrons in the metal atom. It is apparent that A/D is atomic volume, thus nD/A is a free electron concentration term. It is claimed that this kind of sinusoidal curve (which is limited to + 0.6 to - 1.1 on the normal hydrogen electrode scale) is a better fit than the equation of Vasenin. Also, according to Ukshe and Levin the bulk component of $E_{q=0}$ must

depend upon temperature because the density of the metal is dependent upon temperature. The dependence may not be very appreciable but one can expect that zero charge potentials of Pb, Zn, Cd, Te and Cu must shift to more negative values as the temperature increases. The potential of zero charges of Bi and Ag will on the contrary shift to positive values as the temperature increases. But so far no experimental data is found in literature of sufficient accuracy to test such dependence.

Another difficulty of the formula of Ukshe and Levin is that there are ∞ values of potentials of zero charge for a given value of $(Dn/A)^{1/3}$ and this does not have physical meaning.

In another paper Ukshe, Levin and Novakovskii[14] attempt theoretically to arrive at Vasenin's relation. This derivation is given as follows. Let us consider the following cell M_1 / sol^n / M_2. The e.m.f. of such a cell is defined as

$$E = {}^1\Delta^s \bar{\varphi} + {}^2\Delta\bar{\phi} - {}^2\Delta^s \bar{\varphi} \qquad (15)$$

where the three $\Delta\bar{\phi}$'s refer to the phase boundary potentials. Now if one measures the e.m.f. between an electrode i under standard reversible conditions and electrodes of like kind at zero charge, then we have

$$\bar{E}_o = E_o - E_{q=0} = {}^i\Delta^s\bar{\phi}_o - {}^i\Delta^s\bar{\phi}_{q=0} \qquad (16)$$

E_o refers to the electrode's normal potential and $E_{q=0}$ the potential of zero charge. Frumkin has shown[15] that the contact potential difference between metal-solution at potential of zero charge (i.e. ${}^i\Delta^s\bar{\phi}_{q=0}$) cannot <u>a priori</u> be taken equal to zero because the intrinsic potential drop at the metal-solution interface can be different from the sum of the intrinsic potential drops at the metal-vacuum and the vacuum-solution

interfaces owing to the different orientation of the dipole molecules of the solvent at the interfaces with the metal and with the vacuum. This is confirmed by experiments,[16] which served as a basis to evaluate the phase boundary potential difference between a mercury electrode at zero charge and a NaCl solution as 0.33.[20] Also one can in addition, according to Frumkin and Ershler[17] take the magnitude of this potential drop for various electrodes in first approximation as a constant, i.e.

$$^{i}\Delta^{s}\psi_{q=0} \doteq \text{constant} \tag{17}$$

As far as the potential drop $^{i}\Delta^{s}\psi_{o}$ for an electrode in a normal solution is concerned it is defined by the free energy of transfer of ions from metal lattice into their one normal solution. Thus, we can write

$$^{i}\Delta^{s}\psi_{o} = \frac{U_m - U_s}{ze_o^-} \tag{18}$$

where U_m is the energy required in removing a metal ion from the lattice and U_s is the energy for removing an ion from the solution. Now U_m as determined from a thermodynamic cycle is,

$$U_m = \Delta G_s + \Delta G_i - ze_o^- \phi \tag{19}$$

and

$$U_s = \Delta G_h + ze_o^- \chi_s \tag{20}$$

ΔG's are the free energies and the subscripts s,i and h are for sublimation, ionization and hydration respectively. ze_o^- is the charge on the ion, ϕ is the work function and χ_s is the potential drop across the solution-vacuum interface. From equations (17) - (20) it follows that,

$$\bar{E}_o = E_o - E_{q=0} = \frac{\Delta G_s + \Delta G_i - \Delta G_h}{ze_o^-} - \chi_s - \phi - {}^{i}\Delta^{s}\psi_{q=0} \tag{21}$$

Thus $\bar{E}_o$ varies linearly with the electronic work function ϕ. It is not possible, however, to verify the equation (21) because some of the quantities are unknown, e.g., χ_s and ${}^{i}\Delta^{s}\bar{\phi}_{q=0}$. For the calculation Ukshe et al. used the following

$$\bar{E}_o = \frac{\Delta H_s + \Delta H_i - \Delta H_h - T\Delta S}{ze_o^-} - \chi_s - \phi - {}^{i}\Delta^{s}\bar{\phi}_{q=0} \qquad (22)$$

ΔS is the entropy differenee for the ion in the metal lattice and that in the solution. ΔH's are the enthalpies. Table (2) gives the values for the above quantities. If one designates

$$- ze_o^- \phi + \Delta H_s + \Delta H_i - \Delta H_h - T\Delta S = \sum G \qquad (23)$$

then

$$\bar{E}_o = \frac{1}{ze_o} \sum G + \text{constant} \qquad (24)$$

From Table (2) it is seen that almost all of the experimental points with the exception of Al and Ga, are well represented by Eqn. (24). Also it is found that ${}^{i}\Delta^{s}\bar{\phi}_{q=o} + \chi_s$ is a constant and its value is - 0.22 v. Now, these considerations also allow to get an equation relating work function and potential of zero charge. From equation (15) the e.m.f. of a cell composed of an arbitrary electrode at potential of zero charge (i) and another under standard reversible conditions (k) is

$$E_o^k - E_{q=0}^i = {}^{k}\Delta^{s}\bar{\phi}_o + {}^{k}\Delta^{i}\bar{\phi} - {}^{i}\Delta^{s}\bar{\phi}_{q=0} \qquad (25)$$

setting ${}^{i}\Delta^{s}\bar{\phi}_{q=0}$ = constant and since ${}^{k}\Delta^{i}\bar{\phi} = \phi^k - \phi^i$ the difference is work functions we have

$$E_{q=0}^i = (E_o^k - {}^{k}\Delta^{s}\bar{\phi}_o - \phi^k + \text{constant}) + \phi^i \qquad (26)$$

The expression in parenthesis in Eqn. (26) can be calculated for any of the metals represented in Table (2). The experimental values of E_o^k and ϕ^k and $\left[{}^k\Delta^s\bar{\phi}_o = \frac{1}{ze_o^-}\sum G - \text{constant} \right]$ are adduced in the table. Using these data the quantity in the parenthesis in equation (26) is found to remain constant for various metals to a reasonable degree (exceptions Ga and Tl). Table (3) gives these values for several metals. We thus have relationship

$$E_{q=0} = \phi - 4.78 \qquad (27)$$

Equation (27) differs somewhat from Vasenin's equation.

$$E_{q=0} = 0.86\,\phi - 4.25 \qquad (12)$$

If using the data in Table (2) and applying the method of least squares, if one calculates the empirical values of the coefficients of equation (12) one obtains the values of the slope and intercept of the line as 0.92 and - 4.40 v respectively. The point corresponding to thallium falls far out of the line and if one excludes thallium then equation becomes

$$E_{q=0} = 1.02\,\phi - 4.88 \qquad (28)$$

Equation (28) agrees well with equation(27). This equation, however, cannot give accurate values of potential of zero charge but serves as an approximate evaluation of the potentials of zero charge. This is due to the unreliability of the data found in the literature on entropies of hydration or ΔH_h and the electronic work function.

A simple derivation of the relation between potential of zero charge and work function could be obtained fairly rigorously as follows,

$${}^m\Delta^s\bar{\phi} = {}^m\Delta^s\bar{\Psi} + \chi_m - \chi_s \qquad (29)$$

TABLE 2

PHYSICOCHEMICAL CHARACTERISTICS OF THE METALS AND THE CONSTANT IN EQUATION (24)

Metal	z	H_s	H_i	S	T S	H_h	ϕ	$ze_o^-\phi$	$\frac{1}{ze_o^-}G$	E_o	$E_{q=0}$	$\bar{E}_o$	Constant
		kcal	kcal	cal/deg	kcal	kcal	eV	kcal	eV	V	V	V	V
Ag	1	69.1	174.0	7.46	2.2	116.5	4.73	109.0	0.67	+0.80	-0.05	0.85	-0.18
Cu	2	81.5	643.2	-31.6	- 9.4	506.5	4.80	220.8	0.15	+0.34	-0.04	0.38	-0.23
Zn	2	31.2	628.2	-35.4	-10.5	492.5	4.25	196.0	-0.40	-0.76	-0.63	-0.13	-0.27
Cd	2	26.8	594.7	-26.9	- 8.0	436.0	4.01	185.0	0.19	-0.40	-0.90	0.50	-0.31
Hg	2	14.5	670.3	-23.9	- 8.1	442.1	4.53	209.0	0.88	+0.86	-0.21	1.07	-0.19
Pb	2	46.5	515.5	-10.4	- 3.1	359.1	4.15	191.4	0.32	-0.13	-0.69	0.56	-0.24
Sn	2	78.0	503.6	-18.2	- 5.4	384.0	4.38	202.0	0.02	-0.14	-0.35	0.21	-0.19
Al	3	67.5	1223.6	-81.7	-24.3	1102.8	4.25	294.0	-1.18	-1.67	-0.50	-1.17	0.01
Ga	3	52.0	1317.0	-93.2	-27.8	1098.0	4.20	290.5	0.11	-0.52	-0.60	0.08	0.03
Tl	3	42.8	1293.2	-57.4	-17.1	1003.0	3.68	254.0	1.39	+0.72	-0.80	1.52	-0.13
Bi	3	47.8	1126.0	-35.0	-10.1	850.0	4.40	304.5	0.42	+0.23	-0.40	0.63	-0.21

TABLE 3

CALCULATED DATA ON THE QUANTITY ($E_o^k - {}^k\Delta^s\bar{\varphi}_o - \phi^k$ + constant)

FOR VARIOUS METALS

Metal	$E_o^k - \phi^k - \frac{1}{ze_o^-}\sum G$ - 0.22	
Ag	-4.80	
Cu	-4.81	
Zn	-4.81	
Cd	-4.80	
Hg	-4.75	
Pb	-4.80	Average - 4.78
Sn	-4.74	
Al	-4.83	
Ga	-5.00	
Tl	-4.55	
Bi	-4.79	

${}^m\Delta^s\bar{\varphi}$ is inner or galvani potential difference for the metal-solution interface. ${}^m\Delta^s\bar{\Psi}$ the outer or volta potential difference and χ_m and χ_s are the surface potential of the metal and solution respectively. When the charge on the metal is zero, ${}^m\Delta^s\bar{\Psi} = 0$ and

$$ {}^m\Delta^s\bar{\varphi}_{q=0} = \chi_m - \chi_s \qquad (30) $$

Now,

$$ -\phi = \mu_e + ze_o^- \chi_m \qquad (31) $$

where ϕ is the work function and U_e the chemical potential of the electron. Substituting (31) into (30) for χ_m,

$$ {}^{m}\Delta^{s}\bar{\phi}_{q=0} = \frac{-\phi - \mu_e}{ze_o^-} - \chi_s \qquad (32) $$

Now, subtract ${}^{m}\Delta^{s}\bar{\phi}_{N.H.E.}$, the metal-solution inner p.d. of the normal hydrogen electrode, from both the sides of equation (32)

$$ E_{q=0} = {}^{m}\Delta^{s}\bar{\phi}_{q=0} - {}^{m}\Delta^{s}\bar{\phi}_{N.H.E.} = \frac{-U_e}{ze_o^-} - \chi_s - {}^{m}\Delta^{s}\bar{\phi}_{N.H.E.} - \frac{\phi}{ze_o^-} $$
$$ \Delta\bar{\Phi}_{Pt\text{-}m} \qquad\qquad \Delta\bar{\Phi}_{Pt\text{-}m} \qquad (33) $$

Thus we have the relation between potential of zero charge and the work function similar to the one given by Ukshe, Levin and Novakovskii[14]. From equation (32) it also follows,

$$ {}^{m}\Delta^{s}\bar{\phi}^{1}_{q=0} - {}^{m}\Delta^{s}\bar{\phi}^{2}_{q=0} = -\frac{\phi^1 - \phi^2}{ze_o^-} - \frac{U_e^1 - U_e^2}{ze_o^-} - (\chi_s^1 - \chi_s^2) \qquad (34) $$

Superscripts 1 and 2 refer to the metals. Thus, difference in the potentials of zero charge of the two metals is equal to the contact potential difference of the two metals but for difference in the chemical potentials of the electron in the two metals and the two different surface potentials of the solvent on two metals. No calculations are as yet available to test the validity of equations (33) and (34).

In conclusion of this section, we would like to mention that as yet there is no satisfactory theoretical relation between potential of zero charge and a property of the metal, for all the metals. Ukshe, Levin and Novakovskii relation, i.e. equation (28) does not apply to

the transition metals. Also, large deviations to the Vasenin's relation are observed. Also potential of zero charge is a function of the metal surface and the system as well (Section III).

III. ASPECTS OF POTENTIAL OF ZERO CHARGE IN RELATION TO THE SYSTEM

From the treatment given in Section II, it may appear that the potential of zero charge is a property of the metal. However, potential of zero charge does vary under conditions of the experiment. As previously pointed out $\Delta\Psi_{q=0} = \chi_m - \chi_s$. Any change in χ_m or χ_s will change the potential of zero charge. In the presence of ionic adsorption the term $\Delta\Psi$ may not be taken equal to zero. So it is quite obvious that in any process which changes χ_m or χ_s will also have an effect in changing the value of potential of zero charge.

1. Ionic Adsorption

When the ions are specifically adsorbed in the double layer, an excess charge arises due to the presence of the ions in the inner Helmholtz layer and, therefore, ions of the opposite charge gather at the outer Helmholtz plane and the diffuse layer, to maintain electroneutralityin the system. Thus, this causes a potential drop across the dipolar layer of the ions of the opposite sign and also outside the region confined by the planes through the center of the charges.

Thus, the potential of zero charge (value in the absence of specific adsorption) will become more negative as specific adsorption of anions, for example, increases. Also, if there is specific adsorption

of cations the potential of zero charge will shift to more positive values.

In most cases the data for shift of potential of zero charge with specific adsorption have been obtained on Hg. Grahame[18] has determined this shift for various anions and cations. The Table (4) below shows the typical variation of potential of zero charge with ionic adsorption.[13]

TABLE 4

VARIATION OF POTENTIAL OF ZERO CHARGE WITH IONIC ADSORPTION

Solution	$E_{q=0}$ (N.H.E.)	Solution	$E_{q=0}$ (N.H.E.)
1 N KOH	- 0.19	1 N HCl	- 0.30
1 N K_2CO_3	- 0.20	1 N $BaCl_2$	- 0.28
1 N K_2HPO_4	- 0.21	1.0 N $LaCl_3$	- 0.32
1 N Na_2SO_4	- 0.20	1 N KBr	- 0.37
1 N H_2SO_4	- 0.23	3 N KCNS	- 0.49
1 N CH_3COONa	- 0.24	3 N KI	- 0.59
1 N KNO_3	- 0.28		

2. Organic Adsorption

Adsorption of organic molecules is on the competitive basis with water. If it is a neutral molecule it will usually get adsorbed to maximum extent when water gets randomized in its orientation; i.e. when the number of water molecules in each orientation is the same. If the organic molecules get adsorbed to a large extent this will change the

dielectric constant and the number of dipoles on the surface. This will give rise to a change in the magnitude of the surface potential and as a result the potential of zero charge will change. If the organic molecule has a specific interaction with the metal surface (e.g., π electron and d-band interactions, etc.) the shift of the potential of zero charge will be pronounced. As a general rule if the organic dipole's negative end is towards the metal, then the potential of zero charge will shift towards more negative value. And if the positive pole of the organic dipole is towards the metal, potential of zero charge will shift to more positive values.

3. Surfaces Covered with Gases

It is well known in work function measurements that when the surface is covered by adsorbed gases, work function changes. Now,

$$- \phi_m^e = \mu_m^e + Ze_o^- \chi_m \qquad (35)$$

where ϕ_m^e electronic work function, μ is the chemical potential of the electron in the metal and χ_m is the surface potential at the metal surfaee in vacuum. A minus sign arises for ϕ_m^e because the work involved in equation (35) is bringing the electron e_o^- from ∞ into the bulk phase. Thus, when the metal surface is covered by the adsorbed gas, the μ_m^e (bulk property) presumably remains the same and χ_m changes to change the work function of the metal. If the adsorbed layer is negatively charged the work function becomes $\phi e_o^- + 4\pi N\mu$, where $N\mu$ is the electric moment per unit area and $\phi e_o^- - 4\pi N\mu$ when the layer is positively charged. (The adsorbed layer sets up an image charge of opposite sign

in the metal giving rise to the dipole moment.) There is a possibility of covalent linkage which has not been considered here. So, one can see if there is an adsorbed layer of gas on the metal, the potential of zero charge will be different than that in absence of an adsorbed layer, since there is a linear relation between work function and potential of zero charge. Thus, when the adsorbed layer is negatively charged (the work function increases because of the negatively charged layer on the surface) it will shift the potential of zero charge to a more positive value.

If the gas is absorbed inside the metal it will change the bulk properties of the metal. The magnetic susceptibility for instance is changed by absorbed hydrogen. The chemical potential of an electron will be different in case of a metal-hydrogen phase changing the work function. And, hence, potential of zero charge is different when a metal has absorbed hydrogen in its lattice. Krasikov and Kheifets[19] have shown that potential of zero charge of Pt and Co changes to more positive values with the amount of absorbed hydrogen.

4. pH Variation

It is known[19] that the potential of zero charge of metals like Pt, Pd, Ni, Fe, Co varies with hydrogen ion concentration. Whereas metals like Ag, Cu, Zn,Pb and Au do not have a change in their potentials of zero charge with pH. Krasikov and Kheifets[19] have pointed out that the potential of zero charge varies with pH in case of metals which absorb hydrogen. Also, according to them the variation of potential of zero charge with pH is caused due to hydrogen adsorption and/or

absorption in the lattice of the metals. This is not supported by theory or confirmed by experiment. Since hydrogen in the metal decreases the work function (due to increasing the Fermi energy) and shifts potential of zero charge to more negative values; contrary to the idea of Krasikov and Kheifets. And the layer of the adsorbed hydrogen atoms on platinum or palladium (for which the effect of pH on potential of zero charge is very much pronounced) has a positive charge and thus decreases the work function again and potential of zero charge is more negative than it should be. Thus, it can be seen there is no satisfactory explanation for the pH-dependence of the potential of zero charge as yet.

There is no good correlation of the dependence of potential of zero charge on the factors of the system, by which we would be able to predict precisely the effect of the system on potential of zero charge. More work in this regard is to be stressed.

IV. METHODS OF DETERMINATION OF THE POTENTIAL OF ZERO CHARGE

1. Surface Tension Methods

(a) Electrocapillary curves

The electrocapillary curves usually are obtained by capillary electrometer which was first used by Lippmann. The interphase between a liquid metal and the solution is made in a thin capillary tube. The height of mercury required to bring the interphase to a given point on the capillary is proportional to the interfacial tension. The proportionality constant is obtained from a reference solution of known

electrocapillary properties. The modern version has been described by several authors.[20] The obvious limitation of the electrocapillary measurement is that this method can only be used for liquid metals, e.g., Hg, amalgams and liquid metals in molten electrolytes.[21] Karpachev et al.[22] have studied Sn, Pb, Cd, Zn, Tl, Ag, Sb, Bi, Al, Ga, Te as well as Tl, Sn and Bi amalgams and alloys like Sn-Zn, Sn-Au and Bi-Te in LiCi-KCl eutectic. A capillary electrometer can be substituted by a dropping mercury electrode where the dropweight method of measuring interfacial tension is used.

(b) Contact Angle Method

Contact angle measurement can be used to determine the electrocapillary curves. Measurement of the contact angle θ between a gas bubble and a metal surface immersed in an electrolyte makes it possible to observe the interfacial tension changes. The contact angle is related to the interfacial tensions as follows:

$$\text{Cos } \theta = (\gamma_{g,m} - \gamma_{s,m})/\gamma_{g,s} \qquad (36)$$

where $\gamma_{g,m}$ is the interfacial tension of gas/metal and $\gamma_{g,s}$ that of gas/solution. Möller[23] was the first to show that contact angle changed with potential. Frumkin et al.[24] have determined electrocapillary curves for Pt, Ga, Zn, Ag, Hg as well as amalgams of Tl. The values of electrocapillary maximum of mercury obtained by this method compares well with that obtained by other methods. The contact angle method is not as accurate as the electrocapillary method. Frumkin has suggested that while $\gamma_{s,m}$ varies with potential, $\gamma_{g,m}$ and $\gamma_{g,s}$

remain constant. $\gamma_{g,m}$ remains constant because of a moisture film between metal and gas. This type of behavior for ethanol-water mixtures on Hg has been confirmed by Tverdovskii and Frumkin.[25] At higher concentration of ethanol, the contact angle is small and independent of potential. These authors suggested that at high ethanol cnncentrations the moisture film between gas and metal has bulk properties and $\gamma_{g,m}$ then varies with potential in the same way as $\gamma_{s,m}$ resulting in a constant contact angle.

This method seems to be good for getting potential of zero charge of solid metals but difficulties may be associated with it due to contamination of the metal surface due to oxygen, etc. Also, the method is not as accurate as electrocapillary methods.

2. Change of Surface Area

In a dropping mercury electrode since the mercury-solution interface is constantly expanding, a current must be passed if the potential of the electrode (or the charge density on the surface) is to remain constant. Even if the rate of formation of the new interphase is not known, at potential of zero charge no current will flow. Frumkin[27] has used this method to determine electrocapillary maximum of mercury.

This method is also useful for solid metals. While the surface area changes at a fixed potential, the charging current is measured. This charging current will be zero at potential of zero charge and is of opposite sign on either side of the potential of zero charge. The charge q on the electrode is given by

$$q = Aq_m \qquad (37)$$

where A is the area of the electrode and q_m is the charge per unit area. Differentiating equation (37) one has

$$dq = q_m dA + A dq_m \tag{38}$$

Hence,

$$i = dq/dt = q_m (dA/dt) + AC (dE/dt) \tag{39}$$

where C is the capacity per unit area of the interface and E is the potential. If the area of the electrode is increased at constant potential or the rate of change of potential with time is kept small compared to the rate of change of surface area, the second term on the r.h.s. of equation (39) may be considered negligible and the charging current becomes proportional to q_m

$$i \doteq q_m (dA/dt) \tag{40}$$

and approaches zero for any value of dA/dt as the potential approaches the potential of zero charge. There are three methods available to change the surface of the metal-solution interphase.

1. Immersion method.[28]
2. Scraping of the surface.[29]
3. Crystal cleavage.

Results of the first two methods are available. Both of these measurements have been carried out in chloride solutions, where specific adsorption occurs. Another difficulty with the method is that if there is a current due to a Faradaic process taking place, the reversal of current which one would observe may not be at potential of zero charge.

3. Capacity measurements

This method is the most extensively used one for getting potentials of zero charge of solid metals. The capacitance of the electrode is measured by a variety of techniques as a function of potential. A.c. techniques like bridge methods, or measuring a.c. potential difference developed across the cell by passing alternating current can be used for the measurement of capacity of the electrode.

The potential of zero charge is discernible on the capacity-potential relation in dilute solutions of the order of 0.01 M or less. The capacity of an electrode can be represented as,

$$1/(C_{m-s}) = 1/(C_{m-2}) + 1/(C_{2-s}) \tag{41}$$

C_{m-s} is the capacitance of metal-solution interface which can be split up into two terms, C_{m-2} capacitance of the outer Helmholtz plane and C_{2-s} the capacitance of the diffuse double layer. Now,

$$\Phi_{2-s} = (zkT/2\pi)\ \sinh^{-1}\ (q/2A) \tag{42}$$

where

$$A = (kTc/2\pi)^{1/2}$$

$$\frac{1}{C_{2-s}} = \frac{\partial \Phi_{2-s}}{\partial q} = \frac{zkT}{4\pi A} \cdot \frac{1}{(1 + q^2/4A^2)^{1/2}} \tag{43}$$

At the potential of zero charge, it is obvious from equation (43) that C_{2-s} is very large and its contribution to the total capacitance is insignificant and one observes a minimum in the C-E plot. This method has been used very successfully for the determination of the potential of zero charge and seems to be very good. However, it cannot be used

when there is a pseudo-capacitance[30] due to some reaction, since the pseudo-capacitance is usually large compared to the ionic double layer capacitance and acts effectively in parallel with it. In addition the existence of adsorbed species on the surface modifies the double layer capacitance substantially and can also cause a shift in the potential of zero charge.

4. Adsorption Methods

(a) Ionic Adsorption[31]

The charge on the metal q_m can be defined as, $-q_m = z_+ \Gamma_+ F + z_- \Gamma_- F$, where F is the Faraday, z_+ and z_-, the valence of the ions, Γ's are surface excesses, subscripts + and - refer to the cation and anion respectively. When the charge on the metal is zero, $z_+ \Gamma_+ = - z_- \Gamma_-$, z_+ and z_- are related to the number of ions produced from the salt, ν_+ and ν_- as $z_+/z_- = - \nu_-/\nu_+$ and we have $\Gamma_+/\nu_+ = \Gamma_-/\nu_-$. Thus, the number of ions, at potential of zero charge, of a 1:1 electrolyte is equal. Whereas at other potentials there will be different numbers of cations and anions. This is the basis of this method. Thus, if cation and anion are labeled and the radioactive ions emit radiation of different energies, it will be possible to get the number of ions individually which are present in the double layer.

Difficulties associated with this method: specific adsorption of ions (can be avoided by very dilute solutions). And it is not always possible to find a suitable pair of a cation and an anion so that the two tracers can be detected simultaneously. Another problem is that to get fairly large change in concentration of solution a large area of the

electrode must be used. The method is not accurate.

(b) Use of a constant low concentration of radiotracer neutral organic molecule with different concentration of electrolyte

In this method, which was developed in this laboratory[32] the argument is as follows. The adsorption of neutral molecule depends upon the electric field across the Helmholtz layer. Thus, for a given potential difference across the Helmholtz layer the value of the coverage θ of the organic molecule is fixed for a small given concentration of the species. The value of the potential difference across the Helmholtz layer, at the constant $\Delta\phi$ (metal-solution Galvani potential difference), varies with the concentration of the electrolyte. But at potential of zero charge (when there is no field across the double layer except for the $\Delta\chi = \chi^m - \chi^s$ value) the value of p.d. across outer Helmholtz layer is constant irrespective of the concentration of the electrolyte. This would, at potential of zero charge give the same value of θ organic. Thus, if we plot θ_{org} - $E_{N.H.E.}$ varying the concentration of electrolyte which does not give rise to specific adsorption we will observe an intersection of the various θ_{org} - $E_{N.H.E.}$ plots.

Preliminary results of this method are available. Difficulties involved in the method are specific adsorption and the shift in the potential of zero charge due to adsorption of the organic molecules. The θ_{org} - E plot is distinctly unobtainable at very low concentration. The concentration used were 1 N, 0.1 N, 0.01 N, $NaClO_4$. It is very probable[33,34] specific adsorption is involved at 1 N $NaClO_4$. The shift of potential of zero charge may be of the order of 50 - 60 mv. Also the θ_{org} determined is accurate within 10 - 15%. In general potential of zero

charge values obtained are accurate to $\pm$ 50 mv. The shift due to organic adsorption can be small if the θ_{org} is very low. This can be kept within the accuracy of the method by keeping the concentration of the organic low. The presence of specific adsorption is seen in the difference in the magnitude of maximum adsorption at different concentrations.

5. Friction Method

(a) The Pendulum Method

Rehbinder and Wenstrom[35] claimed the existence of a relation between the interfacial tension of the metal-electrolyte system and the hardness or tensile strength of the metal surface. They measured the logarithmic decrement of the oscillations of a Herbert pendulum whose suspension is a small glass sphere about 0.5 mm. diameter resting on the metal surface covered by a drop of an electrolyte solution in which a small luggin capillary and small platinum wire (counter electrode) are dipping. Logarithmic decrement of the oscillations is plotted versus potential. These curves have a close similarity to the electrocapillary curves on Hg. Frumkin[36] has pointed out that if the tension on the metal is high in order to cause deformation of the surface and the fulcrum of the pendulum is made of ground glass the decrement of the oscillations observed is due to the hardness of the metal surface. At the potential of zero charge the hardness is maximum. But if the tension at the fulcrum is reduced and the ground glass ball is replaced by a smooth one, then deformation of the metal is not caused and dispersion or deformation of the surface does not determine the decrement of

the oscillations, but is determined by the external friction as shown first by Bowden and Young.[37] Rehbinder and Wenstrom did not provide any theoretical basis for the dependence of hardness on potential or charge. Bockris and Parry-Jones[38] used a method similar to that of Rehbinder and Wenstrom. However, they have shown that friction probably determines the decrement of the oscillations of the pendulum and not the hardness. This view has been supported by the measurements of Bowden and Young,[37] and Staicopolous.[39] The friction between the two surfaces is the function of the metal-solution potential difference. On the basis of a physical picture, due to the presence of repulsion of charges on the metal-solution interface the friction will be low. As the charge decreases the repulsion decreases, and the friction increases. At potential of zero charge the absence of charge causes the friction to rise to a maximum and in some cases seizure of the metal surfaces occurs. The p.d. across the metal solution interface thus changes the friction between surfaces and probably not the hardness.

(b) The Angle of Inclination Method

The actual measurement of friction is possible as a function of potential. Bowden, Barker and Young[35] have devised an ingenious method for the measurement of static friction as a function of potential. The method in essence is as follows. A platinum wire was stretched taut in a glass cell which could be freed of gases and filled with an electrolyte. There was a platinized platinum auxiliary electrode and a connection for a reference electrode. The wire was provided with a cylindrical platinum slider. The cell was mounted on a system so that the angle of

inclination of the wire could be changed. The angle at which the sliding occurs is a measure of the friction. $\mu = \tan\alpha$, μ is the static coefficient of friction and α is the angle of inclination. This method for the determination of potential of zero charge of various metals, is exceedingly promising. Even if the slider damages the surface of the wire, it will not change the coefficient of friction.[35] Direct measurement of friction is an added advantage. Also slight impurities on the surface do not give high values of friction* (which is a very good indication of the extent of surface contamination). With a similar apparatus and a high purity system potential of zero charge can be measured accurately. This apparatus has not been used except for the measurements made by Bowden and Young on platinum. The method itself is very simple. The difficulties of the method: As yet no direct theoretical correlation between friction and potential difference across the metal-solution interface has been obtained. The pendulum method suffers the drawback of presence of impurities and easy contamination because very small quantities of solution are involved. The second method of angle of inclination is no doubt promising but no experimental data have been obtained for metals other than platinum with this method.

6. Zeta Potential

(a) Electrophoretic Mobility Measurements

The electrophoretic mobility of very thin wires has been

---

*Bowden and Young[35] got μ_{Pt} (at 0.3 volt) = 3.4 and μ_{Pt} (about 1 volt) = 0.7; with H_2s covered wires, the friction was independent of potential.

investigated to obtain potential of zero charge of platinum.[40] Electrophoretic mobility measurement essentially consists of determining the rate of motion of charged particles under the influence of a field (potential gradient). The velocity of the thin wire is given by,

$$V = \zeta DX/4\pi\eta = q\eta X$$

when $q=0\ \zeta = 0$, where X is the field applied to the electrolytic solution, D dielectric constant of the medium. ζ is the zeta potential, η is the intrinsic mobility. As the charge on the metal changes, the direction of the movement of the wire changes. Thus, at potential of zero charge no movement of wire would occur and on either side of it the direction of the movement is different. First, the metal wire must be very thin which is not always possible. Also the problem of specific adsorption is involved. In the presence of specific adsorption when $q^m = o$, $\zeta \neq o$.

(b) Ultrasonic Method[42]

In an acoustic field, due to the periodic distribution of charge, a periodic change in potential ($\Delta\mathcal{E}$) is set up.[41,42] For an electrode, $dq = C\ d\ \bar{E}$, q is the charge, C its capacity and $\bar{E}$ its potential in the rational scale. As the work of distribution of the charges takes place at the expense of the energy of the acoustic wave, so,

$$A = \frac{1}{2} C_{\bar{E}} (\Delta\mathcal{E})^2$$

The work of redistribution is proportional to the energy of acoustic waves.

$$\Delta A/\beta = \Delta\omega = \frac{I}{v} \Delta V$$

where v is the volume element, V and I are velocity and intensity of the acoustic waves. β is the coefficient of transformation of sound energy into electrical energy.

$$\Delta \mathcal{E} = \left(\frac{2\beta I (\Delta V)}{C_E^2 v}\right)^{1/2}$$

At potential of zero charge where capacity is a minimum and double layer is diffuse in character one would get maximum $\Delta \mathcal{E}$ (that is the ultrasonic potential). The method has been speculatively suggested by Kukoz and Kukoz.[42] No experimental work has been carried out. Another difficulty is that the objection is raised on the grounds of low Debye effect. The above authors[42] claim that the field intensities inside the hydration sheath of an ion and the double layer may differ considerably in the magnitude.

7. Repulsion of Double Layers on Two Wires

A repulsive force between charged surfaces acts at distances of the order of the effective depth of the ionic atmosphere. Thus, the liquid film will not rupture and molecular contact will not be established between the two crossed metallic fibres if the external force acting on them is less than the repulsive force barrier. The energy of interaction per unit area u (H) is given by,

$$u\ (H) = N/G$$

N is the force of repulsion between convex surfaces at the closest approach, H, in the solution of the electrolyte G is the geometric factor which depends only on the curvature and orientation of the surfaces in the region of closest approach. For cylindrical fibres of

radii r_1 and r_2,

$$G = 2\pi\sqrt{r_1 r_2}\sin\theta$$

Schematically the apparatus of Veropaeva, Deryagin and Kabanov[43] is shown in the figure (4) below.

Each fibre could be charged to any desired potential. The fibres of platinum were 300 μ in diameter. One of the fibres was attached to an elastic torsion balance of phosphor bronze with a mirror and the other to a moving part driven by a motor which could bring the fibre close to the other. The two fibres rotate around a common axis to avoid slippage of one past another. The whole apparatus was sealed in a vessel. The apparatus was fully automated to record in units of force, as a function of potential. When the fibre attached to drive the system was drawn close to the other fibre, a deflection in the light beam shone on the mirror was caused. An arrangement was provided to reverse the motion of the fibre at the instant of the contact between the two fibres. The fibre attached to torsion balance keeps on moving in the same direction as the fibre approaching it until the two touch each other. The deflection caused thus gives a direct measure of the force barrier. At potential of zero charge, there being no charge on the metal, the repulsive force barrier is at minimum. Figure 6. Thus it can be seen that this method is also a good method to obtain potential of zero charge of metals. The method is rather complex and unless automated which involves a lot of instrumentatinn, is little clumsy to work with. The solutions must be very dilute which means little or no specific adsorption.

V. SUMMARY

Potential of zero charge is one of the important electrochemical characteristics of a metal. This point of view has been stressed with the help of the rational scale of potentials. The next section deals with the semi-empirical and theoretical attempts to relate potential of zero charge with some of the properties of the metal. However, it must be mentioned that potential of zero charge has been found to depend upon the system to some extent and as yet there is no correlation between the factors of the system and the experimental values of potential of zero charge. Among the methods of determination, the capacitance method is the classical method. Friction method of Bowden and Yuung[35] seems to be promising along with the method of repulsion of double layers[43] of two fibres. Dipping wire method of Jekuszewski is also good. The organic adsorption method (Dahms and Green[32]) and the pendulum method[35,38,39] are fairly good. Values of potential of zero charge are compiled in Table 5. It can be seen that the agreement of the potential of zero charge values obtained by different methods is not at all good. This means lots more work is needed under very well defined conditions (Section III). There must be agreement between the values obtained by several different methods. Also, at the present, the theoretical correlations which exist are not very satisfactory for the case of transition metals. Novakovskii, Ukshe and Levin have omitted all of the transition metals from their treatment.

TABLE 5

POTENTIAL OF ZERO CHARGE VALUES OF METALS

Metal	PZC	Method	Ref.
Ag	.08	Cataphoresis of suspended particles	44
	.04	Capacity measurements	44
	.05	Capacity measurements	19
	-.7	Capacity measurements	45
Al	-.52	Electrode dipping	28
Au	.3	Wire stretching	46
	.3	Adsorption shift	32
	.3	Capacity measurements	47
Bi	-.36	Electrode dipping	28
Cd	-.90	Capacity measurements	56
	-.70	Hardness and friction	35
	-.68	Capacity measurements	19
	-.75	Capacity measurements	19
	-.90	Capacity measurements	19
	-.47	Capacity measurements	19
Cr	-.45	Contact angle	49
Cu	-.2	Hardness and friction	39
	.10	Contact angle	12
	-.06	Capacity measurements	50
	+.07	Electrode dipping	28
	-.03	Capacity measurements	19

TABLE 5 (Continued)

Metal	PZC	Method	Ref.
Fe	-.28	Adsorption threshold	51
	-.37	Capacity measurements	46
	-.38	Capacity measurements	19
	-. 85	Capacity measurements	52
Ga	-1.2	Contact angle	20
	-.90	Capillary electrometer	20
	-.62	Capillary electrometer	53
	-.61	Contact angle	24
Hg	-.194	Capillary electrometer	2
	-.194	Dropping Hg electrode	54
	-.19	Contact angle	53
	-.190	Capacity measurements	2
Ni	.21	Work function	3
	+.19	Electrode dipping	28
	-.26	Polarization curves	55
	-.2 to -.35	Capacity measurements	19
	-.33	Capacity measurements	52
Pb	-.69	Capacity measurements	56
	-.69	Capacity measurements	48
	-.56	Hardness and friction	38
	-.62	Hardness and friction	38
Pd	+.2 to -.4	Capacity measurements	19

TABLE 5 (Continued)

Metal	PZC	Method	Ref.
Pt	.17	Zeta potential	40
	.29	Hardness and friction	38
	.32	Hardness and friction	37
	.27	Contact angle	24
	-.5 to .35	Capacity measurements	19
	.20	Repulsion of D.L.	43
	.2	Ion adsorption	57
Sn	-.24	Hardness and friction	38
	-.35	Capacity measurements	38
	-.38	Electrode dipping	28
Te	.51	Hardness and friction	38
	.61	Hardness and friction	35
Tl	-.69	Hardness and friction	35
	-.82	Capacity measurements	56
Zn	-.63	Hardness and friction	35
	-.60	Capacity measurements	19
	-.60 to -.68	Capacity measurements	52
	-.55	Capacity measurements	58

REFERENCES

1. Frumkin: Izv. Khim. Otd., Akad. Nauk. 223 (1945); Frumkin, Bagotshii, Iofa and Kabanov: "Kinetics of electrode processes," (Moscow Univ. Press, USSR) 1952; Frumkin: Vestnik Mosk. Universitèta No. 9, 37 (1952).
2. Grahame: Chem. Rev., 41, 441 (1947).
3. Antropov: Zhur. Fiz. Khim. 25, 1494 (1951) "Kinetics of electrode processes and Null Points of Metals." (Council of Scientific and Industrial Research, New Delhi).
4. Bockris, Devanathan and Müller: Proc. Roy. Soc., A274,55 (1963).
5. Foerster: Electrochemic Wassriger Losungen, (Leipzig) 1934.
6. Frolich and Klark: Z. Electrochem., 31, 649 (1925).
7. Volmer: Zhur. Fiz. Khim., 5, 319 (1934).
8. Vagramyan: Electrodeposition of metals (Akad. Sci. USSR, Moscow) 1950.
9. Kalish and Frumkin: Zhur. Fiz. Khim., 28, 801 (1964).
10. Tanaka and Tamamushi: Electrochimika Acta., 9, 963 (1964).
11. Frumkin and Gorodetskaya: Z.Phys. Chem., 136, 215, 415 (1928); Zhur. Fiz. Khim. 5 240 (1934).
12. Vasenin: Zhur. Fiz. Khim., 27, 878 (1953); ibid 28, 1672 (1954).
13. Ukshe and Levin: Zhur. Fiz. Khim. 29, 219 (1955).
14. Novakovskii, Ukshe and Levin: Zhur. Fiz. Khim. 29, 1847 (1955).
15. Frumkin: J. Chem. Phys. 7, 552 (1939).
16. Klein and Lange: Z. Electrochem. 43, 570 (1947); Latimer, Pfizer and Slansky: J. Chem. Phys. 7, 108 (1939).
17. Ershler: Proceedings of the Conference on Electrochemistry (Publ. Akad. Nauk SSSR, Moscow, 1953) p. 357.

18. Grahame, Coffin, Cummings and Poth: J. Amer. Chem. Soc., 74 1207 (1952).

19. Krasikov and Kheifets: Zhur. Fiz. Khim., 31, 1992 (1957).

20. Parsons: "Equilibrium Properties of Electrified Interfaces" in "Modern Aspects of Electrochemistry," Vol. I. Edited by J. O'M. Bockris. Butterworths Scientific Publications, London (1954).

21. Luggin: Z. Phys. Chem., 17, 677 (1895); Hevsey and Lorenz: ibid. 74, 443 (1910).

22. Karpachev and Stromberg: Z. Phys. Chem. A176, 182; Zhur. Fiz. Khim. 10, 739 (1937); 18, 47 (1944); Acta Physicochim. URSS 12, 523 (1940); 16, 331 (1942); Karpachev, Kockergin and Jordan: Zhur. Phys. Khim., 22, 521 (1948); Karpachev and Rodigini: ibid. 23, 453 (1949).

23. Moller: Z. Phys. Chem. 65, 226 (1908).

24. Frumkin, Gorodetzkaya, Kabanov and Nekrasov: Phys. Z. Soviet, 1, 225 (1932); Gorodetzkaya and Kabanov: ibid. 5, 418 (1934); Frumkin: Actualite's sci. industr. Paris 1937, No. 373.

25. Tverdovskii and Frumkin: Zhur. Fiz. Khim. 21, 819 (1947).

26. Frumkin: Actualites Sci. Industr. Paris, No. 373 (1937).

27. Frumkin: Z. Phys. Chem. 103, 55 (1923).

28. Jakuszewski and Kozlowski: Roczniki Chem. 36, 1873 (1962).

29. Eyring, Anderson and

30. Gileadi and Conway:

31. Balashova: Z. Phys. Chem. (Leipzig) 207, 340 (1957).

32. Dahms and Green: J. Electrochem. Soc., 110, 466 (1963).

33. Anderson and Bockris: Electrochim. Acta, 9, 347 (1964).

34. Wroblowa, Kovac and Bockris:

35. Rehbinder and Wenstrom: Acta Physicochim. URSS, 19, 36 (1944); Dokl. Akad. Nauk SSSR, 68, 329 (1949); Zhur. Fiz. Khim., 26, 12, 12 (1952); Zhur. Fiz. Khim., 26, 1847 (1952).

36. Frumkin: Z. Electrochemie, 59, 807 (1955).

37. Bowden and Young: Young, L., Ph.D. Thesis, Cambridge, 1949.

38. Bockris and Parry-Jones: Nature, 171, 930 (1953).

39. Staicopoulos: J. Electrochem. Soc., 108, 900 (1961).

40. Balashova and Frumkin: Dokl. Akad.Nauk SSSR, 20, 449 (1938).

41. Yeager and Hovorka: J. E. Chem. Soc., 98, 14 (1951).

42. Kukoz and Kukoz: Zhur. Fiz. Khim., 36, 703 (1962).

43. Voropaeva, Deryagin and Kabanov: Izv. Akad. Nauk SSSR, Otd. Khim. Nauk, p. 253 (1963).

44. Conway: "Electrochemical Data," Elsevier Publishing Co.

45. Leikis: Dokl. Akad.Nauk USSR, 135, 1429 (1960).

46. Ayazyan: Dokl. Akad. Nauk SSSR, 100, 473 (1955).

47. Schmid and Hackerman: J. Electrochem. Soc., 109, 243 (1962).

48. Borisova, Ershler and Frumkin: Zhur. Fiz.Khim., 22, 925 (1948).

49. Ukshe and Levin: Compt. rend. Akad. Sci. USSR, 105, 119 (1955).

50. McMullen and Hackerman: J. Electrochem. Soc., 106, 341 (1959).

51. Brasher: Nature, 181, 1060 (1958).

52. Krasikov and Sysoeva: Proc. Sci. USSR, Sect.Phys. Chem., 114, 363 (1957); Dokl. Akad. Nauk SSSR, 114, 826 (1957).

53. Vetter: Electrochemische Kinetic, Springer-Verlag, Berlin (1961).

54. Frumkin: Z.Physik. Chem., 103, 55 (1923).

55. Lukovtsev, Levina and Frumkin: Acta. Physicochim. URSS, 11, 21 (1939); Zhur. Fiz. Khim. SSSR, 13, 916 (1939).

56. Borisova and Ershler: Zhur. Fiz. Khim., 24, 337 (1950).

57. Balashova: Compt. rend. Akad. Sci. USSR, 103, 639 (1955).

58. Tsa, Chuan-sin and Jofa: Dokl. Akad. Nauk, 131, 137 (1960).

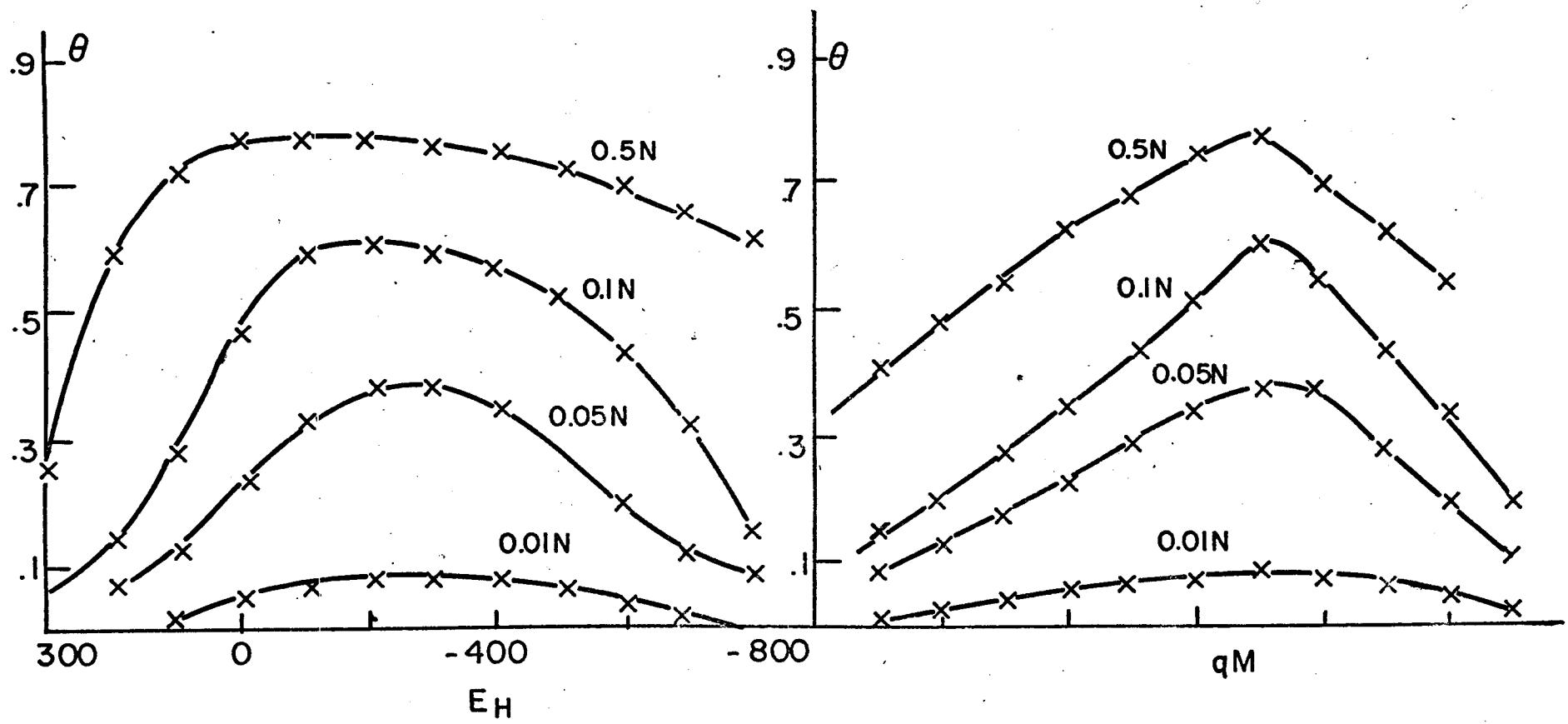
θ
.9
.7
.5
.3
.1
0.5N
0.1N
0.05N
0.01N
300
0
-400
-800
E_H
θ
.9
.7
.5
.3
.1
0.5N
0.1N
0.05N
0.01N
qM

FIG. 1

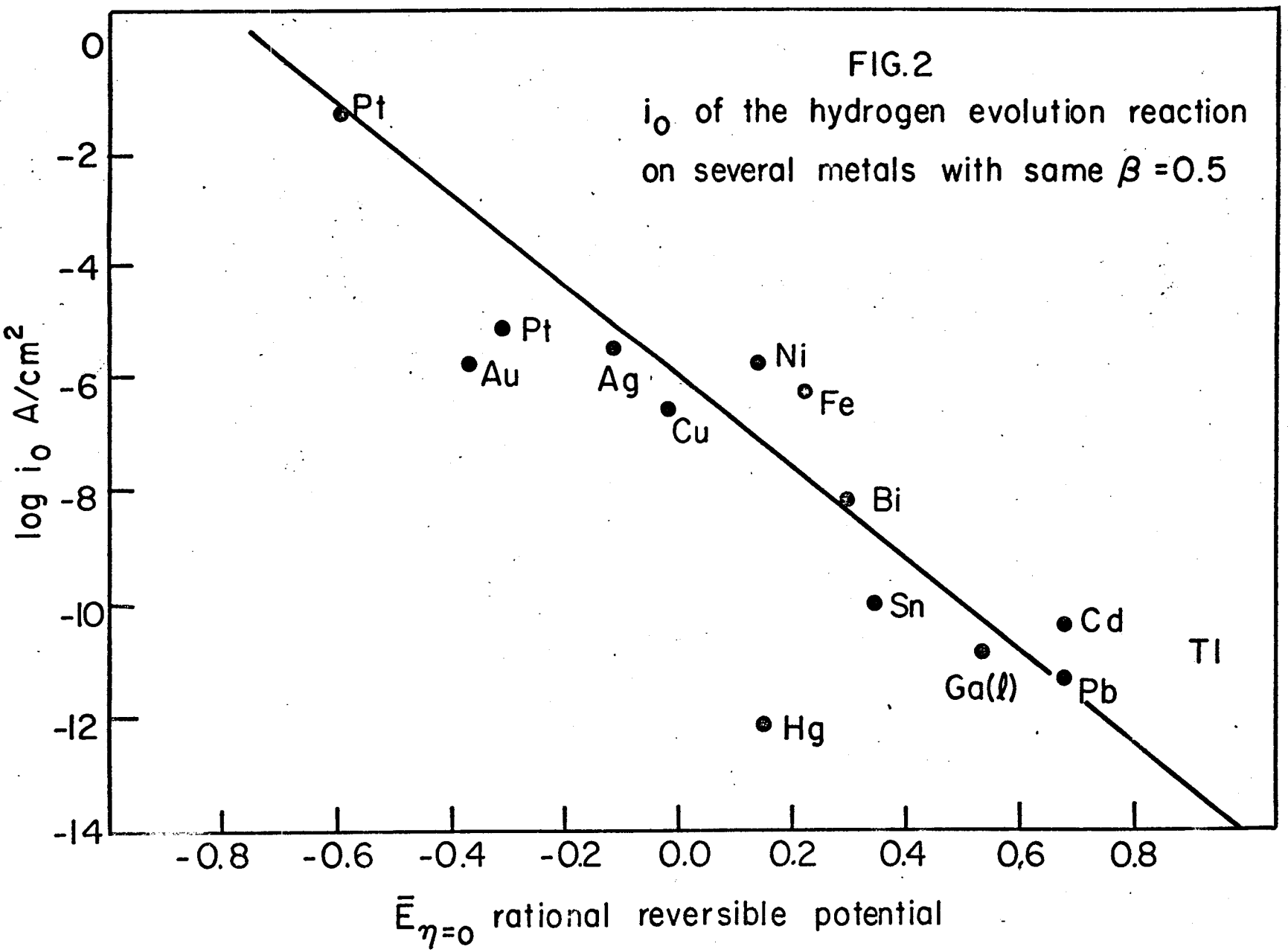
FIG.2
i_o of the hydrogen evolution reaction
on several metals with same β =0.5
log i_o A/cm^2
0
-2
-4
-6
-8
-10
-12
-14
-0.8
-0.6
-0.4
-0.2
0.0
0.2
0.4
0.6
0.8
$\bar{E}_{\eta=0}$ rational reversible potential
Pt
Pt
Au
Ag
Cu
Ni
Fe
Bi
Sn
Cd
Tl
Ga(ℓ)
Pb
Hg

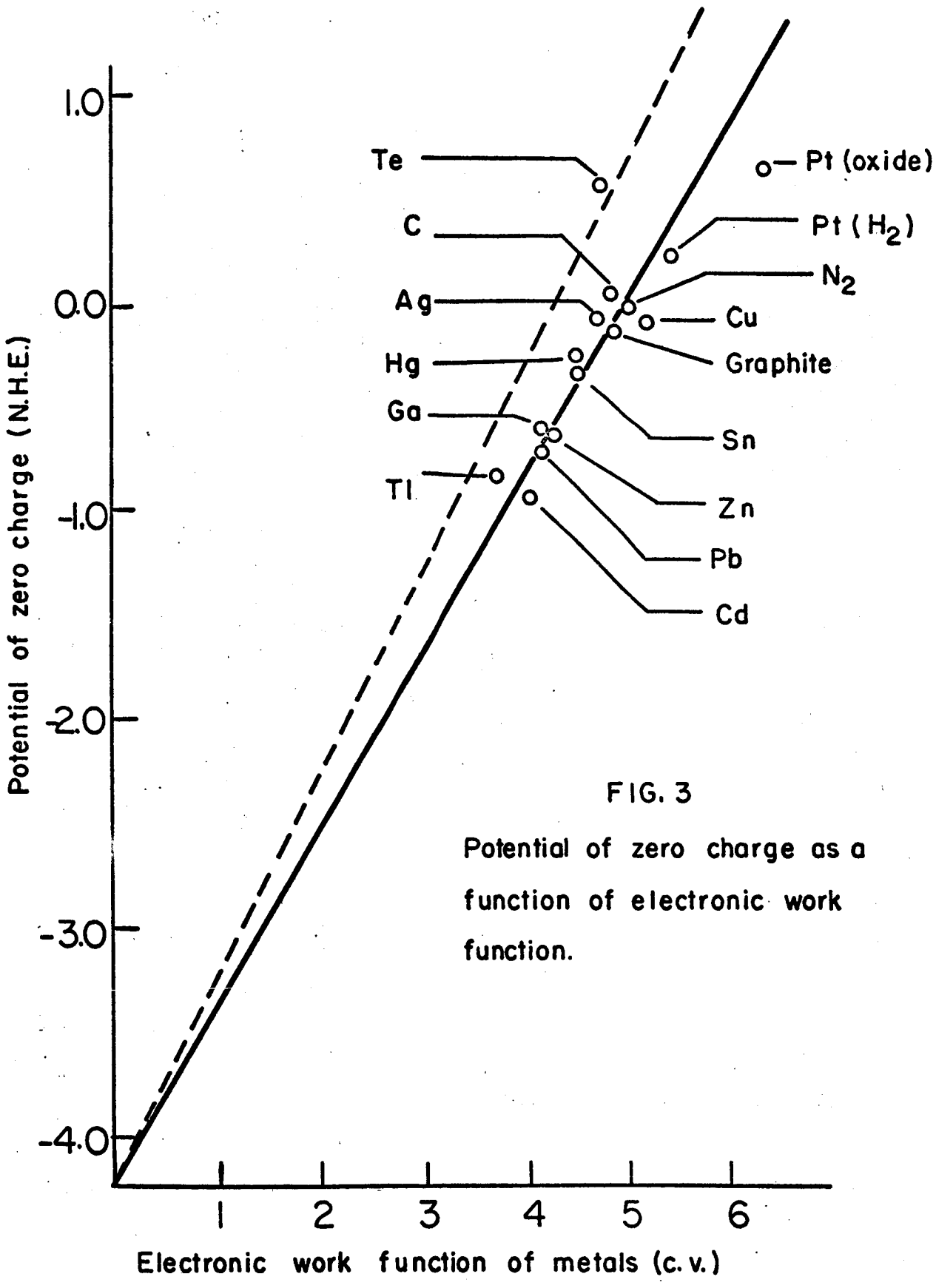

FIG. 3

Potential of zero charge as a function of electronic work function.

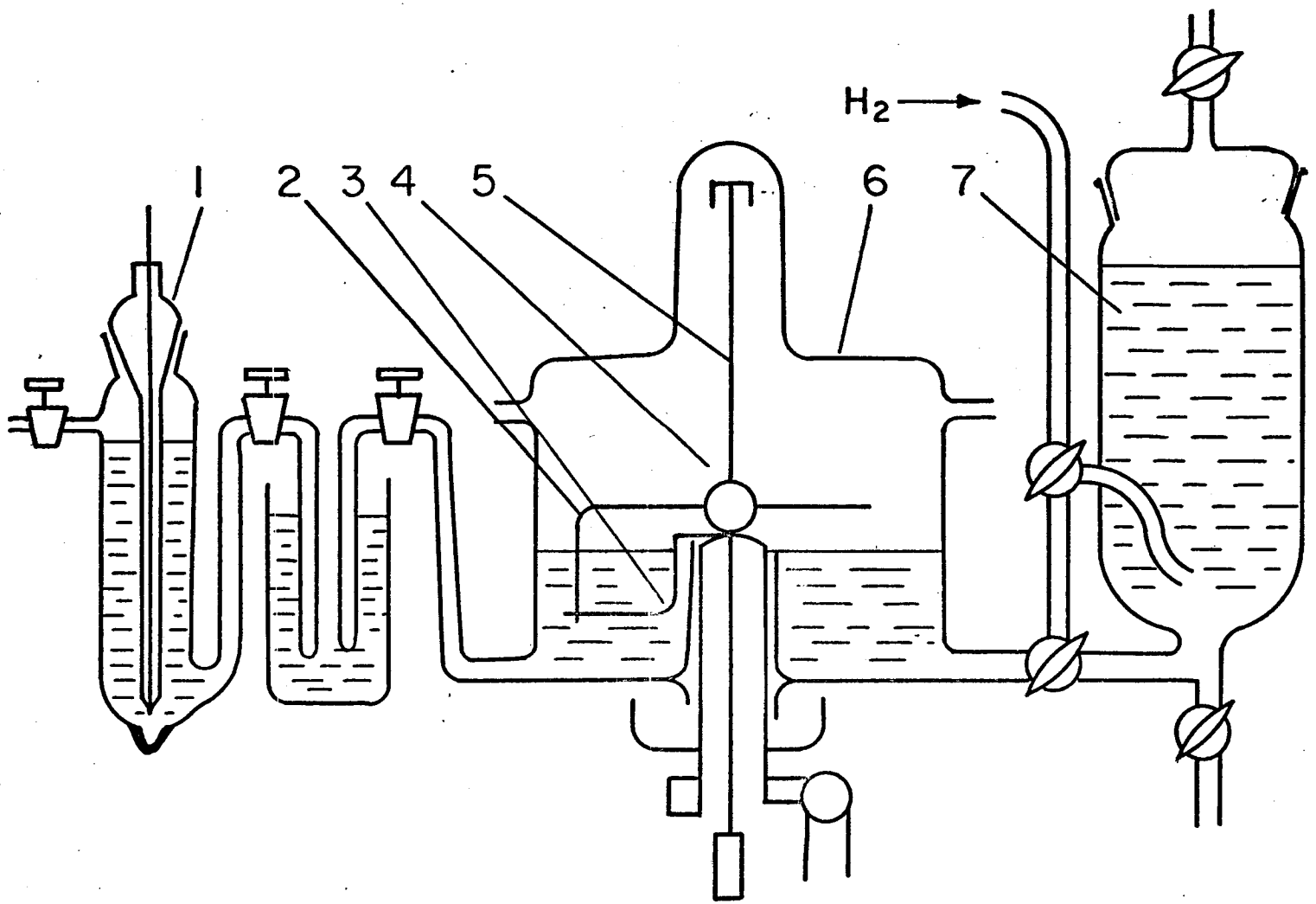

FIG. 4 Schematic diagram of the apparatus of Voropaeva, Deryagin and Kabanov.

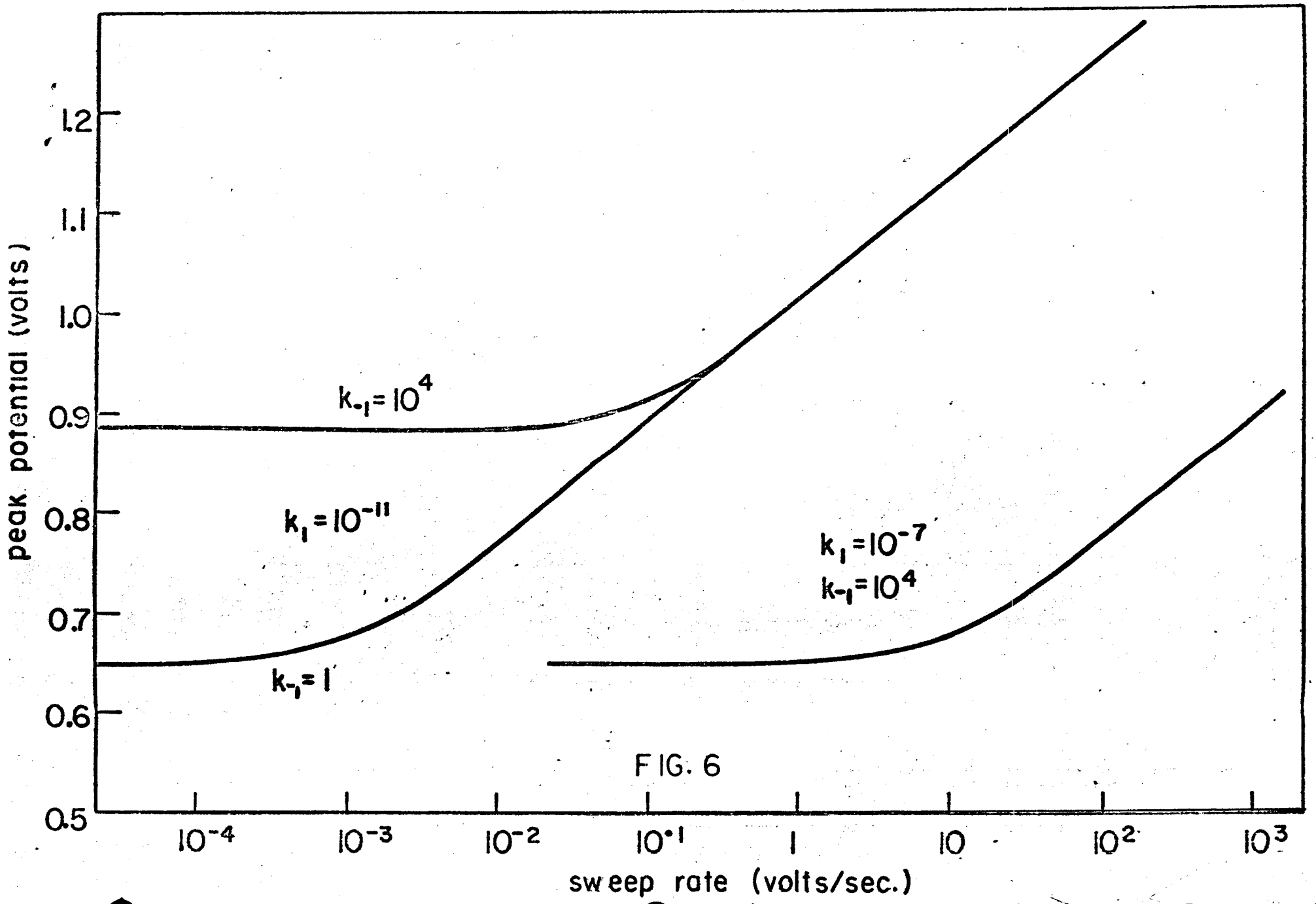
peak potential (volts)
1.2
1.1
1.0
0.9
0.8
0.7
0.6
0.5
$k_{-1}=10^{4}$
$k_1=10^{-11}$
$k_{-1}=1$
$k_1=10^{-7}$
$k_{-1}=10^{4}$
10^{-4}
10^{-3}
10^{-2}
10^{-1}
1
10
10^{2}
10^{3}
sweep rate (volts/sec.)

FIG. 6

APPENDIX II

THE POTENTIAL SWEEP METHOD:

A THEORETICAL ANALYSIS

S. Srinivasan and E. Gileadi

The Electrochemistry Laboratory
The University of Pennsylvania
Philadelphia, Pa. 19104

ABSTRACT

33977

A comparison is made of the current-time curve obtained by the potential sweep method and of the potential-time curve obtained galvanostatically. Limitations of the slow and of the fast potential sweep technique, from the point of view of obtaining kinetic data or coverages in the case of complex reactions (e.g., electroorganic oxidations) are discussed. A detailed mathematical analysis of the method is carried out for a charge transfer reaction of the type $A^- \longrightarrow A + e_o^-$. Three cases which depend on the displacement of the reaction from equilibrium are distinguished. Analytic expressions are derived for the current as a function of potential, peak current and for the peak potential for the cases of quasi-equilibrium and condition under which the reverse reaction may be neglected. For the case where both forward and reverse reactions have to be taken into account, a numerical analysis of the dependence of current on potential is only possible. The capacity-potential plots (capacity = current/sweep rate) are displaced to more positive potentials with departure from equilibrium and the capacity maxima decrease and reach a steady value for considerable departure from equilibrium. The experimental results of Will and Knorr on the adsorption of hydrogen and oxygen on Pt using the potential sweep method serve to verify the present theory.

Author

THE POTENTIAL SWEEP METHOD: A THEORETICAL ANALYSIS

S. Srinivasan and E. Gileadi

The Electrochemistry Laboratory
The University of Pennsylvania
Philadelphia, Pa. 19104

INTRODUCTION

1. General

The potential sweep method is essentially an extension of polarographic techniques, in which the potential of a system is controlled externally and is made to vary, usually at a constant rate. It has been applied first as a triangular sweep method by Sevcik[1] and the corresponding theory in cases where the reaction is partially or completely controlled by diffusion has been given by Delahay.[2] Application of the method for the study of adsorption of electrochemically active intermediates (i.e. species which can be formed on the surface or removed by steps involving charge transfer) has been made by Will and Knorr[3,4] who studied the adsorption of hydrogen and oxygen on noble metal electrodes. These authors have derived relationships between the form of the i-V curves observed experimentally and the sweep rate, and interpreted their results qualitatively in terms of the different degrees of irreversibility of the hydrogen and oxygen desorption steps on these metals.

Following the paper of Will and Knorr, the triangular sweep method has been widely used for the study of anodic oxidation reactions

relevant to fuel cell technology.[4-12]

2. Slow and Fast Potential Sweep

The potential sweep method as applied to anodic oxidation of organic fuels, e.g., alcohols,[5-9] organic acids[8,9] and hydrocarbons[11,12] should really be divided into two classes:

(a) The slow sweep method, with sweep rates in the range of 1 - 100 mV/sec is a quasi-steady state method where it is hoped that the rate of change of potential with time is slow enough for steady state kinetics to be essentially established, while it is fast enough so that impurities cannot accumulate on the electrode surface and affect the current-potential relationship. The aim of such measurements is to obtain current-potential relationships and evaluate the steady state mechanism of the reattions concerned. The conclusions drawn from slow potential sweep method can only be regarded valid if measurements are compared over a wide range of sweep rate $v = dV/dt$ and the observed kinetic parameters are found independent of sweep rate. It may be noted that the actual sweep rate required depends on the type of system studied and its state of purity. Thus, applied to hydrogen evolution studies on mercury in highly purified dilute solutions, a sweep rate as high as a few volts per second could probably be used, while in the study of ethylene oxidation on Pt in 1 N sulfuric acid at 80°C the kinetic parameters were found to depend on sweep rate for $v > 3 \times 10^{-5}$ volt/sec.[13]

(b) The fast potential sweep method ($v > 100$ volt/sec) is a transient method, to be compared with galvanostatic transients. It is

used to measure the concentration of adsorbed species on the electrode surface and finds its best use in the determination of adsorbed intermediates formed on the surface in a charge transfer process.[14,15] The relationship between the V-t curve obtained at constant current and the i-t curve obtained during a potential sweep measurement (at constant $dV/dt = v$) is seen by reference to the schematic diagrams in Fig. 1. The experimentally observed V-t curve (Fig. 1a) can be changed into a V-q curve (Fig. 1b) simply by changing the units on the abscissa, since at constant current

$$\int_{t_1}^{t_2} i\,dt = i(t_2 - t_1) = q \qquad (1)$$

where t_1 and t_2 are times corresponding to the edges of the plateau[14] and q is the charge associated with the process of adsorption taking place in this interval of time. The current-time relatinnship in Fig. 1c can similarly be transformed into a capacity-potential plot by simply changing the units on both coordinates. Thus, since $dV/dt = v = \text{const}$ we can write

$$V = V_i + vt \qquad (2)$$

Also, since in the region of adsorption the observed current is the sum of the double layer charging current and a Faradaic current which is pseudocapacitative in nature we can write

$$i = Cv \qquad (3)$$

where the effective capacity, C, of the interface is the sum of the double layer capacity $C_{D.L.}$ and the adsorption pseudocapacity C_ϕ[16]. Thus, the i-V curves obtained by the fast potential sweep method are

equivalent to the differential of the V-t curves obtained galvanostatically.

An apparent disadvantage of the potential sweep method is that all three variables (i, V, t) change during a sweep, while in galvanostatic or potentiostatic transients the current or the potential respectively is kept constant. However, during a potential sweep the relationship between time and potential is regulated externally and the system therefore has only one independent variable as in the other two cases.

3. Measurement of Adsorption of Organics

Fast potential sweep transients have been used extensively for the determination of the partial coverage θ of electrode by organic compound (e.g., methanol,[17] ethylene[18] or propane[18]) which may be used as fuels in electrochemical energy converters. The main assumptions made in this application are that:

(a) The rate of oxidation of the organic present on the surface at the start of the transient is fast compared to the rate of diffusion, so that no appreciable adsorption from the bulk phase occurs during the transient.

(b) The overall reaction during the transient is the same as that occurring during steady state (even though the mechanism does not necessarily have to be the same).

(c) The reactant and any intermediates formed can only be removed from the surface by complete oxidation.

(d) At the end of the transient the electrode surface is free

of organic molecules or radicals of any kind.

(e) The double layer capacity as well as the adsorption pseudocapacity associated with formation of an oxide layer on the electrode surface are not affected substantially by the presence of the organic on the surface.

Of the five points mentioned above only the first and the fourth can be tested experimentally. Readsorption during the transient can be eliminated if the sweep rate is in excess of ca. 200 volt/sec in the case of methanol.[6,17] Also, if the sweep is continued to high enough potentials so that the current observed in solutions containing the organic coincided with the blank current observed in purified solution through which only nitrogen is bubbled, one may conclude that the electrode surface is free of any organic species. The validity of the other assumptions is questionable and a substantial error of unknown magnitude may be introduced.

In a recent theoretical study[15] of the effect of current density on the θ - V and C_ϕ - V relationship observed in galvanostatic transients it was shown that the partial coverage θ and the pseudocapacity C_ϕ can depend very strongly on the magnitude of the constant current used. At relatively low current densities a parallel shift occurs and the curves can be nearly superimposed if they are moved along the potential axis so that, e.g., the points corresponding to $\theta = 0.5$ or $C_\phi = C_\phi(\max)$ coincide. At high current densities, however, the shape of these curves is also altered and bear no simple relationship to the functional dependence of θ and C_ϕ on V relevant to steady state. In view of the similarity between galvanostatic and potential sweep measurements

discussed above (cf. Fig. 1) an increase in sweep rate would have an effect similar to an increase in current density. This was, in fact, observed experimentally[3] and can be predicted theoretically, as will be shown below.

THEORETICAL DERIVATION

1. Assumptions

In the following we shall consider a simple charge transfer process of the type

$$A^- \underset{k_{-1}}{\overset{k_1}{\rightleftharpoons}} A + e \qquad \text{I}$$

giving rise to an adsorbed species A. The rates of both forward and reverse reactions will be assumed to be activation controlled, with no limitation by mass transfer. It will also be assumed that the adsorbed species A cannot be removed from the surface except by ionization according to reaction (I) in the potential range considered.* The concentration of the reactant A^- in the outer Helmholtz plane will be assumed to be unity and essentially independent of the metal-solution potential difference and the corresponding term will be omitted from the following equations for simplicity. Diffuse double layer effects will be neglected so that the potential drop across the Helmholtz layer will differ from

---

*This is equivalent to the quasi-equilibrium assumption for a fast ion discharge step followed by a slow rate-determining step in which the adsorbed species are removed at a rate negligible in comparison with the exchange rate of their formation and ionization in the first, quasi-equilibrium step.

the potential applied between the test and the reference electrode by a constant.

A case of practical interest corresponding to this model will be the deposition and ionization of atomic hydrogen and of -OH radicals on noble metals in the region of thermodynamic stability of water (i.e. at potentials anodic to the reversible hydrogen evolution potential and cathodic to the reversible oxygen evolution potential in the solution studied). These reactions have been studied extensively by Will and Knorr[3,4] who were the first to introduce the triangular potential sweep method as applied for adsorption measurements. Reaction (I) which will be analyzed below is comparable with the reaction

$$OH^- \rightleftharpoons OH + e \qquad (II)$$

studied by Will and Knorr[3,4] and thus it will be possible to compare the results calculated here directly with experiment.

2. Anodic Sweep

a. Reaction at Quasi-Equilibrium

We start by considering the simplest case of a highly reversible adsorption step.

The Faradaic current (i_F) is expressed as

$$i_F = k_1 (1-\theta) e^{\beta VF/RT} - k_{-1}\theta\, e^{-(1-\beta)VF/RT} \qquad (4)$$

where k_1, k_{-1} are the forward and reverse specific rate constants when the metal-solution potential difference V = 0, and θ is the partial surface coverage by A. During a transient both V and θ change with

time. Our assumption for this case may be written as:

$$i_F \ll k_1 (1-\theta)\, e^{\beta VF/RT} \tag{5}$$

and also

$$\left| i_F \right| \ll k_{-1}\, \theta\, e^{-(1-\beta)VF/RT} \tag{6}$$

This case is then analogous to that of a charge transfer reaction, considered to be virtually in equilibrium preceding the rate-determining step. The latter has been dealt with previously[16,19,20] and expressions for the variation of the adsorption pseudocapacity and coverage with potential were derived. Under these conditions, equation (4) may be rewritten as

$$0 = k_1 (1-\theta) e^{\beta FV/RT} - k_{-1}\, \theta\, e^{-(1-\beta)VF/RT} \tag{7}$$

i.e.

$$\theta/(1-\theta) = k_1\, e^{VF/RT} \tag{8}$$

where

$$K_1 = \frac{k_1}{k_{-1}} \tag{9}$$

hence

$$\theta = \frac{K_1\, e^{VF/RT}}{1 + K_1\, e^{VF/RT}} = \frac{K_1}{e^{-VF/RT} + K_1} \tag{10}$$

The net Faradaic current may also be expressed as

$$i_F = k \frac{d\theta}{dt} \tag{11}$$

where k is the charge required to form a monolayer of adsorbed intermediates according to reaction (I).

From equation (10)

$$\frac{d\theta}{dt} = \frac{K_1}{(e^{-VF/RT} + K_1)^2} \cdot \frac{F}{RT} e^{-VF/RT} \cdot v \qquad (12)$$

Since $V = V_i + vt$ where V_i is the initial potential, v the sweep rate and V is the potential at time t. Combining equations (11) and (12)

$$i_F = \frac{kF}{RT} \cdot \frac{K_1 e^{-VF/RT}}{(e^{-VF/RT} + K_1)^2} \cdot v \qquad (13)$$

It may be noted that the expression multiplying v on the right hand side of equation (12) is that for the adsorption pseudocapacity, as derived by Bockris and Kita.[20] The total current is given by

$$i = i_F + i_{D,L} \qquad (14)$$

In the range of potential where adsorption takes place and θ_A goes from 0.01 to 0.99 it may be assumed that

$$i_{D,L} << i_F \qquad (15)$$

$$i \rightarrow i_F \qquad (16)$$

From equation (13) and (15), it follows that at a constant potential, the current is proportional to the sweep rate. Further, at a constant sweep rate, the current is proportional to the adsorption pseudocapacity for this case.

Determination of peak current and potential: The condition for maximum in i - t curve is

$$\frac{di_F}{dt} = 0 \qquad \text{or} \quad \frac{d^2\theta}{dt^2} = 0 \tag{17}$$

By differentiating equation (12) we find

$$\frac{d^2\theta}{dt^2} = K_1\left(\frac{FV}{RT}\right)^2 \frac{e^{-VF/RT}(e^{-VF/RT} + K_1)^2 - 2e^{-2VF/RT}(e^{-VF/RT} + K_1)}{(e^{-VF/RT} + K_1)^4}$$

$$= K_1 \left(\frac{FV}{RT}\right)^2 e^{-VF/RT}\left[\frac{e^{-VF/RT} + K_1 - 2e^{-VF/RT}}{(e^{-VF/RT} + K_1)^3}\right]$$

$$= K_1 \left(\frac{FV}{RT}\right)^2 e^{-VF/RT}\left[\frac{K_1 - e^{-VF/RT}}{(e^{-VF/RT} + K_1)^3}\right] \tag{18}$$

The potential V_M corresponding to peak current is thus given by

$$V_M = - RT/F \ln K_1 \tag{19}$$

Using equation(19) in (13), the peak current is given by

$$i_{F,M} = (kF/4RT) \cdot v \tag{20}$$

For this case, the peak current is directly proportional to the sweep rate whereas the peak potential is independent of v. The quantity (kF/4RT) is the maximum adsorption pseudocapacity under the assumed conditions which was derived previously in a different manner.[16,19,20]

b. Reverse Reaction Neglected

Here we consider a highly irreversible reaction proceeding at a net rate nearly equal to its forward rate. For brevity this case will be referred to below as the "Tafel approximation."

Under these conditions, equation (4) reduces to

$$i_F = k_1 (1-\theta) e^{\beta VF/RT} \tag{21}$$

or in differential form

$$\frac{di_F}{dt} = k_1 e^{\beta VF/RT} \left[(1-\theta) \beta v F/RT - \frac{d\theta}{dt} \right] \tag{22}$$

The current i_F will reach a maximum when

$$\frac{d\theta}{dt} = (1-\theta) \beta v F/RT \tag{23}$$

Combining equations (11) and (23) we find for the peak current

$$i_{F,M} = (1-\theta) \frac{\beta kF}{RT} v \tag{24}$$

The potential V_M corresponding to peak current can be obtained by combining equations (21) and (24) as

$$V_M = \frac{RT}{\beta F} \ln \frac{k\beta F}{k_1 RT} + \frac{RT}{\beta F} \ln v \tag{25}$$

The peak current may be expressed differently by making use of equation (21) in the form

$$k \frac{d\theta}{dt} = k_1 (1-\theta) e^{\beta VF/RT} \tag{26}$$

Substituting the value of V from equation(2) and rearranging we have

$$- d \ln (1-\theta) = \frac{k_1}{k} e^{\beta V_i F/RT} e^{\beta vtF/RT} dt \qquad (27)$$

whence

$$-\ln(1-\theta) = \frac{k_1}{k} \cdot \frac{RT}{\beta vF} e^{\beta V_i F/RT} e^{\beta vtF/RT} + B \qquad (28)$$

The constant of integration B is evaluated from the boundary condition $\theta = 0$ at $t = 0$ and its value introduced into equation (28) to give

$$- \ln (1-\theta) = \frac{k_1}{k} \frac{RT}{\beta vF} e^{\beta V_i F/RT} (e^{\beta vtF/RT} - 1) \qquad (29)$$

Combining equations (2), (21) and (29) we find

$$\ln i_F = \ln k_1 - \frac{k_1}{k} \frac{RT}{\beta vF} e^{\beta V_i F/RT} \left[e^{\beta (V-V_i)F/RT} - 1 \right] + \beta VF/RT \qquad (30)$$

Equation (30) is of fundamental importance in that it represents the current-potential relationship, independent of θ and time under conditions when only the rate in the forward direction need be considered. It may be noted that a linear Tafel plot with the correct slope of $b = RT/\beta F$ is only predicted under certain conditions, when the second term on the r.h.s. of equation (30) is negligible in comparison with the third. The deviations from this slope will depend on the sweep rate. Under limiting conditions, when the exponent in the square bracket in equation (30) can be linearized, straight Tafel plots can still be obtained, but with slopes varying with sweep rate.

To find $i_{F,M}$ we can use equatinn (30) with $V = V_M$ and substitute the value of V_M from equation (25).

$$\ln i_{F,M} = \ln \left(\frac{k \beta F}{RT} v \right) + \left(\frac{k_1 RT}{k \beta vF} e^{\beta V_i F/RT} - 1 \right) \qquad (31)$$

For the conditions assumed in this section we may write

$$\frac{k_1}{k_{\beta}} \frac{RT}{\beta vF} e^{\beta V_i F/RT} << 1 \qquad (32)$$

Equation (31) then becomes

$$\ln i_{F,M} = \ln \left(\frac{k\beta F}{RT} v\right) - 1 \qquad (33)$$

or

$$i_{F,M} = \frac{1}{e} \cdot \frac{k\beta F}{RT} v \qquad (34)$$

The peak current is again found to be proportional to the sweep rate with an apparent adsorption pseudocapacity of

$$C_{\phi,M}(\text{app.}) = \frac{1}{e} \frac{k\beta F}{RT} = \frac{k F}{5.43\ RT} \qquad (35)$$

(β assumed to be 0.5) as compared to the value of $k'F/4RT$ under quasi-equilibrium conditions (cf. equation 20). Comparison of the two equations obtained in this section for $i_{F,M}$ (equations 24 and 34) shows that the value of the coverage corresponding to peak current is given by

$$1 - \theta = \frac{1}{e} \quad \therefore \theta = 0.63 \qquad (36)$$

In the quasi-equilibrium case, the adsorption pseudocapacity reaches a maximum when $\theta = 0.50$.

c. General case

In this section the more general case will be considered for which quasi-equilibrium in reaction (I) cannot be assumed and both forward and reverse reaction rates must be considered.

Equation (4) may be rewritten in the form:

$$i_F = k_1 e^{\beta VF/RT} - \theta \left(k_1 e^{\beta VF/RT} + k_{-1} e^{-(1-\beta)VF/RT}\right) \qquad (37)$$

From equation (37)

$$\theta = \frac{k_1 e^{\beta VF/RT}}{k_1 e^{\beta VF/RT} + k_{-1} e^{-(1-\beta)VF/RT}} - \frac{i_F}{k_1 e^{\beta VF/RT} + k_{-1} e^{-(1-\beta)VF/RT}}$$

$$= \frac{k_1}{k_1 + k_{-1} e^{-VF/RT}} - \frac{i_F}{k_1 e^{\beta VF/RT} + k_{-1} e^{-(1-\beta)VF/RT}} \qquad (38)$$

$$\frac{d\theta}{dt} = \frac{F}{RT} \frac{k_1 k_{-1} e^{-VF/RT} v}{(k_1 + k_{-1} e^{-VF/RT})^2} - \frac{\frac{di_F}{dt}}{k_1 e^{\beta VF/RT} + k_{-1} e^{-(1-\beta)VF/RT}}$$

$$+ i_F v \frac{k_1 e^{\beta VF/RT}(\beta F/RT) - k_{-1}(1-\beta)F/RT\, e^{-(1-\beta)VF/RT}}{\left[k_1 e^{\beta VF/RT} + k_{-1} e^{-(1-\beta)VF/RT}\right]^2} \qquad (39)$$

$$\frac{di_F}{dt} = \frac{F}{RT} \frac{k_1 k_{-1} v\, e^{-(1-\beta)VF/RT}}{k_1 + k_{-1} e^{-VF/RT}} + i_F \frac{v\left[k_1 \beta F/RT - k_{-1}(1-\beta)(F/RT) e^{-VF/RT}\right]}{k_1 + k_{-1} e^{-VF/RT}}$$

$$- \frac{i_F}{k} e^{\beta VF/RT} (k_1 + k_{-1} e^{-VF/RT}) \qquad (40)$$

This differential equation cannot be solved analytically. Numerical solutions may, however, be obtained for chosen values of the parameters k_1, k_{-1} and v. Alternatively equation (37) may be used to obtain numerical relationships between i_F, V and v for any values of k_1 and k_{-1}.

NUMERICAL COMPUTATIONS

1. Reaction at Quasi-Equilibrium

As in the above theoretical derivation three cases should be distinguished here. The quasi-equilibrium case corresponding to $v \longrightarrow 0$ has been calculated previously[14,16,19,20] and is shown in Figures 4 and 5 for the sake of comparison. The current density at any potential is proportional to the sweep rate (equation 13) and the proportionality factor is the adsorption pseudocapacitance as derived previously.[14,16,19,20] The peak current is proportional to the sweep rate (equation 20) and its position on the potential scale is independent of sweep rate (equation 19). Since the process considered above (I) is an adsorption-desorption process and all the Faradaic current is pseudocapacitative in nature (cf. equation 11), it is best to plot the apparent observed adsorption pseudocapacity $C = 1/v$ as a function of the potential and consider the dependence of the shape of this curve and its position on the V axis on the sweep rate v. Taking then a value of $k = 160\ \mu C/cm^2$ the peak capacity in the quasi-equilibrium case is $C_M = 1.6 \times 10^3\ \mu F/cm^2$. Lower peak values are obtained when the equilibrium in step (I) is disturbed as will be shown below.

2. Reverse Reaction Neglected

In this case an analytical solution can be derived (equation 30). Figure 2 shows the dependence of the C-V plots on sweep rate over a wide range. The peak current is independent of sweep rate as expected (equation 34) and the peak capacity has a value of

$$C_M = \frac{\beta}{e}\frac{kF}{RT} = \frac{1}{5.42}\frac{kF}{RT} = 1.18 \times 10^3 \,\mu F/cm^2 \qquad (41)$$

for $\beta = 0.5$ as compared to a value of $kF/4RT$ for the quasi-equilibrium case discussed above.

The curves in Fig. 2 may all be superimposed by shifting them in parallel along the V axis to an extent of 2.3 x 2RT/F per decade increase in sweep rate. Such behavior was also predicted qualitatively previously as a first approximation for galvanostatic transients (cf. Fig. 2 in ref. 15).

3. General Case

(a) Effect of step size

Equation (37) was used to obtain numerically the C-V relationships for chosen values of the rate constants k_1 and k_{-1} as a function of sweep rate. The procedure here is as follows. At $t = 0$ when $V = V_i$ it is assumed that $\theta = 0$ and i_F is calculated from equation (37). This value of i_F is used to obtain θ at a slightly higher potential $V = V_i + \Delta V$, making use of the relationship $i = k(d\theta/dt) = kv(d\theta/dV)$ (equation 11). The value of θ obtained in this manner is used in equation (37).to obtain a new value of i_F, and so forth. The results of this type of calculatinn depend on the size of the steps used. However, below a certain step size the effect becomes insignificant. In Fig. 3 a plot of C-V is shown for v = 1 volt/sec., $k_1 = 10^{-11}$ and $k_{-1} = 1$ for 50, 10 and 1 mV step sizes. The position of the maximum is not affected but the curves are narrower and higher for larger step size. In all subsequent calculations a step size of 0.1 mV was used which,

according to Fig. 3 would give the true C-V relationship to better than 1%.

(b) Pseudocapacity-potential plots

Figures 4 and 5 show calculated C-V curves for $k_1 = 10^{-11}$; $k_{-1} = 1$ and $k_1 = 10^{-7}$; $k_{-1} = 10^4$ respectively, for a range of sweep rates $v = 10^{-3} - 10^3$ volt/sec. (The quasi-equilibrium case is included for comparison.) At first the peak capacity decreases and the shape of the curves changes with increasing sweep rate. At higher sweep rates a parallel shift in the C-V curves without change in shape is observed. In Fig. 4, the curves for $v \gtrsim 10^{-2}$ volt/sec. are identical to those obtained in Fig. 2 for the "Tafel" case for the same values of k_1 and v. Qualitatively similar behavior is observed in Fig. 5. Here, however, the equilibrium conditions are not substantially effected until a sweep rate of 10 volt/sec is reached and the peak height becomes independent of sweep rate only at $v \gtrsim 10^2$ volt/sec. It may, therefore, be concluded that the equilibrium in the adsorption-desorption process is disturbed to an extent depending on the ratio k_1/v for the forward reaction or $|k_{-1}/v|$ for the reverse step. A certain degree of arbitrariness remains in the choice of V_i, the potential at which a transient is started. The deviations from quasi-equilibrium would better be defined in terms of the ratio (k_1/v) $\exp(\beta V_i F/RT)$ which will only depend on the intrinsic properties of the system and on the applied sweep rate.

Figure 6 shows plots of V_M, the peak potential, vs. the logarithm of the sweep rate for two values of k_1 and k_{-1}. The horizontal section of the curve represents a region of sweep rate in which the equilibrium

in the adsorption-desorption step is not substantially disturbed. The limits of this region depend on both k_1 and k_{-1}, but are more sensitive to the variations in k_1. The curves in Fig. 6 are superimposable, and are shifted one decade in sweep rate per decade increase in k_1 or per two decades increase in k_{-1}. At high sweep rates V_M varies linearly with log v as expected from equation (25) for the "Tafel approximation." Between the region where the reverse reaction may be neglected ("Tafel approximation") and where the quasi-equilibrium assumption is essentially valid, there is only a small range of sweep rates (less than two decades) where the complete equation (37) must be employed. Thus the experimental results may in general be analyzed either in terms of the quasi-equilibrium assumption or in terms of the limiting "Tafel approximation," both of which can be treated analytically.

In the range where the Tafel approximation applies equation (25) may be used to obtain the symmetry factor β and the specific rate constant k_1 from the slope and the intercept of the V_M-log v plot respectively. This may be combined with the equilibrium constant obtained from V_M in the quasi-equilibrium range (equation 19) to obtain k_{-1}, the specific rate constant for the reverse reaction. The latter may also be obtained by studying the effect of sweep rate on V_M for cathodic sweeps.

4. Comparison with Experiment

Of the numerous papers in which the potential sweep technique has been applied, only few have considered the effect of sweep rate on the results. In the original papers of Will and Knorr[3,4] a detailed experimental study of the sweep rate effect is reported. The reactions studied by

these authors (hydrogen and oxygen adsorption and ionization on noble metal electrodes) are of the general type considered here (reaction I), and some of their results will be analyzed below with the aid of the equatinns derived in the present paper.

The plots of the peak potential V_M vs. log v for hydrogen and oxygen adsorption and ionization on Pt (Fig. 16 and 18 in ref. 3) are qualitatively the same as those calculated here (cf. Fig. 6). For hydrogen the adsorption-desorption equilibrium is not detectably disturbed up to a sweep rate of a few volts per sec. For oxygen the equilibrium is disturbed already at the lowest sweep rate (v = 0.1 volt/sec.) studied. Moreover, the hydrogen adsorption step is seen to be more reversible than the hydrogen ionization step on Pt.

The slope of these lines is given according to equation (25) as

$$dV_M/d \log v = 2.3\, RT/\beta F \qquad (42)$$

irrespective of the specific rate constant for the reaction considered. For hydrogen ionization the average slope observed is 0.11 V and for oxygen it is 0.055 V with a rather large scatter around these values. This is consistent with the fact that hydrogen and oxygen adsorption represent one and two electron quasi-equilibria respectively.

A plot of log $i_{F,M}$ vs. log v (Fig. 17 and 19 in Ref. 3) is practically linear, with a slope of unity as expected according to equations (20) and (34).

It is noted that the system studied by Will and Knorr[3] is more complicated than the simple charge transfer adsorption step analyzed mathematically here (step I) on account of the possible absorption of

hydrogen and oxygen in the metal lattice. Thus, the persistence of two hydrogen peaks even on single crystal platinum electrodes has been interpreted[21] as being due to part of the hydrogen being adsorbed in interstitial positions below the outer layer of metal atoms. Direct evidence for the absorption and diffusion of hydrogen in Pt at room temperature has recently been obtained[22] and the absorption of both hydrogen and oxygen in Pt at room temperature has been suggested [23] on the basis of transient measurements.

CONCLUSIONS

The application of the potential sweep or triangular sweep method to organic oxidation and adsorption studies are discussed. A clear distinction between "slow" and "fast" sweeps is made. The relation between galvanostatic and fast potential sweep transients is discussed and the limitations of both for the determination of coverage by organic species are pointed out. It is concluded that meaningful results can only be obtained by this method if in each system studied the effect of sweep rate is measured over a wide range and a suitable value of the sweep rate is chosen.

A detailed mathematical analysis of the current potential transients during application of the potential sweep method is given for a simple adsorption step involving charge transfer assuming Langmuir conditions.* The general equations and two limiting cases are developed.

---

*The treatment can be extended to cases where the apparent standard free energy of adsorption changes substantially with coverage (Temkin conditions). Under such conditions only numerical solution can be obtained, however.

Numerical analysis of the general equations shows that they are applicable only over a narrow range of sweep rates of less than two decades. Thus in most practical cases an analysis by either the quasi-equilibrium or the "Tafel" approximation may be applied. The mode of variation of the peak potential V_M with sweep rate can serve as an indication of the type of equation to be used in any situation.

The extent to which equilbrium in the adsorption-desorption step is disturbed depends on the sweep rate and on the specific rate constants for the reaction concerned. Beyond a certain sweep rate (the numerical value of which depends on the nature of the reaction studied) the shape of the i - V curves becomes independent of sweep rate but the curves shift to higher potentials with increasing sweep rate. Similar behavior has been predicted previously[15] on the basis of a qualitative argument for galvanostatic transients.

Good agreement is obtained between the equations derived here and the experimental results reported by Will and Knorr[3] for hydrogen and oxygen adsorption on Pt electrodes. Complications due to absorption of hydrogen and possibly oxygen in the metal may give rise to some of the deviations from theoretical behavior observed.

ACKNOWLEDGEMENTS

Financial support for this work by the National Aeronautics and Space Administration on Grant No. NSG-325 is gratefully acknowledged.

The authors also wish to thank Professor J. O'M. Bockris for helpful discussion and suggestions, and the Johnson Foundation for use of their digital computor.

REFERENCES

1. A Sevcik, Colln. Czech Chem. Comm., 13, 349 (1948).
2. P. Delahay, "New Instrumental Methods in Electrochemistry," Chapter 6 Interscience Publishers, Inc., N.Y. (1954).
3. F. G. Will and C. A. Knorr, Z. Elektrochem., 64, 258 (1960).
4. F. G. Will and C. A. Knorr, ibid, 64, 270 (1960).
5. W. Vielstich, Z. Instrumenten. 71, 29 (1963), Chem. Ing. Tech., 35, 362 (1963).
6. S. Gilman and M. W. Breiter, J. Electrochem. Soc., 109, 1099 (1962).
7. M. W. Breiter, Electrochim. Acta, 8, 973 (1963).
8. J. Giner, Electrochim. Acta, 9, 63 (1964).
9. V. S. Bagotskii and Yu. B. Vasilyev, Electrochim. Acta, 9, 869 (1964)
10. S. Gilman, J. Phys. Chem., 68, 70 (1964).
11. R. P. Buck and L. R. Griffith, J. Electrochem. Soc., 109, 1005 (1962).
12. D. R. Rhodes, Ibid, 9, 36 (1964).
13. J. O'M. Bockris, G. Stoner and E. Gileadi, to be published.
14. E. Gileadi and B. E. Conway, Modern Aspects of Electrochemistry, Volume 3, Chapter V, Butterworths (1964).
15. B. E. Conway, E. Gileadi and H. Angerstein-Kozlowska, J. Electrochem. Soc., 112, 341 (1965).
16. B. E. Conway and E. Gileadi, Trans. Faraday Soc., 58, 2493 (1962).
17. M. W. Breiter and S. Gilman, J. Electrochem. Soc., 109, 622 (1962).
18. R. Ch. Burshtein, V. S. Tiurin and A. G. Pshenichnikov, Paper presented at the September 1964 Meeting of C.I.T.C.E.
19. A. Eucken and B. Weblus, Z. Electrochem. 55, 114 (1951).

20. J. O'M. Bockris and H. Kita, J. Electrochem. Soc., 108, 676 (1961).

21. F. G. Will, Extended Absts. Theoret. Div. Electrochem. Soc., Vol. 2, No. 1 (1964); see also: J. Electrochem. Soc., 112, 451 (1965).

22. E. Gileadi, M. Fullenwider and J. O'M. Bockris, in course of publication.

23. S. Schuldiner and T. B. Warner, J. Electrochem. Soc., 112, 212 (1965).

CAPTIONS TO FIGURES

Figure 1. Schematic diagrams relating galvanostatic and triangular sweep transients (a) v-i plot at constant current density; (b) V-q plot calculated from (1a); (c) i-t plot for trianbular sweep. (d) calculated C-V plot for triangular sweep.

Figure 2. Calculated pseudocapacity-potential plots for the "Tafel approximation" case ($k_1 = 10^{11}$).

Figure 3. Step size effect in the numerical calculation for the general case.

Figure 4. Calculated C-V plots for the general case $k_1 = 10^{-11}$, $k_{-1} = 1$. Sweep rate as indicated.

Figure 5. Same as Fig. 4 for $k_1 = 10^{-7}$; $k_{-1} = 10^{4}$.

Figure 6. Plots of the peak potential V_M *vs.* the logarithm of the sweep rate.

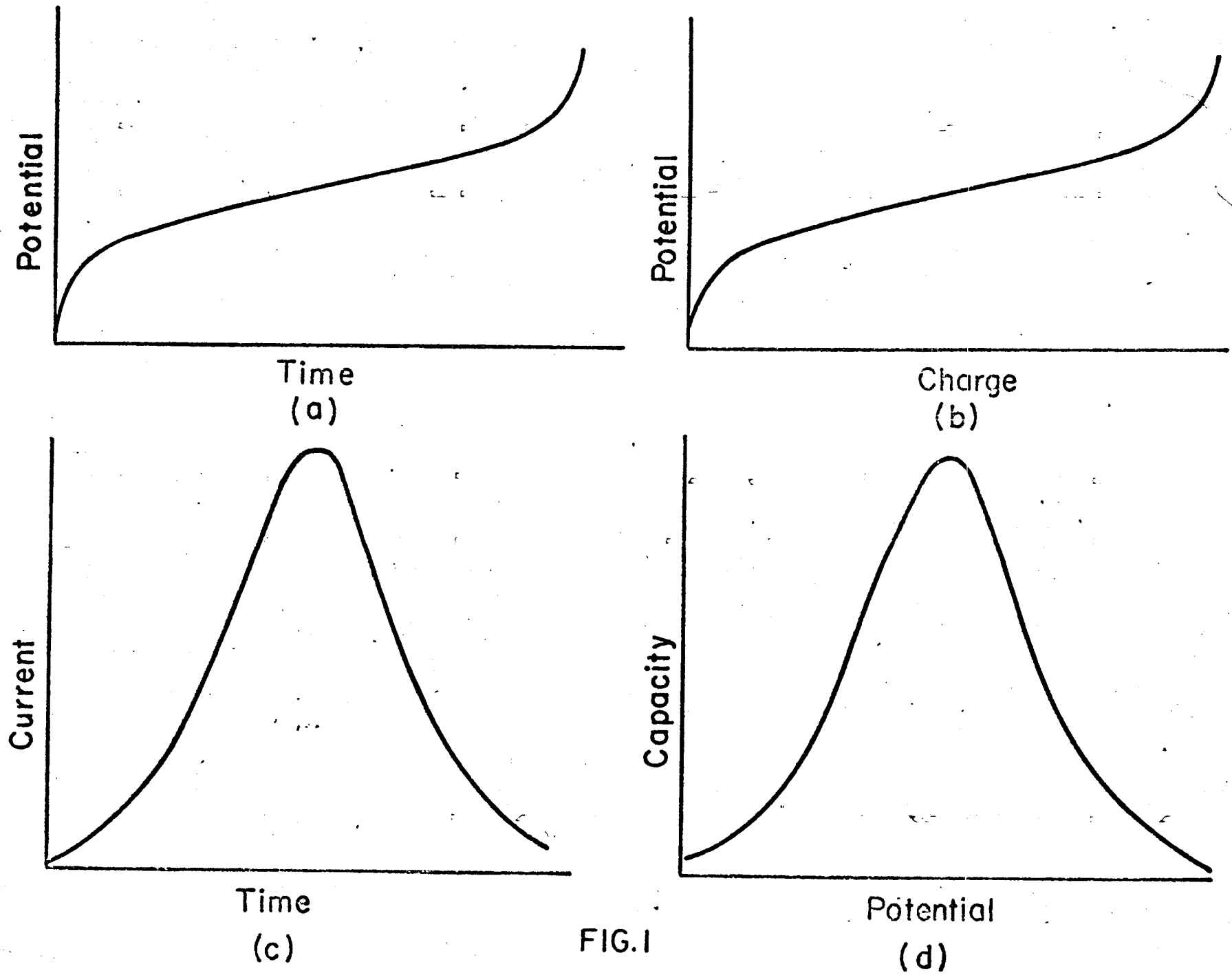
Potential
Time
(a)
Potential
Charge
(b)
Current
Time
(c)
Capacity
Potential
(d)

FIG. 1

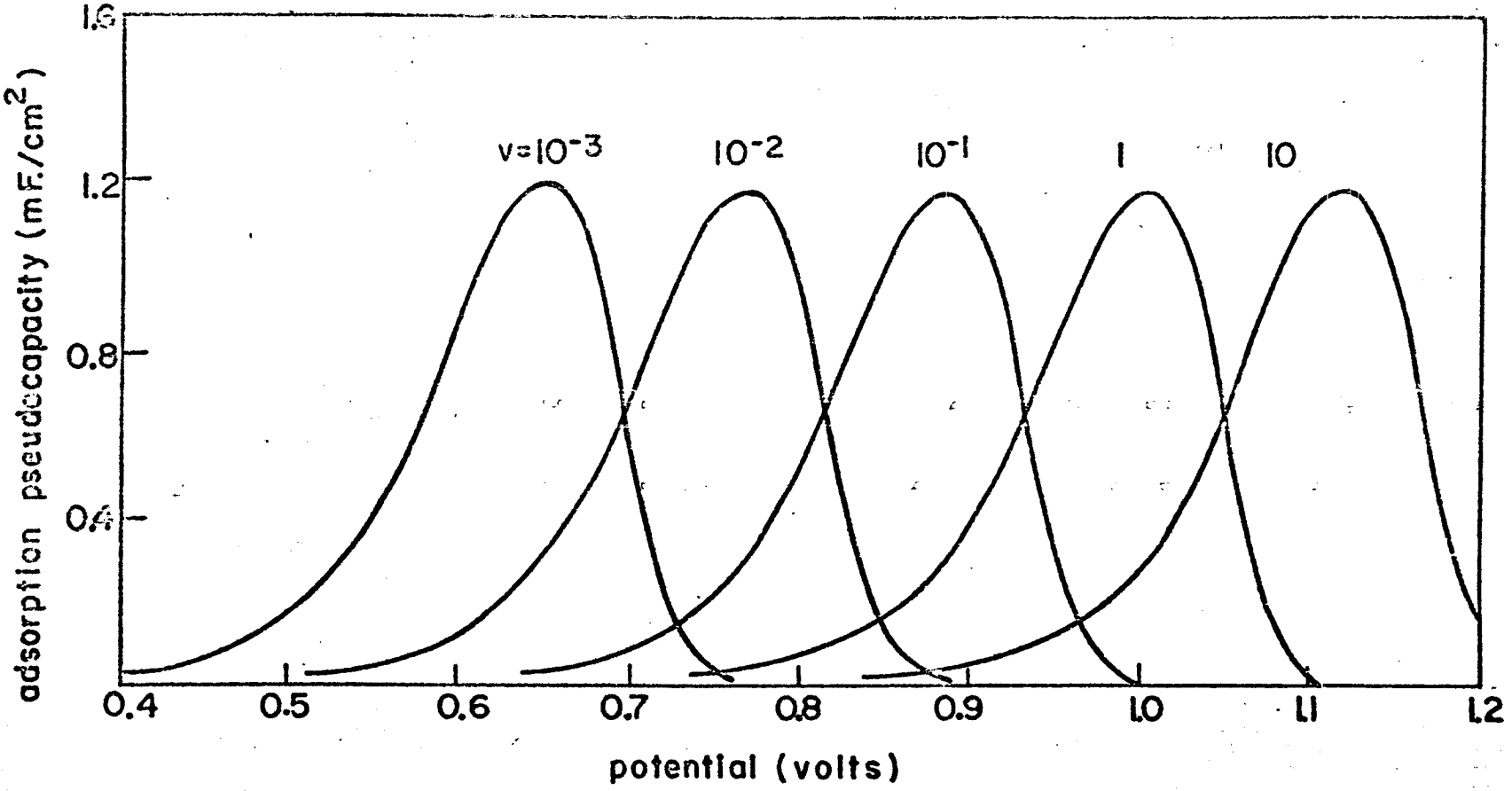
adsorption pseudocapacity (mF./cm²)
1.6
1.2
0.8
0.4
v=10⁻³
10⁻²
10⁻¹
1
10
0.4
0.5
0.6
0.7
0.8
0.9
1.0
1.1
1.2
potential (volts)

FIG.2

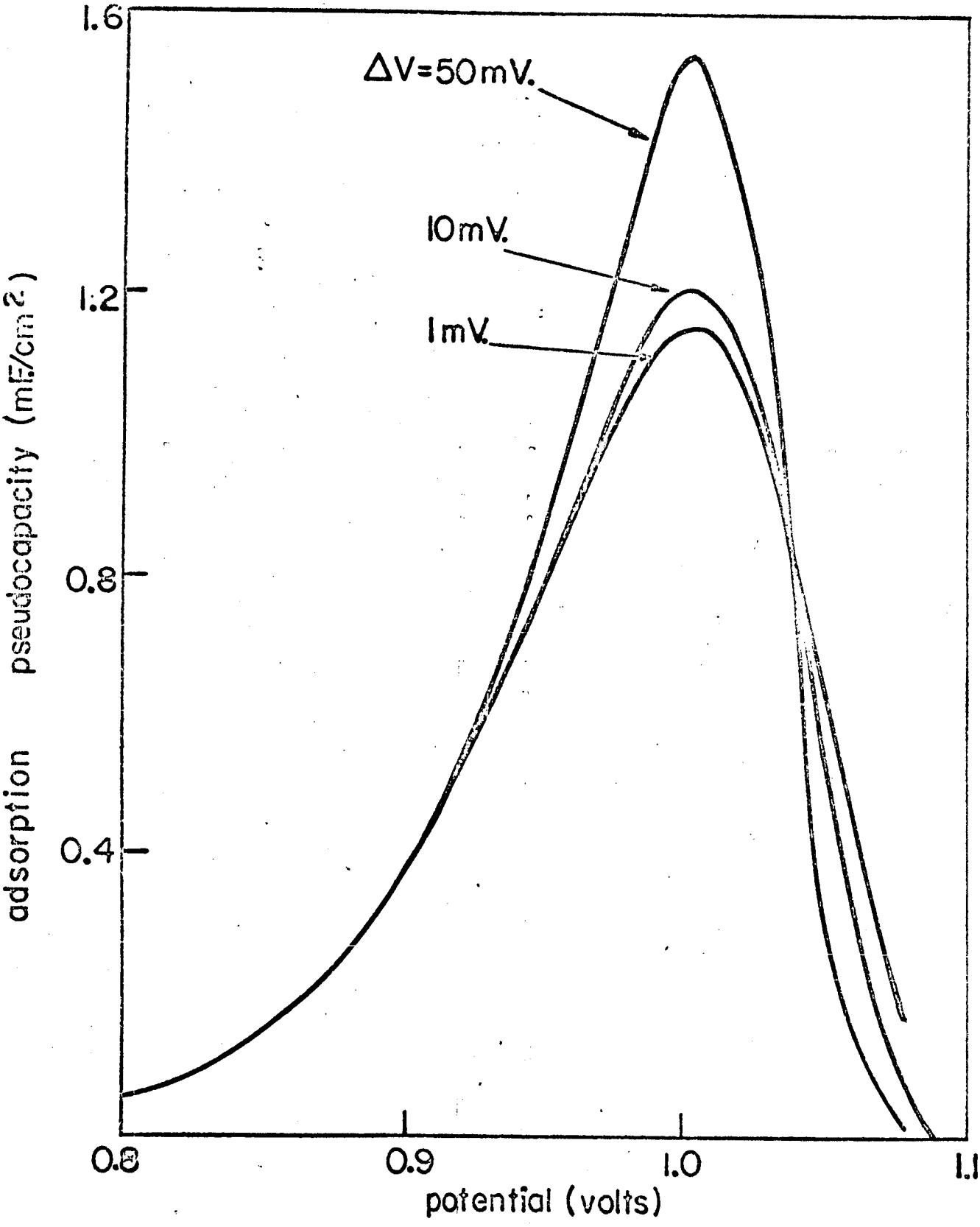
1.6
1.2
0.8
0.4
ΔV=50mV.
10mV.
1mV.
adsorption pseudocapacity (mF/cm²)
0.8
0.9
1.0
1.1
potential (volts)

FIG.3

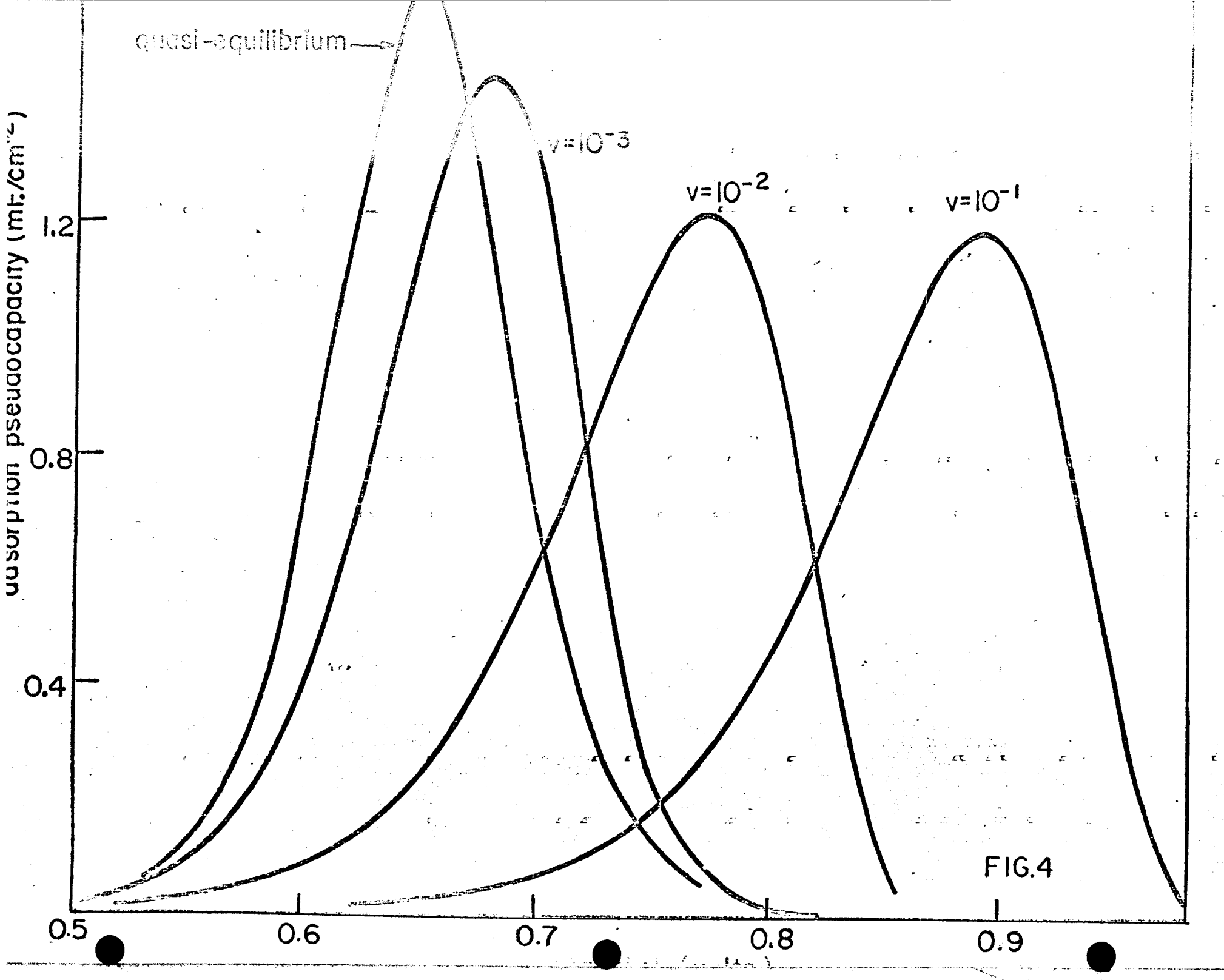

FIG.4

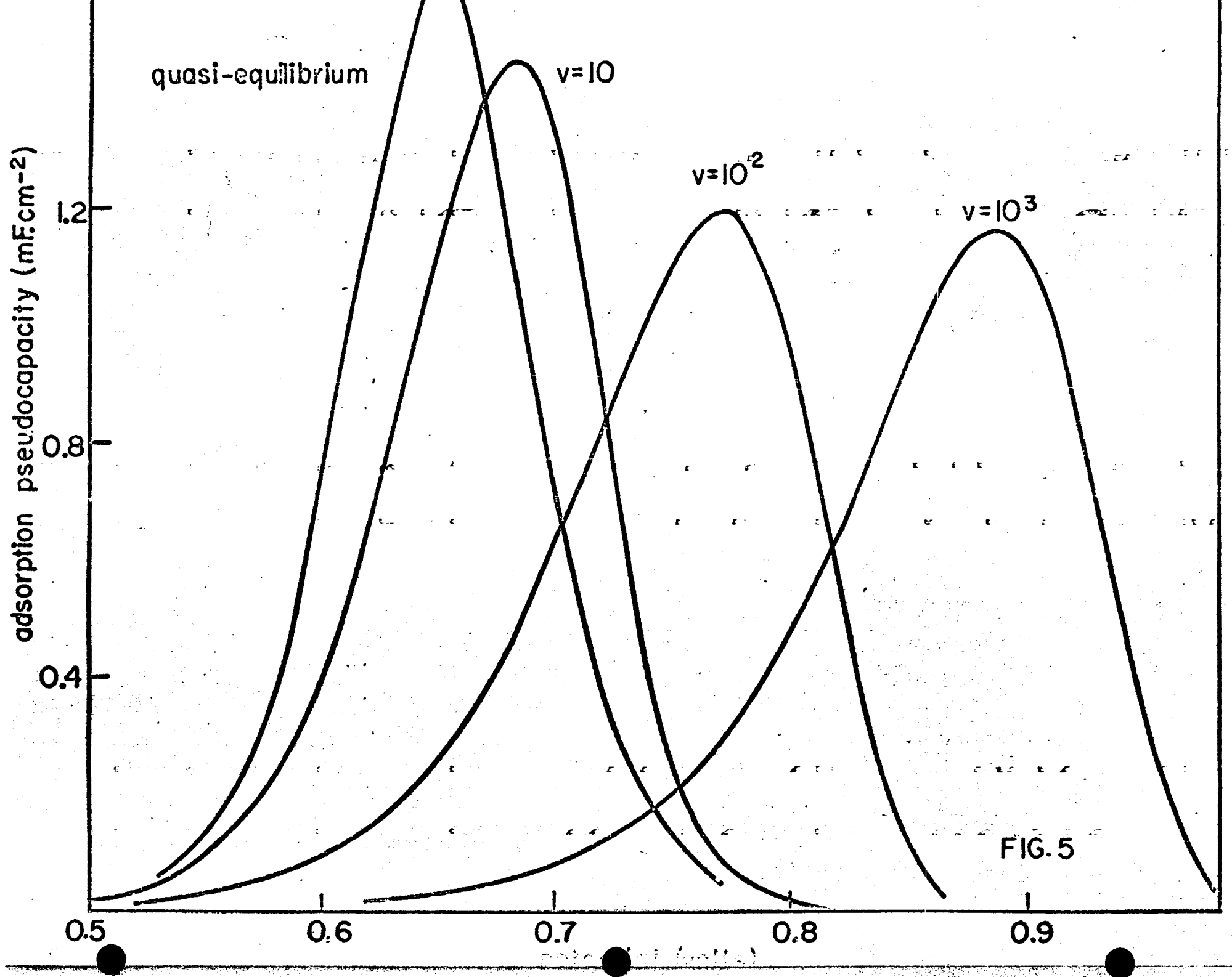
quasi-equilibrium
v=10
v=10^2
v=10^3
adsorption pseudocapacity (mF.cm^-2)
1.2
0.8
0.4
0.5
0.6
0.7
0.8
0.9

FIG. 5

APPENDIX III

PROTON TRANSFER ACROSS DOUBLE LAYERS:

MECHANISM EVALUATION FROM ISOTOPIC EFFECTS

J. O'M. Bockris, S. Srinivasan and D. B. Matthews

The Electrochemistry Laboratory
The University of Pennsylvania
Philadelphia, Pa. 19104
U.S.A.

SUMMARY

The separation factor depends sharply upon the mechanism of the hydrogen evolution reaction. Conway's previous calculations contain errors of principle. Calculations on the basis of classical transition state theory are reported: They consist essentially of the calculation of force constants at the saddle point of potential energy-distance diagrams for several alternative rate-determining steps in the hydrogen evolution reaction. Correspondingly, the relevant partition function ratios for corresponding isotopic situations have been calculated. An essential difference in result of these calculations from previous ones of the Japanese School is that the present calculations take account of the stretching frequency of the O-H bond in the activated state. The separation factor calculated is thus reduced by about 6 times, and allows consistence with a rate-determining proton discharge mechanism upon metals for which the rate constant of the hydrogen evolution reaction is low. Relations are deduced which show that the separation factor is a functinn of the fast reaction following a rate-determining step.

Quantum mechanical calculations of separation factors must be made as corrections to the classical transition state calculations because otherwise the zero point energy level of the activated state is neglected (as was done by Christov). Experimental data reports the unexpected dependence of the separation factor for metals having low rate constants for the hydrogen evolution reaction upon potential. It is shown that explanations in terms of only classical proton transfer rates are improbable. Correspondingly, the variation of the rate of proton transfer with potential is shown to be highly independent of assumptions concerning barrier width, and therefore degree of barrier penetration, within certain ranges of the parameters of barrier height and barrier width. The temperature dependence of the separation factor is also not a sensitive criterion for the degree of barrier penetration in proton transfer. It is shown, however, that the dependence of the separation factor on potential is a particularly sensitive indication of degree of barrier penetration for protons.

The barrier width and height are calculated with the assumption of an Eckart type barrier by solving quantum mechanical equations which relate the rate to the change of potential; to the absolute value of separation factor; and to the variation of the separation factor with potential. In this way, the most probable value of the barrier width and height upon mercury for the proton discharge reaction from 0.1 N acid solutions is shown to be 4 Å and 14 Kcal $mole^{-1}$. Utilizing these parameters, the quantum mechanical correction factors for the separation factor are calculated. Utilizing these values, it is possible to associate the well known alternative paths for the hydrogen evolution

reaction with certain separation factors. Hence, identification of mechanisms can rapidly be made with a few experimentally simple measurements of H-T separation factor concentrations.

The barrier penetration fraction of the proton transfer rate on mercury in 0.1 N HCl at room temperature may amount to about 70% of the total current at an overpotential of 1 V. An important corollary of these calculations is that the barriers assumed in earlier theoretical work in electrode processes have been too narrow. Probable barriers would have to be at least 4 Å. Such conclusions are consistent with recent views on the existence of a water layer on electrodes as an essential constituent of the double layer structure.

PROTON TRANSFER ACROSS DOUBLE LAYERS: MECHANISM EVALUATION FROM ISOTOPIC EFFECTS

J. O'M. Bockris, S. Srinivasan and D. B. Matthews

The Electrochemistry Laboratory
The University of Pennsylvania
Philadelphia, Pa. 19104

Most methods used to determine the mechanism of electrolytic hydrogen evolution involve work at the steady state in the low current density range and thus cannnt be applied to metals which enter mixed potential reactions with the solution.[1] The separation factor method[2] avoids this difficulty. It depends on a theoretical analysis of the separation factors expected from the various mechanisms. Previous calculations[3-8] have been discrepant; tunneling effects have been neglected.

The aim of this paper is to give a theoretical analysis of separation factors associated with proton transfer and related mechanisms of the pasaage of hydrogen across a metal-solution boundary,[9-11] and to assess numerically the neglected effects of tunneling.[12]

CLASSICAL EVALUATION OF SEPARATION FACTORS

Conway's approach[8] (corrected for an error in the calculated ratio of activities of isotopic oxonium ions) gives large isotope effects due to neglect of zero point energy differences of the isotopic activated complexes. Since the calculation procedure by Horiuti et al.[3-7] minimizes the calculation of partition functions of species in solution, the same approach was adopted in the present work.

STEPS IN METHOD OF CLASSICAL CALCULATION

(i) Expression for separation factor

The hydrogen-tritium separation factor is defined by the equation

$$S_T = \left(\frac{C_H}{C_T}\right)_g \Big/ \left(\frac{C_H}{C_T}\right)_s \qquad (1)$$

where $(C_H/C_T)_g$ and $(C_H/C_T)_s$ are the ratios of atomic concentrations of hydrogen to tritium in the gas phase and in solution, respectively. The ratio $(C_H/C_T)_g$ is equal to twice the ratio of the velocities of H_2 and HT evolution since $C_{H_2} >> C_{HT}$. Using this relation S_T may be expressed by

$$S_T = n \frac{\gamma_H}{\gamma_T} \cdot \frac{f_H^{\neq}}{f_T^{\neq}} \cdot \frac{f_{HTO,g}}{f_{H_2O,g}} \cdot K_T \qquad (2)$$

for all mechanisms, except when the diffusion of molecular hydrogen away from the electrode is the rate-determining step. For a linked discharge-electrochemical desorption mechanism,

$$\frac{1}{S_T} = \frac{1}{S_{Dis}} + \frac{1}{S_{El}} \qquad (3)$$

where S_{Dis} and S_{El} are given by expressions of the form (2). In equations (2), n = 1/2 for the slow discharge mechanism, n=1 for all other mechanisms, γ_H/γ_T is the ratio of tunneling correction factors, $f_H^{\neq}/f_T^{\neq}$ is the partition function ratio of the isotopic activated complexes for the particular step considered, $f_{HTO,g}/f_{H_2O,g}$ is the partition function ratio of the HTO and H_2O molecules in the gas phase and K_T is the equilibrium constant for the reaction

$$H_2O_{\ell} + HTO_g \rightleftharpoons HTO_{\ell} + H_2O_g \qquad (4)$$

in equation (3), S_{Dis} refers to an expression of the form of (2) for the discharge step and S_{El} to the electrochemical desorption step.

Thus, the calculations consist of (a) calculation of the force constants at the saddle point of the reactions constituting assumed rate-determining steps and (b) the quantum mechanical penetration and reflection of the barrier. The $f_{HTO,g}/f_{H_2O,g}$ ratio can be calculated from spectroscopic data of the HTO and H_2O molecules in the gas phase; the K_T value is known experimentally.

(ii) Partition function ratio of isotopic water molecules in gas phase ($f_{HTO,g}/f_{H_2O,g}$):

This ratio is given by

$$\frac{f_{HTO,g}}{f_{H_2O,g}} = \frac{\sigma_{H_2O}}{\sigma_{HTO}} \cdot \left(\frac{m_{HTO}}{m_{H_2O}}\right)^{3/2} \cdot \frac{(I_A I_B I_C)^{1/2}_{HTO}}{(I_A I_B I_C)^{1/2}_{H_2O}} \cdot \frac{\prod^{3} \sinh(h\nu_i/2kT)_{H_2O}}{\prod^{3} \sinh(h\nu_1/2kT)_{HTO}} \qquad (5)$$

Spectroscopic data, necessary for the calculation of f_{HTO}/f_{H_2O}, were obtained from the work of Libby.[14] This value is 289.54. Together with the experimental value of K_T,

$$K_T \cdot \frac{f_{HTO,g}}{f_{H_2O,g}} = 316.46 \qquad (6)$$

(iii) Partition function ratios of isotopic activated complexes for the slow discharge mechanism ($f_H^{\neq}/f_T^{\neq}$):

It is assumed that the activated complex H_2O---H---M (or its

isotopic analogue) is similar to a linear triatomic molecule (Fig. 1- cf. Parsons and Bockris[15]). $f^{\neq}_H/f^{\neq}_T$ is given by

$$\frac{f^{\neq}_H}{f^{\neq}_T} = \frac{f^{\neq}_{t,H}}{f^{\neq}_{t,T}} \cdot \frac{f^{\neq}_{r,H}}{f^{\neq}_{r,T}} \cdot \frac{f^{\neq}_{vib,H}}{f^{\neq}_{vib,T}} \qquad (7)$$

where $f^{\neq}_t$, $f^{\neq}_r$ and $f^{\neq}_{vib}$ represent the translational, rotational and vibrational contributions respectively of the indicated species.

(a) Translational partition function ratio ($f^{\neq}_{t,H}/f^{\neq}_{t,T}$):

The activated complex may be regarded as immobile, i.e. the translational partition function ratio is unity. Even if restricted translational motion occurred, there is only a negligible isotope effect, since the heavy metal atoms form a part of the isotopic activated complexes. Translational motion in two dimensions by H_3O^+ is not relevant.

(b) Rotational partition function ratio ($f^{\neq}_{r,H}/f^{\neq}_{r,T}$):

A small isotope effect arises due to the restricted rotation of the isotopic activated complexes about the two axes, through the center of gravity of the activated complex, mutually perpendicular to the axis of the molecule. The partition function ratio due to this restricted rotation is given by

$$\frac{f^{\neq}_{r,H}}{f^{\neq}_{r,T}} = \frac{\sinh^2 h\nu_T/2kT}{\sinh^2 h\nu_H/2kT} \qquad (8)$$

Since the observed librational frequencies are small (e.g., for water 600 cm^{-1}) and are inversely proportional to the square roots of

the corresponding moments of inertia, then

$$\frac{f^{\neq}_{r,H}}{f^{\neq}_{r,T}} = \frac{I^{\neq}_{H}}{I^{\neq}_{T}} \qquad (9)$$

where $I^{\neq}_{H}$ and $I^{\neq}_{T}$ are the moments of inertia of the H and T activated complexes about axes perpendicular to the axis of the molecule and through their respective centers of gravity. The calculated rotational partition function ratio is

$$\frac{f^{\neq}_{r,H}}{f^{\neq}_{r,T}} = 0.962 \qquad (10)$$

(c) Vibrational partition function ratio ($f^{\neq}_{vib,H}/f^{\neq}_{vib,T}$):

For a linear triatomic molecule, there are four degrees of vibrational freedom. Since one of these is imaginary for the activated complex, three frequencies are to be cnnsidered in calculating the vibrational partition function ratio of the isotopic activated complexes, which is given by

$$\frac{f^{\neq}_{vib,H}}{f^{\neq}_{vib,T}} = \frac{\sinh(h\,\nu_T/2kT)_s}{\sinh(h\,\nu_H/2kT)_s} \cdot \frac{\sinh^2(h\,\nu_T/2kT)_b}{\sinh^2(h\,\nu_H/2kT)_b} \qquad (11)$$

The suffices s and b stand for stretching and bending frequencies respectively.

It may be shown that for linear traiatomic molecules with H (or its isotopes) as the central atom and heavy end atoms (in our case the metal atom and H_2O) that

$$\left(\frac{\nu_T}{\nu_H}\right)^2_b = \frac{m_H}{m_T} = \frac{1}{3} \tag{12}$$

where (m_H/m_T) is the ratio of the mass of the H atom to that of the T atom. In addition, since bending frequencies are generally small, we may assume that

$$\frac{\sinh^2(h\nu_T)2kT)_b}{\sinh^2(h\nu_H/2kT)_b} = \frac{m_H}{m_T} = \frac{1}{3} \tag{13}$$

For the calculation of the stretching vibrational frequencies, it is necessary to solve the secular equation:

$$\lambda^2 - \lambda\left[\left(\frac{1}{m_1} + \frac{1}{m_2}\right) k_{11} + \left(\frac{1}{m_2} + \frac{1}{m_3}\right) k_{22} - \frac{2}{m_2} k_{12}\right] + \frac{m_1+m_2+m_3}{m_1 m_2 m_3}(k_{11}k_{22} - k_{12}^2) = 0 \tag{14}$$

where k_{11} is the force constant for the stretching of the bond between m_1 and m_2, k_{22} is the force constant for the stretching of the bond between m_2 and m_3 and k_{12} is a coupling constant. λ is given by the expression

$$\lambda = 4\pi^2 \nu^2 \tag{15}$$

Equation (14) is obtained by setting up the expressions for the potential energy, kinetic energy and then by using Lagrange's equations of motion. In order that the force constants for the activated complex may be determined, it is necessary to express the potential energy as a function of the two variable distances r_1 and r_2. From the table of values of V as a function of r_1 and r_2, which is obtained by a computer calculation, the reaction path and the coordinates, $r_1^{\neq}$ and $r_2^{\neq}$, at the saddle point may be determined. The force constants are obtained by a

calculation of the respective second derivatives [i.e. $(\partial^2 V/\partial r_1^2)_{r_1=r_1^{\neq}}$, $(\partial^2 V/\partial r_2^2)_{r_2=r_2^{\neq}}$ and $(\partial^2 V/\partial r_1 \partial r_2)_{r_1=r_1^{\neq}, r_2=r_2^{\neq}}$] of the potential energy at the saddle point. This method of calculation is the same as that used by Eyring et al.[16] Three such calculations were carried out for the slow discharge mechanism, varying the percentage coulombic-exchange energy ratios in the Heitler-London expression for the potential energy of a three atom system.[16] The results of such calculations are shown in Table 1. It may be seen from this Table that the variations in percentage coulombic energy have little influence on the real stretching frequencies of the activated complexes.

The importance of the effect of the stretching frequency to the isotope effect, is seen from the present calculations. Kodera et al.[6,7] considered only the effect of the bending frequencies of the activated complexes and as a result obtained high separation factors for this mechanism. By the inclusion of the effect of stretching frequencies, the partition function ratios of the activated complexes are considerably lower - hence also the separation factors - than that calculated by the Japanese workers.

This conclusion has also recently been stated, apparently independently, by Conway and Salomon.[17*] These workers obtained higher values for the ratio of partition functions of the isotopic activated complexes (and hence separation factors) in some cases, than those obtained in the present work due to an incorrect choice of the relevant

---

*However, the existence of the importance of the stretching frequency was indicated by the present authors to Professor Conway at a discussion on 14 October 1962.

TABLE 1. FORCE CONSTANT (k's), STRETCHING VIBRATIONAL FREQUENCIES (ω's), PARTITION FUNCTION RATIOS ($f_{H^{\neq}}/f_{D^{\neq}}$ and $f_{H^{\neq}}/f_{T^{\neq}}$) OF ISOTOPIC ACTIVATED COMPLEXES FOR THE SLOW DISCHARGE MECHANISM

Parameter	Calculation number		
	1	2	3
ρ_1 (%)	20	5	39
ρ_2 (%)	20	5	3
$r_1^{\neq}$ (Å)	1.05	1.05	1.05
$r_2^{\neq}$ (Å)	3.40	2.92	3.30
$E^{\neq}$ (kcal mole^{-1})	2	6	4
k_{11} (kcal mole^{-1} Å^{-2})	688.6	635.1	654.8
k_{22} (kcal mole^{-1} Å^{-2})	- 3.9	- 12.7	- 10.6
k_{12} (kcal mole^{-1} Å^{-2})	0	0	0
ω_H (cm^{-1})	2906	2773	2820
ω_D (cm^{-1})	2110	2015	2048
ω_T (cm^{-1})	1763	1686	1714
$\omega_{H^{\neq}}$(cm^{-1})	52 i	90 i	84 i
$\omega_{D^{\neq}}$(cm^{-1})	50 i	88 i	83 i
$\omega_{T^{\neq}}$(cm^{-1})	50 i	89 i	81 i
$\frac{\sinh(h\nu_D/2kT)_s}{\sinh(h\nu_H/2kT)_s}$	0.1465	0.1605	0.1552
$\frac{\sinh(h\nu_T/2kT)_s}{\sinh(h\nu_H/2kT)_s}$	0.0633	0.0725	0.0672
$(f_{H^{\neq}}/f_{D^{\neq}})\ 10^2$	7.207	7.897	7.636
$(f_{H^{\neq}}/f_{T^{\neq}})\ 10^2$	2.030	2.325	2.155

force constants necessary for the solution of the secular equations. These force constants were not calculated but chosen only by analogy of the activated complex with similar molecules in the ground state. It was assumed that the O-H stretching frequency in the activated state is quite small. However, our detailed potential energy calculations, varying the percentage coulombic energy, showed consistently high values of force constants for the stretching of the O-H bond. It is, thus, the opinion of the present authors that the higher partition function ratios obtained by Conway and Salomon are due to the assumptions of a low force constant for the O-H bond in the activated state. Calculations for a dual site adsorption model on similar lines made by these workers showed somewhat lower partition function ratios than those obtained in the present work, due to the greater number of vibrational modes for this model.

CLASSICAL SEPARATION FACTORS FOR THE VARIOUS MECHANISMS.

Using equations (6) and (10) along with the partition function ratios of the activated complexes found in Table 1 in equation (2), the classical value of the separation factor for the slow discharge mechanism may be obtained. The classical separation factors (both H-D and H-T) for all other mechanisms, calculated in a similar manner, along with that for the slow discharge mechanism are given in Table 2. For the calculations of the partition function ratios of isotopic activated complexes for the slow electrochemical and slow recombination mechanisms, the activated complexes were treated as linear pseudo tetra atomic and symmetrical trapezium shaped molecules. Figure 1 shows the models for these activated complexes. As in the case of the slow discharge mechanism, the

TABLE 2

THEORETICAL SEPARATION FACTORS FOR THE DIFFERENT MECHANISMS

AS CALCULATED IN PRESENT INVESTIGATION

Mechanism	Separation factors excluding tunneling corrections		Separation factors including tunneling corrections	
	S_D^*	S_T^*	S_D	S_T
Slow-discharge fast-recombination	2.4	3.4	3.0	4.6
Slow-discharge fast-electrochemical (in equilibrium)	3.8	6.2	3.8	6.2
Linked-discharge electrochemical (either rate-determining)				
(i) Coulombic energy 100% for all interactions	3.4	5.4	4.1	7.0
(ii) Coulombic energy 20% for M-H and H^+-OH_2 15% for H-H interactions	3.6	5.7	4.4	7.5
Fast-discharge slow-recombination				
(i) Ni(d_{Ni-Ni} = 3.52 Å)	5.5	11.3	5.8	13.0
(ii) Pt(d_{Pt-Pt} = 2.77 Å)	4.9	9.4	5.5	11.1
Fast-discharge slow-electrochemical				
(i) Coulombic energy 100% for all interactions	8.3	19.8	9.1	23.0
(ii) Coulombic energy 20% for Ni-H and H^+-OH_2 15% for H-H interactions	9.7	24.7	10.7	28.7
Slow molecular hydrogen diffusion	4.5	8.2	4.5	8.2

saddle point was located from the table of values of the potential energy as a function of the variable distances. The potential energy surface generated from one typical calculation is shown in Fig. 2. The saddle point is represented by a dot on the figure.

QUANTAL CORRECTION TO CLASSICAL SEPARATION FACTOR CALCULATION

THE NEED FOR QUANTUM MECHANICAL CORRECTION

According to the classical theory of reaction rates, γ_H (or γ_T) in equation (2), is zero for the reacting particles with energy less than the activation energy ($E^{\neq}$) and is equal to unity for particles with energy greater than $E^{\neq}$. Quantum mechanically, it is possible for γ to have a finite value for particles with energy less than $E^{\neq}$ and also to have a value less than unity for particles with energy greater than $E^{\neq}$. The net contribution of this non classical penetration and non classical reflection is expressed by the so-called tunneling correction factor, γ_H (or γ_T). The magnitude of γ depends on the dimensions of the energy barrier for the reaction and also on the mass of the particle being transferred. For hydrogen atom or ion transfer (or its isotopes) γ may have appreciable values depending on the height and width of the one dimensional normal mode along the reaction coordinate.

It is necessary to see how the tunnel effects introduce only a correction to the classical rate. The quantum mechanical rate for the proton discharge is given by

$$i_{q,1} = k_1 \, c_{H_3O^+} \int_{E_o}^{\infty} W(E) \, e^{-(E-E_o)/kT} \, dE \qquad (16)$$

where k_1 is a frequency factor, W(E) is the probability of proton tunneling at energy level E and E_o is the zero point energy for the stretching of the H^+-OH_2 bond. Since this motion is assumed to lead to reaction, the zero point energy of the activated state does not enter into the calculation if $i_{q,1}$. For low and wide barriers one attains the classical limit. Under these conditions, W = 0 for $E \leqslant E^{\neq}$ and W = 1 for $E > E^{\neq}$. Thus, equation (16) becomes

$$i_{c,1} = k_1 c_{H_3O^+} kT\, e^{-(E^{\neq} - E_o)/kT} \qquad (17)$$

The tunneling correction γ is given by

$$\gamma = \frac{i_{q,1}}{i_{c,1}}$$

$$= \frac{1}{kT} e^{(E^{\neq} - E_o)/kT} \int_{E_o}^{\infty} W(E)\, e^{-(E - E_o)/kT} dE \qquad (18)$$

The rate of the reaction is then given by

$$i_{q,1} = \gamma i_{c,1} \qquad (19)$$

It is well known that $i_{c,1}$ calculated according to Eq. (18) is not the observed rate when tunneling affects are negligible, since the zero point energy of the activated complex has been neglected according to the above one dimensional model analysis. An a priori calculation using i_q alone would have neglected the zero point energy levels of the activated state - a procedure shown to be invalid.[16,18,19] Thus, in Eq. (19), $i_{c,1}$ is the clasically calculated rate including all modes of vibration (taking into account the zero point energy of the activated state).

PREVIOUS WORK ON TUNNEL EFFECTS IN THE SLOW DISCHARGE MECHANISM

The possibility of proton tunneling effects in the hydrogen evolution reaction were considered fairly early but detailed calculations on these lines were carried out only recently by Christov.[20] There are, however, several factors which were not taken into consideration by Christov. Zero point energy contributions to the activation energy and to the separation factor were ignored. Thus, to explain a separation factor of six solely by tunnel effects, would lead to a higher degree of tunneling than if part of the isotope effect were ascribed as due to zero point energy differences and partly due to tunneling. In fact some workers[8] have been able to explain some observed isotope effects solely on the basis of zero point energy effects without considering the tunnel effect. Further Christov has ignored the important dependence of separation factor on potential since his calculations refer to the reversible potential. Conway[21] has calculated the effect of proton tunneling on the kinetics of the hydrogen evolution reaction as well as the H-D separation factor. Conway, like Christov, used the Eckart barrier in his calculations. However, he used quite narrow barriers (barrier width 0.5 $\mathring{A}$). Though reasonable variations of the separation factor with potential were observed it was found that high and different Tafel slopes were expected for proton and dueteron discharge. Further, if one were to calculate an activation energy, the value would be too low. Conway proposed the criterion of high and different Tafel slopes for the H^+ and D^+ discharge to determine the degree of tunneling. Due to the contradictory views expressed by these authors and the disagreement with experiment, the

role of proton tunneling and its effect on H-T separation factors was examined in the present work.

CRITERIA FOR SIGNIFICANT TUNNELING CONTRIBUTIONS

It is difficult to obtain a clear or sensitive quantitative method for assaying the degree of participation of quantum mechanical effects of proton transfer from solution. Thus,the Tafel slopes become independent of potential over a wide range of potential even though the penetration and reflection currents are very significant.

A striking phenomenon has been observed recently[12] - the separatinn factor on high overpotential metals is markedly dependent on potential. It can be shown that this effect is not explainable on classical lines[12] and consequently is an indication of non-classical contribution to proton transfer current. The degree of dependence of separation factor on potential is therefore a sensitive test of tunneling.

METHODOLOGY OF γ_H/γ_T CALCULATIONS

(i) Expression for tunneling probability

In the calculation of the quantum mechanical rate ($i_{q,1}$) and of the tunneling correction, it is essential to know the shape of the barrier along the one dimensional normal mode. The Eckart barrier[22] appears to have the closest fit to the real barrier and was hence used in the present work. The unsymmetrical Eckart barrier has the form

$$V(x) = \frac{A \exp(2\pi x/d)}{1 + \exp(2\pi x/d)} + \frac{B \exp(2\pi x/d)}{\left\{1 + \exp(2\pi x/d)\right\}^2} \tag{20}$$

where

$$A = A_o + E_o \eta \tag{21}$$

$$A_o = V(\infty) = V(-\infty) \tag{22}$$

$$B = 2E^{\neq} - A + 2\left\{E^{\neq}(E^{\neq} - A)\right\}^{1/2} \tag{23}$$

$$E^{\neq} = E^{\neq}_o - \beta e_o \eta \tag{24}$$

2d is the barrier width and $E^{\neq}_o$ is the barrier height at $\eta = 0$. For this barrier,

$$W(E) = \frac{\cosh 2\pi(\lambda + \mu) - \cosh 2\pi(\lambda - \mu)}{\cosh 2\pi(\lambda + \mu) + \cosh 2\pi\sigma} \tag{25}$$

where

$$\lambda = \frac{d}{h}(2mE)^{1/2} \tag{26}$$

$$\mu = \frac{d}{h}\left\{2m(E - A)\right\}^{1/2} \tag{27}$$

and

$$\sigma = \frac{1}{2}\left\{(8md^2 \frac{B}{h^2}) - 1\right\}^{1/2} \tag{28}$$

For barrier widths greater than 3.0 Å and $E^{\neq}_o \gg 1.0 \times 10^{-12}$ erg, we may use the approximate formula:

$$W = \frac{\exp\left\{2\pi(\lambda + \mu - \sigma)\right\} - \exp\left\{2\pi(\lambda - \mu - \sigma)\right\} - \exp\left\{-2\pi(\lambda - \mu + \sigma)\right\}}{\exp\left\{2\pi(\lambda + \mu - \sigma)\right\} + 1} \tag{29}$$

τ should now be obtained by using euqation (29) in equation (18). But the integral in the resulting equal for τ cannot be solved analytically. Thus, numerical integration was carried out on a digital computer. The results thereby obtained were found to be in agreement with the graphical method to within 5%.

(ii) Choice of barriers

A large number of computations were carried out with various combinations of barrier parameters at several temperatures and over a wide range of temperatures. Comparison of the computed values with the corresponding experimental data was then used to determine the most probable barrier parameters. The experimental data available, for comparison, are the Tafel slope, the separation factor and its variation with potential. Such a comparison should therefore yield a unique set of barrier parameters which are of physical significance.

(iii) Results of calculations

(a) Tafel slopes

The values of J, calculated according to

$$J = \int_{E_o}^{\infty} W(E) \exp\left\{ - (E - E_o)/kT \right\} dE \qquad (30)$$

using equation (29) for $W(E)$ were plotted as a function of potential to obtain the Tafel slopes recorded in Table 3. The Tafel slopes were linear over the entire potential range except at less than 50 mv. The results show that the Tafel slopes increase with increase in degree of proton tunneling. In Fig. 3, the classical dependence of Tafel slope on temperature is compared to the dependence in the presence of proton tunneling. For thin barriers, which lead to an independence of b on temperature at low temperatures, the Tafel slope is considerably larger than the classical value at room temperature. The same conclusion was also reached by Conway.[21] Thus, the present results show that the thin barrier model is not correct.

TABLE 3

COMPUTED TAFEL SLOPES

A_o (10^{-12} erg)	E_o^* (10^{-12} erg)	T °K	2d Å	b(mV) Protium	Deuterium	Tritium
0.0	1.4	298	6.0	118	118	118
	1.6	323	5.0	131	129	129
			4.0	134	130	130
			3.0	142	133	130
		298	6.0	118	118	118
			5.0	121	120	119
			4.0	124	121	119
			3.0	134	123	120
		273	5.0	112	110	109
			4.0	115	110	109
			3.0	127	114	110
		240	5.0	99.3	97.4	95.5
			4.0	104	98.0	96.8
			3.0	120	102	98.0
		198	5.0	84.3	81.4	79.3
			4.0	91.8	81.8	79.3
			3.0	116	88.6	83.6
	1.8	323	4.0	133	129	129
		298	6.0	119	118	118
			4.0	123	119	118
		273	4.0	114	110	108
	2.0	323	4.0	132	130	128
		298	4.0	123	119	118
		273	4.0	113	110	108
0.4	1.6	298	4.0	122	119	118
0.6	1.6	298	4.0	121	119	118
0.8	1.6	298	4.0	121	119	118

(b) Dependence of tunneling correction factor ratio on potential

Equation (2) may be rewritten as

$$S_T = \Gamma_{H,T}\, S_{T,Cl} \qquad (31)$$

where $\Gamma_{H,T}$ is equal to the ratio τ_H/τ_T and $S_{T,Cl}$ is the classical separation factor calculated in the previous sub-section. The variation of separation factor with potential is hence given by

$$\frac{dS_T}{d\eta} = S_{T,Cl}\,\frac{d\Gamma_{H,T}}{d\eta} \qquad (32)$$

The computed figures of τ_H, τ_T and $\Gamma_{H,T}$ for the most probable barrier parameters are given in Table 4. These parameters were arrived at by a comparison of the observed variation of the separation factor with potential. A typical plot, showing variations of A_o, used in the calculation of τ_H, τ_T and hence $\Gamma_{H,T}$, is given in Figure 4. A comparison between the calculated and experimental values of S_T as a function of potential at 27°C and 50°C is shown in Figure 5.

(c) Dependence of separation factor on temperature

The results at 50° and 27°C are in agreement with the theory of proton tunneling as applied to a discharge followed by catalytic mechanism. The results from 5° to - 71°C do not agree with this theory. The results at the lower temperatures may be interpreted on the basis of a change over of the mechanism of the subsequent step to electrochemical desorption mechanism. For this mechanism, the separation factor is given by equation (3). Such a change over leads to a large reduction in $dS/d\eta$, as observed experimentally. Furthermore,

TABLE 4

COMPUTED RESULTS FOR THE MOST PROBABLE BARRIER

$2d = 4.0$ Å, $E_o^* = 1.5 \times 10^{-12}$ ergs, $A_o = -0.6 \times 10^{-12}$ ergs

T	η_i	$\tilde{\tau}$			Γ	
°K	(10^{-12} erg)	H	D	T	H,D	H,T
323	0.8	3.851	1.844	1.488	2.088	2.591
	1.2	3.257	1.730	1.431	1.883	2.280
	1.4	2.957	1.665	1.397	1.777	2.120
	1.6	2.665	1.596	1.359	1.670	1.961
	1.8	2.375	1.522	1.320	1.561	1.802
	2.0	2.079	1.444	1.276	1.440	1.632
300	0.8	5.089	2.053	1.588	2.483	3.215
	1.2	4.107	1.901	1.516	2.163	2.716
	1.4	3.634	1.816	1.474	2.005	2.473
	1.6	3.190	1.727	1.428	1.851	2.239
	1.8	2.768	1.631	1.379	1.698	2.012
	2.0	2.351	1.534	1.326	1.534	1.777
278	0.8	7.417	2.358	1.728	3.158	4.292
	1.2	5.569	2.145	1.634	2.606	3.409
	1.4	4.752	2.028	1.579	2.338	3.009
	1.6	4.015	1.907	1.522	2.116	2.641
	1.8	3.354	1.781	1.459	1.890	2.299
	2.0	2.731	1.655	1.393	1.658	1.962

the values of S calculated at an overpotential of 1.3 V are also in good agreement with experiment at temperatures of 5^{o} and below.

CONCLUSIONS

USE OF H-T SEPARATION FACTORS IN MECHANISM DETERMINATION OF PROTON TRANSFER PROCESSES AT ELECTRODES

The theoretical separation factors (Table 2) indicate that most mechanisms (path and r.d.s.) can be distinguished by means of separation factors except a linked discharge-electrochemical desorption mechanism where the rate-determining step cannot be determined. A knowledge of the degree of coverage of hydrogen on the metal is also required to make such a distinction. The theoretically forecast values for a slow molecular hydrogen diffusion mechanism and for a slow recombination mechanism are also not well separated. However, in this case, the experimental separation factors (S_T) on the platinum group of metals - which should be independent of the metal for the slow molecular diffusion mechanism - or the temperature coefficient of the separation factors should be helpful in distinguishing between the two mechanisms. Secondary isotope effects due to H_2/HDO interchange reactions play a role only in the case of the slow discharge-fast electrochemical desorption mechanism at low overpotentials.

The mechanisms on the metals sutdied in acid and alkaline electrolytes, obtained by this method, are indicated in Table 5.

TABLE 5

EXPERIMENTAL H-T SEPARATION FACTORS AT A c.d. OF 10^{-2} amp cm^{-2} AND AT A TEMPERATURE OF 25°C AND MECHANISMS INDICATED THEREFROM

Metal	Electrolyte	Separation factor	Mechanism
Pt	0.5 N H_2SO_4	9.6 ± 0.4	Fast discharge-slow recombination
Pt	0.5 N NaOH	15.3 ± 0.8	Fast discharge-slow electrochemical desorption
Rh	0.5 N H_2SO_4	10.7 ± 0.4	Fast discharge-slow recombination
W	0.5 N H_2SO_4	6.0 ± 0.2	Linked discharge-electrochemical desorption
W	0.5 N NaOH	4.4 ± 0.5	Slow discharge-fast recombination
Ni	0.5 N H_2SO_4	18.0 ± 0.9	Fast discharge-slow electrochemical desorption
Ni	0.5 N NaOH	4.1 ± 0.3	Slow discharge-fast recombination
Cu	0.5 N H_2SO_4	18.1 ± 2.4	Fast discharge-slow electrochemical desorption
Hg	0.5 N H_2SO_4	5.8 ± 0.3	Slow discharge-fast recombination
Pb	0.5 N H_2SO_4	6.7 ± 0.7	Linked discharge-electrochemical desorption.
Pb	0.5 N H_2SO_4	7.2 ± 0.8	Linked discharge-electrochemical desorption
Cd	0.5 N H_2SO_4	9.2 ± 0.5	Linked discharge-electrochemical desorption

TABLE 5

EXPERIMENTAL H-T SEPARATION FACTORS AT A c.d. OF 10^{-2} amp cm^{-2} AND AT A TEMPERATURE OF 25°C AND MECHANISMS INDICATED THEREFROM

Metal	Electrolyte	Separation factor	Mechanism
Pt	0.5 N H_2SO_4	9.6 ± 0.4	Fast discharge-slow recombination
Pt	0.5 N NaOH	15.3 ± 0.8	Fast discharge-slow electrochemical desorption
Rh	0.5 N H_2SO_4	10.7 ± 0.4	Fast discharge-slow recombination
W	0.5 N H_2SO_4	6.0 ± 0.2	Linked discharge-electrochemical desorption
W	0.5 N NaOH	4.4 ± 0.5	Slow discharge-fast recombination
Ni	0.5 N H_2SO_4	18.0 ± 0.9	Fast discharge-slow electrochemical desorption
Ni	0.5 N NaOH	4.1 ± 0.3	Slow discharge-fast recombination
Cu	0.5 N H_2SO_4	18.1 ± 2.4	Fast discharge-slow electrochemical desorption
Hg	0.5 N H_2SO_4	5.8 ± 0.3	Slow discharge-fast recombination
Pb	0.5 N H_2SO_4	6.7 ± 0.7	Linked discharge-electrochemical desorption.
Pb	0.5 N H_2SO_4	7.2 ± 0.8	Linked discharge-electrochemical desorption
Cd	0.5 N H_2SO_4	9.2 ± 0.5	Linked discharge-electrochemical desorption

USE OF SEPARATION FACTORS IN ASCERTAINING DEGREE OF PROTON TUNNELING IN THE SLOW DISCHARGE MECHANISM.

The most probable barrier parameters for proton discharge on mercury were fonnd to be 2d = 4.0 Å, $E_o^{\neq}$ = 1.5 x 10^{-12} erg and A_o = - 0.6 x 10^{-12} erg. For these parameters it was found that at η = 1V and at 27°C, γ_H = 3.19. From this value of γ_H, it follows that the degree of proton tunneling is 68.7%. With decrease of cathodic potential or decrease in temperature, the degree of proton tunneling decreases.

Christov[20] used A_o = 0 in his calculation and arrived at 70% degree of tunneling at η = 0. With the present values of A_o, the degree of tunneling is 86% at the reversible potential. The assumption that A_o = 0 made by christov is invalid. Further, Christov neglected the effect of zero point energies.

Conway and Salomon[17] claim that proton tunneling effects are not significant. This conclusion was based mainly on the observed independence of activation energy for proton discharge from methanolic acid solution down to - 98°C. The activation energy obtained was 11.2 Kcal $mole^{-1}$ compared to 20 Kcal $mole^{-1}$ in aqueous solutions. The activation energy of 11.2 Kcal $mole^{-1}$ is incompatible with overpotential measurements above 1 V since the barrier height would be less than zero under such conditions, assuming the symmetry factor to be half. Their result appears to be connected with the observed variation of the transfer coefficient with potential.

The low temperature separation factor data indicate that the removal of adsorbed hydrogen is by the electrochemical desorption step.

The present work shows that the Tafel slope and its temperature dependence are not good criteria for determining the role of proton tunneling in the hydrogen evolution reaction.

THE RELATION OF KINETICS OF HYDROGEN EVOLUTION TO DOUBLE LAYER STRUCTURE

Important conclusions of a confirmatory nature, about the structure of the electrode-solution double layer may be made on the basis of the present study. The present results of the most probable width ($2d = 4$ Å) is equivalent to a proton transfer distance of 3.7 Å, between the metal surface and the center of the oxygen bonded to the discharging proton. This distance compares favorably with a distance of 3.8 Å as calculated from the Bockris, Devanathan and Müller[23] theory of the double layer. Further evidence for this arises from the potential energy calculation for the slow electrochemical desorption mechanism. Earlier models of double layer structure showed no activation energy for this reaction but the Bockris, Devanathan and Müller model showed that there is an activation energy for this reaction.

REFERENCES

1. Srinivasan, Ph.D. Thesis, University of Pennsylvania, Philadelphia (1963).
2. Horiuti and Okamoto, Sci. Pap. Inst. Phys. Chem. Res. (Tokyo) 28, 231 (1936).
3. Okamoto and Horiuti and Hirota, Sci. Pap. Inst. Phys. Chem. Res. (Tokyo), 29, 223 (1936).
4. Horiuti, Keii and Hirota, J. Res. Inst. Cat., 2, 1 (1951).

5. Horiuti and Nakamura, J. Res. Inst. Cat., 2, 73 (1951).

6. Keii and Kodera, J. Res. Inst. Cat., 5, 105 (1957).

7. Kodera and Saito, J. Res. Inst. Cat., 7, 5 (1959).

8. Conway, Proc. Roy. Soc., A247, 400 (1958).

9. Bockris and Srinivasan, J. Electrochem. Soc., 111, 844 (1964).

10. Bockris and Srinivasan, ibid., 111, 853 (1964).

11. Bockris and Srinivasan, ibid., 111, 858 (1964).

12. Matthews, Ph.D. Thesis, University of Pennsylvania, Philadelphia (1965).

13. Sepall and Mason, Can. J. Chem., 38, 2024 (1960).

14. Libby, J. Chem. Phys., 11, 101 (1943).

15. Parsons and Bockris, Trans. Farad. Soc., 47, 914 (1951).

16. Glasstone, Laidler and Eyring, Theory of Rate Processes, McGraw-Hill, N. Y.

17. Conway and Salomon, Ber. Buns. Gess., 68, 331 (1964).

18. Melander, Isotope Effects on Reaction Rates, Ronald Press, N.Y. (1960).

19. Sharp and Johnston, J. Chem. Phys., 37, 1541 (1962).

20. Christov, Electrochim. Acta, 4, 306 (1961).

21. Conway, Can. J. Chem., 37, 178 (1959).

22. Eckart, Phys. Rev., 35, 1303 (1930).

23. Bockris, Devanathan and Müller, Proc. Roy. Soc., A274, 55 (1963).

FIG. I Activated complexes for various mechanisms

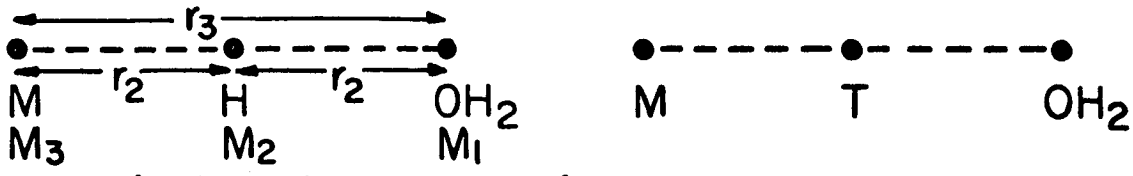

Activated complexes for slow discharge mechanism

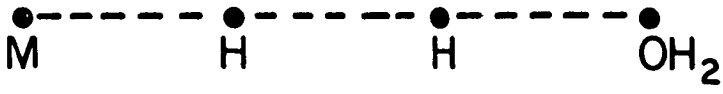

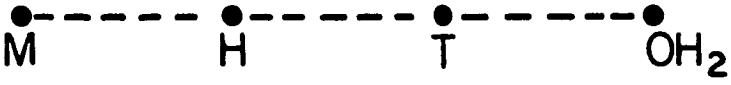

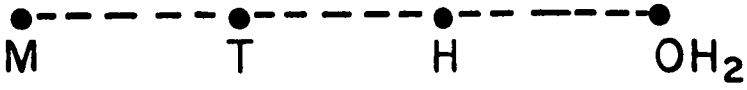

Activated complexes for slow electrochemical desorption mechanism

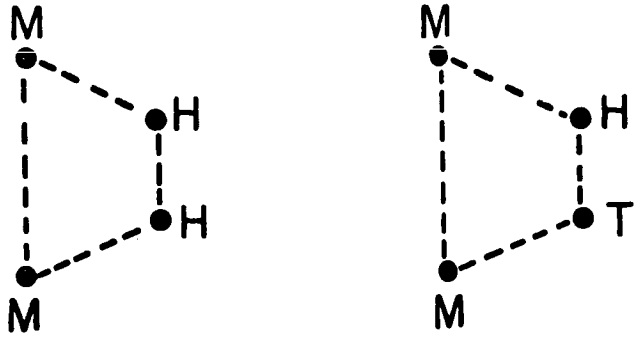

Activated complexes for slow recombination mechanism

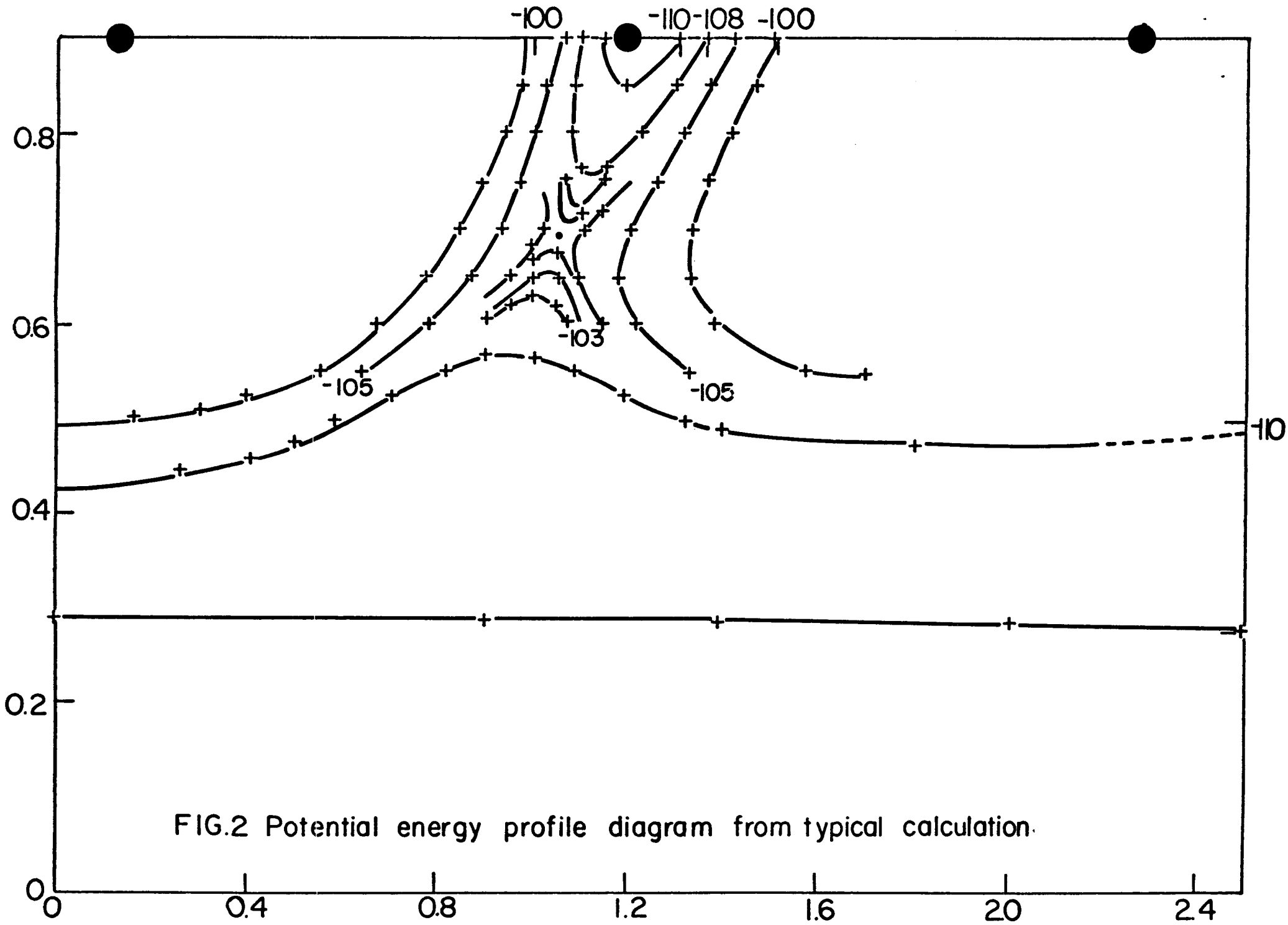

FIG.2 Potential energy profile diagram from typical calculation.

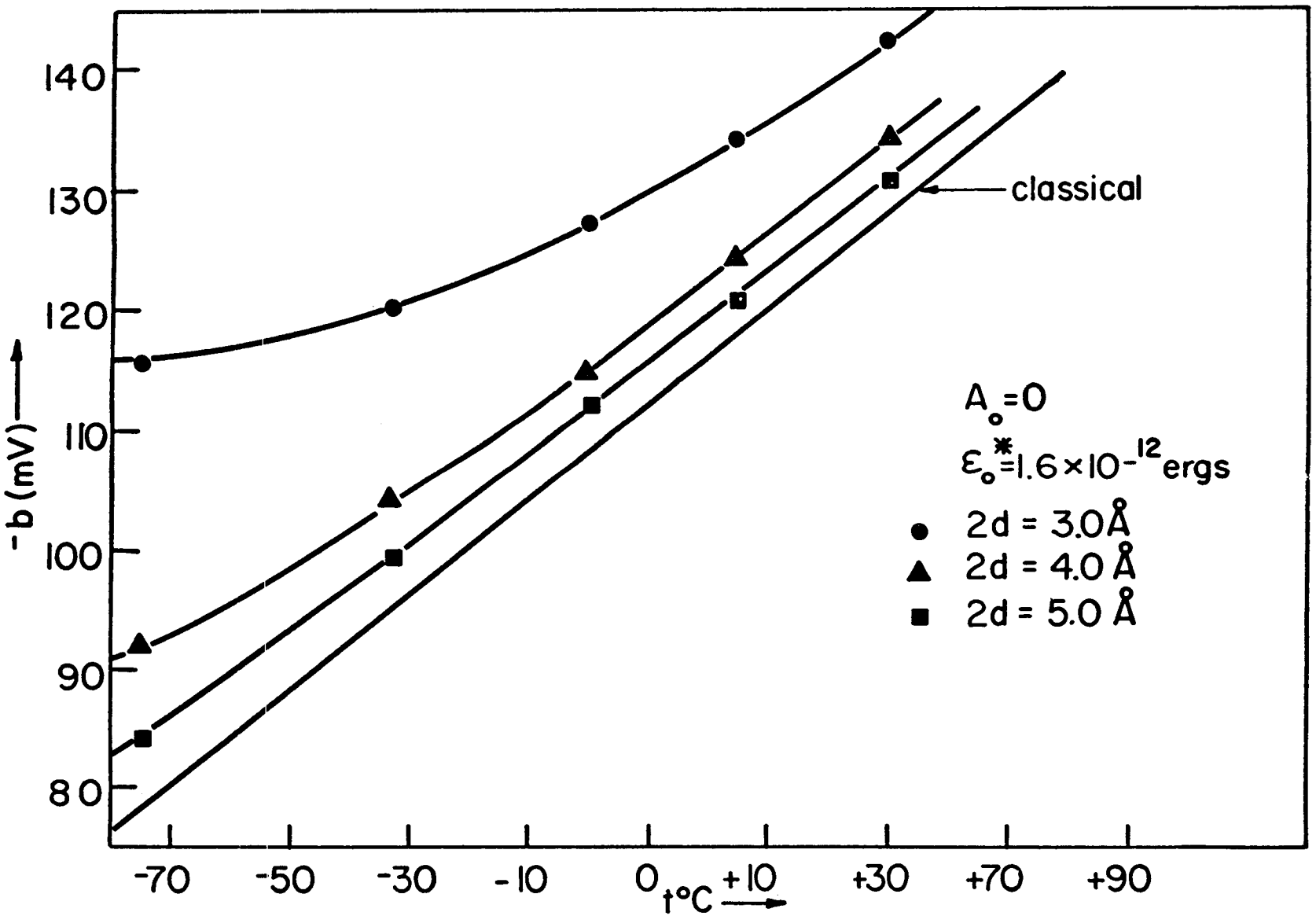

FIG.3 Dependence of computed Tafel slopes on temperature

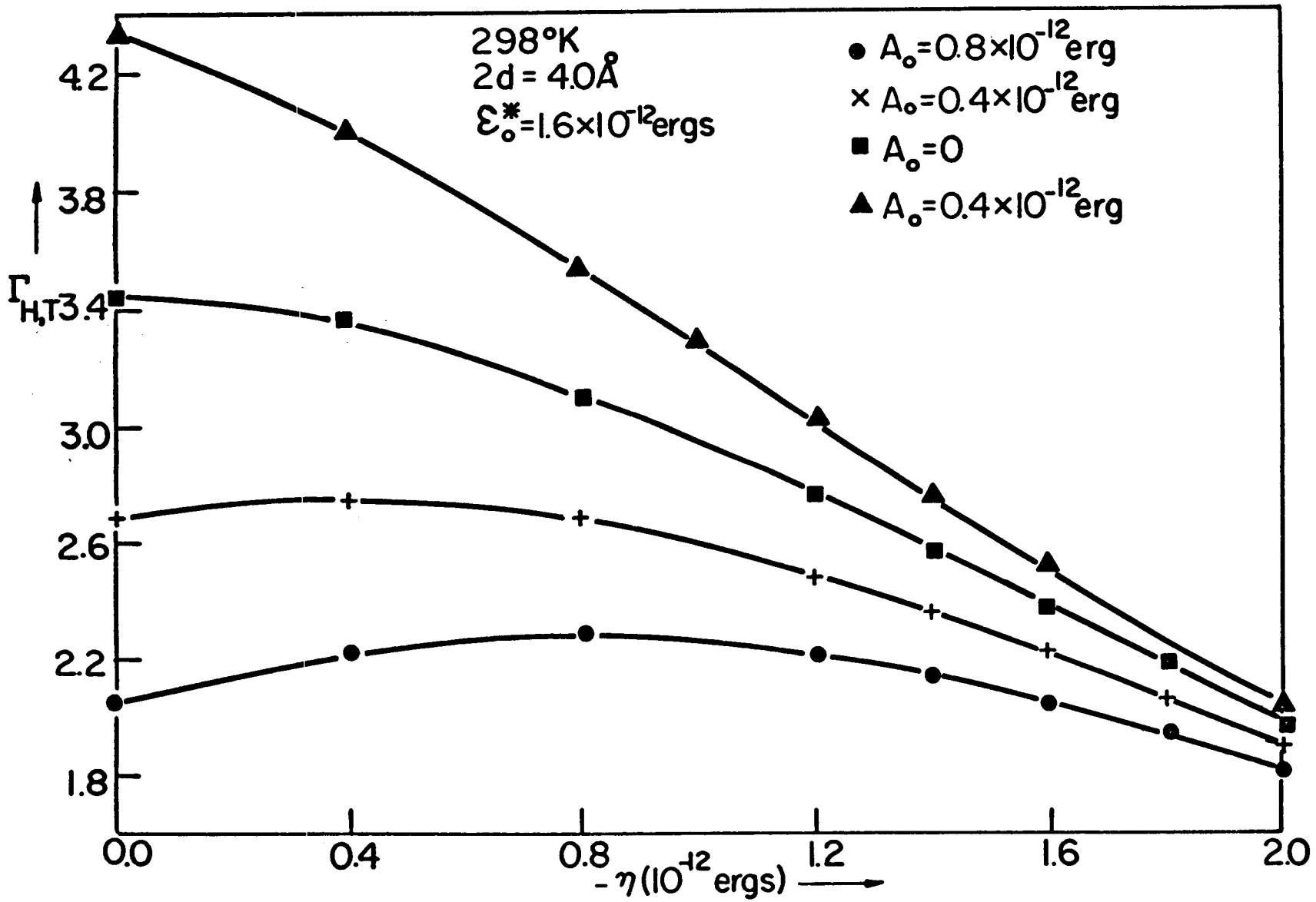

FIG. 4 Dependence of Γ on A_o

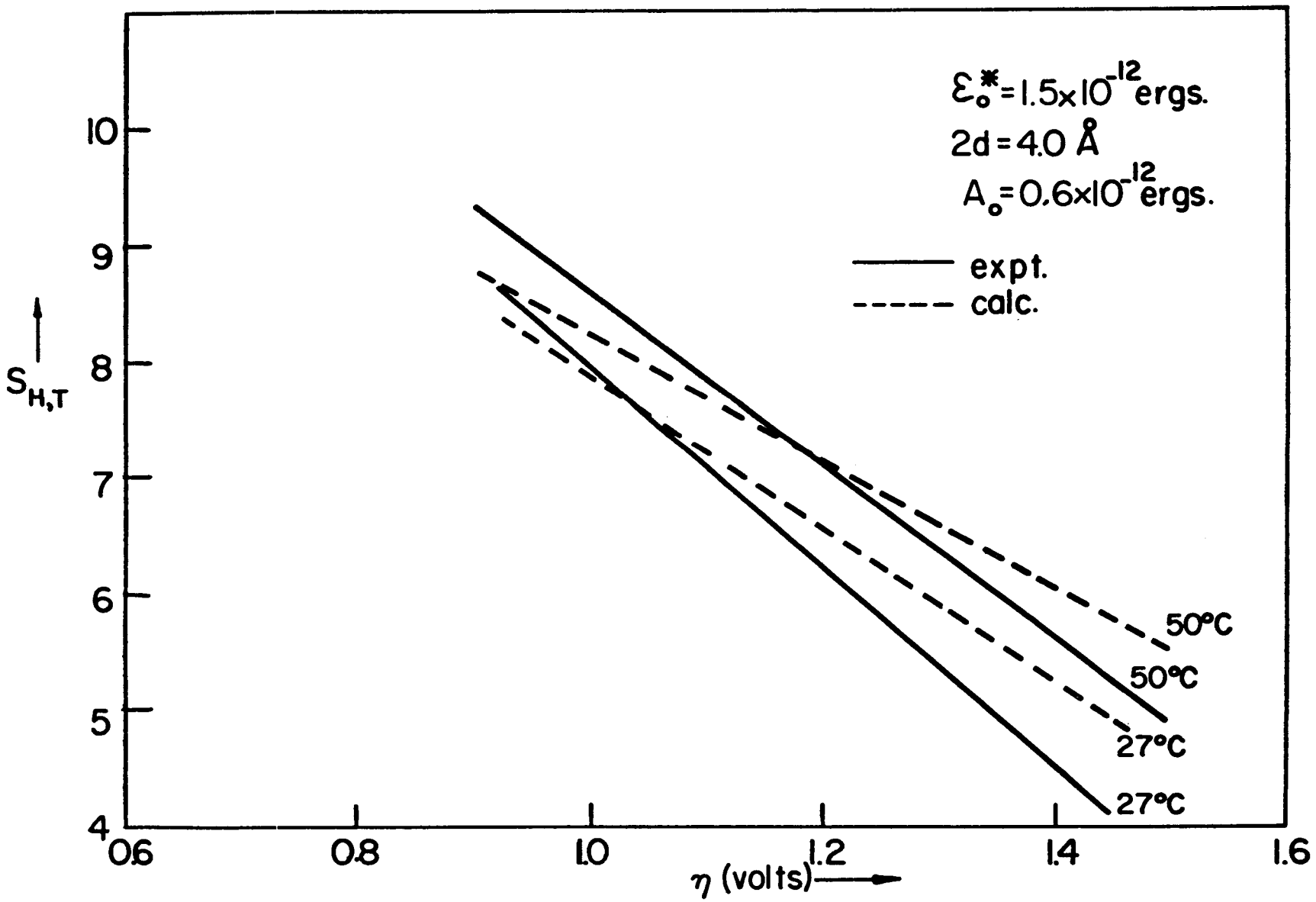

FIG. 5 Comparison of calculated and observed dependence of S on potential

APPENDIX IV

A BRIEF OUTLINE OF ELECTROCATALYSIS

J. O'M. Bockris and S. Srinivasan

The Electrochemistry Laboratory
The University of Pennsylvania
Philadelphia, Pa. 19104

A BRIEF OUTLINE OF ELECTROCATALYSIS

J. O'M. Bockris and S. Srinivasan

The Electrochemistry Laboratory
The University of Pennsylvania
Philadelphia, Pa. 19104

1. Definition of Electrocatalysis

The term electrocatalysis was first used by Grubb[1] in 1962. It is an important term because it makes the role of the electrodes - which are, essentially, simple catalysts of charge transfer reactions - in electrochemical energy conversion clearer.

A formal definition of electrocatalysis is desirable and it could be: "The influence of the inert metal electrode upon the reaction rate, when the influence of mass transfer to or from active sites is eliminated."

2. Empirical Proof of the Existence of Electrocatalysis

In the case of non-porous electrodes - planar or wire - there is no doubt, whatsoever, about the existence of electrocatalysis. It is most apparent when all mass transfer effects are eliminated by stirring, as in the studies of the electrolytic hydrogen evolution reaction.[2] In addition, this reaction is very convenient for elucidating the concept of electrocatalysis because measurements are made in the cathodic region where very many electrode materials may be used without the counter and complicating effects of dissolution. The effect of electrocatalysis may be illustrated in two ways[3,4] as shown in Figs. 1 and 2.

Fig. 1 shows that a plot of work function vs log i_o[3] (i_o = exchange current density) reveals the presence of two distinct groups which are associated with the slow discharge and the slow electrochemical desorption mechanism. In Fig. 2, a plot of D_{MH} (bond energy of M-H bond) vs the overpotential at a constant current density again shows the division between the two groups. For metals in which the slow discharge mechanism is operative, the overpotential decreases with increasing D_{MH}. The opposite behavior is observed for the metals on which the rate-determining step is electrochemical desorption.[4]

In the case of porous electrodes, there is a possibility that electrocatalysis may not play an important role because:

(i) The active area available is now greater so that the real current density is much lower than with planar smooth electrodes. Hence, the overpotential may, in general, be considerably smaller.

(ii) The resistance to transport of ions to or from the active sites is higher when porous electrodes are used than in the corresponding situation with planar electrodes. Therefore, the ohmic components of polarization may become more important than the activation components in the former case and conceivably then vitiate electrocatalytic effects. That these suppositions are, however, not confirmed at least for oxygen reduction and hydrocarbon oxidation are indicated by the large shifts in the potential - log i (i = current density) curves for oxygen reduction and propane oxidatinn with various catalysts.

The only explanation of such shifts - which correspond to about four decades at the same potential in the cases with widest variation - is that there is a difference in particle size distribution. But this

explanation may be excluded because:

(i) A very high difference in particle size and distribution is necessary to explain the results.

(ii) The order of the activity is the same as is obtained by experiments with planar electrodes.

Thus, the only possible theory is that it is the electrocatalytic influence of the materials, which is being observed.

3. Influence of Electrocatalysis on Electrochemical Energy Conversion as Illustrated by a Simple Case

The equations for the variation of efficiency and of power with current density are relatively simple if the cell potential (E) - current density (i) relation is linear as represented by

$$E = E_r - mi \tag{1}$$

where E_r is the cell potential when i = o. m in equation (1) is a constant and may be expressed by

$$m = \sum\left(\frac{RT}{i_o F}\right) + \sum\left(\frac{RT}{i_L F}\right) + R_i \tag{2}$$

where summations represent the resistance due to activation and concentration losses at each of the electrodes; R_i is the internal resistance per cm^2 of the cell. m is thus the effective internal resistance of the cell.

E may also be expressed by the relation

$$E = iR_E \tag{3}$$

where R is the resistance in ohm cm^2 of the external load. From equations (1) and (3), it follows that

$$i = \frac{E_R}{R_E + m} \tag{4}$$

Thus, the rate i increases as m decreases for a constant R_E. From equation (2), m decreases as i_o and i_L increase but as R_i decreases. For the case that $i_L >> i_o$, $R_i \approx 0$, and $(i_o)_{anode} << (i_o)_{cathode}$

$$m = \frac{RT}{i_{o,a}F} \tag{5}$$

where $(i_o)_a$ is the exchange current density for the anodic reaction. Thus, the higher the value of $i_{o,a}$, the higher is the current density obtainable for a constant external load. The maximum power, P_m, is reached when

$$R_E = m \tag{6}$$

P_m is given by

$$P_m = E_r^2/4m \tag{7}$$

Under the conditions when (5) holds,

$$P_m = \frac{E_R^2}{4RT/i_oF} \tag{8}$$

Thus, P_m increases directly with i_o, which parameter is a measure of the electrocatalytic rate constant. A similar conclusion may be reached for the case when the current-potential relation is not linear.

4. Extent to which Electrocatalysis may be Effected:

4.1. Basic principles

In any overall reaction, there is a reaction sequence and within this consecutive mechanism there is a rate-determining step.

Consequently, the central problem in determining the role of electrocatalysts in fuel cell reactions, is to determine the rate-determining step of the reactinn, which depends mainly on the electrode material. This aspect has been generally neglected but is most necessary.

The mechanism of electro-oxidation of ethylene on platinized platinum at 80°C in H_2SO_4 has been investigated in detail.[5] (Fig. 3). It was shown that the water discharge step is rate-determining. In this connection, it is worthwhile to examine the potential energy - distance relation for the water discharge step on a metal (Fig. 4). The vertical distance between the intersection point and the minimum of the initial state curve may be taken as an approximate measure of the activation energy for the reaction. By adjusting the factors such as the heat of adsorption of oxygen on the metal, the electronic work function, etc., it should be possible theoretically, to predict increase in rate of the reaction, depending on the electrocatalyst.

4.2. Practical Realizations

(i) Influence of electronic factors

To some extent, effects predicted theoretically can be tested experimentally. For example, in the Fe^{2+}/Fe^{3+} redox reaction, since no adsorption process is involved a pure work function effect is expected and has been confirmed experimentally by working on Au, Pd and a series of their alloys[6] (Fig. 5). With increasing work function, the exchange current density for the reaction increases. However, the hydrogen evolution reaction on Au-Pd system shows somewhat of a different

behavior.[7] With increasing Au content, there is a sharp decrease in rate till about 60% Au. Thereafter, the rate is almost a constant up to 100% Au (Fig. 6). In this case, from 0 to 60% Au there is a progressive filling up of the d band, which is associated with a decrease in the strength of the M-H band strength and hence of the rate. Above 60%, since the d band is complete, the M-H bond strength and the reaction rate are practically constant.

In the case of the electrooxidation of ethylene, a plot of the rate of the reaction at a constant electrode-solution potential versus the latent heat of sublimation of the metal (or alloy) electrode revealed an interesting behavior[8] (Fig. 7). The result may be summarized as follows: as the heat of sublimation of the metal increases, the strength of the adsorption bond between the metal and oxygen atoms increases, as seen from the Pauling equation.[9]

$$D_{M-O} = \frac{1}{2} (D_{M-M} + D_{O-O} + 23.06 (X_M - X_O)^2 \qquad (9)$$

where D_{M-M} and D_{O-O} are the dissociation energies of the M-M and O-O bonds respectively. (D_{M-M} varies directly with $\overline{C}$ the latent heat of sublimation, L_s). With increasing strength of the M-O bond, the water discharge reaction is accelerated. But eventually, there reaches a stage where the M-O bond strength becomes high enough to make the water discharge rate quite fast and not the rate-determining step. The stronger is the bond between the metal and adsorbed oxygen, the slower is the rate of the succeeding intermediate step between it and the adsorbed ethylene molecule. At the point where the water discharge step ceases to be rate-determining, the latter step may then control the

rate of the overall reaction. The second curve in Fig. 7 is obtained with an alloy made of one metal on the left hand side and the other as the right hand side of the curve 1. This curve, too, has a shape similar to curve 1. Thus, instead of using Pt, which is at the peak of the first curve, alloys of composition corresponding to the peaks may be used.

(ii) Influence of geometric factors:

In the study of the hydrogen evolution reaction on the various crystal planes of Ni, it was found that the (111) plane, which is the most densely packed plane, has the smallest overvoltage.[10] This result is consistent with the view that the electrochemical desorption step is rate-determining. No effect of grain size of Pt was found in the hydrogen evolution and in the Fe^{2+}/Fe^{3+} reactions.[11]

(iii) Activation by radiation:

The activation of an electrode process can also be brought about by radiation from a source which is deposited on the electrode or is situated externally. Schwabe[12] has investigated the influence of α and β emitters, deposited on the electrode, on the activity of the oxygen electrode. In this case, one of the following radioactive elements: Ru 106, Ir 192, Tl 204, Po210 was deposited electrolytically on a Pt or Ni electrode, in the form of sheets, sieves or cylinders. The electrolyte used was 1 N KOH. In the absence of any radiation, the rest potential of an oxygen electrode reached a steady value, 200-250 mv below the reversible potential in about 20 min. In the presence of

radioactive Tl deposited on the electrode (activity 3 mc cm^{-2}), a stationary value, within 150-180 mv of the reversible potential was attained in about 10 min. The current-potential relations also show that the activated electrodes are less polarized than the unactivated ones. The activated electrodes also show a more uniform potential-time behavior under galvanostatic conditions. Schwabe points out that it is not probable that the energy of the β and α radiation influences the activation process but that the activity of the electrode surface is increased.

(iv) Use of redox system to change path of reactions:

The oxygen dissolution reaction is highly irreversible on most electrodes and thus reduces the efficiency of electrochemical energy conversion. One possible way of improving the performance of the cathode in a fuel cell is by the use of redox systems. The nitric acid/nitric oxide redox couple has been successfully used.[13] The electrode reaction is the reduction of nitric acid to nitric oxide instead of the electrochemical reduction of oxygen. Oxygen then oxidizes nitric oxide back again to nitric acid. Thus, though the overall reaction is still the same, the path of the reaction is considerably altered. Since the electrochemical reduction of nitric acid is quite fast and so also is the chemical oxidation of nitric oxide, problems of polarization losses are considerably reduced.

Molybdenum redox couples have been used in two ways for the oxidatinn of methanol - use of a Pt-Mo alloy[14] as the catalyst or the use of molybdates in the electrolyte.[15] The electrode reaction is the

oxidation of the Mo^{5+} to Mo^{6+} ion and the chemical regeneration of Mo^{5+} ion is effected with methanol.

(v) Activation by pulsing

The method of activation by pulsing, which has possible applications in hydrocarbon-oxygen fuel cell, was developed by Bockris et al.[16] In this work, the potential of a platinum electrode, at which anodic oxidation of ethylene occurs, was momentarily increased to a value close to that of oxide formation (e.g., 0.9 - 1.0 V vs N.H.E.), which thereby increased the activity of the electrode. It was suggested that the activation is caused by the removal of some inactive species, which is adsorbed on the electrode at the working potential during the momentary increase of potential. The high activity of the electrode may be maintained by the use of repeated pulses at the fuel electrode. Since the pulse current is in the same direction as the output current, the fuel cell may be activated by continuous momentary short circuiting.

(vi) Active area and meniscus heating effect in porous electrode

Studies are being conducted to understand the mechanisms of electrochemical reactions carried out in a single pore of varying dimensions.[17] Such studies should lead to an understanding of the mode of operation of porous electrodes used in fuel cells. Two important aspects will be briefly mentioned. Steady-state current-potential measurements for the hydrogen dissolution reaction on an inactivated Pt electrode show a linear relation over a considerable range of potential (600 mV). Ohmic behavior is indicated. Optical examination of the meniscus indicates a

finite contact angle. Cahan has carried out a mathematical analysis for the expected current-potential behavior, assuming a contact angle of 45° and that the electrochemical reaction is fast. A linear current-potential relation was obtained theoretically, thus confirming the experimental result. Further, it was shown that most of the reaction was concentrated in a very small region near the top of the meniscus. Due to the extremely high current density in this region considerable heating effects should be expected. Such heating effects are quite clear from the microscopic examination of the meniscus. At fairly high overpotentials, the gas-solution boundary shifted and microscopic droplets covered the electrode. These droplets subsequently grow in size and cover the main liquid. Cahan interpreted this behavior as being due to irreversible heat effects, which raise the temperature in the region of the meniscus. Water, thus evaporates and condenses on the cooler part of the electrode above the meniscus. The meniscus heating effect also supports the view of the absence of a film.

The idea that the reaction takes place only in a small region may be used in the construction of the electrode by preferential location of the catalyst particles in this active region, thereby minimizing the quantity of catalyst and hence its cost.

5. Limitations in a Study of Electrocatalysis

The region of electrical potential in which most reactions of interest to fuel cells are studied is from 0 to 1.2 V vs a hydrogen electrode in the same solution. From the Pourbaix diagrams,[18] it may be seen that the only metals which are stable in acid solutions are Pt,

Rh, Ir, Os, Ru, Re, Au and Tc. In alkaline solutions the choice is wider. The instability of the metal is caused by corrosion or the formation of passive films. With alloys, too, there are the same problems depending on the composition of the alloys. In this case, preferential dissolution of the alloys may take place. Thus, it appears necessary, both from the academic and economic points of view to direct a major part of the future work towards non-metal electrocatalysts, e.g., semicnnduction oxides, carbides, chelates, etc. Chelates may in a sense be considered to play a dual role, i.e. they[1] exert the catalytic properties of the metals and are stable due to the action of the chelating agent.

ACKNOWLEDGEMENTS

Financial support from the National Aeronautics and Space Administration on Grant No. NsG-325 and the U. S. Army Engineer Research and Development Laboratories, Fort Belvoir, under Contract No. DA-44-009-AMC-469(T), for the relevant sections of the above work carried out at the Electrochemistry Laboratory, University of Pennsylvania, is gratefully acknowledged.

REFERENCES

1. Grubb, W. T., Nature, 198, 883 (1963).
2. Bockris, J. O'M., Modern Aspects of Electrochemistry, Vol. I, Chapter IV, Butterworths, London (1954).
3. Matthews, D. B., Ph.D. Thesis, University of Pennsylvania (1965).
4. Conway, B. E., and Bockris, J.O'M., J. Chem. Phys., 26, 532 (1957).
5. Wroblowa, H., Piersma, B. J., and Bockris, J. O'M., J. Electroanal. Chem., 6, 401 (1963).
6. Bockris, J. O'M., Jahan, R., and Damjanovic, A., to be published.
7. Bockris, J. O'M., and Damjanovic, A., to be published.
8. Kuhn, A. T., Bockris, J. O'M., and Wroblowa, H., to be published.
9. Pauling, L., Nature of the Chemical Bond, p. 60, Cornell University Press, Ithaca, New York (1948).
10. Piontelli, R. Peraldo Bicelli, L., and LaVecchia, A., Rend. Acc. Na.2, Linceii VIII, 27 312 (1959).
11. Reddy, A. K.N., and Paunovic, A., NASA Contract (NsA325) Report for semicannual period ending 30th September 1964, submitted by The Electrochemistry Laboratory, University of Pennsylvania, Phila.
12. Schwabe, K., Fuel Cells, Vol. 2, Chapter 6, Editor G. J.Young, Reinhold, N. Y. (1963).
13. Shropshire, J. A., and Tarmy, B. L., Advances in Chemistry Series, 47, 153 (1965).
14. Heath, C. E., Proceedings of 1ith Annual Power Sources Conference, p. 33 (1964).
15. Shropshire, J. A., Electrochemical Society Meeting, Washington, D. C., Oct. 12-15 (1964).

16. Bockris, J. O'M., Piersma, B. J., Gileadi, E., and Cahan, B. D., J. Electroanal. Chem., 7,487 (1964).

17. Bockris, J. O'M., Cahan, B., and Wroblowa, H., to be published.

18. Pourbaix, M., Atlas D'Equilibres Electrochimiques, Cauther-Villars and Co., Paris (1963).

CAPTIONS TO FIGURES

Figure 1: Dependence of exchange current density for hydrogen evolution on the work function of metals.

Figure 2: Dependence of hydrogen overpotential at a current density of 10^{-3} amp cm^{-2} on the metal-hydrogen bond strength.

Figure 3: Typical plot in determination of kinetic parameters for the ethylene oxidation reaction. Case illustrated is effect of ethylene partial pressure (P_E) on current density. P_E is in (1) 10^{-4}, (2) 10^{-3}, (3) 10^{-2}, (4) 10^{-1}, (5) 1 atmos.

Figure 4: Potential energy profile diagram for the water discharge step.

Figure 5: Log i_o for the Fe^{2+}/Fe^{3+} reaction vs % Au composition for Au, Pd and their alloys.

Figure 6: Log i_o for the hydrogen evolution reaction vs % Au composition for Au, Pd and their alloys.

Figure 7: Current at a potential of 600 mv (N.H.E.) vs latent heat of sublimation for ethylene oxidation on some metals and alloys.

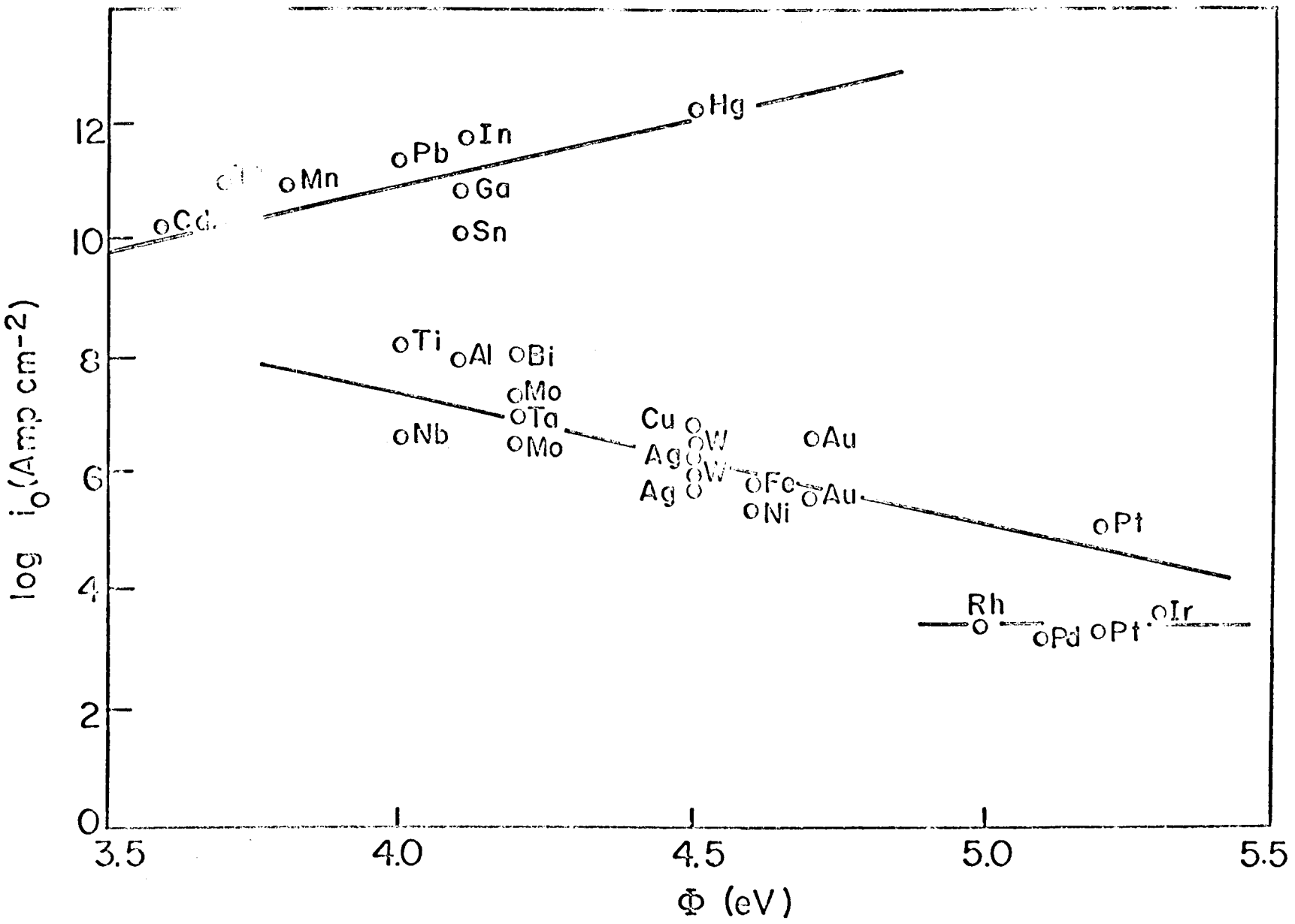
log i_o (Amp cm-2)
12
10
8
6
4
2
0
3.5
4.0
4.5
5.0
5.5
Φ (eV)
oHg
oPb
oIn
oMn
oGa
oCd
oSn
oTi
oAl
oBi
oMo
oTa
oMo
oNb
Cu
Ag
Ag
oW
oW
oFe
oNi
oAu
oAu
oPt
Rh
oPd
oPt
oIr

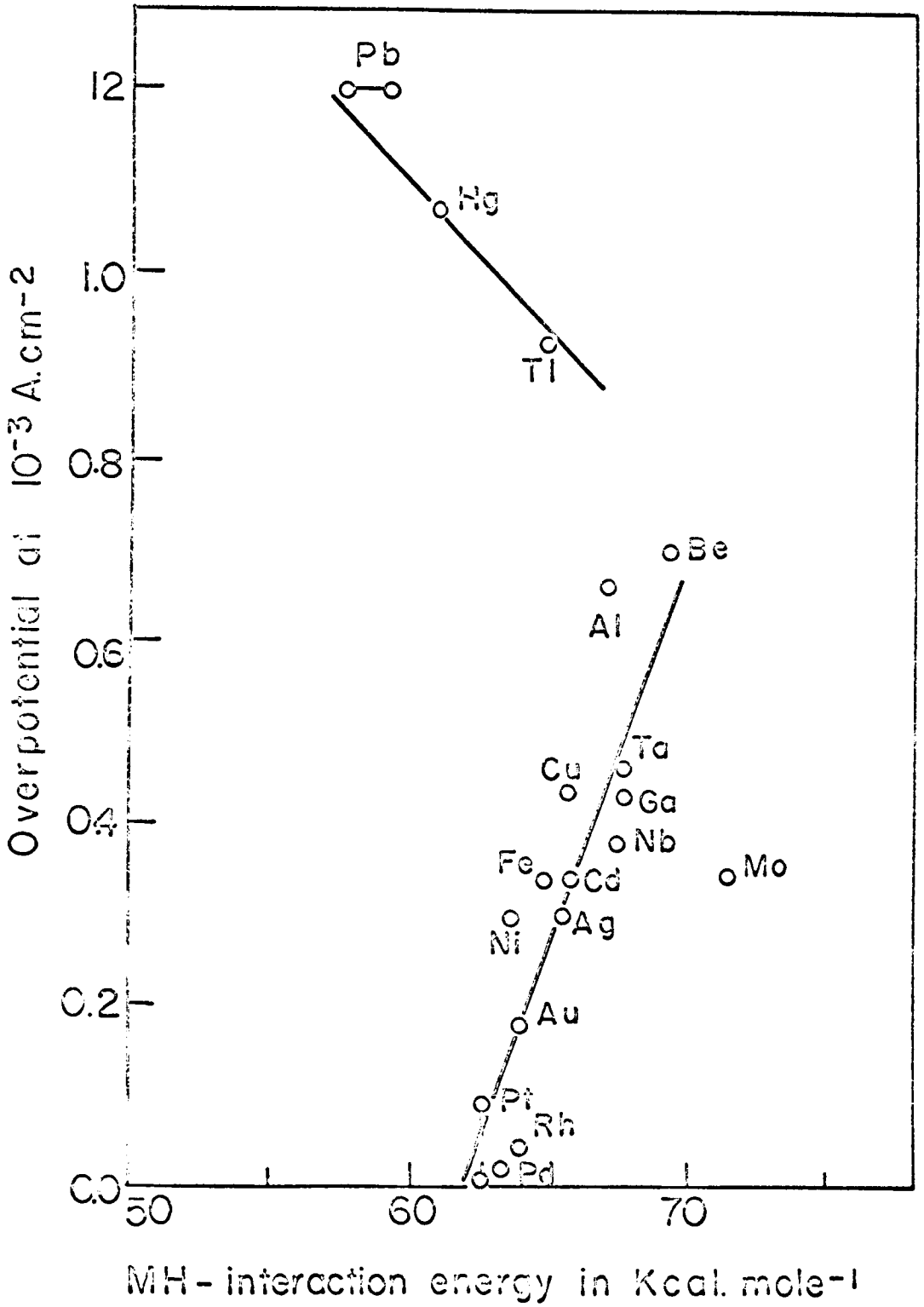
Pb
Hg
Tl
Be
Al
Ta
Cu
Ga
Nb
Fe
Cd
Mo
Ni
Ag
Au
Pt
Rh
Pd
1.2
1.0
0.8
0.6
0.4
0.2
0.0
50
60
70
Overpotential at 10^{-3} A.cm^{-2}
MH - interaction energy in Kcal. mole^{-1}

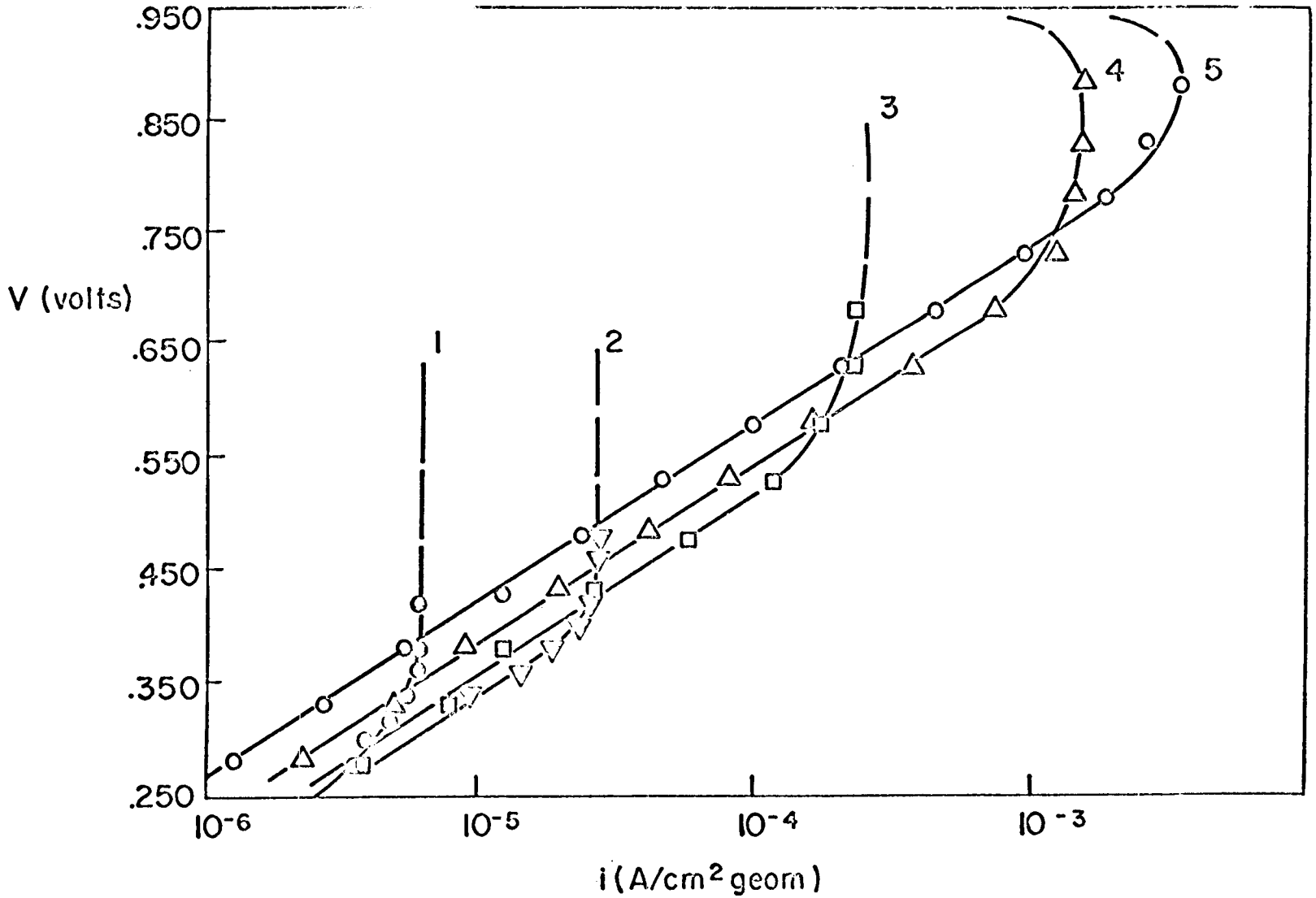
.950
.850
.750
.650
.550
.450
.350
.250
V (volts)
1
2
3
4
5
10-6
10-5
10-4
10-3
i (A/cm2 geom)

Fig. 4.

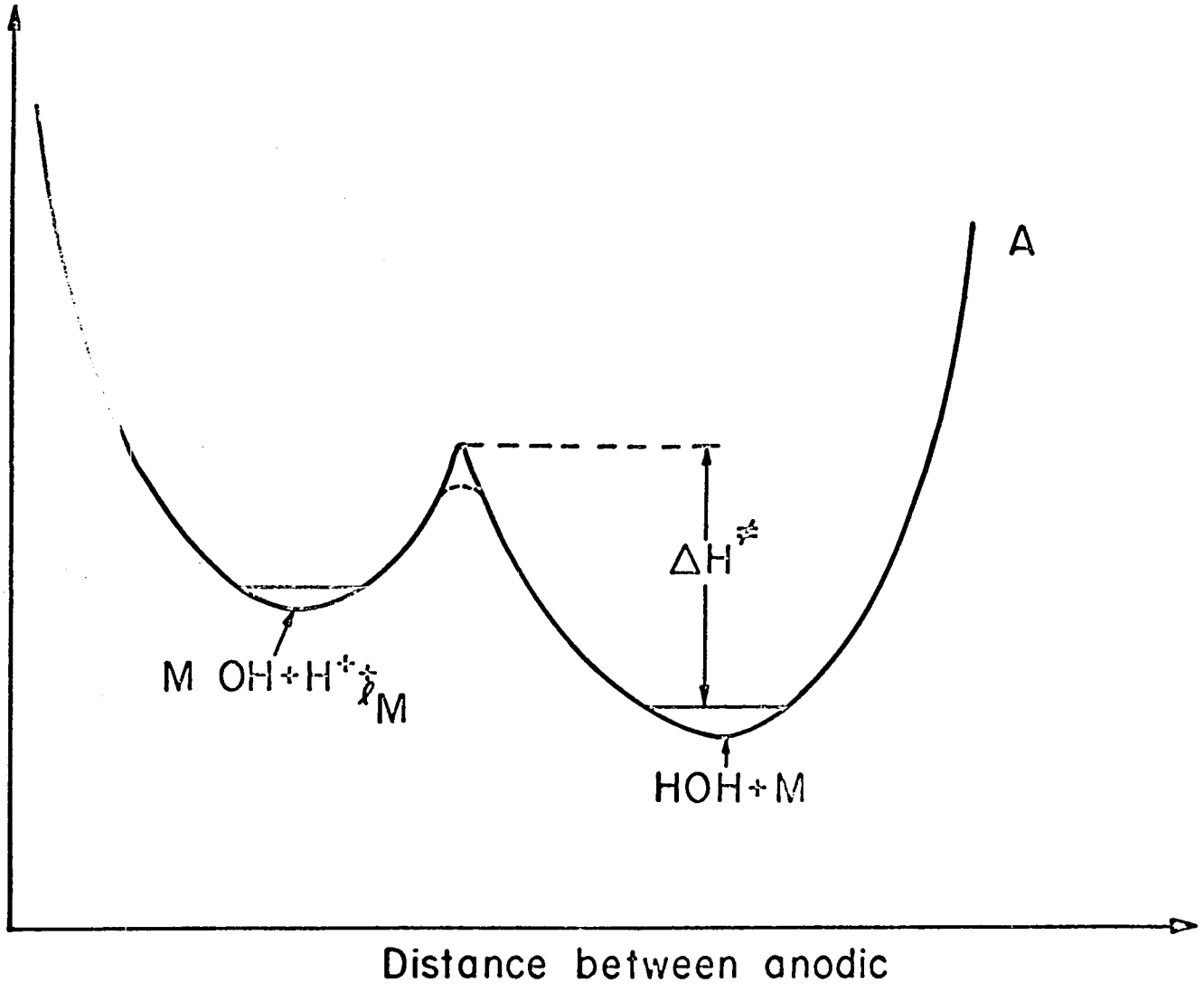

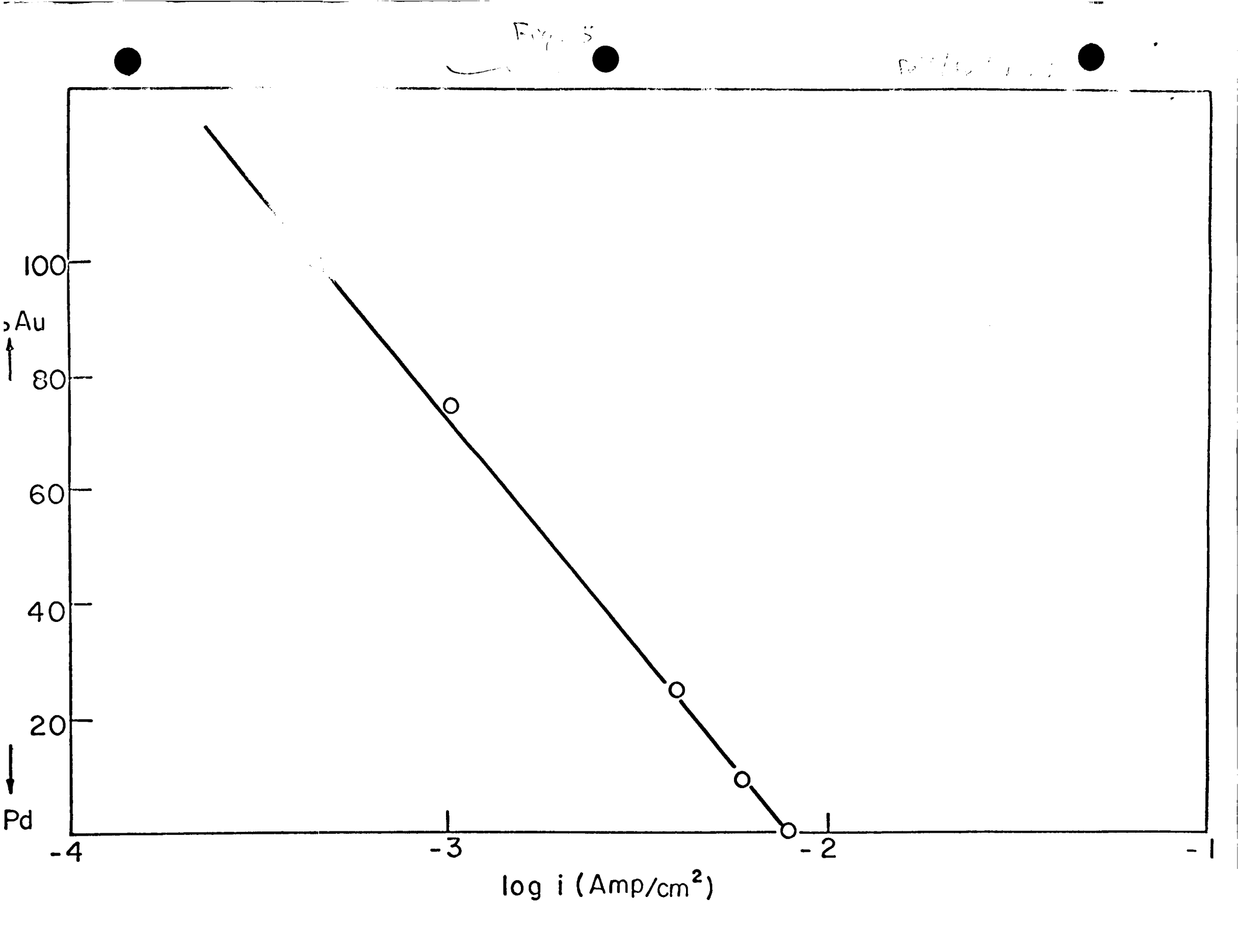
100
Au
80
60
40
20
Pd
-4
-3
-2
-1
log i (Amp/cm²)

Fig. 6.

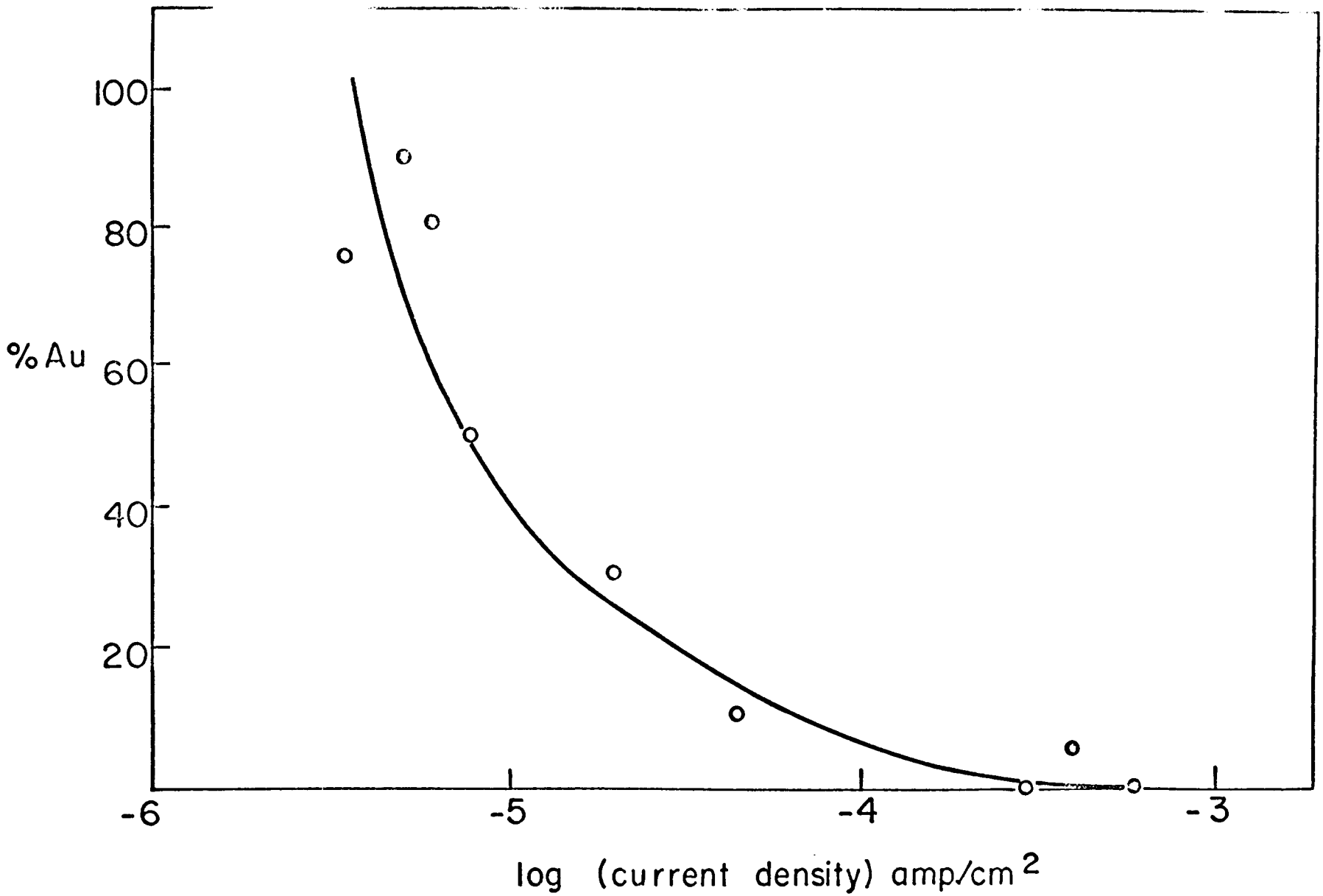

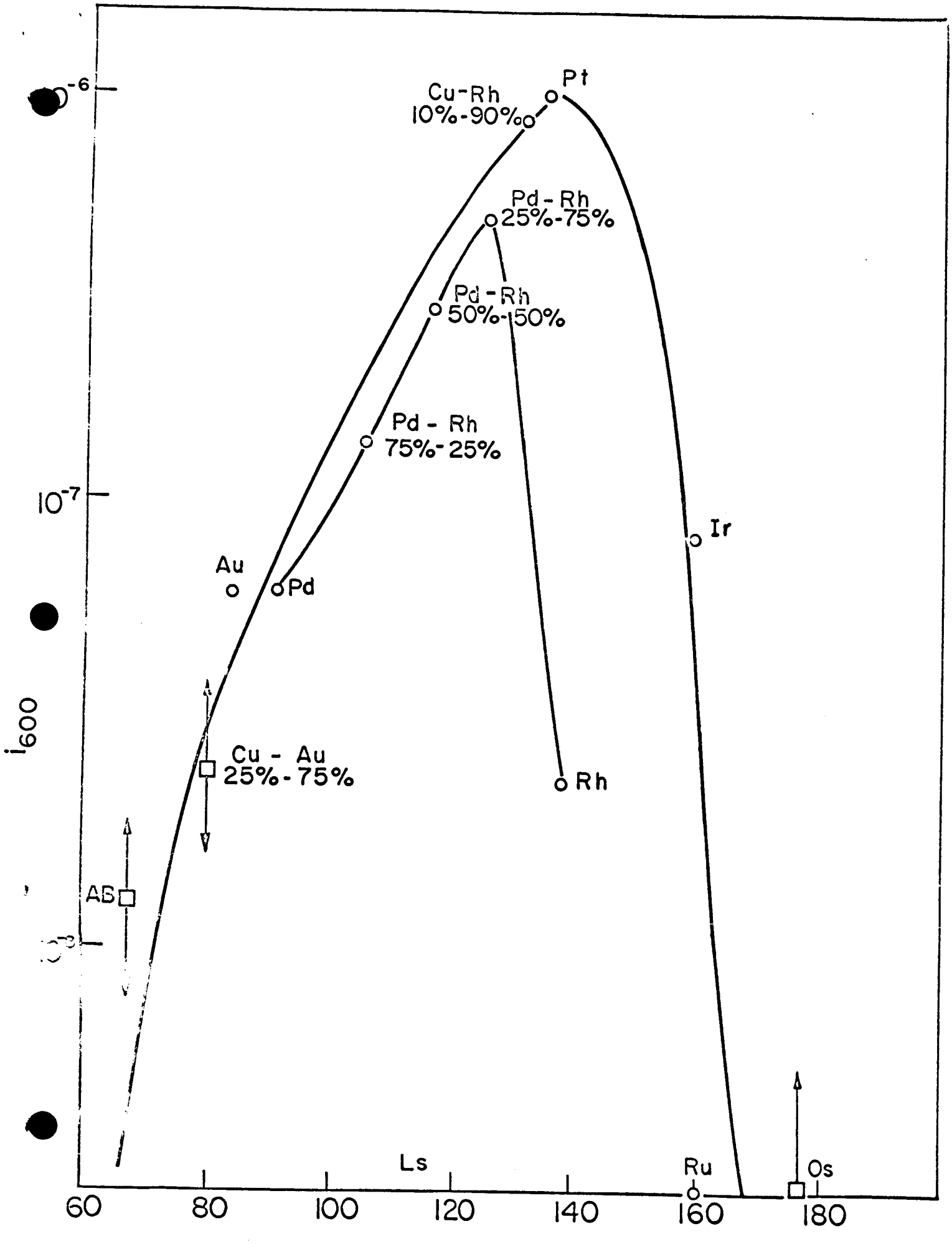
10^{-6}
10^{-7}
10^{-8}
i_{600}
Cu-Rh
10%-90%
Pt
Pd-Rh
25%-75%
Pd-Rh
50%-50%
Pd-Rh
75%-25%
Ir
Au
Pd
Cu - Au
25%-75%
Rh
AB
Ls
Ru
Os
60
80
100
120
140
160
180

DISTRIBUTION LIST FOR FUEL CELL REPORTS

August, 1964

One copy to be sent to each addressee, unless otherwise indicated.
Note that more than one addressee may be shown for the same address.
Name/Name means only one copy needed.

National Aeronautics & Space Administration
Washington, D. C. 20546
Attn: Ernst M. Cohn, Code RNW
George F. Esenwein, Code MAT
A. M. Andrus, Code ST
J. R. Miles, Code SL

National Aeronautics & Space Administration
Scientific and Technical Information Facility
P. O. Box 5700
Bethesda, Maryland, 20014 (3)

National Aeronautics & Space Administration
Goddard Space Flight Center
Greenbelt, Maryland
Attn: Thomas Hennigan

National Aeronautics & Space Administration
Langley Research Center
Langley Station
Hampton, Virginia
Attn: S. T. Peterson

National Aeronautics & Space Administration
Lewis Research Center
21000 Brookpark Road
Cleveland 35, Ohio
Attn: N. D. Sanders
Robert Miller
Robert L. Cummings

National Aeronautics & Space Administration
Marshall Space Flight Center
Huntsville, Alabama
Attn: Philip Youngblood

National Aeronautics & Space Administration
Ames Research Center
Pioneer Project
Moffett Field, California
Attn: James R. Swain

Cell Reports (con't.)

National Aeronautics & Space Administration
Manned Spacecraft Center
Houston 1, Texas
Attn: Richard Ferguson (for EP-5)
Robert Cohen
Forrest E. Eastman, EE-4

National Aeronautics & Space Administration
Ames Research Center
Mountain View, California
Attn: Jon Rubenzer, Biosatellite Project

Jet Propulsion Laboratory
4800 Oak Grove Drive
Pasadena, California
Attn: Aiji Uchiyama

DEPARTMENT OF THE ARMY

U. S. Army Engineer R&D Labs.
Fort Belvoir, Virginia
Attn: Electrical Power Branch

U. S. Army Engineer R&D Labs.
Fort Monmouth, New Jersey
Attn: Arthur F. Daniel (Code SELRA/SL-PS)

U.S. Army R&D Liaison Group (9851 DV)
APO 757
New York, New York
Attn: Chief, Chemistry Branch

U.S. Army Research Office
Physical Sciences Division
3045 Columbia Pike
Arlington Virginia

Harry Daimond Labs.
Room 300, Building 92
Connecticut Ave. & Van Ness St., N.W.
Washington, D.C.
Attn: Nathan Kaplan

Cell Reports (Con't.)

Army Material Command
Research Division
AMCRD-RSCM T-7
Washington 25, D.C.
Attn: John W. Crellin

Natick Labs.
Clothing & Organic Materials Div.
Natick, Massachusetts
Attn: Leo A. Spano/Robert N. Walsh

U.S. Army TRECOM
Physical Sciences Group
Fort Eustis, Virginia
Attn: (SMOFE)

U.S. Army Research Office
Box CM, Duke Station
Durham, North Carolina
Attn: Paul Greer/Dr. Wilhelm Jorgensen

U.S. Army Mobility Command
Research Division
Center Line, Michigan
Attn: O. Renius (AMSMO-RR)

Hq., U.S. Army Material Command
Development Division
Washington 25, D.C.
Attn: Marshall D. Aiken (AMCRD-DE-MO-P)

DEPARTMENT OF THE NAVY

Office of Naval Research
Department of the Navy
Washington 25, D.C.
Attn: Dr. Ralph Roberts/H.W. Fox

Mr. J. H. Harrison
Special Projects Division
U.S. Navy Marine Engineering Lab.
Annapolis, Maryland 21402

Cell Reports (Cont'd.)

Bureau of Naval Weapons
Department of the Navy
Washington 25, D.C.
Attn: (Code RAAE)

U.S. Naval Research Laboratory
Washington, D.C., 20390
Attn: (Code 6160)

Bureau of Ships
Department of the Navy
Washington 25, D.C.
Attn: Bernard B. Rosenbaum/C.F. Viglotti

Naval Ordnance Laboratory
Department of the Navy
Corona, California
Attn: Mr. William C. Spindler (Code 441)

Naval Ordnance Laboratory
Department of the Navy
Silver Spring, Maryland
Attn: Philip B. Cole (Code WB)

DEPARTMENT OF THE AIR FORCE

Wright-Patterson AFB
Aeronautical Systems Division
Dayton, Ohio
Attn: George W. Sherman, APIP

AF Cambridge Research Lab
Attn: CRZE
L. G. Hanscom Field
Bedford, Massachusetts
Attn: Francis X. Doherty/Edward Rasking (Wing F)

Rome Air Development Center, ESD
Griffiss AFB, New York
Attn: Frank J. Mollura (RASSM)

Cell Reports (cont'd.)

Space Systems Division
Attn: SSZAE-11
Air Force Unit Post Office
Los Angeles 45, California

Air Force Ballistic Missile Division
Attn: WEZYA-21
Air Force Unit Post Office
Los Angeles 45, California

ATOMIC ENERGY COMMISSION

Mr. Donald B. Hoatson
Army Reactors, DRD
U.S. Atomic Energy Commission
Washington 25, D.C.

OTHER GOVERNMENT AGENCIES

Office, DDR&E: USW & BSS
The Pentagon
Washington 25, D.C.
Attn: G. B. Wareham

Mr. Kenneth B. Higbie
Staff Metallurgist
Office, Director of Metallurgy Research
Bureau of Mines
Interior Building
Washington, D.C., 20240

Institute for Defense Analyses
Research and Engineering Support Division
400 Army-Navy Drive
Arlington, Virginia 22202
Attn: Dr. George C. Szego/R. Hamilton

Cell Reports (cont'd.)

Power Information Center
University of Pennsylvania
Moore School Building
200 South 33rd Street
Philadelphia 4, Pennsylvania

Office of Technical Services
Department of Commerce
Washington, D.C. 20009

PRIVATE INDUSTRY

Alfred University
Alfred, New York
Attn: Professor T. J. Gray

Allis-Chalmers Mfg. Co.
1100 S. 70th Street
Milwaukee 1, Wisconsin
Attn: Dr. W. Mitchell, Jr.

Allison Division of General Motors
Indianapolis 6, Indiana
Attn: Dr. Robert E. Henderson

American Cyanamid Company
1937 W. Main Street
Stamford, Connecticut
Attn: Dr. R. G. Haldeman

American Machine & Foundry
689 Hope Street
Springdale, Connecticut
Attn: Dr. L.H. Shaffer
Research & Development Division

Astropower, Inc.
2968 Randolph Avenue
Costa Mesa, California
Attn: Dr. Carl Berger

Cell Reports (Cont'd.)

Battelle Memorial Institute
Columbus 1, Ohio
Attn: Dr. C. L. Faust

Bell Telephone Laboratories, Inc.
Murray Hill, New Jersey
Attn: Mr. U. B. Thomas

Clevite Corporation
Mechanical Research Division
540 East 105th Street
Cleveland, Ohio
Attn: A. D. Schwope

Electrochimica Corp.
1140 O'Brien Drive
Menlo Park, California
Attn: Dr. Morris Eisenberg

Electro-Optical Systems, Inc.
300 North Halstead Street
Pasadena, California
Attn: E. Findl

Engelhard Industries, Inc.
497 DeLancy Street
Newark 5, New Jersey
Attn: Dr. J. G. Cohn

Esso Research and Engineering Company
Products Research Division
P.O. Box 215
Linden, New Jersey
Attn: Dr. Carl Heath

The Franklin Institute
Philadelphia, Pennsylvania
Attn: Mr. Robert Goodman

General Electric Company
Direct Energy Conversion Operations
Lynn, Massachusetts
Attn: Dr. E. Glazier

Cell Reports (Cont'd.)

Garrett Corp.
1625 Eye St., N.W.
Washington 6, D.C.
Attn: George R. Shepherd

General Electric Company
Research Laboratory
Schenectady, New York
Attn: Dr. H. Liebhafsky

General Electric Company
Missile and Space Division (Room M1339)
P.O. Box 8555
Philadelphia 1, Pennsylvania
Attn: L. Chasen

General Motors Corp.
Box T
Santa Barbara, California
Attn: Dr. C. R. Russell

Globe-Union, Inc.
Milwaukee 1, Wisconsin
Attn: Dr. C. K. Morehouse

Dr. Joseph S. Smatko
General Motors
Defense Research Laboratories
P.O. Box T
Santa Barbara, California, 93102

Johns Hopkins University
Applied Physics Laboratory
8621 Georgia Avenue
Silver Spring,Maryland
Attn: W. A. Tynan

Leesona Moos Laboratories
Lake Success Park
Community Drive
Great Neck, New York
Attn: Dr. A. Moos

Cell Reports (Cont'd.)

McDonnell Aircraft Corporation
Attn: Project Gemini Office
P.O. Box 516
St. Louis 66, Missouri

Monsanto Research Corporation
Everette 49, Massachusetts
Attn: Dr. J. O. Smith

North American Aviation Co.
S&ID Division
Downey, Calfironia
Attn: Dr.James Nash

Pratt and Whitney Aircraft Division
United Aircraft Corporation
East Hartford 8, Connecticut
Attn: Librarian

Radio Corporation of America
Astro Division
Heightstown, New Jersey
Dr. Seymour Winkler

Radio Corporation of America
Somerville, New Jersey
Attn: Dr. G. Lozier

Speer Carbon Company
Research & Development Laboratories
Packard Road at 47th Street
Niagara Falls, New York
Attn: Dr. L. M. Liggett

Stanford Research Institute
820 Mission Street
So. Pasadena, California
Attn: Dr. Fritz Kalhammer

Thiokol Chemical Corporation
Reaction Motors Division
Denville, New Jersey
Attn: Dr. D. J. Mann

Cell Reports (cont'd.)

Thompson Ramo Wooldridge
2355 Euclid Avenue
Cleveland 17, Ohio
Attn: Mr. Victor Kovacik

Unified Science Associates, Inc.
826 S. Arroyo Parkway
Pasadena, California
Attn: Dr. Sam Naiditch

Union Carbide Corporation
12900 Snow Road
Parma, Ohio
Attn: Dr. George E. Evans

University of California
Space Science Laboratory
Berkeley 4, California
Attn: Prof. Charles W. Tobias

University of Pennsylvania
Philadelphia 4, Pennsylvania
Attn: Dr. Manfred Altman

Western Reserve University
Cleveland, Ohio
Attn: Prof. Ernest Yeager

Yardney Electric Corp.
New York, New York
Attn: Dr. Paul Howard

Lockheed Missiles & Space Co.
3251 Hanover St.
Palo Alto, California
Attn: Dr. George B. Adams

Mr. B. S. Baker
Institute of Gas Technology
State & 34th Streets
Chicago 16, Illinois